Investigating plasma-tissue interactions in the context of wound healing

by

Nishtha Gaur

Bachelor and Master of Technology in Nanotechnology

Amity University (India)

A thesis submitted for the degree of

Doctor of Philosophy

School of Engineering

Division of Information Technology, Engineering and Environment



University of
South Australia

February 2019

Contents

1 Chapter 1 Introduction 1

1.1 Literature Review 4

1.1.1 What is plasma? 4

1.1.2 Plasma medicine and plasma devices 5

1.1.3 Linking plasma to biological processes 9

1.1.4 Cells, cellular components and tissue 15

1.1.5 Potential of plasma to stimulate wound healing 23

1.2 Summary 37

1.3 References 38

2 Chapter 2 Analysis of the plasma generation of RONS in biologically-relevant liquids 61

2.1 Small molecule probes to measure RONS in solution 66

2.1.1 Materials and Methods 69

2.1.2 Results and discussion 71

2.2 Amperometric probes to measure H_2O_2 in solution 81

2.2.1 Materials and Methods 82

2.2.2 Results and discussion 83

2.3 Conclusion 87

2.4 References 89

3 Chapter 3 Assessing plasma delivery of reactive species through tissue 98

3.1 Molecular probes to track RONS delivered by plasma through tissue models 103

3.1.1 Materials and Methods 103

3.1.2 Results and discussion 107

3.2 Real-time monitoring of plasma delivered RONS through tissue model using UVAS 116

3.2.1 Instrumentation techniques 116

3.2.2 Materials and Methods 119

3.2.3 Results and discussion 122

3.3 Tracking penetration of RONS delivered by plasma in tissue model using mass spectrometry 135

3.3.1 Principle and Instrumentation 136

3.3.2 Materials and Methods 137

3.3.3 Results and discussion 139

3.4 Conclusion 148

3.5 References 151
4 Chapter 4 Assessing plasma interactions with cells and biological components 161
4.1 Assessment of DNA damage using MB 164
4.1.1 Materials and methods 164
4.1.2 Results and discussion 171
4.2 Assessment of DNA damage with the γ-H2AX assay 183
4.2.1 Materials and methods 183
4.2.2 Results and discussion 185
4.3 Conclusion 192
4.4 References 194
5 Chapter 5 Assessing the effects of plasma on the skin cells 199
5.1 Materials and methods 200
5.1.1 Cell culture 200
5.1.2 He plasma jet 201
5.1.3 He gas jet and plasma jet treatment 202
5.1.4 Resazurin viability assay 203
5.1.5 UVAS measurements 203
5.1.6 Electrochemical probe measurements 204
5.2 Results and discussion 204
5.3 Conclusion 215
5.4 References 217
6 Chapter 6 Conclusion and future work 220
6.1 References 227
Appendix A Calibration for the detection of H_2O_2 using OPD-HRP 230
Appendix B Calibration for the detection of NO_2^- using Griess reagent 232
Appendix C Calibration for the detection of H_2O_2 using ISO-HPO-2 234
Appendix D Publishing rights for the figures in Chapter 3 (Section 3.1) 236
Appendix E Publishing rights for the figures in Chapter 3 (Section 3.2) 238
Appendix F Publishing rights for the figures in Chapter 3 (Section 3.3) 240
Appendix G Publishing rights for the figures in Chapter 4 241
Appendix H Author declaration for the referred manuscript in Chapter 4 243
Appendix I Publishing rights for the figures in Chapter 5 245

List of Figures

Figure 1.1Various components of plasma 4

Figure 1.2 Schematic of a typical plasma jet assembly used in this thesis (a); and photograph of the plasma jet in operation (b). 9

Figure 1.3 The process of redox homeostasis: Balance between the ROS production and ROS clearance achieved with the help of ROS scavengers [180] 12

Figure 1.4 Generation of RONS through various means in an organism and the signalling pathways followed thereafter. The fate of cell is decided by signal transduction and interaction of RONS with specific molecules. The cell may survive or die depending on the signalling mechanism followed. 15

Figure 1.5 Hooke observed a thin slice of cork under microscope. The small compartments separated by thin walls were named cells [237]. 15

Figure 1.6 An illustration of a prokaryotic and eukaryotic cell [242]. 16

Figure 1.7 A schematic of DNA. The long DNA fits into the small cell in form of a coiled chromosome. The double helical ladder-like DNA structure consists sugar group, phosphate group and bases (collectively referred as nucleotides). The bases are attached to sugar-phosphate backbone and paired to each other via hydrogen bonds. Adenine (A) pairs with Thymine (T) and Guanine (G) pairs with Cytosine (C). This pairing is energetically favoured as the bases are neither too far and nor too close, maintaining a proper helix structure [245]. 17

Figure 1.8 A simplified structure of the plasma membrane and its components. 19

Figure 1.9 An illustration of types of actions performed by proteins embedded in plasma membrane. Channel proteins are small openings which facilitate diffusion of specific molecules through the membrane. Recognition proteins acts as markers whch allow the cells to identify cells as self or foreign body. Enzymatic proteins act as a catalyst to transform a molecule from one form to another and are mainly involved in metabolic acitivity of cell. Receptor proteins have active sites for specific molecules such as hormones, which upon binding to the site trigger signalling cascades in cell. Carrier proteins allow specific molecules to attach to its binding site and transport them across the membrane. [261-264] 19

Figure 1.10 Different types of phospholipids and their chemical structures 21

Figure 1.11 Types of glycolipid molecules and the cholesterol molecule. 21

Figure 1.12 The phospholipid molecule with a hydrophilic head and hydrophobic tail (left); and energetically favourable lipid bilayer formation (right). 22

Figure 1.13 A schematic of the structure of human skin 22

Figure 1.14 Different phases of the wound healing process. 24
Figure 1.15 Differences between (a) acute and (b) chronic wound healing. Acute wound healing initiates with scab formation and a temporary inflammatory response. The growth factors and cytokines released by immune cells stimulate angiogenesis, migration of fibroblasts and collagen deposition. This helps in just sufficient reepithelization and eventually tissue remodelling. Chronic wounds exhibit bacterial invasion and prolonged inflammation (hyper-inflammation). Due to an imbalance in growth factors, the epidermal layer undergoes hyper-proliferation, fibroblasts become senescent and levels of matrix metalloproteinases increases. Angiogenesis is also impaired due to hypoxic state induced by fibrin cuffs on the blood vessels. [311]..... 26

Figure 1.16 Common pathways of ROS, RNS and RSS generation in cells. 29

Figure 2.1 An illustration of the working principle of a (a) fluorescent assay and (b) colourimetric assay. 66

Figure 2.2 Reaction illustrating conversion of non-fluorescent DCFH into highly fluorescent DCF upon interaction with RONS. 67

Figure 2.3 Reactions illustrating the production of $O_2^{\bullet -}$, H_2O_2 and HS• during oxidation of DCFH to DCF..... 67

Figure 2.4 Reaction illustrating the conversion of the colourless OPD into a yellow product DAP upon oxidation with H_2O_2..... 68

Figure 2.5 Reaction illustrating two-step conversion of colourless Griess reagent to a pink colored azo dye upon interaction with NO_2^-. Step one is the formation of diazonium cation from sulfanilamide and step two involves the coupling of the cation with N-(1-naphthyl)ethylenediamine to form a stable pink azo dye. 69

Figure 2.6 A schematic (a) and photograph (b) of the He plasma jet assembly utilised in this study. 69

Figure 2.7 Reaction illustrating removal of the acetyl group in DCFH-DA by NaOH to form DCFH. 70

Figure 2.8 Detection of RONS using DCFH. DCFH was prepared in water, PBS, and DMEM and directly exposed to the plasma jet. Plasma jet was operated at 0.5 slpm for 15, 30 and 60 s. Each column represents the mean value and ± standard error of the mean (SEM) between 3 experiments. The experiments were performed with triplicate samples per experiment (n = 9)..... 72

Figure 2.9 Illustration of the key phases involved in plasma-liquid interactions (for plasma operated into ambient air): gas phase, gas-liquid interface and liquid phase, and likely species to be generated in each phase. 73

Figure 2.10 Detection of plasma delivered RONS in DMEM with and without phenol red using DCFH. Each column represents the mean value and ± standard error of the

mean (SEM) between 3 experiments. The experiments were performed with triplicate samples per experiment (n = 9)..... 74

Figure 2.11 Detection of RONS generated with the plasma jet in DMEM with and without L-glutamine using DCFH. Each column represents the mean value and ± standard error of the mean (SEM) between 3 experiments. The experiments were performed with triplicate samples per experiment (n = 9)..... 74

Figure 2.12 Detection of H_2O_2 in water, PBS and DMEM using the (a) direct method and (b) indirect method. The plasma jet was operated at 0.5 slpm for 15, 30 and 60 s. Each column represents the mean value and ± standard error of the mean (SEM) between 3 experiments. The experiments were performed with triplicate samples per experiment (n = 9)..... 76

Figure 2.13 Detection of NO_2^- in water, PBS and DMEM using the (a) direct method and (b) indirect method. The plasma jet was operated at 0.5 slpm for 15, 30 and 60 s. Each column represents the mean value and ± standard error of the mean (SEM) between 3 experiments. The experiments were performed with triplicate samples per experiment (n = 9)..... 79

Figure 2.14 A schematic of components of the membrane-electrochemical sensor used to measure H_2O_2. 82

Figure 2.15 Photograph of the membrane-electrochemical sensor ISO-HPO-2 (on left) and free radical analyzer TBR4100 (on right) from World Precision Instruments used to measure H_2O_2. 83

Figure 2.16 Concentrations of H_2O_2 measured using ISO-HPO-2 in water, PBS and DMEM after plasma treatment for 15 s, 30 s and 60 s. Each column represents the mean value and ± standard error of the mean (SEM) in the experiment performed with triplicate samples (n = 3). 83

Figure 2.17 Comparison between the concentrations of H_2O_2 measured using amperometric probe ISO-HPO-2 and molecular probe OPD-HRP for H_2O_2 detection in water (a,d), PBS (b,e) and DMEM (c,f). In the panel, figures a, b and c panel represent the measurements with indirect method; and d, e and f represent the measurements with direct method Two-way ANOVA was used to determine the statistical significance of the values. The values with ****,!!!! and ++++ marks represent statistically significantly different values ($p < 0.05$), whereas ! and + were statistically insignificant. The marks *, ! and + denote statistical difference in 15 s, 30 s and 60 s values. 85

Figure 3.1 ‘Oxy-nitroso shield burst model’ illustrating transport of plasma generated RONS deep into the tissue via cell-to-cell communication. 100

Figure 3.2 Schematic of the He plasma jet used for this study. 104

Figure 3.3 Schematic of the experimental set-up to assess (a) concentration of RONS delivered by plasma through gelatin and PVA tissue target; (b) the role of fluid proteins in plasma delivery of RONS upon direct plasma exposure; (c) the role of fluid proteins in delivery of RONS through gelatin tissue target; (d) how proteins embedded in gelatin

tissue model impact RONS delivery; and (e) how fluid proteins and tissue-embedded proteins together influence plasma generation of RONS. In all cases the plasma plume is in contact with the target. 106

Figure 3.4 (a) Experimental scheme for the plasma-delivery of RONS in the reporter solution with and without gelatin and PVA tissue targets. The absolute concentrations of (b) H_2O_2 and (c) NO_2^- were elucidated using the calibrations curves, and (c) •OH data is presented as a normalised FI. Direct plasma exposure for 1 min was the control. The symbols *, **, *** indicate a significant difference ($p<0.05$) between corresponding datasets. Below the dashed line, all numbers are effectively zero. Each column represents the mean value and ± standard error of the mean (SEM) between triplicate samples (n = 3). 108

Figure 3.5 (a) The experimental setup for assessing the role of proteins in plasma generation of ROS. (b) The production of ROS is measured as normalised FI without (0 mg ml^{-1}) and with (50 mg ml^{-1}) BSA dispersed in DCFH solution. The symbol * indicates a significant difference ($p<0.05$) between corresponding datasets. Below the dashed line all numbers are effectively zero. Each column represents the mean value and ± standard error of the mean (SEM) between triplicate samples (n = 3). 110

Figure 3.6 (a) The experimental setup to assess the plasma generation of ROS without BSA (0 mg ml^{-1}) and with BSA (1, 25 and 50 mg ml^{-1}) through gelatin using DCFH reporter solution. (b) Total ROS production after plasma treatment of 1, 5 and 10 min is depicted as normalised FI. Below the dashed line all numbers are effectively zero. Each column represents the mean value and ± standard error of the mean (SEM) between triplicate samples (n = 3). 110

Figure 3.7 The experimental setup to assess the effect of gelatin incorporating BSA ("BSA-loaded") on plasma generation of ROS in PBS (a) without BSA and (c) with BSA. BSA is dispersed in gelatin ("BSA-loaded") at concentrations of 0 and 50 mg ml^{-1}. (b) Total ROS production in) PBS (without BSA) after the plasma treatment for 1, 5 and 10 min through agarose with BSA. Total ROS production in PBS (with BSA) after plasma treatment for 1 min (d) directly and (e) indirectly through a BSA-loaded agarose. The symbols *, **, *** indicate a significant difference ($p<0.05$) between corresponding datasets. Below the dashed line all numbers are effectively zero. Each column represents the mean value and ± standard error of the mean (SEM) between triplicate samples (n = 3). 112

Figure 3.8 Schematic of the working principle of UVAS. The light from the source passes through a diffraction grating and slit to reach the filter. Through the filter the light then reaches the sample cell (cuvette), at fixed wavelength. The transmittance of light incident on the sample cell (**I**) and exiting out of the cell (**I0**) is detected by a detector. The output is collected by the computer as an absorbance spectra at specific wavelengths. 117

Figure 3.9 Schematic of a current monitor. The current carrying conductor to be measured passes through the current monitor. The output voltage is measured using an oscilloscope. 118

Figure 3.10 An illustration of the electronic, vibrational and rotational energy levels in a molecular spectra. The horizontal lines represent the energy levels and the vertical lines

represent the transitions (electronic, vibrational and rotational) between different energy levels. 118

Figure 3.11 Schematic of the plasma jet used in this study. The jet consists a 150 mm glass tube which was purged with He gas at a flow rate of 1 slpm. A 15 mm long Cu electrode was wound on the glass tube such that distance between the end of glass tube and the electrode is 40 mm. An oscilloscope was used to monitor the voltage and frequency supplied to the unit by the high voltage power unit. 120

Figure 3.12 Schematic of the experimental setup utilised in this study. A volume of 4.1 ml of the DI water was exposed to the plasma jet in a cuvette (a) with and, (b) without an agarose target on top (at d = 15 mm). Electrical measurements were conducted using a current monitor and high voltage probe. UVAS was utilised to measure the transmittance in each case before (**I0**) and after (**I**) plasma treatment at a specific wavelength (λ). OES was performed using a fiber optic probe with collimating lens and a spectrometer. The absorption and emission spectra were recorded on the computer. 122

Figure 3.13 Electrical diagnosis of the He plasma jet operated at a He gas flow rate of 1 slpm. (A) The voltage waveform at an applied peak-to-peak voltage (V_{p-p}) of 7 kV were measured using the voltage probe. (B) The total current (I_t) and displacement current (I_{dis}) were measured using the current monitor. (C) The discharge current calculated (I_d) by subtracting I_{dis} from I_t. The duration of positive and negative peaks are denoted by Δt_p and Δt_n, respectively. 123

Figure 3.14 The OES generated emission spectrum of He plasma jet in the range of (A) 280-480 nm and (B) 640-840 nm. (C) The experimental spectra (circles) of N_2 second positive system from 370 nm to 385 nm was fitted against the calculated spectra (red line) provided kindly by Prof. Hiroshi Akatsuka at Tokyo Institute of Technology. ... 124

Figure 3.15 UV absorption profile showing time-dependent changes upon plasma treatment of DI water for 15 min (A) directly and (B) indirectly (through 2.5 mm thick agarose) at t=15, 30, 45 and 60 min. (C) The total absorbance between 190 and 340 nm after 15 min (green shaded region) of direct and indirect plasma treatment through the agarose target (1.3, 2.5 and 5.8 mm thick). Total absorbance was measured for up to 60 min. Open arrows indicate the point at which RONS production increased and solid arrows indicate points where rate of RONS generation slowed down. Each error bar represents ± standard error of the mean (SEM) between triplicate samples (n = 3). 126

Figure 3.16 Concentrations of RONS in DI water after direct and indirect (through agarose) plasma treatment determined using an automated UVAS curve fitting technique. Reference UV absorbance peaks of neat solutions of (A) H_2O_2, (B) HNO_2, (C) HNO_3 and (D) O_2 (aq) were used to determine concentrations of RONS in DI water after plasma exposure. Plasma and helium gas flow were extinguished after 15 min (t = 15 min) as represented using green shaded region. Curve fitted spectra for (E) direct and (F) indirect plasma treatment through 2.5 mm agarose were recorded. The spectra was recorded up to t = 60 min i.e. 45 min after plasma and He gas were switched off. Dynamic changes in concentrations of (G) H_2O_2, (H) NO_2^-, (I) NO_3^- and (J) O_2 (aq) were investigated by plotting concentrations of each RONS against time. The positive and negative inflections in concentrations were shown using open and solid arrows,

respectively. . Each error bar represents ± standard error of the mean (SEM) between triplicate samples (n = 3). 129

Figure 3.17 Schematic of a mass spectrometer. The species are differentiating based on the m/z ratio in three major steps – ionization by electron beam bombardment, sorting by a mass analyser and detection to get a mass spectrum. 137

Figure 3.18 A pictorial representation of mass spectrometry of a He plasma jet. The jet was mounted onto an x-y-z stage for the molecular beam alignment. The HPR60 has a three-stage differentially pumped system which is separated by the three skimmer cones. The cones and the turbo molecular pumps help to maintain vacuum condition in the chamber. The plasma species were detected for (a) direct plasma treatment and (b) through-agarose plasma treatment. 139

Figure 3.19 Time resolved changes in mass intensities of neutral species (a) N_2, (b) O_2, (c) H_2O (in ambient air) during plasma treatment, and (d) intensity of He during plasma jet as well as neutral He gas treatment. The species were detected in RGA mode using an internal ioniser (EQP300). 140

Figure 3.20 Ambient mass spectra of positive species delivered by plasma jet treatment (a) without agarose at t=1 min; (b) through agarose at t=10 min; and (c) through agarose at t=20 min. All measurements were done in positive SIMS mode. 142

Figure 3.21 Time-dependent changes in mass intensities of positive ions O^+(16 amu), O_2^+(32 amu), and $H^+(H_2O)_4$ (73 amu). 144

Figure 3.22 Ambient mass spectra of negative species delivered by plasma jet treatment (a) without agarose at t=1 min; (b) through agarose at t=10 min; and (c) through agarose at t=20 min. All measurements were done in negative SIMS mode..... 145

Figure 3.23 Time-dependent changes in mass intensities of negative ions O_2^-(32 amu), NO_2^-(46 amu), CO_3^- (60 amu), and $O_2^-(H_2O)_2$ (68 amu)..... 147

Figure 4.1 A schematic of the structure of a molecular beacon (MB). The MB used in this study consists of a single-stranded loop and double-stranded stem with a quencher (black circle) and a fluorophore (open circle) on either ends of the stem. Upon breakage of the DNA strands, the quencher separates from the fluorophore resulting in fluorescence of the fluorophore (green circle)..... 162

Figure 4.2 (a) A photograph of the He plasma jet. (b) A schematic of the plasma jet assembly and specifications of the plasma jet. 165

Figure 4.3 A schematic of the methodology to assess DNA-strand breaks using the MB in models of tissue fluid, tissue and cells. DNA-strand breaks were assessed with (a) the MB dispersed in the tissue fluid model, (b) dispersed within the tissue fluid model underneath the tissue model, (c) dispersed within the tissue model, and (d) encapsulated inside the cell model dispersed within the tissue fluid model. 169

Figure 4.4 Photograph of the He plasma jet in operation under different experimental parameters. The plasma jet is shown operated at (a, c, e) 0.05 slpm or (b, d, f) 0.5 slpm

into the ambient air (a, b), or during treatment of the HEPES tissue fluid model (c, d), or during treatment of the gelatin tissue model (e, f). 171

Figure 4.5 (a) DNA-strand breaks in the tissue fluid model after plasma jet treatment at 0.05 and 0.5 slpm. (b) The concentration of H_2O_2 delivered by the plasma jet under the same treatment parameters. (c) Assessment of DNA-strand breaks (shown as FI values of the MB) from different concentrations of H_2O_2 solution added to the MB suspension. 172

Figure 4.6 DNA-strand breaks and concentration of H_2O_2 after the plasma jet treatment of the MB through the gelatin tissue model. The plasma jet was operated at a He gas flow rate of 0.5 slpm for 10 min. 174

Figure 4.7 The assessment of DNA-strand breaks when MB is dispersed within the gelatin tissue matrix after the treatment with (a) He plasma jet and (b) He gas jet, both at 0.5 slpm for 10 min. The figures are the overlay of images obtained using the fluorescence and phase-contrast microscopy. The scale bar of images is 250 µm..... 175

Figure 4.8 Typical ESR spectrum of HEPES containing the CYPMPO spin-trap for the •OH after plasma jet treatment. Two plasma jet treatment conditions were assessed: direct plasma treatment of HEPES and treatment of HEPES through the gelatin target. The plasma jet was operated at 0.5 slpm. The ESR spectrometer settings were: center magnetic field = 335.6 mT; and sweep width = +/- 7.5 mT. 176

Figure 4.9 Plasma jet treatment of the MB encapsulated within the phospholipid vesicles. (a) Results showing the normalised FI of the MB treated at the two different flow rates of 0.05 slpm for 10 and 20 min, and 0.5 slpm for 15, 30 and 60 s. (b) Plasma jet treatment of the vesicles encapsulating CF and (c) corresponding results showing the normalised FI of the CF with control treatments with 0.05 slpm (for 20 min) and 0.5 slpm (for 60 s) He gas flow alone, and treatment with 0.01% (v/v) Triton X-100 solution as a positive control. 177

Figure 4.10 (a) Photograph and (b) schematic of the experimental methodology used to assess indirect plasma jet treatment of the MB suspended in HEPES underneath a commercial hydrogel dressing (Intrasite Conformable). (c) Corresponding results showing the normalised FI of the MB (indicator of DNA-strand break) and concentration of H_2O_2 delivered the dressing into HEPES under the same treatment conditions. The plasma jet was operated at 0.5 slpm for 10 min..... 180

Figure 4.11 The phosphorylation of H2AX to γ-H2AX following various plasma jet treatments. The first, second and third row show the immunofluorescence images of DAPI stained nuclei, γ-H2AX positive nuclei and the merged image, respectively. ... 187

Figure 4.12 Percentage of DNA-strand breaks observed after the different plasma treatments of HaCaT cells. The cells were plasma-treated with the hydrogel dressing for 240 s and also without the hydrogel dressing (contact and non-contact) for 15, 30 and 60 s, respectively. Untreated control cells are shown for comparison. 188

Figure 4.13 The ESR spectrum of the CYPMPO-OH adduct in HEPES adduct after it was directly treated with the plasma jet and indirectly through the hydrogel dressing.

The ESR was operated with the center magnetic field at 335.6 mT and sweep width of +/- 7.5 mT. 189

Figure 4.14 The relative signal intensities of the •OH after the direct plasma jet treatment of the CYMPO spin-trap in HEPES. The peak intensities were calculated by referencing to a Mn^{+2} internal standard. Data are expressed as the mean ± standard deviation (n=3). The plasma jet treatment of 15, 30 and 60 s was conducted in two conditions – non-contact (plasma plume not touching the liquid) and contact (plasma plume touching the liquid). 190

Figure 4.15 Concentrations of H_2O_2 generated by the plasma jet into HEPES after the direct plasma treatment (without hydrogel dressing) and through the hydrogel dressing. The direct treatments were performed in two conditions – (i) contact (when the plasma plume is touching HEPES), and (ii) non-contact (when the plasma plume is not touching HEPES). 191

Figure 5.1 Schematic of the He plasma jet unit used in this study. 200 µl of cell suspension was exposed to plasma (or He gas) in a 96-well plate at a fixed distance of 2 mm. 202

Figure 5.2 The dynamic changes in the concentration of H_2O_2, NO_2^-, NO_3^- and O_2 (aq) in water during and after the treatments with (a) 30 min of He gas jet, (b) 15 min of He plasma jet, (c) 15 min of He gas jet followed by 15 min of He plasma jet, and (d) 15 min of He plasma jet followed by 15 min of He gas jet. Both the jets were operated at a gas flow rate of 0.5 slpm. 205

Figure 5.3 The effect on HaCaT cell viability after the treatments with (a) 60, 180 and 300 s of 0.5 slpm He gas jet and 15 and 30s of 0.5 or 0.05 slpm He plasma jet, (b) 300 s of 0.5 slpm He gas jet followed by 15 and 30s of 0.5 or 0.05 slpm He plasma jet, (c) 15 and 30s of 0.5 or 0.05 slpm He plasma jet followed by 300 s of 0.5 slpm He gas jet .. 208

Figure 5.4 The effect on HFF-1 cell viability after the treatments with (a) 60, 180 and 300 s of 0.5 slpm He gas jet and 15 and 30s of 0.5 or 0.05 slpm He plasma jet, (b) 300 s of 0.5 slpm He gas jet followed by 15 and 30s of 0.5 or 0.05 slpm He plasma jet, (c) 15 and 30s of 0.5 or 0.05 slpm He plasma jet followed by 300 s of 0.5 slpm He gas jet .. 209

List of Tables

Table 1.1 Types of RONS detected in an APPJ 10

Table 1.2 Examples of membrane proteins and their functions. 20

Table 1.3 Changes in the expression of growth factors in chronic wound and their subsequent effects. [86, 312, 313] 26

Table 1.4 Effect of O_2 in wound healing [323]. 27

Table 2.1 Composition of various biologically relevant solutions used as tissue models – water being the simplest solution and DMEM being the most complex. 65

Table 2.2 The factorial difference between the concentrations of H_2O_2 measured with the ISO-HPO-2 sensor and OPD-HRP molecular probe (indirect or direct method). The difference was calculated by dividing the concentrations measured from OPD-HRP (direct or indirect) with the measurements from ISO-HPO-2. 86

Table 3.1 The wavelengths corresponding to the emission spectral lines in N_2^+ FNS and N_2^*SPS systems when transitioning from v' to v". 124

Table 3.2 Concentrations of RONS in micromolar (µM) after direct and indirect (through agarose) plasma treatment of DI water. Plasma and gas flow were both switched off after 15 min i.e at t= 15 min. Concentrations were measured at (A) t=15 min; (B) t=30 min; and (C) t= 60 min. 130

Table 5.1 The O_2 (aq) tension (%) and H_2O_2 (µM) delivered by He gas jet and He plasma jet in DMEM. The symbols … denotes values which could not be measured and * denotes the extrapolated values from calibration curves using longer treatment times of minutes. 213

List of Abbreviations

AP-1 - Activator protein

APPJ - Atmospheric pressure plasma jet

ATM - Ataxia telangiectasia mutated

BCD - Barrier coronal discharge

BSA - Bovine serum albumin

CO_2 - Carbon dioxide

$CO_3^{\bullet-}$ - Carbonate ion

Cl^- - Chlorine

CAP - Cold Atmospheric Plasma

Cu - Copper

CF- 5,6-carboxyfluorescein

cGMP - Cyclic guanosine-3',5'-monophosphate

DAP - 2,3-diaminophenazine

DAPI - 4′,6-diamidino-2-phenylindole

DBD - Dielectric barrier discharge

DNA - Deoxyribonucleic acid

DDR - DNA damage response

DI Water – Deionized water

DMEM - Dulbecco's Modified Eagle Medium

DCFH - Dichlorodihydrofluorescein

DOPC - Dipalmitoylphosphatidylcholine

ESR - Electron spin resonance

ETC - Electron Transport Chain

eNOS - Endothelial NOS

EGF - Epidermal growth factor

EGF-R - Epidermal growth factor receptors

ECM - Extracellular matrix

Fe^{+2} - Ferrous ion

Fe $(NO_3)_3$ - Ferric nitrate

FGF - Fibroblasts growth factor

FNS - First negative systems

FE-DBD - Floating electrode

FI - Fluorescent intensity

γ-H2AX - Gamma-H2AX

He - Helium

HEPES - 4-(2-hydroxyethyl)-1-piperazineethanesulfonic acid

HEA - Hydroxylethylacrylate

H_2O_2 - Hydrogen peroxide

H_2S - Hydrogen sulphide

H_2S_2 - Hydrogen disulphide

RSSH - Hydropersulfide

•OH - Hydroxyl radicals

HP - Hydroxyl-proline

HOO• - Hydroperoxyl radical

HBOT - Hyperbaric oxygen therapy

HOCl - Hypochlorous acid

HIF-1 - Hypoxia-inducible factor-1

IBU - Ibuprofen

ROS - Include reactive oxygen species

iNOS - Inducible NOS

IL - Interleukins

HaCaT -Keratinocytes

kHz - Kilo Hertz

kPa - Kilo Pascal

kV - Kilo Volts

MIP-1α - Macrophage inflammatory protein 1 alpha

MS - Mass spectrometry

MMP - Metalloproteinases

µM - Micro molar

µm – Micro meter

mm – Milli meter

µL - Micro liter

ml – Milli liter

mM - Milli molar

MΩ – Mega ohm

MAPK - Mitogen-activated protein kinase

MB - Molecular beacon

MCP-1- Monocyte chemoattractant protein

MPa - Mega pascal

MPO - Myeloperoxidase

NWPT - Negative pressure wound therapy

NOX - Nicotinamide adenine dinucleotide phosphate oxidase

NO_3^- - Nitrate

NO - Nitric oxide

NO_2^- - Nitric dioxide

NOS - Nitric oxide synthase

nm – Nano meter

nM - Nano molar

$NaNO_2$ - Sodium Nitrite

$NaNO_3$ - Sodium Nitrate

NF-ĸB - Nuclear factor-ĸB

OES - Optical emission spectroscopy

O_2 - Molecular oxygen

O_3 - Ozone

OPD-HRP - o-Phenylenediamine dihydrochloride–horseradish peroxidase

PDGF-R - PDGF receptors

V_{p-p} - Peak-to-peak voltage

$ONOO^-$ - Peroxynitrite

ONOOH - Peroxynitrous acid

PI - Phosphatidylinositol

PBS - Phosphate buffer saline

PC - Phosphotidylcholine

PE - Phosphotidylethanolamine

PG - Phosphotidylglycerol

PS - Phosphotidylserine

PDGF - Platelet derived growth factor

PoC - Point-of-care

PTFE - Polytetrafluoroethylene

PVA - Poly vinyl alcohol

K^+ - Potassium

RNS - Reactive nitrogen species

ROS - Reactive oxygen species

RONS - Reactive oxygen and nitrogen species

RSS - Reactive sulphide species

RBC - Red blood cells

$^1O_2$ - Singlet oxygen

RSNO - S-nitrosothiols

Na^+ - Sodium

NaOH - Sodium hyroxide

Slpm - Standard litres per minute

$O_2^{-\bullet}$ - Superoxide

SIMS - Secondary ion mass spectrometry

SOD - Superoxide dismutase

SPS - Second positive systems

TF - Tissue factor

HS• - Thiyl radical

H_2S_3 - Trisulfane

H_2S_4 - Tetrasulfane

TGF-β - Transforming growth factor beta

TNF-α - Tumour necrosis factor alpha

UV - Ultraviolet rays

UVAS - UV-visible absorption spectroscopy

VEGF - Vascular endothelial growth factor

XO - Xanthine oxidase

Summary

Renewed optimism that plasma can be developed as a medical tool has in the past two decades stimulated a surge in research into both the fundamentals and applications of plasma devices. A wide range of plasma devices and potential medical uses are currently being investigated, and relevant to this work are plasma jet designs and their uses in wound healing and management. Non-healing chronic wounds are a major healthcare challenge often resulting in limb amputation and death, and the direct cost of chronic wounds to Australia is $2.8bn p.a. In the context of wounds, it has been speculated that in both wound decontamination and wound healing the plasma jet delivery of reactive oxygen and nitrogen species (RONS) are likely to have a number of beneficial effects. And, although a wide range of studies are being conducted globally, to understand the generation of different types of RONS and their delivery to cells and tissue, still a plethora of questions remain outstanding. Such outstanding questions relate to issues such as: (a) the basic accuracy of the metrology of RONS whether using common detection methods (b) the mechanism(s) of delivery of RONS into cell culture, into cells and deeper into tissues; and (c) how the various "plasma-delivered" RONS interact with the different cellular components.

This PhD project, employing a plasma jet device, focuses on understanding the measurement of RONS within the jet effluent and the fundamentals of plasma jet delivery of RONS into models of biological fluids, cells and tissue and the possible mechanisms involved in plasma-induced stimulation of wound healing. These are achieved by developing an arsenal of detection systems using molecular probes, electrochemical sensors, electron spin resonance or mass spectrometry to accurately and reliably quantify RONS delivered into *in vitro* models: into an artificial cell model (employing vesicles), tissue fluid, and tissue surrogates (using hydrogels). In order to elucidate the effects of RONS on cells significant in wound environments, fibroblasts and keratinocytes have been used as models of the principal skin cells.

In the development of new medical therapies, safety is equally important as efficacy. Therefore, this thesis also aims to assess the safety of the plasma jet in assays of cell viability and DNA damage. This project foreshadows the future development of 'tailored' plasma devices that could deliver controlled RONS dosages to, for example, the wound site, and tailored depending on nature of the disease and/or patient status.

Declaration

This thesis presents work carried out by myself and does not incorporate without acknowledgment any material previously submitted for a degree or diploma in any university; to the best of my knowledge it does not contain any materials previously published or written by another person except where due reference is made in the text; and all substantive contributions by others to the work presented, including jointly authored publications, are clearly acknowledged.

Nishtha Gaur 02-02-2019

Acknowledgments

Firstly, I would like to thank my supervisors, Prof. Rob Short and Dr. Endre Szili for accepting me as an intern in 2014 and later as a PhD student. There could not have been a better place to embark my journey as a researcher. Your wisdom and knowledge will forever be a source of motivation for me. Thank you so much for not just being a PhD mentor but also a friend (those skype meetings were therapeutic!).

I am also grateful to my co-supervisor Prof. Allison Cowin for her guidance in the field of biology and ever-ready to help me in the absence of Rob and Endre. Additionally, I thank my co-supervisor Prof. David Graves for supervising me all the way from USA whenever needed.

I would like to acknowledge the financial support from the University of South Australia, Australian Government's Cooperative Research Centre's Program and the Wound Management Innovation CRC.

I am thankful to A/Prof. Jun-Seok Oh and Dr. Hirofumi Kurita for hosting me as a visiting researcher in Japan. I also extend my gratitude to Prof. Sarah Allison, Dr. Howard Lindsay and Prof. Ruth Cameron for the successful collaborative work in UK.

Also a huge thanks to my colleagues in university, especially Sunny, Sue and Alex who helped me a lot laboratory and answered all my questions with great patience for 3 years! Thanks to all my friends or rather a little family in Australia for the endless venting-out coffee sessions and great laughter that made this PhD little smoother. I express my gratitude to Apoorva and Parth for helping me with proof-reading.

This journey wouldn't have been possible without the support of my family. Thank you Mumma and Daddy for being my pillars of strength and my brother Nishkarsh for tabdasingo.

I must also acknowledge myself for working hard to achieve this PhD thesis in time!

Chapter 1 Introduction

Modern medical science endeavours to serve humankind by providing reliable methods of preventing, diagnosing and treating diseases. Recent advancements have armed us to "beat" diseases through vaccination such as polio [1-3], smallpox [4] and rabies [5], and through other strategies we have been able to "manage" treatment for diseases such as diabetes [6-8], hepatitis B [9], hepatitis C [10] and tuberculosis [11]. Medical research is also making substantial progress towards the effective management of cancer [12-19], chronic wounds [20-22] and ulcers [23, 24].

Current medical treatments are commonly based on pharmaceutical drug formulations. Drugs are the most common and most popular type of treatment method which involves administering pharmaceutical formulations (e.g. drugs, vaccines, etc.) into the body via oral (enteral formulations such as tablets, capsules and powders), intravenous (parenteral formulations such as liquid and lyophilised drugs), nasal (nasal drops, nasal sprays), ocular (eye drops, contact lens, ointments) or transdermal (topical formulations such as ointment, gel, paste, patch) means [25-29]. But limitations include poor solubility, drug accumulation causing tissue damage, rapid breakdown *in vivo*, poor pharmacokinetics and non-specific delivery leading to side-effects [30].

Nanotechnology is the next stage of orthodox drug delivery, with attempts to overcome the current limitations. Nanotechnology-based drug delivery platforms such as nanoemulsions, nanogels, functionalised nanoparticles, drug solid lipid nanoparticles and dendrimers have emerged as suitable drug delivery vehicles [25, 31-34]. Characteristics such as excellent biocompatibility, enhanced solubility and stability, and multi-functional surfaces enable them to improve the drug bioavailability, target specific tissue, and control drug pharmacokinetics [30, 35]. But the toxicity and safety associated with nanotechnology based drugs such as immunogenicity arising from

increased reactivity and bioaccumulation due to small size still remain a concern [35, 36].

Radiation based treatment, generally a part of cancer therapy, is another popular medical therapy. The year 1895 marked the discovery of X-rays [37]. Within one year of its discovery, X-rays were used for diagnosis of a broken wrist of a schoolboy in the US [38]. In 1899, the first successful treatment of an ulcer and epithelium using radiation therapy was reported [39]. Today, radiation therapy is a well-known technique which includes the use of X-rays [40, 41], gamma rays [42, 43] and charged particles such as protons, neutrons, and helium (He) ions to treat cancer and skin diseases [39, 44-49]. Phototherapy using lasers is another example of radiation therapy wherein low intensity laser radiations are exploited to induce non-destructive biochemical processes in the body [50, 51].

'Plasma medicine' is a potential further such innovation in healthcare, wherein the ionised gas (plasma) is directly applied to the living tissue for the purpose of medical treatment [52-59]. The potential role of plasma in the biomedical field is gaining considerable attraction all over the world. *In vitro* studies have successfully demonstrated the lethal [60], sub-lethal [61] and non-lethal [62] effects of plasma gas and its applications for sterilization (as anti-fungal, anti-bacterial and disinfectant) [60], stimulation of cell signalling [61], wound healing [62], the treatment of implants [63] and the localised treatment (e.g.- tooth root canal and targeted cancer therapy) [64] and, large area tissue treatment (e.g.- wound decontamination and dermatology) [64, 65]. Amongst, the wide range of plasma devices available for medical use, an atmospheric pressure plasma jet is most common and widely reported. This has been explained in greater detail in Section 1.1.2.

The biological effects induced by plasma gas are directly linked to the constituents of the gas. Plasma gas comprises ions, electrons, ultraviolet rays (UV), transient electric field and RONS, amongst which the role of RONS had been extensively studied (discussed in detail in Section 3.1 and 3.2). Studies across the globe point to the potential significance of RONS in plasma-based therapeutics [66-70]. The sterilization and decontamination of surgical tools [71-73] and the potential to decontaminate wounds [64, 65, 74] are often reported. Section 3.3 highlights species generated by plasma that have been implicated to have the ability to deactivate lipid A and

endotoxins. These RONS include reactive oxygen species (ROS) such as hydrogen peroxide (H_2O_2), superoxide (O_2^-), hydroxyl radicals (OH•) [75], and high-energy reactive nitrogen species (RNS) such as peroxynitrite ($ONOO^-$) [76]. Whilst RNS, such as nitric oxide (NO), have been shown to promote endothelial cell proliferation, induce angiogenesis and trigger vascular endothelial factors [77, 78]. NO had also been reported to control blood flow, tissue oxygenation and vasodilatation, opening new gateways for tumor treatment [79].

Plasma based treatments have been shown to be systemic or highly localised, depending upon the application [80-85]. Localisation implies plasma therapy can be used to induce biological effects in specific cells without affecting nearby cells, unlike current less targeted conventional drug and radiation therapies. The selective or cell-specific effect of plasma has promising applications. This study focuses on the application of plasma in wound healing processes. The process of wound healing can be regarded as an evolutionarily-conserved interplay between various types of cells such as keratinocytes, fibroblasts, endothelial cells, macrophages and platelets; and cell growth factors such as vascular endothelial growth factor (VEGF), transforming growth factor beta (TGF-β), fibroblasts growth factor (FGF), platelet derived growth factor (PDGF) and cytokines [86]. Growing interest and confidence in plasma therapy has led to a wide range of *in vitro* and *in vivo* studies to understand the role of RONS in wound healing. Section 3.4 highlights these studies involved with the effect of plasma on wound healing processes and signalling mechanisms.

To date, we know that plasma retains its beneficial therapeutic effects even after multiple applications, but in order to introduce this nascent technology as an alternative or adjunct to current wound-healing therapies, after demonstration of potential beneficial effects many significant aspects need to be addressed, starting as with any new therapeutic, safety concerns. Although a number of clinical devices including kinPen MED [59], MicroPlaSter [56, 57], PlasmaDerm [87] are being widely used on patients, reports on safety of these devices have not been well-examined yet [66, 88, 89]. Furthermore, the wider biological effects of plasma treatment have yet to be investigated. For example, the role of each type of RONS has yet to be established and issues such as deep surface effects, the interactions of plasma with the tissue and diffusion of plasma-delivered RONS into the tissue have barely been commented upon [66, 90-92].

Therefore, in considering the potential applications of plasma to stimulate wound healing, this thesis will cover multidisciplinary research focusing on basic plasma physics and chemistry, physical chemistry of plasma-tissue interactions, through to the biology of plasma-cell interactions. The literature review and research is carried out in the context of the known biological processes involved in the maintenance of healthy tissue and the repair of damaged skin tissue. The sections below will cover the relevant literature of these aspects.

1.1 Literature Review

1.1.1 What is plasma?

The term ‘plasma’ was coined by Langmuir in 1928 [93]. Plasma is an ionized gas comprising a cocktail of ions, electrons, UVA, UVB, UVC, heat, reactive species/radicals, metastables and neutrals [65, 94, 95] (Figure 1.1). Since plasma gases are made up of charged particles, they behave differently to neutral gases because their movement is influenced by electric and magnetic fields. Hence, plasmas are considered a distinct "fourth state of matter" [96].

Plasma occurs abundantly in nature. For example, inside interstellar gas clouds, large scale structures of galaxies, interplanetary matter, stars and the sun, the solar wind, comet tails, ionosphere, auroras, lightning and fire [97]. In short, plasma is everywhere – 99.9% of the universe is made up of plasma [98-101].

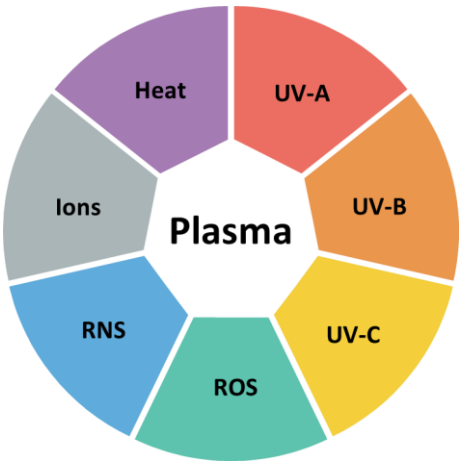


Figure 1.1Various components of plasma

Apart from naturally occurring plasmas, a variety of technologies have been devised to create plasma artificially (referred to herein as technological plasma). Technological plasmas can be generated by applying an electrical energy to ‘ignite’ the background

gas [102]. With a sufficient amount of applied voltage, electrons dissociate from atoms (or molecules) leading to a 'breakdown' of the gas [103]. Light is emitted within the gas as the electrons relax from a higher energy state to a lower energy state; therefore plasmas usually exhibit a characteristic glow.

Plasmas can be created and operated over a wide range of parameters such as [102, 104-112]:

- **Applied power** including AC or DC excitation over a range of voltages and frequencies (Hz, kHz, RF and microwave);
- **Pressures** from above atmospheric pressure (760 Torr) to pressures well below atmospheric pressure; and
- **A wide range of gases** like helium, neon, xenon, oxygen, nitrogen, carbon dioxide, argon, air, etc.

Plasmas can be non-thermal with the gas temperature ranging from 300 K to 350 K and thermal with temperatures exceeding 1000K. Owing to the possibility of operating plasma over a wide range of parameters and configurations, plasmas offer many applications in semiconductor manufacturing, electronics, energy and power production, textile industries and healthcare [55, 113-116].

1.1.2 Plasma medicine and plasma devices

Technological plasma can be categorised into two main types: thermal plasma and non-thermal plasma [117]. Thermal plasmas have gas temperatures much higher than ambient air temperature with the electron temperature being close to the gas temperature, and are used in applications which require high temperature such as in plasma spraying to produce high temperature-resistant coatings, plasma chemical vapor deposition for thin film deposition, plasma metallurgy for scrap melting, alloying, welding and metal cutting, waste treatment/vitrification to destroy hazardous waste, and material synthesis such as nanomaterials [118-120]. Non-thermal plasmas have gas temperature close to ambient air, and are used in applications requiring low temperatures such as for surface treatment to add functionality to heat-sensitive materials (e.g. semiconductors, plastics and biomaterials) [121]. They are often referred to as "cold" plasma. Since non-thermal plasma operates at low temperature (as low as

room temperature) and can operate into open air, plasma sources can be constructed for plasma use in point-of-care (PoC) applications to treat thermally sensitive materials such as human tissues [122, 123].

In 1869, Johann Hittorf discovered cathode rays in, what has become to be known as a Crookes tube [124]. Plasma was first reported by Sir William Crookes in 1879 as a 'radiant matter' in the Crookes tube [125]. Later in 1897, Sir J.J. Thomson identified electrons as the constituents of the cathode rays [126]. But it was not until the turn of the twentieth century when Wilson [127] and Elster and Geital [128], simultaneously, used the term 'atmospheric ions' or 'air ions' to describe the electrically charged nature of air.

1900-1980 covers an early, sporadic, era in ***"plasma medicine"*** exploration, wherein attempts to quantitatively study the interaction of plasma with biological matter such as tissues were first made [129]. Investigations initially commenced to achieve stable plasma operation at low or ambient gas pressure [103, 130-132]. Afterwards, applications of atmospheric pressure plasma sources (or cold plasma) were typically limited to thin film deposition and etching, but recent developments in plasma sciences have led to cold plasma-based medical therapies [133, 134]. A quick Google Scholar search on "plasma medicine" results in just 244 research articles from 1998-2008. However, a clear growth can be seen with 4780 research publications in next 10 years (2008-2018). Expansion in the field of plasma medicine has been witnessed in last 15 years through various biological experiments and computer simulation techniques [135]. Now, plasma based treatments are regarded to have the potential to augment current medical therapies. The following features of plasma jets make them suitable as the basis for new medical therapies:

- Thermally sensitive surfaces, such as tissues, can be treated using non thermal plasma without causing potential burn damage, as would be the case with thermal radiations [136].

- Plasma based treatment is postulated to be highly specific and localised, purportedly preventing exposure of any nearby cells from the effects of plasma [89, 137, 138]. Radiation therapies and chemotherapy drugs lack this property as they also damage bystander "normal" or healthy cells, thus causing harmful side effects [139].

- Cold Atmospheric Plasma (CAP) devices can be operated at room temperature and the treatment can be carried out in atmospheric conditions without any special requirements [140].

- The diverse constituents of plasma contribute to its multi-mode action against microorganisms such as bacteria and spores [104, 141]. As a result, it is argued that microorganisms will struggle to develop resistance against CAP treatment, unlike with antibiotic drugs [104, 142].

- Plasma devices are proposed to be cheaper and more cost-effective than other redox inducing mechanisms such as electrical stimulation, electromagnetic fields and ionizing radiation [122, 143].

The above characteristics of plasma medicine are widely cited as rationales for the concept of using plasma devices for wound treatment [56, 144], dentistry [53, 123], disinfection and sterilization, cancer therapy [122, 145], dermatology [65], drug delivery [146] and gene therapy [147].

Introduced by W. Siemens in 1857 for ozonisation [148], the dielectric barrier discharge (DBD) now forms the foundation of most CAP devices [64, 112, 149]. An insulating (dielectric) material placed in the electrical discharge path is characteristic feature of DBD. At high voltage, the gas gets ionised and results in migration of ionised species (radicals, electrons) towards the dielectric electric material. This charge deposition on dielectric material diminishes the charge on the electrode and subsequent decline in electric field in the gap. Eventually the discharge stops and high current build-up is prevented. Limited currents also helps in achieving a low power device and suitability for tissue treatment [141, 148, 150, 151]. In plasma medicine, a DBD device can be operated in three modes- *direct*, *indirect* and *hybrid* [152].

Conventionally, a DBD device consists of two electrodes separated by a dielectric material [148, 150, 151]. In *direct* mode, the human body surface itself serves as the second (ground) electrode. Since the electrode of the plasma device itself is not grounded, it is referred as the floating electrode-DBD (FE-DBD) [133, 152, 153]. When the tissue is treated with a direct DBD, current flows through the living tissue electrode and with the current there is a concomitant flux of active reactive species like charged particles, RONS, UV-light, etc., to the surface of tissues [152, 154].

In the *indirect* configuration, plasma is generated in similar fashion, but the plasma is contained in a device (jet) and there is a flux of longer-lived reactive species, radicals, and uncharged atoms and molecules present in the plasma 'after-glow' or post-discharge plasma to the specimen surface. This process uses an inert gas (usually helium or argon) to aid the flow of these species to the tissue specimen [52, 66, 153].

The *hybrid* devices incorporate the design of direct plasma mode plasma device and the current-free nature of an indirect mode plasma device. They are referred as 'barrier coronal discharge' (BCD) [83, 133, 152, 155]. These devices may include a system with a grounded metal mesh that separates the plasma from the tissue and the gas. The mesh has low electrical resistance than the tissue, such that the current passes through the mesh and there is an indirect direct flux of charged species to the tissue surface [156].

Today plasma medical research involves the use of a wide range of plasma devices based upon various designs such as plasma jets [69, 80, 140], plasma needles [157-160], plasma torches [161, 162] and plasma arrays [163-166]

This thesis focuses on developing a firmer understanding of the mechanisms underlying an atmospheric pressure plasma jet (APPJ), referred to as a "plasma jet" hereafter. A plasma jet is arguably the most common plasma design [112]. The main components of a plasma jet assembly used in this thesis are:

i. Capillary glass tube

ii. Powered electrode such as copper (Cu) electrode

iii. High voltage power supply

iv. Measurement acquisition device such as an oscilloscope

v. Inert gas supply such as a helium (He) gas cylinder

As shown in Figure 1.2, in this study a capillary plasma jet is used. A hollow glass tube, mounted in a thick polytetrafluoroethylene (PTFE) housing to protect the user from the high voltage electrode, is purged with He gas (BOC, high purity grade). The gas flow rate is controlled using a digital mass flow controller. A Cu electrode is wound onto the glass tube and connected to a high voltage power supply. A sinusoidal peak-to-peak voltage ($V_{p\text{-}p}$) of 5-10 kV is applied at a frequency ranging from 25-50 kHz. The

electrical properties are measured using a voltage probe and current monitor and recorded on an oscilloscope.

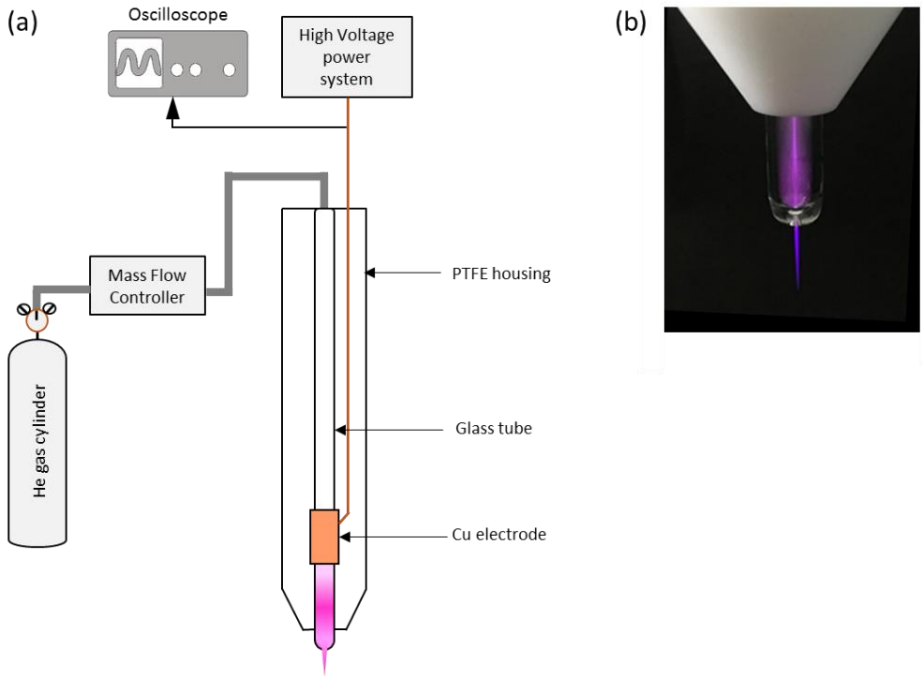


Figure 1.2 Schematic of a typical plasma jet assembly used in this thesis (a); and photograph of the plasma jet in operation (b).

This PhD focuses on measuring physical, chemical and biological changes brought about by a plasma jet to understand its potential modes of action in wound healing. This required using a variety of characterization techniques such as electrical measurements using voltage and current probes; optical analysis using optical emission spectroscopy (OES) and mass spectrometry (MS); and chemical analysis using electron spin resonance (ESR), UV-visible absorption spectroscopy (UVAS), electrochemical sensors and molecular reporters. The majority of the work reported herein was conducted at the University of South Australia. But certain analysis such as MS, ESR and UVAS were carried out during my research collaborative visit to Meijo University and Toyohashi University of Technology in Japan. Therefore, some experiments in this thesis are conducted in Japan which involved minor variations in plasma jet assembly specifications. The plasma parameters and configurations have been described in detail in 'materials and method' section of each chapter.

1.1.3 Linking plasma to biological processes

Plasma is a cocktail of active species comprising positive ions, electrons and RONS thus creating a unique and complex environment. Table 1.1 lists some of the different types of RONS that have been detected in atmospheric plasma jets [74, 109, 167-170].

The therapeutic action of plasma is most often attributed to an interplay between reactive species, radicals, ions and UV photons with the tissue/cell target [60, 75, 94, 95].

Table 1.1 Types of RONS detected in an APPJ

Type of ROS detected	Type of RNS detected
H_2O_2	$ONOO^-$
O_2^-	NO
•OH	Nitrate (NO_3^-)
Hypochlorous acid (HOCl)	Nitrite (NO_2^-)
Singlet oxygen ($^1O_2$)	Peroxynitrous acid (ONOOH)
Ozone (O_3)	
Atomic oxygen (O, O+, O^-)	

1.1.3.1 Free Radical Theory of Ageing

Over a century ago, it was a common orthodox view that the organisms with a higher metabolic activity are prone to shorter life-spans [171]. In 1956, the 'free radical theory' of D. Harman appeared to substantiate this belief by stating that free radical reactions are the causative agent of aging [172]. Put very simply, the theory advocates that higher metabolic activity leads to more free radical formation and free radical reactions, resulting in detrimental changes in the organism [172-174]. The free radical theory of aging is based on the fact that mitochondria were thought (at that time) to be the only source of RONS generation (within the cell) and consequently it was considered that RONS were only destructive agents. The theory missed the highly significant (and specific) signalling pathways that RONS control and that RONS are also actively generated by enzymes like urate oxidase, xanthine oxidase and NADPH oxidase during various cellular processes [171, 175-178].

1.1.3.2 The biological role of RONS

More recent advancements in the study of RONS in biology have helped to identify the role of RONS in regulating cell signalling and other biological functions [179-182]. For

instance, whilst H_2O_2 is lethal for the cell at concentrations of 0.1 mM, but through very specific and highly regulated mechanisms it induces cell proliferation, cell differentiation and mitochondrial genesis generally at lower concentrations of up to 10μM [183-185]. H_2O_2 is also necessary for synthesis of thyroid hormone by the thyroid gland [186]. Similarly other ROS are also a key feature of immune cells. A large concentration of HOCl, O_2^- and •OH along with H_2O_2 are produced by the neutrophils and the macrophages during the process of phagocytosis [187-189]. This acts as a potent microbiocidal agent that kill specific bacteria and virus [190, 191].

RNS such as $ONOO^-$ and NO have been reported as important intercellular messenger molecules for cell signalling and neural network activation at low concentrations (nM range) [192]. NO is generated in endothelium and neurons (dendrites) and plays key roles in shock absorbance (medical) and neuronal activity, respectively [193]. Nitric oxide synthase (NOS) generates NO to control the vascular tone (smooth muscle relaxation) and the cyclic guanosine-3',5'-monophosphate (cGMP)-dependent physiological functions of the nervous system [180]. NO is also formed by decomposition of the oxidant $ONOO^-$ and competes against oxygen to reversibly inhibit cytochrome oxidase and NO further controls oxygen consumption by mitochondria [174, 192]. NO deficiency is a common symptom in patients with malnutrition, diabetes and in cases of steroid use [194].

A synergistic action between both ROS and RNS (or RONS) results in appropriate cellular responses. For instance, during an injury, RONS are released on active inflammation and detected by enzymes and proteins leading to fibroblast proliferation, change in cell metabolism and/or effect on the Na^+ and Ca^{+2} channels [179, 193]. Lymphocytes and phagocytes also detect any increase in RONS production and initiate cell defence mechanisms [177].

To summarise, RONS are the key players, particularly as cell-signalling molecules, within our body. And whether beneficial or harmful to the cell system, depends on various factors such as the location of synthesis of RONS in a cell, the type of RONS generated, the RONS concentration in the cell and the cell signalling mechanisms followed after generation. It is reported that a change in RONS concentration is not always followed by activation of anti-oxidant systems. The major role of anti-oxidant systems is to balance the amount of oxidative species (and not to simply) eliminate

them entirely) [171, 195]. Within different cell types, there is usually a specific threshold of RONS concentration required to activate an anti-oxidant system [196].

1.1.3.3 Oxidative Stress: a necessary evil

Oxidative stress can be defined as an imbalance in concentration of RONS inside our body [187, 197]. Oxidative stress occurs when the rate of generation of RONS exceeds the rate of clearance, thus overwhelming the cellular defence mechanisms [190, 198]. The extent of accumulation of RONS in the cell is determined by anti-oxidant systems. Accumulation of RONS can cause lipid peroxidation, deamination of DNA strand bases, formation of methaemoglobin, trigger autoimmunity and interfere in the Electron Transport Chain (ETC) within mitochondria (also resulting in formation of new ROS such as O_2^-) [199, 200]. In order to prevent damage, the cell undergoes a systemic RONS mediated *redox regulation* to protect itself against oxidative damage and maintain the state of "redox homeostasis" as illustrated in Figure 1.2.

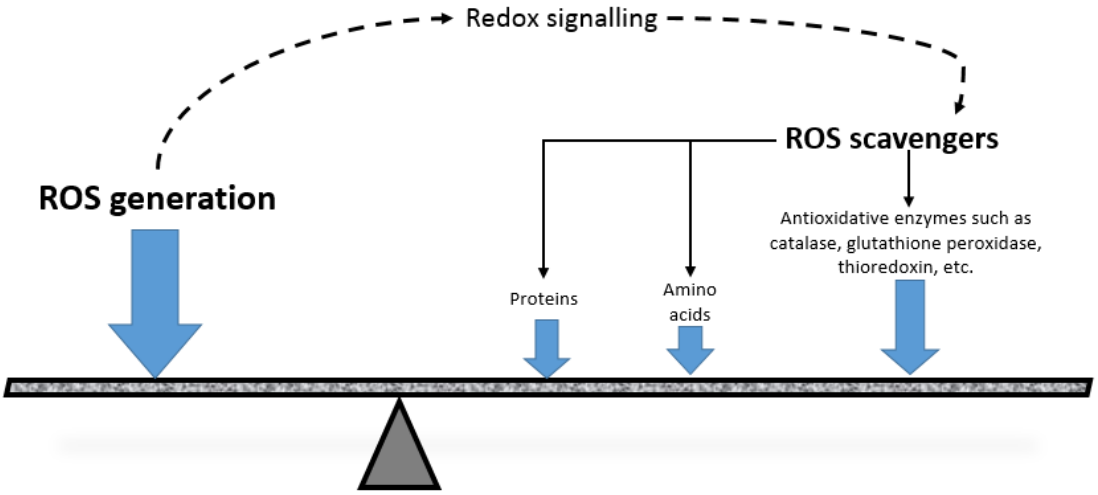


Figure 1.3 The process of redox homeostasis: Balance between the ROS production and ROS clearance achieved with the help of ROS scavengers [180]

Up until the 1990s, biologists considered that oxidative stress only leads to deleterious effects within cells [177, 199, 201]. However, this view was challenged from the 1970s onwards – Mittal and Murard [202], Ignarro and Kadowitz [203], Moncada and his colleagues [204], Roth and Dröge [205], Keyse and Tyrell [206], to name a few. These studies emphasised the fact that oxidative stress plays a major role in the redox regulation in cells and may activate proteins controlling apoptosis, gene transduction, cell proliferation and angiogenesis. [77, 122, 145, 194, 198, 207-210]. For example, oxidative stress arising from H_2O_2 also is a secondary messenger in signal transduction. H_2O_2 is a key player in ligand-stimulated activation of nuclear factor-ĸB (NF-ĸB)

[207]. Under oxidative stress, mitochondria produce excess O_2^- and H_2O_2, which in turn activates NF-ΚB. Other signalling pathways activated by the oxidative stress include hypoxia-inducible factor-1 (HIF-1), activator protein-1 (AP-1) and mitogen-activated protein kinase (MAPK) [211].

1.1.3.4 RONS overproduction: cause or consequence?

RONS have relevance right from the origins of life to the activation of cell defence systems in eukaryotes [212]. In response to the oxidative stress, the organism adapts and overcomes the stressors such as excess RONS, toxins, cell membrane damage and calcium ions. Cells follow various adaptation mechanisms including altering the apoptotic pathways to inhibit apoptosis, gene transduction involving various proteins for damage repair, synthesis of protective molecules such as anti-oxidants and anti-apoptotic proteins, autophagy wherein cytoplasmic components within lysosomes are engulfed and degraded [175, 213-215] (Figure 1.4).

Diseases are often associated with elevated (or altered concentrations from) physiological levels of RONS. For example, atherosclerosis is caused by imbalance between NO and O_2^- and neurogenerative diseases such as Parkinson's disease caused by RONS induced mitochondrial impairment [174]. An imbalance in RONS can have impacts from molecular level to the whole organism. For instance, excess $ONOO^-$ causes:

- at the molecular level, deamination of DNA bases and oxidative modifications of bases and the sugar phosphate chain which leads to DNA damage [216, 217],
- at the cellular level, overproduction of O_2^- in mitochondria playing pivotal role in diabetic complications [218-220], and
- at the whole system level, heart failure to respond to vasorelaxing agents under excessive RONS exposure [221, 222].

But does this "label" RONS as the causative agent? Could increases in RONS levels be an outcome of the disease, rather than the causative agent? In case of some neurological diseases such as Parkinson's disease, it still remains unclear whether ROS-induced oxidative stress is the 'initiator' of cell injury. However, it is well established that oxidative stress associated with elevated levels of ROS are detected in 'propagation' of

signalling events during cell injury [223]. In murine models of constipation-associated colorectal cancer, signalling pathways such as HIF-1 induced by oxidative stress, do not participate in tumorigenesis [224]. Similarly, an increase in RONS levels in tissue after ischemic injury is considered to be a downstream consequence of increased cytosolic calcium content [225].. Presence of calcium blockers is shown to abate RONS formation, thus questioning the causative role of RONS in post-ischemic injury [225]. Other studies have demonstrated that oxidative stress pathways do not contribute to disuse muscle atrophy [226]. It may be possible that increase in RONS concentrations (observed in a disease) are the result of oxidising products formed through various redox pathways and signalling cascades, which facilitate to more RONS production, DNA damage, carcinogenesis, etc. [181, 227].

A number of modern medical treatments focus on eliminating RONS. The most common method is flooding the system with anti-oxidants. Yet it has been reported that elevated levels of antioxidants may act as pro-oxidants and contribute to more serious illness [228-232]. 100-300 μM of urate control oxidative stress but higher concentrations of urate lead to multiple secrosis and Parkinson's disease. [173]. Higher uric acid in blood is the cause of a high cardiovascular rate, hypertension, obesity and visceral adiposity [233]. In the process of eliminating RONS, antioxidants may unintentionally cause inactivation of the immune system and down-regulation of endogenous anti-oxidants [231, 234] . This is one primary reason why the current antioxidant drug-based medical therapies have appeared to fail to effectively combat diseases [235, 236].

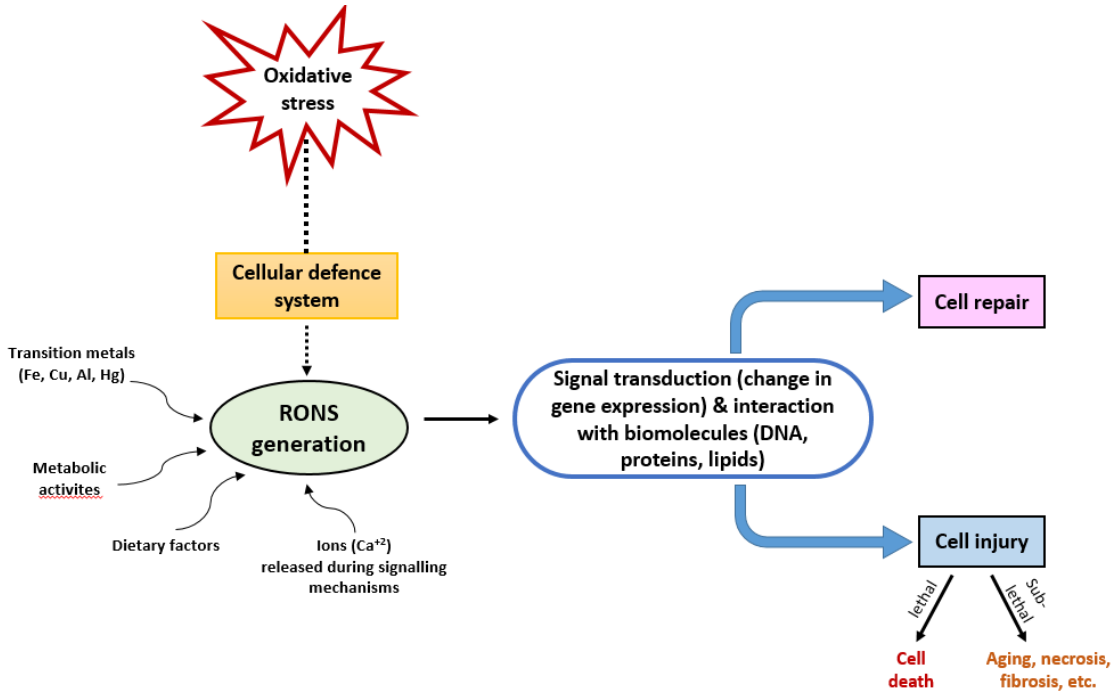


Figure 1.4 Generation of RONS through various means in an organism and the signalling pathways followed thereafter. The fate of cell is decided by signal transduction and interaction of RONS with specific molecules. The cell may survive or die depending on the signalling mechanism followed.

1.1.4 Cells, cellular components and tissue

1.1.4.1 The cell

The term 'cell' was first coined in 1665 by Robert Hooke while observing a cork under microscope (Figure 1.5) [237]. Commonly referred as the "building blocks of life", cells are the fundamental biological unit of life [238]. Originating from the Latin word *cella*, meaning a small room, cells act as a small compartment with cytoplasm, proteins, nucleic acids (section 3.5.3) and other organelles such as mitochondria, nucleus, golgi apparatus and ribosomes enveloped within a membrane [238].

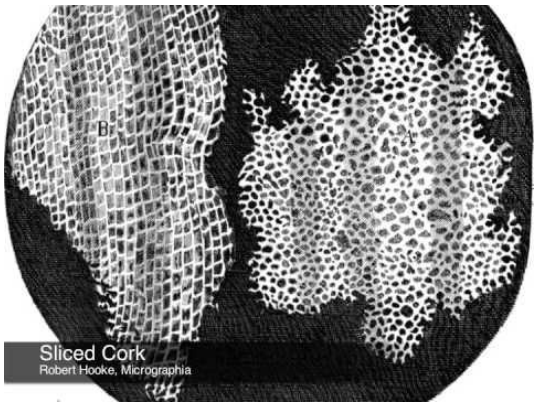


Figure 1.5 Hooke observed a thin slice of cork under microscope. The small compartments separated by thin walls were named cells [237].

The human body is made up of more than 10 trillion (10^{12}) cells ranging from 1-100 µm and performing a myriad of functions. Cells provide a number of important functions such as structure and support to an organism, growth and tissue repair through cell division and metabolism, facilitate interactions with the exterior environment and participate in reproduction [238, 239].

Based on the packaging of their genetic material, cells are classified into prokaryotes (bacteria and archae) and eukaryotes (plant and animal cell) [240]. This classification is based upon the separation of cell's generic material from the cytoplasm, by means of a membrane (forming a distinct organelle, the nucleus). While prokaryotic cells do not have a nucleus and their DNA is not separated from the cytoplasm, eurkaryotic cells have their DNA encapsulated within the nucleus [241]. All cells comprise complex structures containing organelles specialised to specific functions (Figure 1.6).

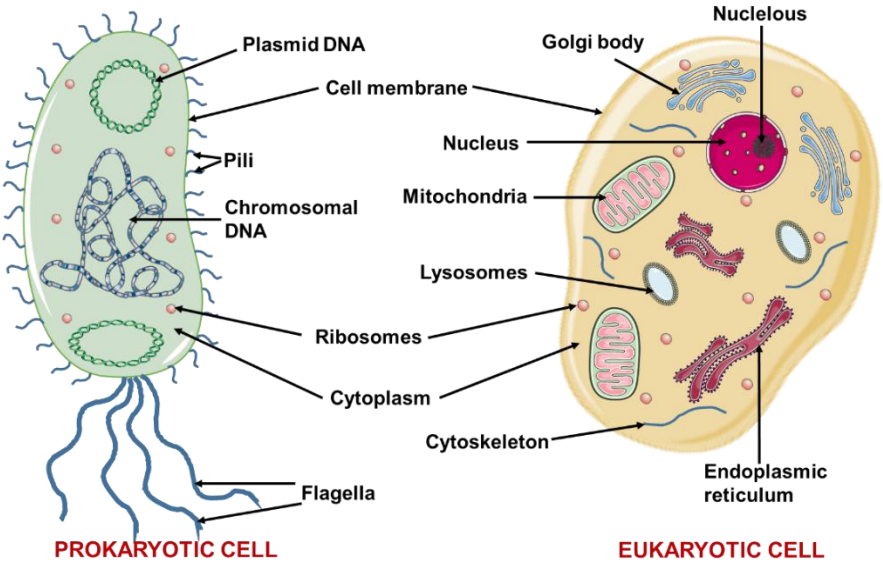


Figure 1.6 An illustration of a prokaryotic and eukaryotic cell [242].

1.1.4.2 The DNA

The genetic and hereditary information in all organisms is encoded within the DNA, which is coiled tightly as chromosomes in the nucleus of the cell [243]. DNA was discovered by the German scientist Frederich Miescher in 1869, who wasn't aware of its significance [244]. There was growing awareness of the potential role DNA played throughout 19th and 20th centuries, but it wasn't until 1953 when the Nobel Prize winners Watson, Crick and Wilkins discovered the double helical structure of DNA that it was fully appreciated how genetic information is fabricated and stored using chemical

bases- Adenine (A), Guanine (G), Tyrosine (T) and Cytosine (C) [243, 244]; shown in Figure 1.7.

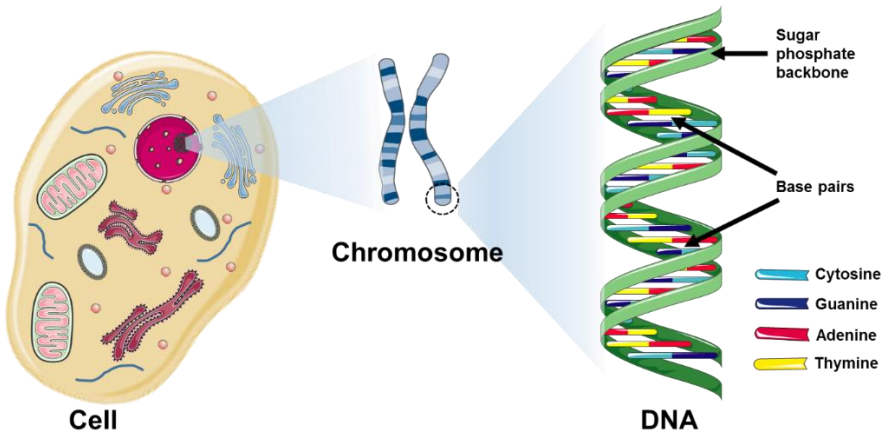


Figure 1.7 A schematic of DNA. The long DNA fits into the small cell in form of a coiled chromosome. The double helical ladder-like DNA structure consists sugar group, phosphate group and bases (collectively referred as nucleotides). The bases are attached to sugar-phosphate backbone and paired to each other via hydrogen bonds. Adenine (A) pairs with Thymine (T) and Guanine (G) pairs with Cytosine (C). This pairing is energetically favoured as the bases are neither too far and nor too close, maintaining a proper helix structure [245].

The sugar phosphate backbone of DNA is called a "strand" where each end is labelled as 5' and 3'. The 5' end has phosphate group attached to the ribose ring and 3' end is usually unmodified hydroxyl group. In double helix, the strands run in opposite directions, which mean if one strand is 5' to 3' , the second strand will be in opposite direction of 3' to 5'. in the process of replication the DNA template is read in a 5' → 3' direction [246]. The chemical bases (or nucleotides) can be arranged in a group of three, where each group is known as a *codon* [247]. Codons combine together in a non-overlapping manner to code for specific amino acids. The arrangement of these bases is specific to a particular amino acid. For example: leucine has a combination of codons AAT, AAC, GAA, GAG GAT, GAC but methionine has only one codon TAC as its DNA base code. The amino acids, thus decoded, assemble together to form proteins [248]. Thus, it can be said that the sequence of nucleotide bases is critical to protein encoding.

Broadly, the DNA in humans and all other organisms is responsible for several different functions including growth and development; cell division and reproduction; protein transcription, translation and modification; disease control; and maintaining a genetic diversity [249, 250].

DNA is also susceptible to damage, due to various endogenous and environmental factors. There are approximately 10^{13} cells in human body and each cell undergoes more than 10,000 DNA damages per day [251]. These DNA damages are in form of lesions, strand breaks, DNA adducts, base pair mismatch, telomerase shortening [252, 253]. To counter the potential threat damage poses, DNA must identify the damage and signal for a repair. This process is known as DNA damage response (DDR) mechanism which includes mismatch repair, base excision repair and nucleotide excision repair [254].

The context of a new medical therapy, it is important to conduct an in-depth analysis of DDR, cellular pathways activated during DDR in response to the therapy and monitor DNA damage, if any. In this thesis, the effects of plasma on DNA *in vitro* are assessed with the following assays:

- Synthetic oligonucleotides (also known as molecular beacons) to monitor DNA strand breaks; and
- H2AX histone phosphorylation at the site of DDR in living cells;

These assays are discussed in details in Chapter 5.

1.1.4.3 The plasma membrane

The plasma (bilayer) membrane is a thin envelope (approximately 5 nm) of proteins and fatty molecules that acts as container for all the cellular matrix and cell organelles. The plasma membrane is very critical to cell survival. It not only separates and protects the components of cell from the outside world but also acts as an "inlet" for the nutrients and "outlet" for the waste products. The membrane also plays vital role in cell expansion and contraction, which controls important cellular functions such as endocytosis, exocytosis, motility and actin-driven edge extension and it determines cell morphology [255, 256]. The membrane contributes to the mechanical properties of the cell allowing the cell to grow, change shape and move. [257-260]. Lipids, proteins and carbohydrates are the principal components of a plasma membrane (Figure 1.8).

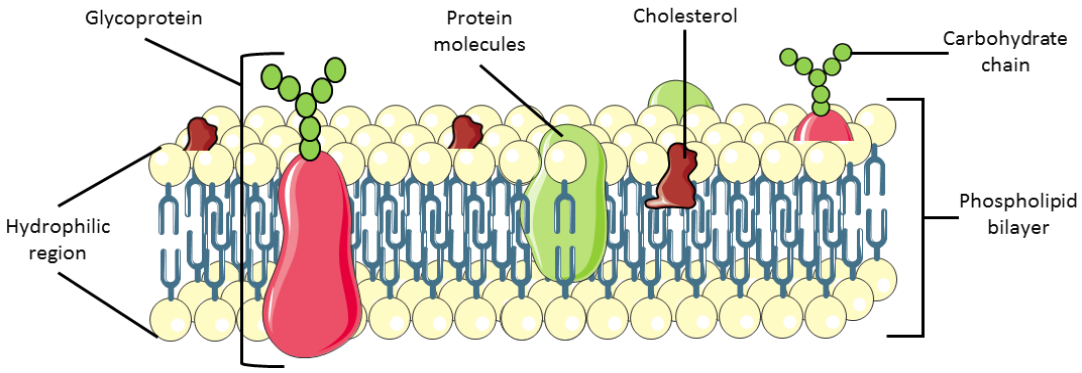


Figure 1.8 A simplified structure of the plasma membrane and its components.

Membrane proteins participate in (amongst other activities) signal transduction, maintaining the cell structure, controlling the chemical and electrical gradients [238]. The presence of membrane proteins including highly selective channels and transporters making the plasma membrane semi-permeable in nature with the ability to send and receive information and contribute to signal transduction (Figure 1.9) [257-260]. Table 1.2 lists a few examples of the classes of membrane proteins and their functions.

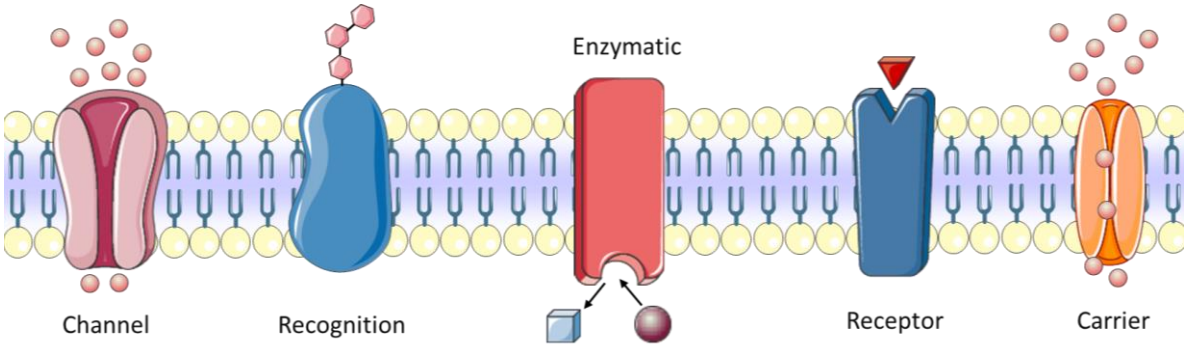


Figure 1.9 An illustration of types of actions performed by proteins embedded in plasma membrane. Channel proteins are small openings which facilitate diffusion of specific molecules through the membrane. Recognition proteins acts as markers whch allow the cells to identify cells as self or foreign body. Enzymatic proteins act as a catalyst to transform a molecule from one form to another and are mainly involved in metabolic acitivity of cell. Receptor proteins have active sites for specific molecules such as hormones, which upon binding to the site trigger signalling cascades in cell. Carrier proteins allow specific molecules to attach to its binding site and transport them across the membrane. [261-264]

Membrane proteins can be classified into *intrinsic* and *extrinsic* proteins [265, 266]. Also referred as integral protein, the intrinsic proteins are either buried deep in the lipid bilayer or have one (or more) region embedded in the bilayer. The intrinsic proteins have their hydrophobic domain lying inside the bilayer, and hydrophilic domains exposed to either the cytoplasm or extracellular fluid. Unlike intrinsic proteins, the extrinsic proteins are located only on the periphery of the plasma membrane (either side of the bilayer membrane) and do not reside in the hydrophobic core of the bilayer) [265,

266]. Extrinsic proteins are loosely anchored to the phospholipids or intrinsic proteins via weak non-covalent interactions (ionic, hydrogen or Van der Waals bonding).

Table 1.2 Examples of membrane proteins and their functions.

Protein	**Function**	**Examples**
Transporter protein	Facilitate movement of ions and molecules across the cell membrane.	Sodium (Na^+) pump [267], serum albumin [268]
Ion channel protein	Transport of ions through the pores in cell membrane.	Potassium (K^+) leak channel, Chlorine (Cl^-) channel [269]
Cytoskeletal protein	maintain the cellular structure and stability, cell division, cellular mobility and cell adhesion	Spectrin, Actin , Tubulin [270-272]
Receptor protein	Transmit signals between cell's external to internal environment.	PDGF receptors (PDGF-R), Epidermal growth factor receptors (EGF-R) [273]
Enzymatic protein	Help in cellular signalling process by converting a substrate from one form to another.	Lactose, pepsin, catalase, adenylyl cyclase [274]

The plasma membrane comprises three major kinds of membrane lipids- *phospholipids, glycolipids* and *cholesterol* [262]. Phospholipids are amphipathic in nature with a hydrophilic head and two hydrophobic hydrocarbon tails. A variety of phospholipids are present in the lipid bilayer; a few listed in Figure 1.10. *Phosphotidylcholine* (PC) is the most common one. The others include *phosphotidylserine* (PS), *phosphotidylethanolamine* (PE), *phosphotidylglycerol* (PG) and, *phosphatidylinositol* (PI) [258, 259, 261, 275-279].

Glycolipids comprise a carbohydrate monosaccharide or polysaccharide unit attached to the lipid moiety by covalent glycosidic bond (Figure 1.11). Glycolipids act as receptors for cell-to-cell interactions. For example, they act as receptor in red blood cells and help in determining the blood group of an individual [258, 259, 261, 275-279].

Cholesterol, also known as sterol, is an exclusive component found only in the eukaryotic plasma membrane. It contains four hydrocarbon rings to form a steroid structure (Figure 1.11). The cholesterol molecules are scattered in the lipid bilayer to

help in maintaining the integrity and fluidity of the cell membrane [258, 259, 261, 275-279].

Since the cell resides in an aqueous environment, the lipid molecules align themselves in a fluid-mosaic structure with the hydrophilic head exposed to the aqueous environment outside and inside the cell and the hydrophobic tails shielded from water (Figure 1.12); i.e. the most energetically favourable configuration [258, 259, 261, 275-279].

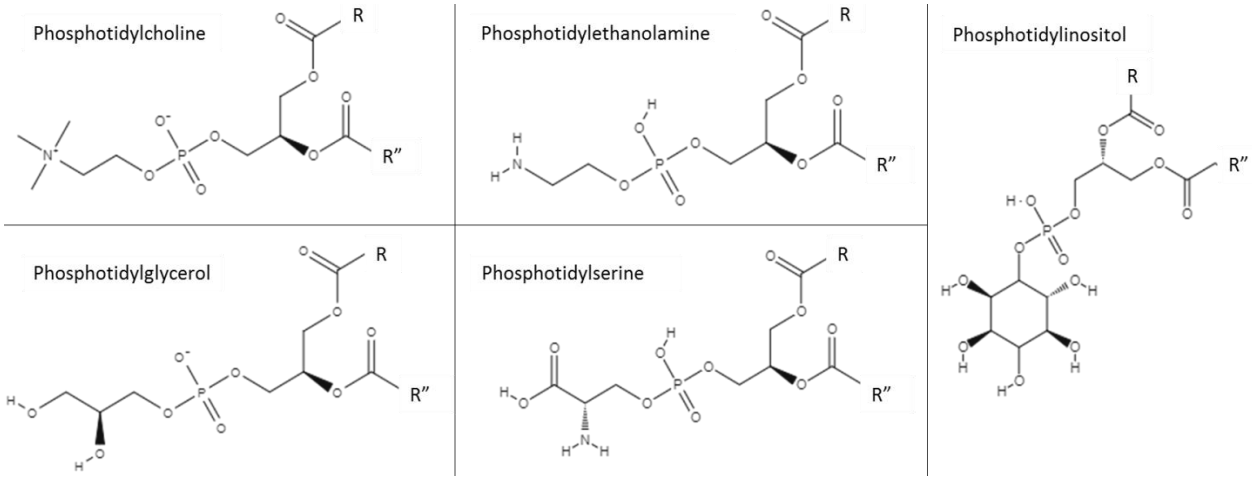


Figure 1.10 Different types of phospholipids and their chemical structures

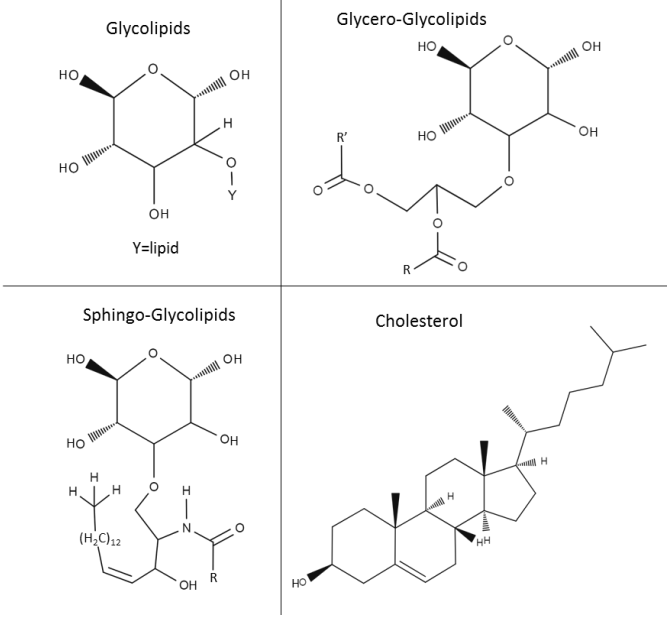


Figure 1.11 Types of glycolipid molecules and the cholesterol molecule.

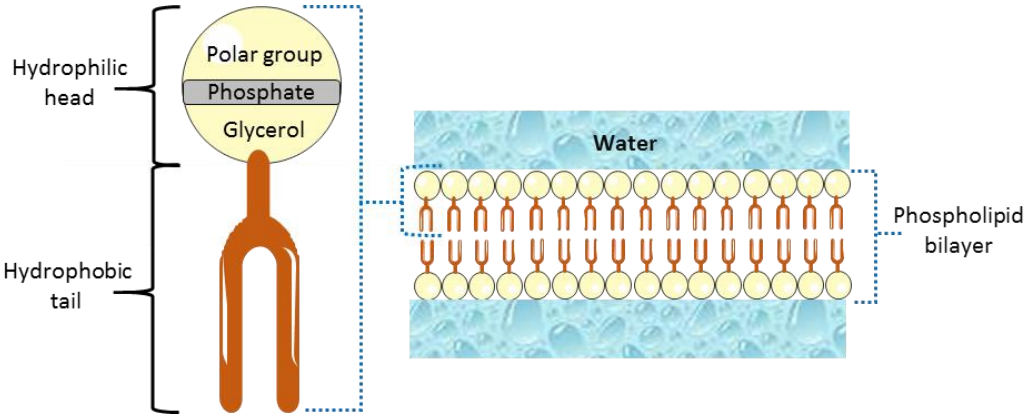


Figure 1.12 The phospholipid molecule with a hydrophilic head and hydrophobic tail (left); and energetically favourable lipid bilayer formation (right).

1.1.4.4 The skin

Skin is the largest organ of the body protecting the underlying internal organs such as muscles and bones from the external environment [280]. Besides acting as a barrier, the skin also plays a key role in regulating body temperature, fighting infection, endowing sensation and skin colour and endocrine functioning [281]. In order to unravel the interactions of plasma with tissues, cells and cell organelles, it is a prerequisite to understand the structure of skin. Skin comprises three layers – epidermis including the stratum corneum, dermis and hypodermis (Figure 1.13) [282].

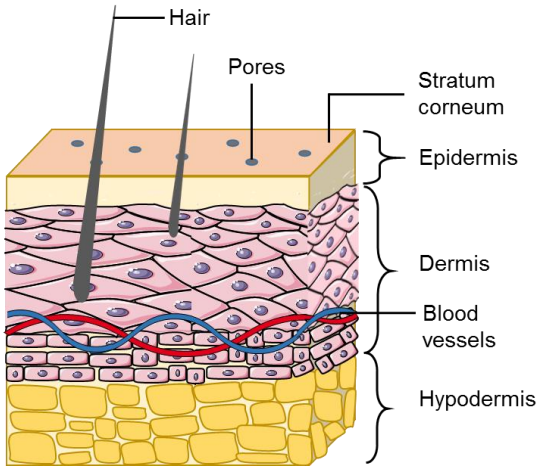


Figure 1.13 A schematic of the structure of human skin

Stratum corneum (thickness: 10-20 µm) is the outermost hydrophobic layer of skin made up of dead cells (corneocytes), which serves as a barrier to for example pathogens and chemicals. The dead cells of stratum corneum also determine the electrical properties of skin [283, 284].

The epidermal layer (thickness: 50-100 µm), just below the stratum corneum, is essentially made up of keratinocytes [284]. Keratinocytes initiate the process of migration of cells from basement membrane, up towards the top of the epidermis and replace dead cells of stratum corneum. Other significant cells in the epidermis are melanocytes and Langerhans cells [283, 285]. Melanocytes are responsible for skin and hair colour pigmentation via the production of melanin [286]. Abnormal levels of melanin can lead to pigmentation disorders such as malignant melanoma [287]. Langerhans cells are known to be the dendritic immune cells which provide protection from infection [288]. The epidermis is uneven and irregular due to presence of hair shafts and sweat gland pores [282].

Below the epidermis is the dermis (thickness: 300-3000 µm) which is rich in collagen and fibroblasts [285]. Extracellular matrix (ECM) proteins such as collagen, elastin and fibronectin contribute to the elasticity of the dermis, which also consists of blood vessels, nerves, sweat glands, hair follicles, mast cells and dermal dendritic cells [289].

The hypodermis also known as the deep subcutaneous tissue includes a layer of fat cells and connective tissues insulating the body from heat and cold. The thickness of the fat layers varies across the body – very thick on buttocks to very thin on eye lids [290].

1.1.5 Potential of plasma to stimulate wound healing

The previous sections outline that oxidative stress can be useful to control various cell signalling processes and is essential for normal processes within the human body. This PhD project focuses on linking plasma with wound healing. In order to assess the role of RONS in wound healing processes such as cell proliferation, epithelialization and angiogenesis, it is essential to first discuss the process of wound healing briefly.

1.1.5.1 Wound healing

The highly complex and well-orchestrated process of wound healing can be divided into four phases, as shown in Figure 1.14 [291, 292]:

1. Coagulation: stop bleeding
2. Inflammation: removal of foreign bodies and organisms (e.g. bacteria)
3. Reepithelization/Proliferation: angiogenesis, epithelisation and wound contraction

4. Remodelling: ECM deposition and maturation, collagen deposition

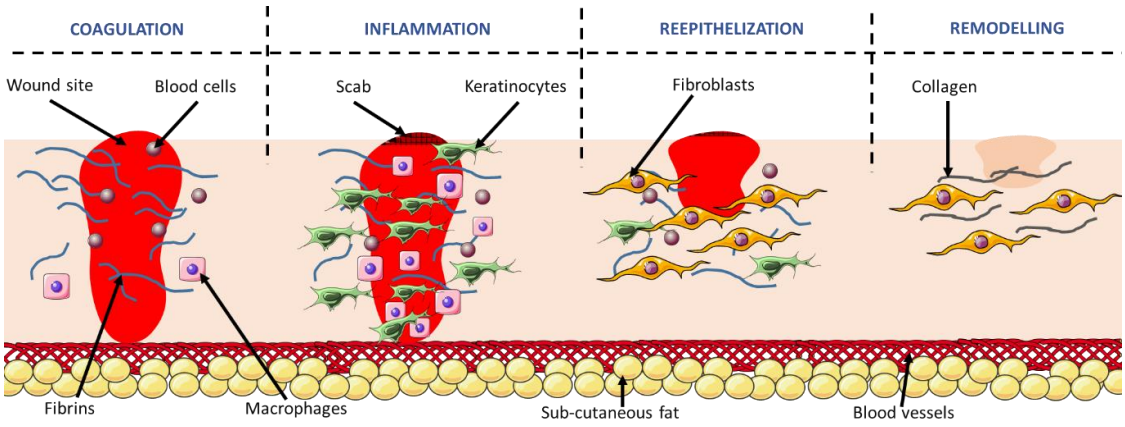


Figure 1.14 Different phases of the wound healing process.

Immediately after an injury, thrombocytes are recruited to the injury site to form a blood clot and stop bleeding [293]. This process is also defined as haemostasis [294]. Different types of growth factors and cytokines are released from thrombocytes which initiate the inflammatory phase. For instance, PDGF and TGF-β are important signalling molecules for recruiting macrophages, neutrophils, fibroblasts and collagen to the wound site [295]. Macrophages in the wound milieu also secrete more signalling molecules such as FGF, PDGF, tumour necrosis factor alpha (TNF-α), and interleukins (IL). During inflammation the neutrophils locate, identify, phagocytize, kill and digest the bacteria and microorganisms and eliminate wound debris [296].

Within a few days of the injury, the process of reepithelization begins [297]. Keratinocytes are the key players in this phase. They migrate to the wound site and undergo proliferation and migration. TGF-β is up-regulated in the reepithelization stage and stimulates the expression of integrins, which, in turn promote adhesion and keratinocyte migration [298]. TGF-β also promotes wound contraction by stimulating the expression of fibroblasts and myofibroblasts [298].

After acute injury, TGFβ1 is rapidly up-regulated and secreted by keratinocytes, platelets, monocytes, macrophages, and fibroblasts.[1] TGFβ1 is essential for initiating inflammation and granulation tissue formation. It also stimulates wound contraction through induction of smooth muscle alpha actin expression in fibroblasts, and induction of myofibroblast differentiation. Further, TGFβ1 is involved in angiogenesis by up-regulating vascular endothelial growth factor.[1] Lastly, TGFβ1 promotes keratinocyte migration during wound closure.TGFβ1 clearly promotes keratinocyte migration by

increasing the expression of different integrins, which, in turn, promotes the adhesion and migration of keratinocytes.

The final stage is remodelling which may continue for up to a year to form scar tissue and new skin [299]. Various signalling molecules such as IL-10, IL-6, monocyte chemoattractant protein (MCP-1), macrophage inflammatory protein 1 alpha (MIP-1α), IL-1β, monocyte chemoattractant protein 1 (MCP-1), and macrophage inflammatory protein 1 alpha (MIP-1α); and growth factors including FGF, PDGF, VEGF, TGF-β and epidermal growth factor (EGF) are released from macrophages, fibroblasts, keratinocytes, thrombocytes and endothelial cells [86, 300, 301]. Collectively, these signalling molecules and growth factors govern remodelling of connective tissues and recruitment of blood vessels.

1.1.5.2 Chronic wounds

The process of wound repair can be impaired by a number of factors. The healing impairment may arise due to intrinsic factors such as neuropathy (motor, sensory, autonomic fibres affected), vascular problems (reduction in capillary size and thickening of basal membrane) and systemic effects and/or extrinsic factors such as bacterial infection, callus formation and external pressure to the site [302]. When wound healing does not progress normally in an orderly fashion, it leads to the condition of 'chronic wounds'. A chronic wound can be defined as a wound that does not heal within 4 to 6 weeks [303, 304].

As shown in Figure 1.15, a chronic wounds can be characterised by – (i) prolonged inflammation with excessive levels of macrophages and MMP which contribute to bacterial invasion and degradation of extracellular matrix [305, 306]; (ii) epidermis undergoing hyper-proliferation and turning into a necrotic ulcer [307]; (iii) poor angiogenesis and vascularisation due to hypoxia caused by fibrin cuffs developed on blood vessels [308]; and (iv) reduced migration capacity in prematurely senesced fibroblasts [309]. The aberrations in normal wound healing process have been linked to an imbalance in levels of growth factors and cytokines [310]. Table 1.3 briefly enlists changes in levels of growth factors and its consequence on wound healing.

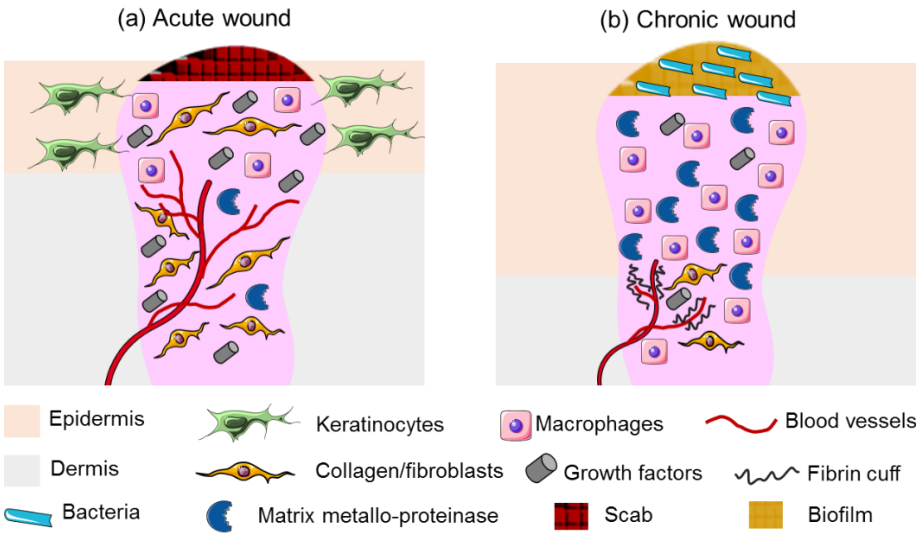


Figure 1.15 Differences between (a) acute and (b) chronic wound healing. Acute wound healing initiates with scab formation and a temporary inflammatory response. The growth factors and cytokines released by immune cells stimulate angiogenesis, migration of fibroblasts and collagen deposition. This helps in just sufficient reepithelization and eventually tissue remodelling. Chronic wounds exhibit bacterial invasion and prolonged inflammation (hyper-inflammation). Due to an imbalance in growth factors, the epidermal layer undergoes hyper-proliferation, fibroblasts become senescent and levels of matrix metalloproteinases increases. Angiogenesis is also impaired due to hypoxic state induced by fibrin cuffs on the blood vessels. [311]

Table 1.3 Changes in the expression of growth factors in chronic wound and their subsequent effects. [86, 312, 313]

Growth factor	Levels in chronic wounds	Effect
EGF	Decreased	Aberrant epithelization; poor angiogenesis
PDGF	Decreased	Diminished keratinocyte, fibroblast and collagen migration resulting in abnormal reepithelization and remodelling
VEGF	Decreased	Poor angiogenesis and tissue granulation
FGF	Decreased	Reduced TGF and VEGF levels, which eventually impair granulation and reepithelization
TGF-β	Decreased	Problems in scar formation, matrix deposition and tissue remodelling; inability to recruit inflammatory cells

TNF-α	Increased	Increase in MMP production resulting in prolonged inflammation that impairs cell migration and reepithelization.
IL-1, IL-6	Increased	Same effect as TNF-α

Most common chronic wounds, but not limited to the following, are – venous ulcers, diabetic ulcers and pressure ulcers [311]. Venous ulcers are common in lower extremities of body (such as legs), when fibril cuffs deposit on blood vessels and deteriorate the blood circulation [314]. Venous ulcers may also occur due to slow migration of leukocytes, resulting in blockage of blood capillaries. Impaired angiogenesis and vascular systems can also lead to ulcers in diabetic patients, especially in feet and are termed as diabetic foot ulcers [315]. Pressure ulcers are common in sacrum, shoulder blades and heels. These ulcers arise due to prolonged pressure-induced ischemia [316]. Treatment for chronic wounds varies based on the type of ulcer. For instance, while diabetic foot ulcer treatment focuses on bacterial disinfection and "offloading", venous leg ulcer are treated using compression bandaging [315, 317]. The current status of wound treatments are discussed in details in section 1.5.3.

1.1.5.3 Linking RONS with wound healing

Chronic hypoxia and ischemia are known to be the cause of most chronic wounds (diabetic, venous and pressure ulcers). *In vitro* and *in vivo* studies indicate that in the state of chronic hypoxia there is a decrease in fibroblasts proliferation rate, collagen deposition, keratinocyte migration [318-321]. Molecular oxygen (O_2), therefore, is an essential element in wound healing for its role in cell metabolism and redox signalling [322, 323]. A review by Tandara *et al.* states in detail the importance of O_2 in wound healing at sub-cellular, cellular and supra-cellular levels [323]; briefly discussed in Table 1.4.

Table 1.4 Effect of O_2 in wound healing [323].

	Examples
Sub-cellular level	• Mitochondria require O_2 to produce energy for oxidative phosphorylation. • Respiratory burst in inflammatory cells, to prevent infection, requires O_2.

	• Upon interaction with proline, O_2 forms hydroxyl-proline (HP). Without HP, the pro-collagen molecules cannot form stable triple helices; thus unable to synthesise collagen.
Cellular level	• Proliferation activity of fibroblasts decreases in hypoxic state. • During hypoxia, dermal fibroblasts cannot produce collagen. • Anti-microbial activity of leucocytes depends on the high amount of oxidants produced from oxygen.
Supra-cellular level	Poor blood flow in capillaries and oxygen consumption by metabolically active and proliferative cells can lead to decrease in oxygen tension in wounds. This delays the process of wound healing, and leads to wound infection and poor wound tensile strength.

The beneficial role of O_2 is attributed to the oxidants derived from reduction of O_2. These oxidants (ROS) react with other biomolecules to form more ROS, RNS and reactive sulphide species (RSS) as shown in Figure 1.16. ROS ($O_2^{-\bullet}$) can be produced through the ETC in mitochondria via electron reduction and/or through enzymatic catalysis by nicotinamide adenine dinucleotide phosphate oxidase (NOX) or xanthine oxidase (XO) present in cell membrane. In the presence of superoxide dismutase (SOD) isoforms, $O_2^{-\bullet}$ undergoes dismutation to form H_2O_2. Exogenously generated H_2O_2 (via NOX and XO) can enter through aquaporins in cell membrane and reacts with biomolecules and other RONS inside the cell. For instance, H_2O_2 undergoes Haber-Weiss reaction with $O_2^{-\bullet}$ or Fenton reaction in presence of metal ions Fe^{+2} to form highly reactive oxidant $\bullet OH$. H_2O_2 can also react with myeloperoxidase (MPO) present in phagocytic cells to form highly reactive HOCl.

RNS including NO are generated mainly through conversion of L-arginine to L-citrulline, catalysed by NOS enzyme isoforms- inducible NOS (iNOS) and endothelial NOS (eNOS). Both iNOS and eNOS are expressed in macrophages, endothelial cells, fibroblasts and keratinocytes. A rapid reaction between NO and $O_2^{-\bullet}$ leads to formation of highly reactive $ONOO^-$.

Proteins (amino acids) are a significant component of cells, and may undergo reactions with RONS including H_2O_2, NO, $ONOO^-$, $\bullet OH$, and HOCl. The interactions between the thiol-groups of amino acids and RONS result in production of RSS such as S-nitrosothiols (RSNO), hydrogen sulphide (H_2S), hydropersulfide (RSSH), etc.

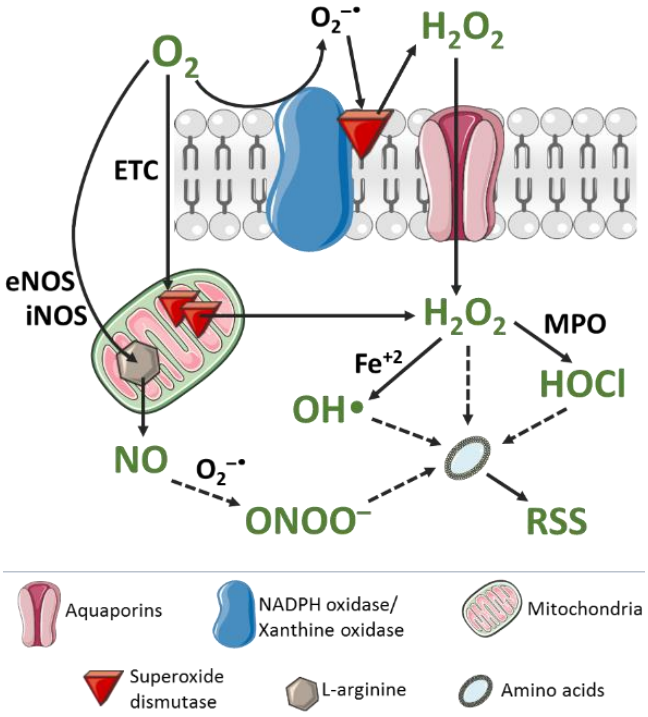


Figure 1.16 Common pathways of ROS, RNS and RSS generation in cells.

Reactive species generated in cells govern major signalling pathways in wound healing. A comprehensive review of redox signalling and gene expression is outside the scope of this thesis, and can be found in [297, 324-335]. Briefly the role of only major RONS, focussing on ROS and RNS, in each wound healing phase is discussed below.

Redox signalling modulates wound healing process from the initial phase. An increase in ROS production at the wound site is observed during the haemostasis/coagulation stage [336]. Coagulation is initiated by production of thrombin by active tissue factor (TF). Thrombin also leads to generation of ROS (H_2O_2) in vascular cells via NOX enzymes and increase in TF expression [328]. To maintain haemostasis in injured tissue, platelet aggregation and activation is also important. Activated platelets can produce ROS and participate in upregulation of TF expression in vascular cells [337]. Collagen-induced platelet aggregation also depends on NOX-mediated ROS generation [338]. Upon activation, platelets also release PDGF which is important for cell proliferation and its expression is dependent on H_2O_2 [339]. PDGF also participates in production of $O_2^{-\bullet}$, which in turn modulates the signalling of NF-ĸB and MCP-1 in smooth muscle cells [340]. Excessive platelet aggregation causing poor vasodilation is prevented by NO generated by both platelets and other non-phagocytic cells [341].

It is well established that during inflammation, RONS are released by inflammatory cells (leucocytes and macrophages), arming these cells to eliminate bacteria and decontaminate the wound site [187, 188, 322, 325, 342-344]. The NOX-mediated respiratory burst generates a large amount of H_2O_2. This oxidative stress leads to DNA damage and lipid-peroxidation in the phagocytised bacteria. Besides directly killing microbes, H_2O_2 also acts as a secondary messenger for inducing PDGF, TGF-β, TNF-α and IL-6 that facilitates recruitment and adhesion of macrophages and neutrophils to the wound site [343]. NO released by macrophages and its derivatives such as $ONOO^-$also have deleterious effects on microbes [345]. NO-producing enzymes iNOS and eNOS are also expressed in macrophages and neutrophils, highlighting the role of NO in inflammatory phase of wound healing [342, 345]. NO also acts as a chemoattractant for IL-1 and TGF-β, monocytes and neutrophils in keratinocytes [344]. RONS can also facilitate an anti-inflammatory and pro-inflammatory signalling loop to promote acute healing and prevent chronic (non-transient) inflammation [322, 327, 342].

In the reepithelization process, H_2O_2 activates MMP and EGF expression in keratinocytes [322, 346, 347]. MMP degrade extracellular matrix to help migration of epidermal cells and EGF promotes keratinocytes proliferation. Keratinocyte proliferation also depends on iNOS expression, indicating the role of NO in wound reepithelization. NO and H_2O_2 also enhance in VEGF and FGF expression in wound cells that promotes angiogenesis and endothelial cell migration and adhesion [348, 349]. ROS enhances PDGF and TGF-α expression in fibroblasts that promotes granulation in the tissue and wound contraction [340, 350]. H_2O_2 and NO are both relevant for collagen (I, II, III) deposition and cross-linking to acquire tensile strength in the remodelled wound [351, 352].

1.1.5.4 Advances in wound management techniques

Wound healing practices were first recorded in a Mesopotamian clay tablet, written around 2200 BC [353]. Since then wound healing practices have undergone an exciting, though often punctuated long journey from Edwin Smith Papyrus (1650 BC), Sushruta (600 BC) and Hippocrates (460-377 BC) [354]. Since Hippocrates (almost 2000 years!), there had been a slow evolution in wound healing, until late in the 19^{th} century with the advancement in disinfection and covering (bandaging) the wounds [355]. One of the major advancement occurred when Joseph Lister contributed to the idea of "antiseptic" healing techniques by demonstrating the use of carbolic acid in

dressings to disinfect the wounds. [356]. Later, William Halsted introduced the use of silver foil as an antiseptic in wound dressings [357]. Thereafter, the practice of debridement and wound cleaning became common.

The 19th century also witnessed impactful advancements to improve the knowledge about wound biology. In 1908, Elie Metchnikoff introduced the concept of 'phagocytosis' in inflammation and wound debridement [358]. In 1962, Winter and Scales demonstrated that in pigs, the moist wounds heal faster than the dry wounds, contrary to the original belief [359]. These results were later (in 1963) confirmed in human subjects by Hinman and Maibach [360]. Following these findings, the focus of wound healing techniques evolved from the outdated "dry dressings" to "moist dressings" [361].

Since the beginning of 20th century, enhanced knowledge about wound biology and improved technology have led to emergence of a variety of wound care techniques such as biological dressings, off-loading, debridement, skin grafts (or substitutes), growth factor-delivery systems, compression therapy, negative pressure wound devices, enzymatic debridement, topical drugs, and oxygen and nitrogen gas therapy.

Dressings and the topical application of drugs is the most popular method of wound treatment. Drug loaded wound dressings made of various biomaterials such as polyurethane, alginates, hydrocolloids, and hydrogels are utilised to deliver antimicrobial agents (such as iodine, silver, H_2O_2) and growth factors (such as FGF, PDGF and EGF) to the wound bed [362]. Dressings are more favourable than ointments as they can protect the wound site from further trauma by providing moisture and absorb excess wound exudate. Major limitations of topical drugs and dressings include drug-resistance developed in bacteria, frequent re-application of ointment or dressing for many days, exudate absorption in the dressing and skin stripping upon removal of dressings. Topical treatments and standard dressings cannot replace the techniques essential for off-loading, debridement, and prevention of ischemia.

Debridement involves removal of non-proliferating tissue (debris) and biofilms from tissue to terminate chronic inflammation and initiate proliferation phase. This can be carried out using different methods such as proteolytic enzyme-based debridement, sharp debridement using surgical tools, ultrasonic debridement, high pressure water based debridement, and bio-debridement using maggots [362, 363]. Although

debridement is very effective and arguably an essential step for wound healing, frequent and too extensive debridement practise can impair (or delay) the wound healing process. Surgical complications such as excessive bleeding and removal of healthy tissue can also pose danger. Hydro-debridement uses a high pressure streams of water which may push the bacteria further inside the wound and also lead to water-borne contamination. The process is not only costly but also painful for the patients [363].

Negative pressure wound therapy (NWPT) is conducted using a portable vacuum device to create a negative pressure or sub-atomic pressure (100-125 mm Hg) inside the wound [363]. The pump attached to the device then draws out all the exudates and other infectious materials present in the fluid. Before starting the vacuum suction, the wound bed is filled with several layers of small pieces of dressings (gauze or foam). The movement of skin and wound fluid can sometimes push the pieces of dressings deep into the wound bed. These pieces can be easily missed by clinicians while removing the dressing, which can lead to further complications [364]. Other limitations of NWPT include noisy device which may interrupt patient's sleep and social engagement, changes in negative pressure setting depending on wound state (for dry wound negative pressure need to be reduced while for wet wound the pressure need to be increased), skin stripping upon removal of dressing, inability to debride and disinfect wounds, and pressure lesions developed due to improper positioning of the pump tubing [365, 366].

Growth factors-based therapies aim to deliver exogenous cytokine and growth factors to the wound site and accelerate wound healing process [362]. Growth factor-loaded dressings, gel-based creams and direct injection to the wound site are popular methods, but new methods utilising gene therapy (for example, viral vectors loaded with growth factor gene) are evolving [367]. Growth factors in a normal wound healing process have a pleiotropic nature. Different types of growth factors play key roles in different stages of wound healing and interact with different types of cells. This multitude of biological signalling in wound healing is difficult to achieve with delivery of a single growth factor, considering chronic wounds have a compromised wound milieu deficit in several types of growth factors and cells. These therapies have the lack of patient-specific protocols, heterogeneity in wounds, and inconsistent and unpromising outcomes, which has resulted in limited number of global trials [367].

The role of oxygen in promoting revascularization, collagen deposition and bacterial killing has been discussed in previous sections [368]. These potential benefits of oxygen are harnessed in the hyperbaric oxygen therapy (HBOT) to promote tissue oxygenation and as a potential wound therapy [20]. In the HBOT procedure, patients are placed in a sealed chamber with 100% oxygen at increased atmospheric pressure. The procedure is not localised and does not target specifically the wound site, which may lead to potential risks including sinus damage, middle ear rupture due to fluid build-up at high pressure, lung damage due to barotrauma, seizures, temporary myopia, and claustrophobia. Besides oxygen, NO gas therapy is also used for wounds as anti-microbial agent as well as for healing [193]. Similar to HBOT, the NO gas therapy also requires a special chamber equipped with gas tanks, pressure regulators, heaters and humidifiers which can be cumbersome and costly, and has similar risks as HBOT [193]. Extra caution is required to prevent oxygen from interacting with NO and form NO_2 which may be toxic for cells.

The antioxidant dietary supplements of Vitamin A, Vitamin E, Vitamin C, selenium and β-carotene had been successfully marketed as potential wound healing treatment measures [189, 230, 369]. However the efficacy of antioxidants to heal wounds still remains unclear. While some studies claim that antioxidants when topically applied to wounds can speed up the wound process and improve appearance of scars, other studies show either no effect or a negative impact on wound healing. For example, vitamin E did not have any cosmetic benefit on scar appearance and also increased chances of dermatitis in a clinical trial [370]. Ibuprofen is a common anti-inflammatory drug which also enhances the concentration of antioxidants but seems to inhibit proliferation, fibroblast formation, angiogenesis and epithelization [371, 372]. Ascorbate and β-carotene may act as pro-oxidants instead of antioxidants and enhance RONS formation, eventually increasing the chances of DNA damage and lipid peroxidation [373]. The application of uric acid antioxidant actually increased the wound severity and worsened the condition of chronic wounds by promoting inflammation [374]. These studies reflect the strange paradox associated with antioxidants based healing mechanisms where anti-oxidants may act as pro-oxidants and/or impede the functions of RONS to perform signal transduction and generation of intracellular RONS crucial for wound healing [373].

Oxidant-rich pharmaceutical formulations are emerging as therapies to speed up the process of wound repair and effectively disinfect the wound. For example creams composed of H_2O_2 enhance the cutaneous blood recruitment in ischemic ulcers in guinea pigs [375]; allopurinol (which produces O_2^- upon interactions with xanthine oxidase) increased the tensile strength of healing tissue [299, 375, 376], and acidified nitrite creams (produce NO via reaction between nitrite and ascorbic acid) enhance wound closure time in diabetic mice [377, 378] with no adverse effects. A few studies have also highlighted the limited efficacy of oxidants as wound therapy. For instance, no difference in control and H_2O_2 treated groups were observed in appendectomy wound healing rate [379] or wounds infected with *Staphylococcus aureus* [380].

Skin grafts or human skin equivalents are also used to augment tissue remodelling in case of severe skin loss. Acellular (synthetic) and human (donor) skin subsitutes are now clinically in use. Examples include Dermagraft® (a human fibroblast-derived dermal substitute) [381], Apligraf ® (neonatal keratinocytes and fibroblasts on bovine collagen) [382], TheraSkin® (a human skin allograft) [383], TransCyte® (porcine collagen and newborn human fibroblasts on silicone membrane) [384], and MySkin® (autologous keratinocytes on plasma co-polymer dressing) [385, 386] Skin grafting can undergo complications such as predisposed infection in chronic wounds, haematoma due to inappropriate pressure or excessive patient movements, mismatch in overall skin topography, skin discolouration, which may require further cosmetic interventions [387], and high skin graft failure rate in obese and diabetic patients [388].

Despite of so many emerging techniques, wound healing still remains a socio-economic challenge globally (discussed in section 1.5.3). Limited efficacy of the current wound therapies is credited to the complex wound healing mechanisms (still not fully understood), incorrect wound diagnosis, diverse wound aetiologies in patients, unspecific treatment protocols and dosages, limitations in chronic wound models, and multi-factorial limited (and ambiguous) clinical trials.

1.1.5.5 Economic and humanistic burden of chronic wounds in Australia

In order to appreciate the need for innovative wound healing technologies, it is essential to understand the growing burden of chronic wounds in Australia. Chronic wounds pose a threat to Australia (and globally) by causing (i) patient suffering, constant pain, and

reduced mobility, and complications such as infection and amputation (which may eventually result in death); (ii) mental distress (depression and anxiety) in patients arising from social isolation, fear of body shaming and poor lifestyle and (iii) an economic burden placed on individuals as well as on the whole healthcare system.

As per the July 2017 report by Australian Centre for Health Services Innovation, almost half a million people in Australia suffer from chronic wounds [389]. Chronic wounds drain $3 billion annually from the Australian health care system which is 2-3% of the total health expenditure [389, 390]. There is also a financial burden at individual level. For instance, old patients (60 years and above) spend $27.5 million annually from their pockets on expenses including cost for doctor's visit, expensive products and therapies such as dressings, compression therapy, pharmacological therapy, surgical intervention, home nursing services, etc. [389, 391]. Other factors contributing to the expense include the aetiology (i.e. longevity) of wounds wherein approximately 83% of chronic wounds take 24 weeks of treatment [392].

Non-healing wounds are a serious problem in the older and diabetic population. As per the reports, diabetic patients are at a 15-25% lifetime risk of developing foot ulcers [302, 393] and 90% of patients suffering from leg ulcers are above 60 years old [394-397].

The problem of chronic wounds is not restricted to Australia and affects the people and healthcare system globally. The magnitude of the problem can be estimated from the fact that an amputation occurs every 30 s in a part of the planet due to diabetic ulcer [398]. Approximately 1.5-2 million people in Europe and around 6.5 million people in USA are living with chronic wounds [399, 400].

These appalling statistics mentioned above act as a catalyst to identify chronic wounds as a priority in healthcare systems of several countries and invest in new approaches which are needed to circumvent the problem of chronic wound healing.

1.1.5.6 Plasma for wound healing

Plasma is emerging as a promising tool for wound healing. A plasma-based wound therapy has following advantages [57, 93, 122, 291, 401-404]:

- Plasma treatment is localised and minimally-invasive.

- Plasma treatment can be tailored to be localised (e.g. toe) wound or to cover larger areas (e.g. leg).
- It has the potential to improve the wound healing.
- Plasma has anti-microbial properties against multi-pathogenic infection and biofilms.
- Many plasma devices do not need to be in contact with the wound, thus preventing the inadvertent spread of infection.
- It is easier to install and use than other therapies such as viral vectors for growth factors delivery, NPWT and HBOT.
- Randomized trials with patients reported plasma treatment as a painless procedure.

A range of *in vivo* and *in vitro* experiments have demonstrated the potential beneficial effects of plasma in wound decontamination and healing including the elimination of wound pathogens [142, 158, 405-410], stimulation of skin cell proliferation [62, 88, 291, 410-412] and migration [62, 291, 412, 413], improve angiogenesis by increasing oxygen tension in tissue [93, 122, 414] and enhancement in the synthesis of growth factors such as IL-6, IL-8, MCP-1, TGF-β, FGF [415-418].

The recent boost in plasma medicine research which has given rise to a number of plasma medical devices such as kINPen Med (INP Greifswald, Germany), PlasmaDerm® (CINOGY, Germany), Maxium® (KLS Martin, Germany), and MicroPlaSter (ADTEC Plasma Technology Co., Japan). Randomized clinical trials from these devices have demonstrated positive outcomes. A phase II study with MicroPlaSter on 38 chronic wounds in 36 patients (average age of 70.8 years) successfully reduced the bacterial load in wounds without any noted side-effects [57]. The antibacterial efficacy of kINPen Med was examined in clinical trial with 26 patients. The results indicate that kINPen Med (in combination with other antiseptics) was highly efficacious against bacteria [419]. In another study, the kINPen Med and an antiseptic Octenisept were compared. Known to be the most effective antiseptic, Octenisept showed a comparable reduction in bacterial load to the kINPen [420], but with a significantly

lower level of wound reduction (closure). The antiseptic group showed just 19% of wound reduction and whilst plasma group showed a 56% reduction [421].

While the ‘cocktail’ nature of plasma is a strength and a motivation for plasma medicine development, it also poses some challenges. The major challenge is defining how each component in plasma (UV photons, ions, electric field, RONS, heat, etc.) interacts with the biological system (tissue). Due to the complexities of the plasma environment and biological environment it is difficult to unravel the exact mechanisms of action of plasma. Questions can be divided broadly into “physical questions” about plasma delivery, for example, (i) which component of plasma are delivered into the target? (ii) what are the concentrations of the species delivered? (iii) how deep into the tissue are these delivered, and questions around the subsequently triggered “biological responses”, for example, (i) how does these concentrations affect the biological response? (ii) how much does each component actually contribute to the biological response? These questions must be addressed to understand the importance of each component on wound healing and formulate ‘safe’ plasma doses to fully realise the potential of plasma as a medical device.

1.2 Summary

The aforesaid sections describe in details the physical and biological properties of plasma. In terms of the physics, the different types of cold plasma designs and key constituents of plasma were discussed. This was followed by a discussion of the plasma biochemistry including discussion of the known roles of RONS in cellular functioning and thus the potential of plasma delivered RONS in wound healing. This review serves as a motivation and optimism to pursue this study further.

This PhD project is an attempt to unravel the mechanisms involved in plasma generation of RONS in various physiological environments: tissue fluid, deep within tissues, in cells and cellular components such as DNA.

The motivation for this study is to show that plasma-delivered RONS can linked to the stimulation of the processes involved in wound healing. To establish the basis for such a hypothesis the following objectives were assessed:

1. *The development of protocols to accurately assess the plasma delivery of RONS into the wound environment.*

This was achieved by exploring various RONS detection techniques including small molecular probes (Chapter 2), amperometric sensors (Chapter 2), UV-Visible spectroscopy (Chapter 3), and mass spectroscopy (Chapter 3). The plasma jet used in this study was diagnosed using voltage probe, current monitor and optical emission spectroscopy wherever needed.

2. *The investigation of plasma-induced effects in tissues cells and cellular components.*

   The effects of plasma delivered RONS were assessed using synthetic models for tissue fluid, tissue, cells, and DNA. Phospholipid vesicles were employed as synthetic cell models to monitor cell membrane damage (Chapter 4). Similarly, synthetic oligonucleotides (molecular beacons) were utilised as a quick and versatile assay for DNA strand breaks (Chapter 4). To monitor the plasma delivery of RONS deep within the tissues, hydrogel films of various thicknesses made from gelatin and agarose were used (Chapter 3 and 4). Tissue cell culture studies were conducted using two different types of skin cells-keratinocytes and fibroblasts. Cell proliferation and viability in response to plasma exposure was studied (Chapter 5). Furthermore, DNA damage within skin cells was examined using the gamma-H2AX (γ-H2AX) assay (Chapter 4). A patented concept of "plasma screen" was also utilised to regulate the delivery of ROS in tissue environment (Chapter 4) and limit the damaging effects of plasma.

The experimental methodologies and protocols devised in this project can be adopted by other researchers. The results and conclusions drawn from the studies strengthen our knowledge about the plasma-tissue interactions and can help in future development of plasma devices for wound healing and other biomedical applications.

1.3 References

1. Hanlon, P., et al., *Trial of an attenuated bovine rotavirus vaccine (RIT 4237) in Gambian infants.* The Lancet, 1987. **329**(8546): p. 1342-1345.
2. Fine, P.E. and I.A. Carneiro, *Transmissibility and persistence of oral polio vaccine viruses: implications for the global poliomyelitis eradication initiative.* American Journal of Epidemiology, 1999. **150**(10): p. 1001-1021.
3. John, T.J., *Antibody response of infants in tropics to five doses of oral polio vaccine.* BMJ, 1976. **1**(6013): p. 812-812.
4. Fenner, F., et al., *Smallpox and its eradication.* Geneva: WHO, 1987.

5. Brochier, B., et al., *Large-scale eradication of rabies using recombinant vaccinia-rabies vaccine.* Nature, 1991. **354**(6354): p. 520-522.
6. Nathan, D.M., et al., *Intensive diabetes treatment and cardiovascular disease in patients with type 1 diabetes.* The New England journal of medicine, 2005. **353**(25): p. 2643.
7. Rother, K.I., *Diabetes treatment—bridging the divide.* The New England Journal of Medicine, 2007. **356**(15): p. 1499-501.
8. Gillies, C.L., et al., *Pharmacological and lifestyle interventions to prevent or delay type 2 diabetes in people with impaired glucose tolerance: systematic review and meta-analysis.* BMJ (Clinical research ed.), 2007. **334**(7588): p. 299.
9. Soriano, V., et al., *Hepatitis C cure with antiviral therapy–benefits beyond the liver.* Antiviral therapy, 2015. **21**(1): p. 1-8.
10. Kao, J.-H. and D.-S. Chen, *Global control of hepatitis B virus infection.* The Lancet Infectious Diseases, 2002. **2**(7): p. 395-403.
11. Lönnroth, K., et al., *Tuberculosis control and elimination 2010–50: cure, care, and social development.* The Lancet. **375**(9728): p. 1814-1829.
12. Kuderer, N.M., et al., *A meta-analysis and systematic review of the efficacy and safety of anticoagulants as cancer treatment.* Cancer, 2007. **110**(5): p. 1149-1161.
13. Noordijk, E.M., et al., *Radiotherapy as an alternative to surgery in elderly patients with resectable lung cancer.* Radiotherapy and Oncology, 1988. **13**(2): p. 83-89.
14. Frei Iii, E. and G.P. Canellos, *Dose: A critical factor in cancer chemotherapy.* The American Journal of Medicine, 1980. **69**(4): p. 585-594.
15. Kiselyov, A., et al., *Recent Progress in Discovery and Development of Antimitotic Agents.* Anti-Cancer Agents in Medicinal Chemistry- Anti-Cancer Agents), 2007. **7**(2): p. 189-208.
16. Glimelius, B., et al., *Chemotherapy improves survival and quality of life in advanced pancreatic and biliary cancer.* Annals of Oncology, 1996. **7**(6): p. 593-600.
17. Mullard, A., *2011 FDA drug approvals.* Nature reviews. Drug discovery, 2012. **11**(2): p. 91-94.
18. Atkins, J.H. and L.J. Gershell, *Selective anticancer drugs.* Nature Reviews. Drug Discovery, 2002. **1**(7): p. 491-492.
19. Garattini, S. and V. Bertele, *Efficacy, safety, and cost of new anticancer drugs.* BMJ : British Medical Journal, 2002. **325**(7358): p. 269-271.
20. Kranke, P., et al., *Hyperbaric oxygen therapy for chronic wounds.* The Cochrane database of systematic reviews, 2004(2): p. Cd004123.
21. Ubbink, D., et al., *A systematic review of topical negative pressure therapy for acute and chronic wounds.* British Journal of Surgery, 2008. **95**(6): p. 685-692.
22. Lipsky, B.A. and C. Hoey, *Topical antimicrobial therapy for treating chronic wounds.* Clinical infectious diseases, 2009. **49**(10): p. 1541-1549.
23. Sonnenberg, A. and W.F. Townsend, *Costs of duodenal ulcer therapy with antibiotics.* Archives of Internal medicine, 1995. **155**(9): p. 922-928.
24. Sun, D.C.H. and H. Shay, *Optimal effective dose of anticholinergic drug in peptic ulcer therapy.* AMA archives of internal medicine, 1956. **97**(4): p. 442-452.
25. Tiwari, G., et al., *Drug delivery systems: An updated review.* International Journal of Pharmaceutical Investigation, 2012. **2**(1): p. 2-11.

26. Prausnitz, M.R. and R. Langer, *Transdermal drug delivery.* Nature Biotechnology, 2008. **26**(11): p. 1261-1268.
27. Gaudana, R., et al., *Ocular Drug Delivery.* The AAPS Journal, 2010. **12**(3): p. 348-360.
28. Suman, J.D., *Nasal Drug Delivery.* Expert Opinion on Biological Therapy, 2003. **3**(3): p. 519-523.
29. Langer, R., *New methods of drug delivery.* Science, 1990. **249**(4976): p. 1527-1533.
30. Allen, T.M. and P.R. Cullis, *Drug Delivery Systems: Entering the Mainstream.* Science, 2004. **303**(5665): p. 1818-1822.
31. Brocchini, S., S.R. Hanson, and J.B. Kohn, *Polymeric drug formulations*. 1999, Google Patents.
32. Muller, R.H., K. Mader, and S. Gohla, *Solid lipid nanoparticles (SLN) for controlled drug delivery-a review of the state of the art.* European journal of pharmaceutics and biopharmaceutics, 2000. **50**(1): p. 161-177.
33. Ekambaram, P., A.A.H. Sathali, and K. Priyanka, *Solid lipid nanoparticles: a review.* Scintific Reviews Chemical Communications, 2012. **2**(1): p. 80-102.
34. Nanjwade, B.K., et al., *Dendrimers: Emerging polymers for drug-delivery systems.* European Journal of Pharmaceutical Sciences, 2009. **38**(3): p. 185-196.
35. Ventola, C.L., *The Nanomedicine Revolution: Part 1: Emerging Concepts.* Pharmacy and Therapeutics, 2012. **37**(9): p. 512-525.
36. Galvin, P., et al., *Nanoparticle-based drug delivery: case studies for cancer and cardiovascular applications.* Cellular and Molecular Life Sciences 2012. **69**(3): p. 389-404.
37. Staff, H.c., *German scientist discovers X-rays*, in *History.com*. 2009, A+E Networks.
38. Behling, R., *Modern Diagnostic X-Ray Sources: Technology, Manufacturing, Reliability*. 2015: CRC Press.
39. Brady, L.W., *The changing role of radiation oncology in cancer management.* CA: A Cancer Journal for Clinicians, 1983. **33**(2): p. 66-73.
40. Orton, C.G., *Uses of therapeutic x rays in medicine.* Health physics, 1995. **69**(5): p. 662-76.
41. Burns, F.S., *Some Observations on X-Ray Therapeutics in Skin Diseases.* The Boston Medical and Surgical Journal, 1903. **149**(18): p. 481-483.
42. Hall, E.J. and J.S. Bedford, *Dose Rate: Its Effect on the Survival of HeLa Cells Irradiated with Gamma Rays.* Radiation Research, 1964. **22**(2): p. 305-315.
43. Leon, M.B., et al., *Localized Intracoronary Gamma-Radiation Therapy to Inhibit the Recurrence of Restenosis after Stenting.* New England Journal of Medicine, 2001. **344**(4): p. 250-256.
44. Terasawa, T., et al., *Systematic Review: Charged-Particle Radiation Therapy for Cancer.* Annals of Internal Medicine, 2009. **151**(8): p. 556-565.
45. Lawrence, J.H., et al., *Alpha particle and proton beams in therapy.* JAMA, 1963. **186**(3): p. 236-245.
46. Parker, R.G., *An appraisal of particle radiation therapy research.* International Journal of Radiation Oncology Biology Physics, 1988. **15**(6): p. 1435-1439.
47. Parker, R.G., *Particle radiation therapy. Current status and future potential.* Cancer, 1977. **39**(S2): p. 802-805.
48. Castro, J.R., et al., *Current status of clinical particle radiotherapy at Lawrence Berkeley laboratory.* Cancer, 1980. **46**(4): p. 633-641.

49. Linfoot, J.A., et al., *The Alpha Particle or Proton Beam in Radiosurgery of the Pituitary Gland for Cushing's Disease.* New England Journal of Medicine, 1963. **269**(12): p. 597-601.
50. Schindl, A., et al., *Low-intensity laser therapy: a review.* Journal of investigative medicine : the official publication of the American Federation for Clinical Research, 2000. **48**(5): p. 312-326.
51. Bjordal, J.M., et al., *A systematic review of low level laser therapy with location-specific doses for pain from chronic joint disorders.* Australian Journal of Physiotherapy, 2003. **49**(2): p. 107-116.
52. Fridman, G., *Direct plasma interaction with living tissue*. 2008.
53. Z. Xiong, Y.C., X. Lu, and T. Du, *Plasmas in Tooth Root Canal.* IEEE Transactions on Plasma Science, 2011. **39**(11): p. 2968.
54. Hammann, A., et al., *Antiseptic efficacy and tolerance of tissue-tolerable plasma compared with two wound antiseptics on artificially bacterially contaminated eyes from commercially slaughtered pigs.* Skin Pharmacol Physiol, 2010. **23**(6): p. 328-32.
55. Weltmann, K.-D., et al., *Plasma Processes and Plasma Sources in Medicine.* Contributions to Plasma Physics, 2012. **52**(7): p. 644-654.
56. Isbary, G., et al., *Successful and safe use of 2 min cold atmospheric argon plasma in chronic wounds: results of a randomized controlled trial.* Br J Dermatol, 2012. **167**(2): p. 404-10.
57. Isbary, G., et al., *A first prospective randomized controlled trial to decrease bacterial load using cold atmospheric argon plasma on chronic wounds in patients.* Br J Dermatol, 2010. **163**(1): p. 78-82.
58. Lee, H.W., et al., *Tooth bleaching with nonthermal atmospheric pressure plasma.* Journal of endodontics, 2009. **35**(4): p. 587-591.
59. Weltmann, K.D., et al., *Atmospheric pressure plasma jet for medical therapy: plasma parameters and risk estimation.* Contributions to Plasma Physics, 2009. **49**(9): p. 631-640.
60. von Keudell, A., et al., *Inactivation of Bacteria and Biomolecules by Low-Pressure Plasma Discharges.* Plasma Processes and Polymers, 2010. **7**(3-4): p. 327-352.
61. Kim, S.J., H.M. Joh, and T.H. Chung, *Production of intracellular reactive oxygen species and change of cell viability induced by atmospheric pressure plasma in normal and cancer cells.* Applied Physics Letters, 2013. **103**(15): p. 153705.
62. Ngo, M.-H.T., et al., *Increased Fibroblast Cell Proliferation and Migration Using Atmospheric N2/Ar Micro-Plasma for the Stimulated Release of Fibroblast Growth Factor-7.* Plasma Processes & Polymers, 2014. **11**: p. 80-88.
63. Danna, N.R., et al., *Assessment of Atmospheric Pressure Plasma Treatment for Implant Osseointegration.* BioMed Research International, 2015. **2015**: p. 761718.
64. Von Woedtke, T., H-R. Metelmann, and K-D. Weltmann, *Clinical Plasma Medicine: State and Perspectives of in Vivo Application of Cold Atmospheric Plasma.* Contributions to Plasma Physics 2014. **54**(2): p. 104-117.
65. Heinlin, J., et al., *Plasma applications in medicine with a special focus on dermatology.* Journal of the European Academy of Dermatology and Venereology, 2011. **25**(1): p. 1-11.

66. Eva Stoffels, Y.S., and David B. Graves, *Cold Atmospheric Plasma: Charged Species and Their Interactions With Cells and Tissues.* IEEE Transactions on Plasma Science, 2008. **36**(4): p. 1441-1457.
67. Graves, D.B., *Oxy-nitroso shielding burst model of cold atmospheric plasma therapeutics.* Clinical Plasma Medicine, 2014. **2**: p. 38-49.
68. Oh, J.-S., et al., *How plasma induced oxidation, oxygenation, and de-oxygenation influences viability of skin cells.* Applied Physics Letters, 2016. **109**(20): p. 203701.
69. Endre, J.S., et al., *The assessment of cold atmospheric plasma treatment of DNA in synthetic models of tissue fluid, tissue and cells.* Journal of Physics D: Applied Physics, 2017. **50**(27): p. 274001.
70. Hong, S.-H., et al., *Genotoxicity and cytotoxicity of the plasma jet-treated medium on lymphoblastoid WIL2-NS cell line using the cytokinesis block micronucleus cytome assay.* Scientific Reports, 2017. **7**(1): p. 3854.
71. Baxter, H.C., et al., *Surgical Instrument Decontamination: Efficacy of Introducing an Argon:Oxygen RF Gas-Plasma Cleaning Step as Part of the Cleaning Cycle for Stainless Steel Instruments.* IEEE Transactions on Plasma Science, 2006. **34**(4): p. 1337-1344.
72. Whittaker, A.G., et al., *Plasma cleaning of dental instruments.* J Hosp Infect, 2004. **56**(1): p. 37-41.
73. Rossi, F., et al., *Low pressure plasma discharges for the sterilization and decontamination of surfaces.* New Journal of Physics, 2009. **11**(11): p. 115017.
74. Korachi M., A.N., *Low temperature atmospheric plasma for microbial decontamination.* 2013.
75. Ting-Ying Chung, N.N., Jhih-Wei Chu, David B. Graves, Elliot Bartis, Joonil Seog, Gottlieb S. Oehrlein, *Plasma Deactivation of Endotoxic Biomolecules: Vacuum Ultraviolet Photon and Radical Beam Effects on Lipid A.* Plasma Processes and Polymers, 2013. **10**: p. 167-180.
76. Shintani, H., et al., *Inactivation of Microorganisms and Endotoxins by Low Temperature Nitrogen Gas Plasma Exposure.* Biocontrol Science, 2007. **12**(4): p. 131-143.
77. Arjunan, K.P., Clyne A. M., *A Nitric Oxide Producing Pin-to-Hole Spark Discharge Plasma Enhances Endothelial Cell Proliferation and Migration.* Plasma Medicine, 2011. **1**(3-4): p. 279-293.
78. Frank, S., et al., *Nitric oxide triggers enhanced induction of vascular endothelial growth factor expression in cultured keratinocytes (HaCaT) and during cutaneous wound repair.* FASEB J., 1999. **13**: p. 2002-2014.
79. Coller G., *e.a.*, *Plasma jet-induced tissue oxygenation: potentialities for new therapeutic strategies.* Plasma Sources Science and Technology, 2014. **23**: p. 012005.
80. Endre, J.S., et al., *Modelling the helium plasma jet delivery of reactive species into a 3D cancer tumour.* Plasma Sources Science and Technology, 2018. **27**(1): p. 014001.
81. Sun, Y., et al., *Inactivation of Candida Biofilms by Non-Thermal Plasma and Its Enhancement for Fungistatic Effect of Antifungal Drugs.* PLoS ONE, 2012. **7**(7): p. e40629.
82. Keping, Y.A.N., et al., *Pulsed cold plasma-induced blood coagulation and its pilot application in stanching bleeding during rat hepatectomy.* Plasma Science and Technology, 2018. **20**(4): p. 044005.

83. Fridman, G., et al., *Comparison of direct and indirect effects of non-thermal atmospheric-pressure plasma on bacteria.* Plasma Processes and Polymers, 2007. **4**(4): p. 370-375.
84. Stoffels, E., I.E. Kieft, and R.E.J. Sladek, *Superficial treatment of mammalian cells using plasma needle.* Journal of Physics D: Applied Physics, 2003. **36**(23): p. 2908.
85. Sladek, R.E.J., et al., *Plasma treatment of dental cavities: a feasibility study.* IEEE Transactions on Plasma Science, 2004. **32**(4): p. 1540-1543.
86. Barrientos, S., et al., *Growth factors and cytokines in wound healing.* Wound Repair and Regeneration, 2008. **16**(5): p. 585-601.
87. Brehmer, F., et al., *Alleviation of chronic venous leg ulcers with a hand-held dielectric barrier discharge plasma generator (PlasmaDerm((R)) VU-2010): results of a monocentric, two-armed, open, prospective, randomized and controlled trial (NCT01415622).* Journal of the European Academy of Dermatology and Venereology, 2015. **29**(1): p. 148-55.
88. Lloyd G., *e.a., Gas Plasma: Medical Uses and Developments in Wound Care.* Plasma Process. Polym., 2010. **7**: p. 194-211.
89. Laroussi, M., *From Killing Bacteria to Destroying Cancer Cells: 20 Years of Plasma Medicine.* Plasma Processes and Polymers 2014. **11**(12): p. 1138-1141.
90. *al.*, T.v.W.*e.*, *Plasmas for medicine.* Physics Reports, 2013. **530**: p. 291-320.
91. Weltmann Klaus, D., et al., *Atmospheric-pressure plasma sources: Prospective tools for plasma medicine*, in *Pure and Applied Chemistry*. 2010. p. 1223.
92. Morfill, G., M.G. Kong, and J. Zimmermann, *Focus on plasma medicine.* New Journal of Physics, 2009. **11**(11): p. 115011.
93. Haertel, B., et al., *Non-Thermal Atmospheric-Pressure Plasma Possible Application in Wound Healing.* bt, 2014. **22**(6): p. 477-490.
94. Vandamme, M., et al., *ROS implication in a new antitumor strategy based on non-thermal plasma.* International Journal of Cancer, 2012. **130**(9): p. 2185-2194.
95. Vandamme, M., et al., *Antitumor Effect of Plasma Treatment on U87 Glioma Xenografts: Preliminary Results.* Plasma Processes and Polymers, 2010. **7**(3-4): p. 264-273.
96. Eliezer, S. and Y. Eliezer, *The fourth state of matter: an introduction to plasma science*. 2001: CRC Press.
97. Miyamoto, K., *Plasma Physics and Controlled Nuclear Fusion*. Springer Series on Atomic, Optical, and Plasma Physics. Vol. 38. 2005: Springer Science & Business Media. 372.
98. Peratt, A., *Electric space: Evolution of the plasma universe.* Astrophysics and Space Science, 1996. **244**(1-2): p. 89-103.
99. Peratt, A., *Plasma and the Universe: Large Scale Dynamics, Filamentation, and Radiation*, in *Plasma Astrophysics and Cosmology*, A. Peratt, Editor. 1995, Springer Netherlands. p. 97-107.
100. Encrenaz, T., et al., *The solar system*. 2013: Springer Science & Business Media.
101. Dessler, A.J., *Solar wind and interplanetary magnetic field.* Reviews of Geophysics, 1967. **5**(1): p. 1-41.
102. Popov, O.A., *High density plasma sources: design, physics and performance*. 1996: Elsevier.

103. Schutze, A., et al., *The atmospheric-pressure plasma jet: a review and comparison to other plasma sources.* Plasma Science, IEEE Transactions on, 1998. **26**(6): p. 1685-1694.
104. Van Gils, C., et al., *Mechanisms of bacterial inactivation in the liquid phase induced by a remote RF cold atmospheric pressure plasma jet.* Journal of Physics D: Applied Physics, 2013. **46**(17): p. 175203.
105. Barekzi, N. and M. Laroussi, *Dose-dependent killing of leukemia cells by low-temperature plasma.* Journal of Physics D: Applied Physics, 2012. **45** (42): p. 422002.
106. N Barekzi, M.L., *Effects of Low Temperature Plasmas on Cancer Cells.* Plasma Process. Polym. , 2013. **10**: p. 1039–1050.
107. Chen, F.F. and M.D. Smith, *Plasma*, in *Van Nostrand's Scientific Encyclopedia*. 1984, Wiley Online Library.
108. Boulos, M.I., P. Fauchais, and E. Pfender, *Thermal plasmas: fundamentals and applications*. 2013: Springer Science & Business Media.
109. Zhang, Q., et al., *Assessment of the roles of various inactivation agents in an argon-based direct current atmospheric pressure cold plasma jet.* Journal of Applied Physics, 2012. **111**(12): p. 123305.
110. Chu, P.K., et al., *Plasma-surface modification of biomaterials.* Materials Science and Engineering: R: Reports, 2002. **36**(5–6): p. 143-206.
111. Luo D., D.Y., *Microplasmas for analytical applications of lab-on-a-chip.* Trends in Analytical Chemistry, 2012. **39**: p. 254-266.
112. Claire Tendero, C.T., Pascal Tristant, Jean Desmaison, Philippe Leprince, *Atmospheric pressure plasmas: A review.* Spectrochimica Acta Part B, 2006. **61**: p. 2-30.
113. Priest, C., et al., *Microplasma patterning of bonded microchannels using high-precision "injected" electrodes.* Lab Chip, 2011. **11**(3): p. 541-4.
114. Sameer A. Al-Bataineh, E.J.S., Apurva Mishra, Sung-Jin Park, J. Gary Eden, Hans J. Griesser, Nicolas H. Voelcker, Robert D. Short, David A. Steele, *Design of a Microplasma Device for Spatially Localised Plasma Polymerisation.* Plasma Process. Polym., 2011. **8**: p. 695–700.
115. Haruhiko, A., Y. Masahiro, and F. Nobuo, *Developments of Plasma Etching Technology for Fabricating Semiconductor Devices.* Japanese Journal of Applied Physics, 2008. **47**(3R): p. 1435.
116. Morent, R., et al., *Non-thermal plasma treatment of textiles.* Surface and coatings technology, 2008. **202**(14): p. 3427-3449.
117. Fridman, G., et al., *Applied plasma medicine.* Plasma Processes and Polymers, 2008. **5**(6): p. 503-533.
118. Gomez, E., et al., *Thermal plasma technology for the treatment of wastes: A critical review.* Journal of Hazardous Materials, 2009. **161**(2–3): p. 614-626.
119. Fauchais, P. and A. Vardelle, *Thermal plasmas.* Plasma Science, IEEE Transactions on, 1997. **25**(6): p. 1258-1280.
120. Pfender, E., *Thermal plasma processing in the nineties.* Pure and Applied Chemistry, 1988. **60**(5): p. 591-606.
121. Moisan, M., et al., *Low-temperature sterilization using gas plasmas: a review of the experiments and an analysis of the inactivation mechanisms.* International Journal of Pharmaceutics, 2001. **226**: p. 1-21.
122. Arjunan, K.P., et al., *Non-thermal dielectric barrier discharge plasma induces angiogenesis through reactive oxygen species.* Journal of the Royal Society Interface, 2012. **9**(66): p. 147-57.

123. Arora, V., et al., *Cold Atmospheric Plasma (CAP) in Dentistry.* Dentistry, 2014. **4**(1): p. 1-6.
124. Wikipedia. *Cathode ray tube*. 2016; Available from: https://en.wikipedia.org/w/index.php?title=Cathode_ray_tube&oldid=707414560.
125. Crookes, W., *On radiant matter; a lecture delivered to the British Association for the Advancement of Science, at Sheffield, Friday, August 22, 1879.* American Journal of Science, 1879. **Series 3 Vol. 18**(106): p. 241-262.
126. Thomson, J.J., *XL. Cathode Rays.* The London, Edinburgh, and Dublin Philosophical Magazine and Journal of Science, 1897. **44**(269): p. 293-316.
127. Wilson, C.T.R., *On the leakage of Electricity through dust-free air*, in *Proceedings of the Cambridge Philosophical Society*. 1900, Cambridge Philosophical Society.: Cambridge. p. 32.
128. Elster, J. and H. Geitel, *Über die Existenz electrischer Ionen in der Atmosphäre.* Terrest. Magnetism, 1899b. **4**: p. 213-234.
129. Chen, C., et al., *A model of plasma-biofilm and plasma-tissue interactions at ambient pressure.* Plasma Chemistry and Plasma Processing, 2014. **34**(3): p. 403-441.
130. Kanazawa, S., et al., *Stable glow plasma at atmospheric pressure.* Journal of Physics D: Applied Physics, 1988. **21**(5): p. 838.
131. Inomata, K., et al., *Open air deposition of SiO2 film from a cold plasma torch of tetramethoxysilane-H2-Ar system.* Applied physics letters, 1994. **64**(1): p. 46-48.
132. Ha, H.K., et al., *Open air plasma chemical vapor deposition of highly dielectric amorphous TiO2 films.* Applied physics letters, 1996. **68**(21): p. 2965-2967.
133. M G Kong, G.K., G Morfill, T Nosenko, T Shimizu, J van Dijk and J L Zimmermann, *Plasma Medicine: an introductory review* New Journal of Physics 2009. **11**(11): p. 115012.
134. Graves, D.B., *Mechanisms of Plasma Medicine: Coupling Plasma Physics, Biochemistry, and Biology.* IEEE Transactions on Radiation and Plasma Medical Sciences, 2017. **1**(4): p. 281-292.
135. Neyts, E.C., et al., *Computer simulations of plasma–biomolecule and plasma–tissue interactions for a better insight in plasma medicine.* Journal of Physics D: Applied Physics, 2014. **47**(29): p. 293001.
136. Burts, M.L., et al., *Use of atmospheric non-thermal plasma as a disinfectant for objects contaminated with methicillin-resistant Staphylococcus aureus.* Am J Infect Control, 2009. **37**(9): p. 729-33.
137. Ishaq, M., M.M. Evans, and K.K. Ostrikov, *Effect of atmospheric gas plasmas on cancer cell signaling.* Int J Cancer, 2014. **134**(7): p. 1517-28.
138. Ratovitski, E.A., et al., *Anti-Cancer Therapies of 21st Century: Novel Approach to Treat Human Cancers Using Cold Atmospheric Plasma.* Plasma Processes and Polymers, 2014. **11**(12): p. 1128-1137.
139. Crawford, S., *Is it time for a new paradigm for systemic cancer treatment? Lessons from a century of cancer chemotherapy.* Frontiers in Pharmacology, 2013. **4**: p. 68.
140. Gaur, N., et al., *Combined effect of protein and oxygen on reactive oxygen and nitrogen species in the plasma treatment of tissue.* Applied Physics Letters, 2015. **107**(10): p. 103703.
141. Gaunt, L.F., C.B. Beggs, and G.E. Georghiou, *Bactericidal action of the reactive species produced by gas-discharge nonthermal plasma at atmospheric pressure: a review.* Plasma Science, IEEE Transactions on, 2006. **34**(4): p. 1257-1269.

142. Alkawareek, M.Y., et al., *Eradication of Pseudomonas aeruginosa biofilms by atmospheric pressure non-thermal plasma.* PLoS One, 2012. **7**(8): p. e44289.
143. von Woedtke, T., et al., *Introduction to Plasma Medicine*, in *Comprehensive Clinical Plasma Medicine: Cold Physical Plasma for Medical Application*, H.-R. Metelmann, T. von Woedtke, and K.-D. Weltmann, Editors. 2018, Springer International Publishing: Cham. p. 3-21.
144. A. B. Shekhter, R.K.K., A. V. Pekshev, N. P. Kozlov, and Yu. L. Perov, *Experimental and Clinical Validation of Plasmadynamic Therapy of Wounds with Nitric Oxide.* Byulleten' Eksperimental'noi Biologii i Meditsiny, 1998. **126**(8): p. 210-215.
145. Trachootham, D., J. Alexandre, and P. Huang, *Targeting cancer cells by ROS-mediated mechanisms: a radical therapeutic approach?* Nat Rev Drug Discov, 2009. **8**(7): p. 579-91.
146. Lademann, O., et al., *Drug delivery through the skin barrier enhanced by treatment with tissue-tolerable plasma.* Exp Dermatol, 2011. **20**(6): p. 488-90.
147. Ogawa, Y., et al., *An epoch-making application of discharge plasma phenomenon to gene-transfer.* Biotechnol Bioeng, 2005. **92**(7): p. 865-70.
148. Siemens, W., *Induction Tube of W. Siemens.* Poggendorff ’s Ann. Phys. Chem., 1857. **102**: p. 66-122.
149. Blackert, S., et al., *Influence of non-thermal atmospheric pressure plasma on cellular structures and processes in human keratinocytes (HaCaT).* Journal of dermatological science, 2013. **70**(3): p. 173-81.
150. Andrei Vasile Nastuta, I.T., Constantin Grigoras, Valentin Pohoata, Gheorghe Popa, *Stimulation of wound healing by helium atmospheric pressure plasma treatment.* J. Phys. D: Appl. Phys., 2011. **44**: p. 105204.
151. Kogelschatz, U., B. Eliasson, and W. Egli, *Dielectric-barrier discharges. Principle and applications.* Le Journal de Physique IV, 1997. **7**(C4): p. C4-47-C4-66.
152. Fridman, G., et al. , *Applied plasma medicine.* Plasma Processes and Polymers, 2008. **5**(6): p. 503-533.
153. Gregory Fridman, A.S., Monika M. Jost, Ari D. Brooks, Alexander Fridman, Alexander Gutsol, Victor Vasilets, Gary Friedman, *Floating electrode dielectric barrier discharge plasma in air promoting apoptotic behavior in melanoma skin cancer cell lines.* Plasma Chemistry and Plasma Processing, 2007. **27.2**: p. 163-176.
154. Dobrynin, D., et al., *Physical and biological mechanisms of direct plasma interaction with living tissue.* New Journal of Physics, 2009. **11**(11): p. 115020.
155. Babaeva, N.Y. and M.J. Kushner. *Direct and indirect treatment of living tissue: Dielectric barrier discharges VS. plasma jets*. in *2011 Abstracts IEEE International Conference on Plasma Science*. 2011. IEEE.
156. Morfill, G.E., et al., *Nosocomial infections—a new approach towards preventive medicine using plasmas.* New Journal of Physics, 2009. **11**(11): p. 115019.
157. Stoffels, E., et al., *Plasma needle: a non-destructive atmospheric plasma source for fine surface treatment of (bio)materials.* Plasma Sources Science and Technology, 2002. **11**(4): p. 383.
158. Goree J., *e.a., Killing of S. mutans Bacteria Using a Plasma Needle at Atmospheric Pressure.* IEEE Transactions on Plasma Science, 2006. **34**(4): p. 1317-1324.

159. Stoffels, E., et al., *Plasma needle for in vivo medical treatment: recent developments and perspectives.* Plasma Sources Science and Technology, 2006. **15**(4): p. S169.
160. Zirnheld, J.L., et al., *Nonthermal plasma needle: development and targeting of melanoma cells.* IEEE Transactions on Plasma Science, 2010. **38**(4): p. 948-952.
161. Zucker, S.N., et al., *Preferential induction of apoptotic cell death in melanoma cells as compared with normal keratinocytes using a non-thermal plasma torch.* Cancer Biol Ther, 2012. **13**(13): p. 1299-306.
162. Shimizu, T., et al., *Characterization of Microwave Plasma Torch for Decontamination.* Plasma Processes and Polymers, 2008. **5**(6): p. 577-582.
163. Cao, Z., J.L. Walsh, and M.G. Kong, *Atmospheric plasma jet array in parallel electric and gas flow fields for three-dimensional surface treatment.* Applied Physics Letters, 2009. **94**(2): p. 021501.
164. Cao, Z., et al., *Spatially extended atmospheric plasma arrays.* Plasma Sources Science and Technology, 2010. **19**(2): p. 025003.
165. Feng, L., et al., *Jet-to-jet interactions in atmospheric-pressure plasma jet arrays for surface processing.* Plasma Processes and Polymers, 2018. **15**(1): p. 1700114.
166. Ghasemi, M., et al., *Interaction of multiple plasma plumes in an atmospheric pressure plasma jet array.* Journal of Physics D: Applied Physics, 2013. **46**(5): p. 052001.
167. M. Laroussi, X.L., *Room-temperature atmospheric pressure plasma plume for biomedical applications.* Appl. Phys. Lett., 2005. **87**: p. 113902.
168. S.K. Pankaj, C.B.-F., N.N. Misra, V. Milosavljevi, C.P. O'Donnell, P. Bourke, K.M. Keener and P.J. Cullen, *Applications of cold plasma technology in food packaging.* Trends in Food Science & Technology, 2014. **35** p. 5-17.
169. S Reuter, *e.a., Generation of atomic oxygen in the effluent of an atmospheric pressure plasma jet.* Plasma Sources Science and Technology, 2009. **18**: p. 015006.
170. E Stoffels, *e.a., A plasma needle generates nitric oxide.* Plasma Sources Science and Technology, 2006. **15**: p. 501–506.
171. Finkel T., H.N.J., *Oxidants, oxidative stress and the biology of ageing.* Nature, 2000. **408**: p. 239-247.
172. Harman, D., *Free Radical Theory Of Aging.* Mutation Research/DNAging, 1992. **275**(3-6): p. 257-266.
173. Beckman, J.S., *Understanding peroxynitrite biochemistry and its potential for treating human diseases.* Archives of biochemistry and biophysics, 2009. **484**(2): p. p. 114.
174. Pacher, P., J.S. Beckman, and L. Liaudet, *Nitric oxide and peroxynitrite in health and disease.* Physiological reviews, 2007. **87**(1): p. 315-424.
175. D'Autreaux, B. and M.B. Toledano, *ROS as signalling molecules: mechanisms that generate specificity in ROS homeostasis.* Nature reviews. Molecular cell biology, 2007. **8**(10): p. 813-24.
176. A., F.B., *Redox Signaling Across Cell Membranes.* Antioxidants & Redox Signaling, 2009. **11**(6): p. 1349-1356.
177. V. Darley-Usmar, H.W., Barry Halliwell, *Nitric oxide and oxygen radicals: a question of balance.* FEBS Lett, 1995. **369**: p. 131-135.
178. Rhee, S.G., *H2O2, a necessary evil for cell signaling.* Science, 2006. **312**(5782): p. 1882-1883.

179. Graves, D.B., *The emerging role of reactive oxygen and nitrogen species in redox biology and some implications for plasma applications to medicine and biology.* Journal of Physics D: Applied Physics 2012. **45**: p. 263001.
180. Dröge, W., *Free Radicals in the Physiological Control of Cell Function.* Physiological Reviews, 2002. **82**(1): p. 47-95.
181. Valko, M., et al., *Free radicals and antioxidants in normal physiological functions and human disease.* The International Journal of Biochemistry & Cell Biology, 2007. **39**(1): p. 44-84.
182. Mittler, R., et al., *ROS signaling: the new wave?* Trends in Plant Science, 2011. **16**(6): p. 300-309.
183. Klyubin, I.V., K.M. Kirpichnikova, and I.A. Gamaley, *Hydrogen peroxide-induced chemotaxis of mouse peritoneal neutrophils.* European journal of cell biology, 1996. **70**(4): p. 347-351.
184. Murrell, G.A., M.J. Francis, and L. Bromley, *Modulation of fibroblast proliferation by oxygen free radicals.* Biochemical Journal, 1990. **265**(3): p. 659-665.
185. Stone, J.R. and T. Collins, *The role of hydrogen peroxide in endothelial proliferative responses.* Endothelium, 2002. **9**(4): p. 231-238.
186. Ohye, H. and M. Sugawara, *Dual oxidase, hydrogen peroxide and thyroid diseases.* Exp Biol Med (Maywood), 2010. **235**(4): p. 424-33.
187. Schafer, M. and S. Werner, *Oxidative stress in normal and impaired wound repair.* Pharmacol Res, 2008. **58**(2): p. 165-71.
188. Darr, D. and I. Fridovich, *Free radicals in cutaneous biology.* J Invest Dermatol, 1994. **102**(5): p. 671-5.
189. Martin, A., *The Use of Antioxidants in Healing.* Dermatologic Surgery, 1996. **22**(2): p. 156-160.
190. Riley, P.A., *Free radicals in biology: oxidative stress and the effects of ionizing radiation.* International journal of radiation biology, 1994. **65**(1): p. 27-33.
191. Wang, L., et al., *Hypochlorous Acid as a Potential Wound Care Agent: Part I. Stabilized Hypochlorous Acid: A Component of the Inorganic Armamentarium of Innate Immunity.* Journal of Burns and Wounds, 2007. **6**: p. e5.
192. Liebmann, J., et al., *Biological effects of nitric oxide generated by an atmospheric pressure gas-plasma on human skin cells.* Nitric Oxide, 2011. **24**(1): p. 8-16.
193. Schairer, D.O., et al., *The potential of nitric oxide releasing therapies as antimicrobial agents.* Virulence, 2012. **3**(3): p. 271-9.
194. Schulz, G. and J. Stechmiller, *Wound healing and nitric oxide production: too little or too much may impair healing and cause chronic wounds.* The international journal of lower extremity wounds, 2006. **5**(1): p. 6-8.
195. Gutteridge, J.M.C., and Barry Halliwell, *Free Radicals and Antioxidants in the Year.* 2000.
196. Loo, A.E., et al., *Effects of hydrogen peroxide on wound healing in mice in relation to oxidative damage.* PLoS One, 2012. **7**(11): p. e49215.
197. Seiler, A., et al., *Glutathione peroxidase 4 senses and translates oxidative stress into 12/15-lipoxygenase dependent- and AIF-mediated cell death.* Cell Metab, 2008. **8**(3): p. 237-48.
198. Ray, P.D., B.W. Huang, and Y. Tsuji, *Reactive oxygen species (ROS) homeostasis and redox regulation in cellular signaling.* Cell Signal, 2012. **24**(5): p. 981-90.

199. *al.*, E.D.*e.*, *The effects of nitroxide radicals on oxidative dna damage.* Free Radic Biol Med, 2000. **28**(8): p. 1257-1265.
200. Radi R, P.G., Alvarez MN, Naviliat M, Cayota A., *Unraveling peroxynitrite formation in biological systems.* Free Radical Biology and Medicine 2001. **30**(5): p. 463-488.
201. Halliwell, B., *The wanderings of a free radical.* Free Radic Biol Med, 2009. **46**(5): p. 531-42.
202. Mittal, C.K. and F. Murad, *Activation of guanylate cyclase by superoxide dismutase and hydroxyl radical: a physiological regulator of guanosine 3',5'-monophosphate formation.* Proceedings of the National Academy of Sciences of the United States of America, 1977. **74**(10): p. 4360-4364.
203. Ignarro, L.J. and P.J. Kadowitz, *The pharmacological and physiological role of cyclic GMP in vascular smooth muscle relaxation.* Annual review of pharmacology and toxicology, 1985. **25**: p. 171-191.
204. Radomski, M.W., R.M. Palmer, and S. Moncada, *The anti-aggregating properties of vascular endothelium: interactions between prostacyclin and nitric oxide.* British journal of pharmacology, 1987. **92**(3): p. 639-46.
205. Roth, S. and W. Dröge, *Regulation of T-cell activation and T-cell growth factor (TCGF) production by hydrogen peroxide.* Cellular Immunology, 1987. **108**(2): p. 417-424.
206. Keyse, S.M. and R.M. Tyrrell, *Heme oxygenase is the major 32-kDa stress protein induced in human skin fibroblasts by UVA radiation, hydrogen peroxide, and sodium arsenite.* Proceedings of the National Academy of Sciences of the United States of America, 1989. **86**(1): p. 99-103.
207. T, F., *Oxygen radicals and signaling.* Curr Opin Cell Biol, 1998. **10**: p. 248-253.
208. Meier, B., *Reactive oxygen intermediates involved in cellular regulation.* Protoplasma, 2000. **217**: p. 101-116.
209. Choi, J.H., et al., *Low-temperature atmospheric plasma increases the expression of anti-aging genes of skin cells without causing cellular damages.* Archives of dermatological research, 2013. **305**(2): p. 133-40.
210. Arjunan K. P., C.A.M., *Hydroxyl Radical and Hydrogen Peroxide are Primarily Responsible for Dielectric Barrier Discharge Plasma-Induced Angiogenesis.* Plasma Processes & Polymers, 2011. **8**: p. 1154-1164.
211. Li, C. and R.M. Jackson, *Reactive species mechanisms of cellular hypoxia-reoxygenation injury.* American Journal of Physiology - Cell Physiology, 2002. **282**(2): p. C227-C241.
212. Naviaux, R.K., *Oxidative shielding or oxidative stress?* J Pharmacol Exp Ther, 2012. **342**(3): p. 608-18.
213. Mizushima, N., *Autophagy: process and function.* Genes Dev, 2007. **21**(22): p. 2861-73.
214. Milisav, I., B. Poljsak, and D. Šuput, *Adaptive Response, Evidence of Cross-Resistance and Its Potential Clinical Use.* International Journal of Molecular Sciences, 2012. **13**(9): p. 10771.
215. Glick, D., S. Barth, and K.F. Macleod, *Autophagy: cellular and molecular mechanisms.* The Journal of pathology, 2010. **221**(1): p. 3-12.
216. Burney, S., et al., *The chemistry of DNA damage from nitric oxide and peroxynitrite.* Mutat Res, 1999. **424**(1-2): p. 37-49.
217. Niles, J.C., J.S. Wishnok, and S.R. Tannenbaum, *Peroxynitrite-induced oxidation and nitration products of guanine and 8-oxoguanine: Structures and mechanisms of product formation.* Nitric Oxide, 2006. **14**(2): p. 109-121.

218. Hoeldtke, R.D., et al., *Peroxynitrite versus nitric oxide in early diabetes.* American journal of hypertension, 2003. **16**(9 Pt 1): p. 761-6.
219. Guzik, T.J., et al., *Mechanisms of increased vascular superoxide production in human diabetes mellitus: role of NAD(P)H oxidase and endothelial nitric oxide synthase.* Circulation, 2002. **105**(14): p. 1656-62.
220. Suarez-Pinzon, W.L., C. Szabo, and A. Rabinovitch, *Development of autoimmune diabetes in NOD mice is associated with the formation of peroxynitrite in pancreatic islet beta-cells.* Diabetes, 1997. **46**(5): p. 907-11.
221. Pacher, P., et al., *Potent metalloporphyrin peroxynitrite decomposition catalyst protects against the development of doxorubicin-induced cardiac dysfunction.* Circulation, 2003. **107**(6): p. 896-904.
222. Mungrue, I.N., et al., *Cardiomyocyte overexpression of iNOS in mice results in peroxynitrite generation, heart block, and sudden death.* The Journal of Clinical Investigation, 2002. **109**(6): p. 735-743.
223. Andersen, J.K., *Oxidative stress in neurodegeneration: cause or consequence?* Nature Reviews Neuroscience, 2004. **10**: p. S18.
224. Keely, S., et al., *Letter: oxidative stress, cause or consequence of constipation-associated colorectal cancer?* Alimentary Pharmacology & Therapeutics, 2015. **42**(7): p. 941-942.
225. Juranek, I. and S. Bezek, *Controversy of free radical hypothesis: reactive oxygen species--cause or consequence of tissue injury?* Gen Physiol Biophys, 2005. **24**(3): p. 263-78.
226. Powers, S.K., A.J. Smuder, and A.R. Judge, *Oxidative stress and disuse muscle atrophy: cause or consequence?* Curr Opin Clin Nutr Metab Care, 2012. **15**(3): p. 240-5.
227. van der Vliet, A., *Cigarettes, cancer, and carotenoids: a continuing, unresolved antioxidant paradox.* The American Journal of Clinical Nutrition, 2000. **72**(6): p. 1421-1423.
228. Halliwell, B., *Are polyphenols antioxidants or pro-oxidants? What do we learn from cell culture and in vivo studies?* Archives of biochemistry and biophysics, 2008. **476**(2): p. 107-12.
229. Doughan, A.K. and S.I. Dikalov, *Mitochondrial redox cycling of mitoquinone leads to superoxide production and cellular apoptosis.* Antioxidants & redox signaling, 2007. **9**(11): p. 1825-36.
230. Halliwell, B., *Antioxidants in human health and disease.* Annu Rev Nutr, 1996. **16**: p. 33-50.
231. Gutteridge, J.M. and B. Halliwell, *Antioxidants: Molecules, medicines, and myths.* Biochemical and biophysical research communications, 2010. **393**(4): p. 561-4.
232. Sarangarajan, R., et al., *Antioxidants: Friend or foe?* Asian Pacific Journal of Tropical Medicine, 2017. **10**(12): p. 1111-1116.
233. Sautin, Y.Y. and R.J. Johnson, *URIC ACID: THE OXIDANT–ANTIOXIDANT PARADOX.* Nucleosides, nucleotides & nucleic acids, 2008. **27**(6): p. 608-619.
234. Halliwell, B. and J.M. Gutteridge, *Free radicals in biology and medicine*. Vol. 3. 1999: Oxford university press Oxford.
235. Rishton, G.M., *Failure and success in modern drug discovery: guiding principles in the establishment of high probability of success drug discovery organizations.* Medicinal Chemistry, 2005. **1**(5): p. 519-527.
236. Borst, P., et al., *A family of drug transporters: the multidrug resistance-associated proteins.* J Natl Cancer Inst, 2000. **92**(16): p. 1295-302.

237. House, P. *Robert Hooke and The Discovery of the Cell*. 2009; Available from: https://www.science-of-aging.com/timelines/hooke-history-cell-discovery.php#r0rqwcZgs48ld9TE.99.
238. *Molecular Biology of the Cell, 4th Edition*.
239. Holy, J., *Structure and Function of Cell Organelles*, in *Introduction to Bioinformatics: A Theoretical and Practical Approach*, S.A. Krawetz and D.D. Womble, Editors. 2003, Humana Press: Totowa, NJ. p. 25-54.
240. Wikipedia. *Cell (biology)*. 2017 08 October 2017]; Available from: https://en.wikipedia.org/w/index.php?title=Cell_(biology)&oldid=798003429.
241. Education, S.b.N. What is a Cell? 2014 [cited 2017 08- October - 2017]; Available from: https://www.nature.com/scitable/topicpage/what-is-a-cell-14023083.
242. Fields, D. *Eukaryotic and Prokaryotic Cells: Similarities and Differences*. 2017 [cited 2017 08-october - 2017]; Available from: https://www.news-medical.net/life-sciences/Eukaryotic-and-Prokaryotic-Cells-Similarities-and-Differences.aspx.
243. Medicine, U.S.N.L.o. *What is DNA?* 2017 [cited 2017 08- October- 2017]; Available from: https://ghr.nlm.nih.gov/primer/basics/dna.
244. Rettner, R. *DNA: Definition, Structure & Discovery*. 2013 [cited 2017 08-October- 2017]; Available from: https://www.livescience.com/37247-dna.html.
245. Wikipedia. *Base pair*. 2018 3 November 2018 [cited 2018 22 November 2018]; Available from: https://en.wikipedia.org/w/index.php?title=Base_pair&oldid=867078325.
246. Wikipedia. *Reading frame*. 2018 [cited 2018 20 September 2018]; Available from: https://en.wikipedia.org/w/index.php?title=Reading_frame&oldid=846213533.
247. Biro, J.C., et al., *A common periodic table of codons and amino acids.* Biochemical and Biophysical Research Communications, 2003. **306**(2): p. 408-415.
248. Clancy, S.a.B., W., *Translation: DNA to mRNA to Protein.* Nature Education, 2008. **1**(1): p. 101.
249. Mandal, A. *DNA Biological Functions*. 2014 [cited 2017 08- October- 2017]; Available from: https://www.news-medical.net/life-sciences/DNA-Biological-Functions.aspx.
250. Wikipedia. *DNA*. 2017 [cited 2017 08 October 2017]; Available from: https://en.wikipedia.org/w/index.php?title=DNA&oldid=804246694.
251. Lindahl, T. and D.E. Barnes, *Repair of endogenous DNA damage.* Cold Spring Harb Symp Quant Biol, 2000. **65**: p. 127-33.
252. Jackson, S.P. and J. Bartek, *The DNA-damage response in human biology and disease.* Nature, 2009. **461**(7267): p. 1071-1078.
253. Uryga, A., K. Gray, and M. Bennett, *DNA Damage and Repair in Vascular Disease.* Annual Review of Physiology, 2016. **78**(1): p. 45-66.
254. Li, G.-M., *Mechanisms and functions of DNA mismatch repair.* Cell Res, 2008. **18**(1): p. 85-98.
255. Keren, K., *Membrane tension leads the way.* Proceedings of the National Academy of Sciences, 2011. **108**(35): p. 14379-14380.
256. Gauthier, N.C., et al., *Temporary increase in plasma membrane tension coordinates the activation of exocytosis and contraction during cell spreading.* Proceedings of the National Academy of Sciences, 2011. **108**(35): p. 14467-14472.

257. Walker, N.A., *The Structure of Biological Membranes*, in *Transport in Plants II*, U. Lüttge and M.G. Pitman, Editors. 1976, Springer Berlin Heidelberg. p. 3-11.
258. Wikipedia. *Cell membrane*. 2015; Available from: https://en.wikipedia.org/w/index.php?title=Cell_membrane&oldid=691698787.
259. Alberts, B., et al., *The lipid bilayer*. 2002.
260. Alberts, B., et al., *Principles of membrane transport.* 2002.
261. Watson, H., *Biological membranes.* Essays In Biochemistry, 2015. **59**: p. 43-69.
262. Cooper, G.M., *Structure of the Plasma Membrane*, in *The Cell: A Molecular Approach. 2nd edition*. 2000.
263. Berg, J.M., J.L. Tymoczko, and L. Stryer, *Biochemistry 5th edition, 2002*. WH Freeman. Available online through the NCBI Bookshelf: link.
264. O'Connor, C.M., J.U. Adams, and J. Fairman, *Essentials of cell biology.* Cambridge, MA: NPG Education, 2010. **1**.
265. Alberts, B., et al., *Cell junctions, cell adhesion, and the extracellular matrix*, in *Molecular Biology of the Cell. 4th edition.* 2002, Garland Science: New York.
266. Berk, A., S. Zipursky, and H. Lodish, *Molecular Cell Biology 4th edition.* 2000.
267. Wikipedia. *Na+/K+-ATPase*. 2015; Available from: https://en.wikipedia.org/w/index.php?title=Na%2B/K%2B-ATPase&oldid=692837803.
268. Choi, J.-K., et al., *Interactions of very long-chain saturated fatty acids with serum albumin.* Journal of Lipid Research, 2002. **43**(7): p. 1000-1010.
269. Alberts, B., et al., *Membrane transport of small molecules and the electrical properties of membranes.* 2002.
270. Zhang, R., et al., *Spectrin: structure, function and disease.* Sci China Life Sci, 2013. **56**(12): p. 1076-85.
271. Lodish, H. and S.L. Zipursky, *Molecular cell biology.* Biochem Mol Biol Educ, 2001. **29**: p. 126-133.
272. Howard, J., *Mechanics of motor proteins and the cytoskeleton.* 2001.
273. Chegini, N., M.J. Rossi, and B.J. Masterson, *Platelet-derived growth factor (PDGF), epidermal growth factor (EGF), and EGF and PDGF beta-receptors in human endometrial tissue: localization and in vitro action.* Endocrinology, 1992. **130**(4): p. 2373-2385.
274. Chemguide. *Proteins as enzymes*. 2007; Available from: http://www.chemguide.co.uk/organicprops/aminoacids/enzymes.html.
275. Kimball, J.W., *Cell Biology*. 2018: Addison Wesley Publishing Company.
276. Berg, J.M., J.L. Tymoczko, and L. Stryer, *Section 12.3, There Are Three Common Types of Membrane Lipids*, in *Biochemistry. 5th edition.* 2002: New York.
277. Masterjohn, C., *Cholesterol's Importance to the Cell Membrane*. 2005, July.
278. Wikipedia. *Glycolipid*. 2016; Available from: https://en.wikipedia.org/w/index.php?title=Glycolipid&oldid=698653397.
279. Wikibooks. *Structural Biochemistry/Lipids/Cholesterol - Wikibooks,The Free Textbook Project*. 2015; Available from: https://en.wikibooks.org/w/index.php?title=Structural_Biochemistry/Lipids/Cholesterol&oldid=3008111.
280. Wikipedia. *Human skin*. 2017 [cited 2017 03 October 2017]; Available from: https://en.wikipedia.org/w/index.php?title=Human_skin&oldid=803585287.
281. Rittié, L. and G.J. Fisher, *Natural and Sun-Induced Aging of Human Skin.* Cold Spring Harbor Perspectives in Medicine, 2015. **5**(1).

282. Lacouture, M.E., et al., *Characterization and Management of Dermatologic Adverse Events With the NovoTTF-100A System, a Novel Anti-mitotic Electric Field Device for the Treatment of Recurrent Glioblastoma.* Seminars in Oncology, 2014. **41**(Supplement 4): p. S1-S14.
283. Babaeva, N.Y. and M.J. Kushner, *Intracellular electric fields produced by dielectric barrier discharge treatment of skin.* Journal of Physics D: Applied Physics, 2010. **43**(18): p. 185206.
284. Jatana, S. and L. Delouise, *Understanding engineered nanomaterial skin interactions and the modulatory effects of ultraviolet radiation skin exposure*. Vol. 6. 2014.
285. Kolarsick, P.A.J., M.A. Kolarsick, and C. Goodwin, *Anatomy and Physiology of the Skin.* Journal of the Dermatology Nurses' Association, 2011. **3**(4): p. 203-213.
286. Simon, J.D., et al., *Current challenges in understanding melanogenesis: bridging chemistry, biological control, morphology, and function.* Pigment Cell Melanoma Res, 2009. **22**(5): p. 563-79.
287. Yamaguchi, Y. and V.J. Hearing, *Melanocytes and their diseases.* Cold Spring Harbor perspectives in medicine. **4**(5): p. a017046.
288. Chomiczewska, D., et al., *[The role of Langerhans cells in the skin immune system]*. Pol Merkur Lekarski, 2009. **26**(153): p. 173-7.
289. Rossetti, F.b.C., L.v.V. Depieri, and M.V.r.L.B. Bentley, *Confocal Laser Scanning Microscopy as a Tool for the Investigation of Skin Drug Delivery Systems and Diagnosis of Skin Disorders*, in *Confocal Laser Microscopy - Principles and Applications in Medicine, Biology, and the Food Sciences*, N. Lagali, Editor. 2013, InTech: Rijeka. p. Ch. 06.
290. Page, E.H. *Structure and Function of the Skin*. 2017 Accessed on 03/10/2017]; Available from: http://www.msdmanuals.com/en-gb/home/skin-disorders/biology-of-the-skin/structure-and-function-of-the-skin.
291. Tipa, R.S. and G.M. Kroesen, *Plasma-stimulated wound healing.* Plasma Science, IEEE Transactions on, 2011. **39**(11): p. 2978-2979.
292. Wende, K., A. Schmidt, and S. Bekeschus, *Safety Aspects of Non-Thermal Plasmas*, in *Comprehensive Clinical Plasma Medicine*. 2018, Springer. p. 83-109.
293. Nurden, A.T., et al., *Platelets and wound healing.* Front Biosci, 2008. **13**: p. 3532-48.
294. Rodvien, R. and C.H. Mielke, Jr., *Role of platelets in hemostasis and thrombosis.* The Western journal of medicine, 1976. **125**(3): p. 181-186.
295. Greenhalgh, D.G., *The role of growth factors in wound healing.* J Trauma, 1996. **41**(1): p. 159-67.
296. de Oliveira, S., E.E. Rosowski, and A. Huttenlocher, *Neutrophil migration in infection and wound repair: going forward in reverse.* Nature reviews. Immunology, 2016. **16**(6): p. 378-391.
297. Koivisto, L., L. Häkkinen, and H. Larjava, *Re-epithelialization of wounds.* Endodontic Topics, 2011. **24**(1): p. 59-93.
298. Ramirez, H., S.B. Patel, and I. Pastar, *The Role of TGFbeta Signaling in Wound Epithelialization.* Adv Wound Care (New Rochelle), 2014. **3**(7): p. 482-491.
299. Sen, C.K., et al., *Oxidant-induced vascular endothelial growth factor expression in human keratinocytes and cutaneous wound healing.* Journal of Biological Chemistry, 2002. **277**(36): p. 33284-33290.

300. Landén, N.X., D. Li, and M. Ståhle, *Transition from inflammation to proliferation: a critical step during wound healing.* Cellular and molecular life sciences : CMLS, 2016. **73**(20): p. 3861-3885.
301. Eming, S.A., P. Martin, and M. Tomic-Canic, *Wound repair and regeneration: mechanisms, signaling, and translation.* Science translational medicine, 2014. **6**(265): p. 265sr6-265sr6.
302. Falanga, V., *Wound healing and its impairment in the diabetic foot.* The Lancet, 2005. **366**(9498): p. 1736-1743.
303. Fowler, E., *Chronic wounds: an overview.* Chronic wound care: a clinical source book for healthcare professionals, 1990: p. 12-18.
304. Siddiqui, A.R. and J.M. Bernstein, *Chronic wound infection: Facts and controversies.* Clinics in Dermatology, 2010. **28**(5): p. 519-526.
305. Trengove, N.J., et al., *Analysis of the acute and chronic wound environments: the role of proteases and their inhibitors.* Wound Repair and Regeneration, 1999. **7**(6): p. 442-452.
306. Diegelmann, R.F., *Excessive neutrophils characterize chronic pressure ulcers.* Wound Repair and Regeneration, 2003. **11**(6): p. 490-495.
307. Stojadinovic, O., et al., *Increased number of Langerhans cells in the epidermis of diabetic foot ulcers correlates with healing outcome.* Immunol Res, 2013. **57**(1-3): p. 222-8.
308. Burnand, K.G., et al., *Pericapillary fibrin in the ulcer-bearing skin of the leg: the cause of lipodermatosclerosis and venous ulceration.* Br Med J (Clin Res Ed), 1982. **285**(6348): p. 1071-2.
309. Jun, J.I. and L.F. Lau, *The matricellular protein CCN1 induces fibroblast senescence and restricts fibrosis in cutaneous wound healing.* Nat Cell Biol, 2010. **12**(7): p. 676-85.
310. Barrientos, S., et al., *Growth factors and cytokines in wound healing.* Wound Repair Regen, 2008. **16**(5): p. 585-601.
311. Nunan, R., K.G. Harding, and P. Martin, *Clinical challenges of chronic wounds: searching for an optimal animal model to recapitulate their complexity.* Disease Models & Mechanisms, 2014. **7**(11): p. 1205-1213.
312. Mast, B.A. and G.S. Schultz, *Interactions of cytokines, growth factors, and proteases in acute and chronic wounds.* Wound Repair and Regeneration, 1996. **4**(4): p. 411-420.
313. Robson, M.C., *The role of growth factors in the healing of chronic wounds.* Wound repair and regeneration, 1997. **5**(1): p. 12-17.
314. Grey, J.E., K.G. Harding, and S. Enoch, *Venous and arterial leg ulcers.* BmJ, 2006. **332**(7537): p. 347-350.
315. Jeffcoate, W.J. and K.G. Harding, *Diabetic foot ulcers.* The lancet, 2003. **361**(9368): p. 1545-1551.
316. Grey, J.E., K.G. Harding, and S. Enoch, *ABC of wound healing: pressure ulcers.* BMJ: British Medical Journal, 2006. **332**(7539): p. 472.
317. Barwell, J.R., et al., *Comparison of surgery and compression with compression alone in chronic venous ulceration (ESCHAR study): randomised controlled trial.* The Lancet, 2004. **363**(9424): p. 1854-1859.
318. Xia, Y.-P., et al., *Differential activation of migration by hypoxia in keratinocytes isolated from donors of increasing age: implication for chronic wounds in the elderly.* Journal of investigative dermatology, 2001. **116**(1): p. 50-56.

319. Wu, L., et al., *Transforming growth factor-beta1 fails to stimulate wound healing and impairs its signal transduction in an aged ischemic ulcer model: importance of oxygen and age.* Am J Pathol, 1999. **154**(1): p. 301-9.
320. Brucker, M.J., et al., *Differential expression of platelet-derived growth factor receptor-β in an aging model of wound repair.* Wound Repair and Regeneration, 1996. **4**(2): p. 219-223.
321. Siddiqui, A., et al., *Differential effects of oxygen on human dermal fibroblasts: acute versus chronic hypoxia.* Wound Repair and Regeneration, 1996. **4**(2): p. 211-218.
322. André-Lévigne, D., et al., *Reactive Oxygen Species and NOX Enzymes Are Emerging as Key Players in Cutaneous Wound Repair.* International Journal of Molecular Sciences, 2017. **18**(10): p. 2149.
323. Tandara, A.A. and T.A. Mustoe, *Oxygen in wound healing—more than a nutrient.* World journal of surgery, 2004. **28**(3): p. 294-300.
324. Dunnill, C., et al., *Reactive oxygen species (ROS) and wound healing: the functional role of ROS and emerging ROS-modulating technologies for augmentation of the healing process.* International Wound Journal, 2017. **14**(1): p. 89-96.
325. Sen, C.K. and S. Roy, *Redox signals in wound healing.* Biochimica et Biophysica Acta (BBA) - General Subjects, 2008. **1780**(11): p. 1348-1361.
326. Novo, E. and M. Parola, *Redox mechanisms in hepatic chronic wound healing and fibrogenesis.* Fibrogenesis & Tissue Repair, 2008. **1**(1): p. 5.
327. Sen, C.K., *The general case for redox control of wound repair.* Wound Repair and Regeneration, 2003. **11**(6): p. 431-438.
328. Görlach, A., *Redox regulation of the coagulation cascade.* Antioxidants & redox signaling, 2005. **7**(9-10): p. 1398-1404.
329. Herkert, O., et al., *Insights into the redox control of blood coagulation: role of vascular NADPH oxidase-derived reactive oxygen species in the thrombogenic cycle.* Antioxid Redox Signal, 2004. **6**(4): p. 765-76.
330. Essex, D.W. and M. Li, *Redox control of platelet aggregation.* Biochemistry, 2003. **42**(1): p. 129-36.
331. Piette, J., et al., *Multiple redox regulation in NF-kappaB transcription factor activation.* Biol Chem, 1997. **378**(11): p. 1237-45.
332. Clancy, R.M., P.F. Gomez, and S.B. Abramson, *Nitric oxide sustains nuclear factor kappaB activation in cytokine-stimulated chondrocytes.* Osteoarthritis and Cartilage, 2004. **12**(7): p. 552-558.
333. Goldkorn, T., et al., *EGF-Receptor phosphorylation and signaling are targeted by H2O2 redox stress.* Am J Respir Cell Mol Biol, 1998. **19**(5): p. 786-98.
334. Maulik, N., *Redox regulation of vascular angiogenesis.* Antioxid Redox Signal, 2002. **4**(5): p. 783-4.
335. Hunt, T.K., et al., *Aerobically derived lactate stimulates revascularization and tissue repair via redox mechanisms.* Antioxid Redox Signal, 2007. **9**(8): p. 1115-24.
336. Gregg, D., D.D. de Carvalho, and H. Kovacic, *Integrins and coagulation: a role for ROS/redox signaling?* Antioxidants and Redox Signaling, 2004. **6**(4): p. 757-764.
337. Herkert, O., et al., *NADPH oxidase mediates tissue factor–dependent surface procoagulant activity by thrombin in human vascular smooth muscle cells.* Circulation, 2002. **105**(17): p. 2030-2036.

338. Krötz, F., et al., *NAD (P) H oxidase–dependent platelet superoxide anion release increases platelet recruitment.* Blood, 2002. **100**(3): p. 917-924.
339. Sundaresan, M., et al., *Requirement for generation of H2O2 for platelet-derived growth factor signal transduction.* Science, 1995. **270**(5234): p. 296-299.
340. Marumo, T., et al., *Platelet-derived growth factor-stimulated superoxide anion production modulates activation of transcription factor NF-kappaB and expression of monocyte chemoattractant protein 1 in human aortic smooth muscle cells.* Circulation, 1997. **96**(7): p. 2361-7.
341. Riddell, D.R. and J.S. Owen, *Nitric oxide and platelet aggregation.* Vitam Horm, 1999. **57**: p. 25-48.
342. Rizk, M., M.B. Witte, and A. Barbul, *Nitric Oxide and Wound Healing.* World Journal of Surgery, 2004. **28**(3): p. 301-306.
343. Soneja, A., M. Drews, and T. Malinski, *Role of nitric oxide, nitroxidative and oxidative stress in wound healing.* Pharmacological reports, 2005. **57 Suppl**: p. 108-19.
344. Luo, J.-d. and A.F. Chen, *Nitric oxide: a newly discovered function on wound healing.* Acta Pharmacologica Sinica, 2005. **26**: p. 259.
345. Childress, B.B. and J.K. Stechmiller, *Role of Nitric Oxide in Wound Healing.* Biological Research For Nursing, 2002. **4**(1): p. 5-15.
346. Yoon, S.-O., et al., *Sustained Production of H2O2Activates Pro-matrix Metalloproteinase-2 through Receptor Tyrosine Kinases/Phosphatidylinositol 3-Kinase/NF-κB Pathway.* Journal of Biological Chemistry, 2002. **277**(33): p. 30271-30282.
347. Peus, D., et al., *H2O2 is an important mediator of UVB-induced EGF-receptor phosphorylation in cultured keratinocytes.* Journal of Investigative Dermatology, 1998. **110**(6): p. 966-971.
348. Frank, S., et al., *Nitric oxide triggers enhanced induction of vascular endothelial growth factor expression in cultured keratinocytes (HaCaT) and during cutaneous wound repair.* FASEB J., 1999. **13**(14): p. 2002-14.
349. Lee, K.S., et al., *Hydrogen peroxide induces vascular permeability via regulation of vascular endothelial growth factor.* American journal of respiratory cell and molecular biology, 2006. **35**(2): p. 190-7.
350. Vivekananda, J., et al., *Acute inflammatory injury in the lung precipitated by oxidant stress induces fibroblasts to synthesize and release transforming growth factor-alpha.* Journal of Biological Chemistry, 1994. **269**(40): p. 25057-25061.
351. Thornton, F.J., et al., *Enhanced Collagen Accumulation Following Direct Transfection of the Inducible Nitric Oxide Synthase Gene in Cutaneous Wounds.* Biochemical and Biophysical Research Communications, 1998. **246**(3): p. 654-659.
352. Nath, K.A., et al., *Redox regulation of renal DNA synthesis, transforming growth factor-β1 and collagen gene expression.* Kidney international, 1998. **53**(2): p. 367-381.
353. Shah, J.B., *The History of Wound Care.* The Journal of the American College of Certified Wound Specialists, 2011. **3**(3): p. 65-66.
354. Bhattacharya, S., *Wound healing through the ages.* Indian Journal of Plastic Surgery : Official Publication of the Association of Plastic Surgeons of India, 2012. **45**(2): p. 177-179.
355. Hobson, D.W., et al., *The First Cut Is the Deepest:The History and Development of Safe Treatments for Wound Healing and Tissue Repair.* International Journal of Toxicology, 2016. **35**(5): p. 491-498.

356. Cohen, I., *A brief history of wound healing.* Yardley, Pa: Oxford Clinical Communications Inc, 1998.
357. Broughton, G., 2nd, J.E. Janis, and C.E. Attinger, *A brief history of wound care.* Plast Reconstr Surg, 2006. **117**(7 Suppl): p. 6s-11s.
358. Tauber, A.I., *Metchnikoff and the phagocytosis theory.* Nature Reviews Molecular Cell Biology, 2003. **4**: p. 897.
359. Winter, G.D., *Formation of the Scab and the Rate of Epithelization of Superficial Wounds in the Skin of the Young Domestic Pig.* Nature, 1962. **193**: p. 293.
360. Hinman, C.D. and H. Maibach, *Effect of Air Exposure and Occlusion on Experimental Human Skin Wounds.* Nature, 1963. **200**: p. 377.
361. Spear, M., *Wet-to-dry dressings-evaluating the evidence.* Plast Surg Nurs, 2008. **28**(2): p. 92-5.
362. Han, G. and R. Ceilley, *Chronic Wound Healing: A Review of Current Management and Treatments.* Advances in therapy, 2017. **34**(3): p. 599-610.
363. Sarabahi, S., *Recent advances in topical wound care.* Indian Journal of Plastic Surgery : Official Publication of the Association of Plastic Surgeons of India, 2012. **45**(2): p. 379-387.
364. Fife, C. and D. Weir, *The challenges of negative pressure wound therapy in clinical practice.* Today's Wound Clinic, 2010. **4**(6).
365. Frykberg, R.G. and J. Banks, *Challenges in the Treatment of Chronic Wounds.* Advances in wound care, 2015. **4**(9): p. 560-582.
366. Kirby, M., *Negative pressure wound therapy.* The British Journal of Diabetes & Vascular Disease, 2007. **7**(5): p. 230-234.
367. Rizzi, S.C., et al., *Recent advances in dermal wound healing: biomedical device approaches.* Expert Review of Medical Devices, 2010. **7**(1): p. 143-154.
368. Hunt, T.K., B. Zederfeldt, and T.K. Goldstick, *Oxygen and healing.* Am J Surg, 1969. **118**(4): p. 521-5.
369. MacKay, D. and A.L. Miller, *Nutritional support for wound healing.* Altern Med Rev, 2003. **8**(4): p. 359-77.
370. Baumann, L.S. and J. Spencer, *The effects of topical vitamin E on the cosmetic appearance of scars.* Dermatol Surg, 1999. **25**(4): p. 311-5.
371. Steiling, H., et al., *Different Types of ROS-Scavenging Enzymes Are Expressed during Cutaneous Wound Repair.* Experimental Cell Research, 1999. **247**(2): p. 484-494.
372. Guo, S. and L.A. DiPietro, *Factors Affecting Wound Healing.* Journal of Dental Research, 2010. **89**(3): p. 219-229.
373. Devasagayam, T., et al., *Free radicals and antioxidants in human health: current status and future prospects.* Japi, 2004. **52**(794804): p. 4.
374. Fernandez, M.L., et al., *Elevated uric acid correlates with wound severity.* International wound journal, 2012. **9**(2): p. 139-149.
375. Tur, E., L. Bolton, and B.E. Constantine, *Topical hydrogen peroxide treatment of ischemic ulcers in the guinea pig: blood recruitment in multiple skin sites.* Journal of the American Academy of Dermatology, 1995. **33**(2): p. 217-221.
376. Galbusera, C., et al., *Superoxide radical production by allopurinol and xanthine oxidase.* Biochemical Pharmacology, 2006. **71**(12): p. 1747-1752.
377. Weller, R. and M.J. Finnen, *The effects of topical treatment with acidified nitrite on wound healing in normal and diabetic mice.* Nitric Oxide, 2006. **15**(4): p. 395-399.

378. Phillips, R., et al., *Pilot Randomized Double-Blind Trial of Treatment of Mycobacterium ulcerans Disease (Buruli Ulcer) with Topical Nitrogen Oxides.* Antimicrobial Agents and Chemotherapy, 2004. **48**(8): p. 2866-2870.
379. Lau, W.Y. and S.H. Wong, *Randomized, prospective trial of topical hydrogen peroxide in appendectomy wound infection.* The American Journal of Surgery, 1981. **142**(3): p. 393-397.
380. Leyden, J.J. and N.M. Bartelt, *Comparison of topical antibiotic ointments, a wound protectant, and antiseptics for the treatment of human blister wounds contaminated with Staphylococcus aureus.* The Journal of family practice, 1987. **24**(6): p. 601-604.
381. Pham, C., et al., *Bioengineered skin substitutes for the management of burns: a systematic review.* Burns, 2007. **33**(8): p. 946-57.
382. Falanga, V., et al., *Rapid healing of venous ulcers and lack of clinical rejection with an allogeneic cultured human skin equivalent. Human Skin Equivalent Investigators Group.* Arch Dermatol, 1998. **134**(3): p. 293-300.
383. Landsman, A.S., et al., *A retrospective clinical study of 188 consecutive patients to examine the effectiveness of a biologically active cryopreserved human skin allograft (TheraSkin(R)) on the treatment of diabetic foot ulcers and venous leg ulcers.* Foot Ankle Spec, 2011. **4**(1): p. 29-41.
384. Hansen, S.L., et al., *Using skin replacement products to treat burns and wounds.* Adv Skin Wound Care, 2001. **14**(1): p. 37-44; quiz 45-6.
385. Moustafa, M., et al., *Randomized, controlled, single-blind study on use of autologous keratinocytes on a transfer dressing to treat nonhealing diabetic ulcers.* 2007.
386. Haddow, D.B., et al., *Plasma-polymerized surfaces for culture of human keratinocytes and transfer of cells to an in vitro wound-bed model.* Journal of Biomedical Materials Research Part A, 2003. **64A**(1): p. 80-87.
387. Leibovitch, I., et al., *Incidence of host site complications in periocular full thickness skin grafts.* British Journal of Ophthalmology, 2005. **89**(2): p. 219-222.
388. Reddy, S., et al., *The Incidence and Risk Factors for Lower Limb Skin Graft Failure.* Dermatology Research and Practice, 2014. **2014**: p. 3.
389. Pacella, R., *Chronic Wounds in Australia.* 2017.
390. Graves, N. and H. Zheng, *Modelling the direct health care costs of chronic wounds in Australia*. Vol. 22. 2014. 20-33.
391. Norman, R.E., et al., *Improved wound management at lower cost: a sensible goal for Australia.* Int Wound J, 2016. **13**(3): p. 303-16.
392. Santamaria, N., D. Austin, and L. Clayton, *A multi-site clinical evaluation trial of the Alfred/Medseed Wound Imaging System prototype.* Primary Intention: The Australian Journal of Wound Management, 2002. **10**(3): p. 120.
393. Singh, N., D.G. Armstrong, and B.A. Lipsky, *Preventing foot ulcers in patients with diabetes.* Jama, 2005. **293**(2): p. 217-228.
394. Kumar, S., et al., *The prevalence of foot ulceration and its correlates in type 2 diabetic patients: a population-based study.* Diabet Med, 1994. **11**(5): p. 480-4.
395. Gould, L.J., *Wound healing in older adults.* Rhode Island Medical Journal, 2016. **99**(2): p. 34.
396. Wicke, C., et al., *Aging influences wound healing in patients with chronic lower extremity wounds treated in a specialized wound care center.* Wound Repair and Regeneration, 2009. **17**(1): p. 25-33.

397. Gould, L., et al., *Chronic wound repair and healing in older adults: Current status and future research.* Wound Repair and Regeneration, 2015. **23**(1): p. 1-13.
398. *Diabetes in North America: millions of feet at risk of amputations.* in *65th Annual Sessions of the American Diabetes Association*. 2005. San Diego: International Diabetes Federation.
399. Sen, C.K., et al., *Human skin wounds: a major and snowballing threat to public health and the economy.* Wound Repair Regen, 2009. **17**(6): p. 763-71.
400. Lindholm, C. and R. Searle, *Wound management for the 21st century: combining effectiveness and efficiency.* International Wound Journal, 2016. **13**(S2): p. 5-15.
401. Choi, J.H., et al., *Treatment with low-temperature atmospheric pressure plasma enhances cutaneous delivery of epidermal growth factor by regulating E-cadherin-mediated cell junctions.* Arch Dermatol Res, 2014. **306**(7): p. 635-43.
402. Izadjoo, M., et al., *Medical applications of cold atmospheric plasma: state of the science.* Journal of Wound Care, 2018. **27**(Sup9): p. S4-S10.
403. Schmidt, A., et al., *A cold plasma jet accelerates wound healing in a murine model of full-thickness skin wounds.* Experimental Dermatology, 2017. **26**(2): p. 156-162.
404. García-Alcantara, E., et al., *Accelerated Mice Skin Acute Wound Healing In Vivo by Combined Treatment of Argon and Helium Plasma Needle.* Archives of Medical Research, 2013. **44**(3): p. 169-177.
405. Ermolaeva, S.A., et al., *Bactericidal effects of non-thermal argon plasma in vitro, in biofilms and in the animal model of infected wounds.* J Med Microbiol, 2011. **60**(Pt 1): p. 75-83.
406. Yoon, S.-Y., et al., *Effects of metastable species in helium and argon atmospheric pressure plasma jets (APPJs) on inactivation of periodontopathogenic bacteria.* Journal of the Korean Physical Society, 2016. **68**(10): p. 1176-1191.
407. Lackmann, J.W. and J.E. Bandow, *Inactivation of microbes and macromolecules by atmospheric-pressure plasma jets.* Appl Microbiol Biotechnol, 2014. **98**(14): p. 6205-13.
408. Sun, P., et al., *Atmospheric pressure cold plasma as an antifungal therapy.* Applied Physics Letters, 2011. **98**(2): p. 021501.
409. T Nosenko, T.S.a.G.E.M., *Designing plasmas for chronic wound disinfection.* New J. Phys., 2009. **11**: p. 115013.
410. Xu, G.M., et al., *Dual effects of atmospheric pressure plasma jet on skin wound healing of mice.* Wound Repair and Regeneration, 2015. **23**(6): p. 878-884.
411. Yu, Y., et al., *Non-thermal plasma suppresses bacterial colonization on skin wound and promotes wound healing in mice.* Journal of Huazhong University of Science and Technology [Medical Sciences], 2011. **31**(3): p. 390-394.
412. Fathollah, S., et al., *Investigation on the effects of the atmospheric pressure plasma on wound healing in diabetic rats.* Scientific Reports, 2016. **6**: p. 19144.
413. Miller, V., et al., *Plasma stimulation of migration of macrophages.* Plasma Processes and Polymers, 2014. **11**(12): p. 1193-1197.
414. Ngo Thi, M.-H., et al., *Enhancement of Angiogenesis and Epithelialization Processes in Mice with Burn Wounds through ROS/RNS Signals Generated by Non-Thermal N2/Ar Micro-Plasma.* Plasma Processes and Polymers, 2014. **11**(11): p. 1076-1088.

415. Arndt, S., et al., *Cold Atmospheric Plasma (CAP) Changes Gene Expression of Key Molecules of the Wound Healing Machinery and Improves Wound Healing In Vitro and In Vivo.* PLOS ONE, 2013. **8**(11): p. e79325.
416. Arndt, S., et al., *Effects of Cold Atmospheric Plasma (CAP) on ß-Defensins, Inflammatory Cytokines, and Apoptosis-Related Molecules in Keratinocytes In Vitro and In Vivo.* PLOS ONE, 2015. **10**(3): p. e0120041.
417. Haertel, B., et al., *Differential influence of components resulting from atmospheric-pressure plasma on integrin expression of human HaCaT keratinocytes.* Biomed Res Int, 2013. **2013**: p. 761451.
418. Kalghatgi, S., et al., *Endothelial cell proliferation is enhanced by low dose non-thermal plasma through fibroblast growth factor-2 release.* Annals of biomedical engineering, 2010. **38**(3): p. 748-57.
419. Klebes, M., et al., *Combined antibacterial effects of tissue-tolerable plasma and a modern conventional liquid antiseptic on chronic wound treatment.* Journal of Biophotonics, 2015. **8**(5): p. 382-391.
420. Ulrich, C., et al., *Clinical use of cold atmospheric pressure argon plasma in chronic leg ulcers: A pilot study.* J Wound Care, 2015. **24**(5): p. 196, 198-200, 202-3.
421. Lademann, J., et al. *Application of tissue-tolerable plasma in dermatology: risk assessment and prospects (oral presentation).* in *Fifth International Conference on Plasma Medicine, ICPM5*. 2014. Nara, Japan.

Chapter 2 Analysis of the plasma generation of RONS in biologically-relevant liquids

RONS are considered pertinent to major cellular signaling and physiological processes [1] such as redox homeostasis [2], signal transduction through membrane receptors [3], vascular tone regulation (smooth muscle relaxation) [4], inhibition of platelet adhesion [5], production of inflammatory cells [6], cell adhesion [7], angiogenesis [8], and apoptosis [9]. In the context of wounds, H_2O_2 and NO are thought to have an important role in regulating the healing response [4, 10-18].

With highest concentrations found in wound fluids [19], H_2O_2 is thought to have a prominent role in wound disinfection and closure [10, 20-23]. During the inflammatory phase, neutrophils and macrophages produce H_2O_2, which prevents bacterial infection in wounds [24]. H_2O_2 acts as a secondary messenger and induces growth factors such as PDGF and VEGF [23, 25]. This is important for angiogenesis and re-epithelization [26, 27]. Removal of H_2O_2 using enzymes (e.g. catalase) has shown to impair wound healing by inhibiting angiogenesis and collagen proliferation [20, 28].

Owing to its presence in all phases of wound healing, NO is arguably the most significant RONS in wound healing [8, 19, 29-32]. NO is produced by macrophages in the inflammatory stage for up to 10 days [31, 33], playing a role as an anti-microbial [34] and vasodilator [30] in wound healing. NO also acts as a secondary messenger and stimulates VEGF, thus promoting angiogenesis [15]. NO is essential for collagen synthesis in fibroblasts and for the proliferation of keratinocytes which are important for wound closure and tissue remodeling [4, 29, 35].

Topical treatments of wounds using H_2O_2 and NO-generating systems or donors are standard methods to promote wound healing. Solutions of H_2O_2 (1-3%) are popular tools for eliminating bacterial colonization in wounds [36-39]. Bacterial and fungal disinfection and vasodilation can also be achieved using topical nitrite creams [40-42]. NO and its donors incorporated within hydrogel dressings and polymeric films have shown to promote collagen deposition and enhance wound closure [43-45]. Application of NO gas has also been used successfully for wound disinfection and for accelerating healing [46, 47]. Plasma, being a rich source of H_2O_2 and NO, is being explored as a

wound decontamination and healing therapy [16, 46, 48-59]. The inactivation of antibiotic-resistant bacteria and subsequent acceleration in the wound closure rate has been demonstrated *in vivo* and in randomized clinical trials [51, 54, 59-63].

Due to their pleiotropic nature, interactions of RONS with tissues (and cells) are very complex. The pathological effects of RONS in cells depends on the location of RONS production, type of RONS generated and the concentration of each type of RONS [1, 57, 64, 65]. For example, at a relatively low concentration of 10µM, H_2O_2 enhances neutrophil motility [66] and skin cell proliferation [67, 68]. At slightly higher concentrations of 0.1-0.5 mM, H_2O_2 can stimulate an inflammatory response and angiogenesis. However, overexpression of H_2O_2 at 50 mM is detrimental to wound closure [28]. Thomas *et al.* investigated NO activity at various concentrations and elucidated that in the nM range, NO can promote protective mechanisms in cells and proliferation [64]. However, at a higher concentration of 1 µM, it leads to nitrosative stress causing cell cycle arrest and apoptosis [65]. Therefore, maintaining a redox balance (homeostasis) is critical to any redox-based wound healing therapy, including plasma treatments.

Plasma treatment of tissues and tissue fluids generates different types of RONS such as $O_2^{\bullet-}$, OH•, HOO•, $ONOO^-$ and NO. The highly reactive and shorter-lived species such as $O_2^{\bullet-}$ (half-life < 10 s) and NO (half-life < 30s) rapidly decay and are converted to more stable longer-lived redox products H_2O_2, NO_3^-, and NO_2^- as per reactions below [52, 69-72]:

$$2O_2^{\bullet-} + 2H^+ \rightarrow H_2O_2 + O_2$$

$$2NO + O_2 \rightarrow N_2O_4 \xrightarrow{H_2O} NO_2^- + NO_3^- + 2H^+$$

This chapter focuses on the plasma-generation of H_2O_2 and NO_2^- in models of tissue fluids. However, later in the thesis (Chapter 3), the detection of NO_3^- is the subject of the development of UVAS to monitor RONS.

H_2O_2 is the major component of wound fluids as compared to any other bodily fluids [28, 73], and its significance in wound healing has been discussed earlier in this chapter. Owing to its short half-life, assessment of NO is usually performed 'indirectly' by measuring its downstream product NO_2^-. Studies have shown that NO_2^- is also an important molecule in wound healing. For example, it is expressed in macrophages

during the inflammatory phase [74]. It also promotes wound healing, especially in ischemic (hypoxic) tissues by stimulating NO production and vasodilation [75, 76].

Plasma is also applied for wound disinfection and to prevent biofilm formation due to its anti-microbial property [77-79]. For instance, the plasma treated solutions such as water or DMEM have shown the potential to reduce the bacterial load and remove biofilms [80-82]. The plasma treatment of aqueous solutions leads to a drastic reduction in pH levels via formation of nitrous acid (HNO_2) and nitric acid (HNO_3) from NO and the hydronium ion (H_3O^+) from H_2O_2 [83]. In an acidic environment, H_2O_2 and NO species react synergistically to form $ONOO^-$, which is also significant in the anti-bacterial action of plasma [84]. It should be noted that the reactions between the ROS and RNS are post-discharge reactions and contribute in the prolonged therapeutic (anti-microbial) effects of plasma treated solutions.

Measuring concentrations of H_2O_2 and NO_2^- delivered by a plasma jet is essential to fully understand the redox biology governing plasma jet treatment of tissues, determine *safe* doses, and ultimately design plasma jets suitable for wound healing. This can be achieved by establishing probes to detect the concentrations of H_2O_2 and NO_2^-, both *in vitro* and *in vivo*.

A "good" probe has the following characteristics:

i. High selectivity and specificity towards a specific type of RONS;

ii. High sensitivity with a low signal-to-noise ratio. A broad detection range (nM to mM) is important because plasma devices can generate RONS over this wide concentration range. Furthermore, it is necessary to measure RONS over a broad range with high sensitivity to ensure high enough concentrations of RONS are delivered to induce wound healing, and to avoid delivering too higher concentrations that can have detrimental effects on tissue [8, 21];

iii. Stability against external environmental factors such as light, pH and temperature;

iv. Easy to prepare and employ over a wide range of experimental conditions; and

v. Non-toxic to cells for assessing RONS chemistry in cell cultures.

There are different types of RONS detection probes available including spectroscopic probes based on fluorescence, luminescence and absorbance, electrochemical sensors, electron spin resonance, mass spectrometry, etc. This chapter focuses on two types of RONS probes – small molecule probes and amperometric sensors. Molecular probes include fluorescent and colorimetric dyes (Section 2.1), and amperometric sensors includes membrane-based electrochemical sensors (Section 2.2).

The exact mechanisms of how plasma-generated RONS traverse the atmosphere (liquid)/tissue interface and through a "bulk" (hydrated) tissue are yet to be elucidated; however, a number of recent studies have highlighted the potential synergistic role of electric fields and cell-to-cell communication in this context [52, 85-91]). After crossing the tissue barrier, plasma delivered RONS interact with tissue fluid and other biomolecules such as fluid proteins. The RONS ultimately reach cells and inside cellular components such as DNA, which are also dispersed within a (cytoplasmic) fluid. A common element in the interaction of plasma with the physiological environment is tissue fluid. Therefore, determining the nature of RONS reactions prevailing in tissue fluid is a vital step which can be achieved by accurate identification and quantification of RONS delivered by plasma jet in tissues and cells.

In this chapter, tissue fluid models were utilized to study the influence of the fluid itself, fluid proteins and other fluid components in RONS generation. Biologically relevant aqueous solutions were chosen as candidates for tissue fluid. The simplest tissue fluid mimics were water and phosphate buffer saline (PBS) solution. Water is not only important because the human body is made of approximately 65% of water by weight [92], but also because most wound fluids contain 93% water [93]. PBS was used to match the ionic concentrations and pH of tissue fluid. In addition, Dulbecco's Modified Eagle Medium (DMEM) was investigated because it is a widely used growth medium for mammalian cells *in vitro*. DMEM has a very complex composition rich in vitamins, amino acids, media supplements, glucose, salts, and antibiotics. Table 2.1 lists the composition of each tissue fluid model investigated in this chapter. These three tissue models were chosen because the complexity in the composition varied from simple (water) to moderate (PBS) to high (DMEM).

Table 2.1 Composition of various biologically relevant solutions used as tissue models – water being the simplest solution and DMEM being the most complex.

Water	**PBS**	**DMEM**
Water	0.01 M or 1 X PBS solution contains: 2.7 mM potassium chloride, 137 mM sodium chloride, 8.0 mM sodium phosphate, 8.0 mM potassium phosphate Prepared in water.	Amino acids: 0.4 mM Glycine, 0.4 mM L- arginine hydrochloride, 0.2 mM L- cysteine hydrochloride, 4.0 mM L- glutamine, 0.2 mM L-histidine hydrochloride, 0.8 mM L-isoleucine, 0.8 mM L-leucine, 0.8 mM L-lysine hydrochloride, 0.2 mM L-methionine, 0.4 mM L-phenylamine, 0.4 mM L-serine, 0.8 mM L-theonine, 0.8 mM L-tryptophan, 0.4 mM L-tyrosine disodium salt dihydrate, 0.8 mM L-valine, Vitamins: 0.03 mM choline chloride, 0.01 mM calcium pantothenate, 0.01 mM folic acid, 0.03 mM niacinamide, 0.02 mM pyridoxine hydrochloride, 0.001 mM riboflavin, 0.01 mM thiamine hydrochloride, 0.04 mM inositol Inorganic salts: 1.8 mM calcium chloride,

		2.4 x 10^{-4} mM ferric nitrate, 0.8 mM magnesium sulfate, 5.3 mM potassium chloride, 44 mM sodium bicarbonate, 110 mM sodium chloride, 0.9 mM sodium phosphate Other components: 0.04 mM phenol red Prepared in water.

2.1 Small molecule probes to measure RONS in solution

Small molecule probes are vital tools to monitor the RONS delivered by plasma in solution. Two types of small molecule probes are commonly used for RONS detection – fluorescent probes and colourimetric probes (Figure 2.1) [94, 95].

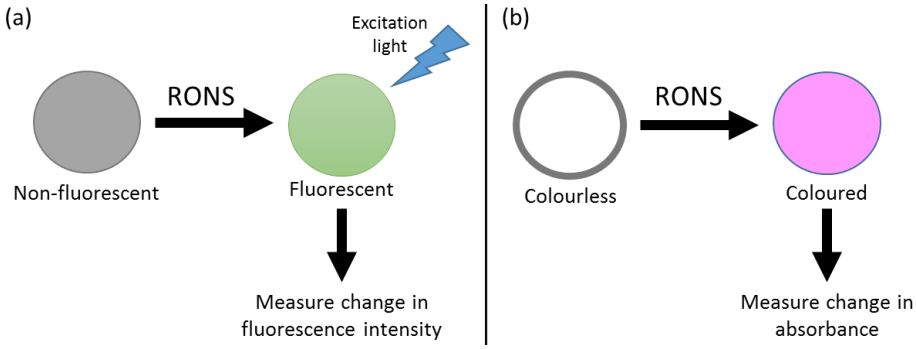


Figure 2.1 An illustration of the working principle of a (a) fluorescent assay and (b) colourimetric assay.

For this study, three types of molecular probes are used:

i. Dichlorodihydrofluorescein (DCFH) for detecting a broad range of RONS;

ii. o-Phenylenediamine dihydrochloride–horseradish peroxidase (OPD-HRP) to detect H_2O_2; and

iii. Griess reagent to detect NO_2^-.

Developed more than 45 years ago and used in over 2000 research studies, DCFH is arguably the most popular probe for detecting RONS both *in vitro* and *in vivo* [96-98]. Non-fluorescent DCFH molecule reacts with a wide range of RONS to form a fluorescent compound DCF (Figure 2.2).

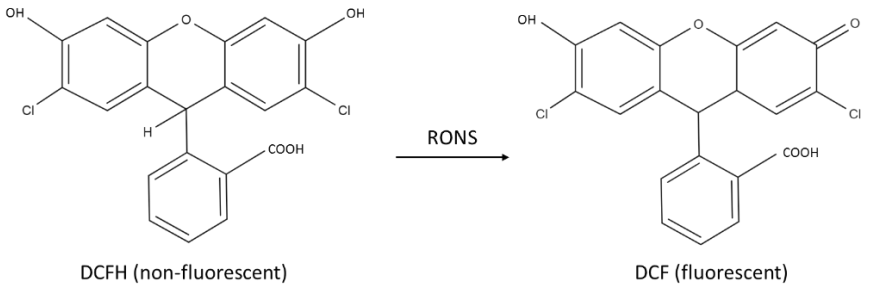


Figure 2.2 Reaction illustrating conversion of non-fluorescent DCFH into highly fluorescent DCF upon interaction with RONS.

DCFH can react with many different molecules/agents such as H_2O_2, NO_2^-, OH•, HOCl, $ONOO^-$, carbonate ion ($CO_3^{\bullet-}$), redox active metals such as ferrous ion (Fe^{+2}) and the thiyl radical (HS•) [97, 99-101]. A challenge associated with DCFH is 'artefactual amplification' in fluorescence intensity (Figure 2.3). For instance, $O_2^{\bullet-}$ and H_2O_2 are common by-products in the DCFH oxidation reaction, and these molecules further oxidise DCFH leading to a "falsely" amplified fluorescence signal [102]. Photo-excitation of DCF to DCF* can lead to oxidation of thiols to HS• radicals, which can also oxidise DCFH [97]. Thiyl radicals in presence of O_2 can produce H_2O_2 [103]. The above by-products can falsely lead to an overestimation of the initial RONS present in the solution if the data is not compared to appropriate calibrations and controls.

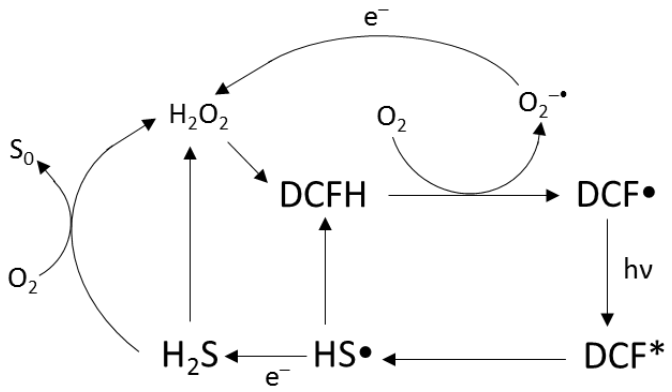


Figure 2.3 Reactions illustrating the production of $O_2^{\bullet-}$, H_2O_2 and HS• during oxidation of DCFH to DCF.

OPD-HRP and Griess reagent have been used to quantify the plasma jet delivery of H_2O_2 and NO_2^-, respectively [90, 104-106]. The colourless OPD substrate undergoes a HRP-catalysed oxidation in presence of H_2O_2 to form a yellow colored product 2,3-diaminophenazine (DAP) with an absorption maximum of 450 nm [107-110]. The enzymatic reaction between OPD-HRP and H_2O_2 occurs in two steps – (i) the formation of an intermediate compound, and (ii) the intermediate compound forms a yellow product DAP (Figure 2.4).

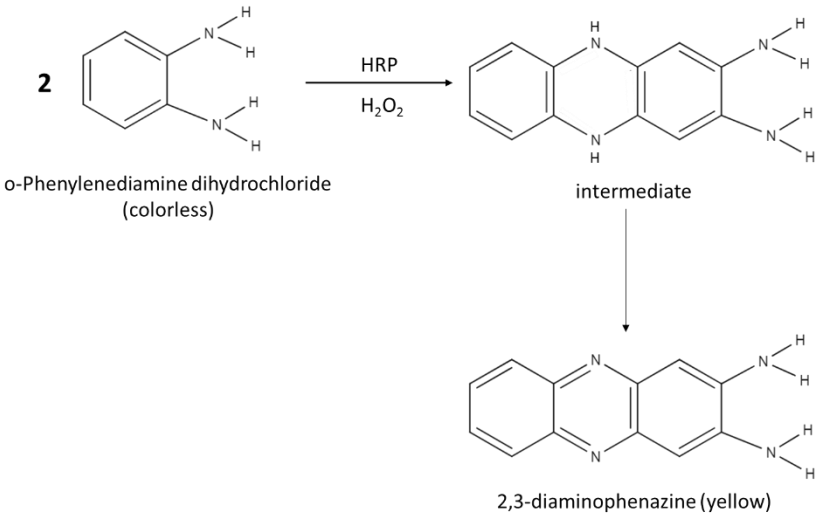
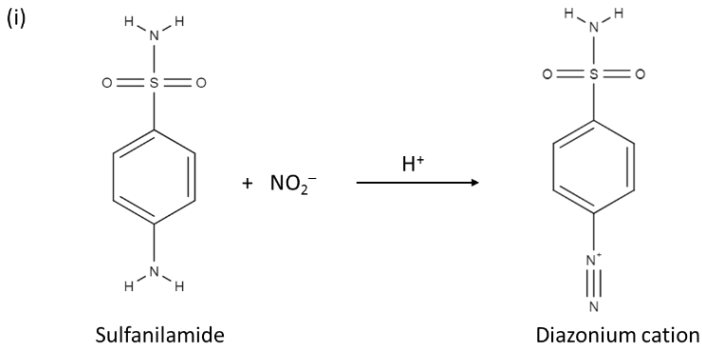


Figure 2.4 Reaction illustrating the conversion of the colourless OPD into a yellow product DAP upon oxidation with H_2O_2.

Griess reagent is used to monitor NO_2^- production in solution (Figure 2.5). The assay involves two-steps – (i) diazotization of sulfanilamide by NO_2^- and (ii) coupling of diazonium cation with N-(1-naphthyl)ethylenediamine to form a pink azo-dye compound with an absorption maximum of 548 nm [111]. Griess reagent can be used as a method for the indirect detection of NO because auto-oxidation of NO generates NO_2^- and NO_3^- as the stable end-products [112]. To measure total NO production, NO_3^- ions must be reduced to NO_2^-. This can be achieved by using enzymes such as NO_3^- reductase or chemical agents such as cadmium and vanadium chloride [95]. However, NO_3^- reductase enzymes and chemicals have been reported to interfere with the diazotization process [95, 113], and may require further research, which is out of the scope for this study. NO_3^- is likely to be reduced to NO_2^- via UV photolysis (UV is an integral component of plasma) [114-117]. Therefore, NO_2^- quantification is the focus of this study and acknowledging it as an indirect marker of NO production.



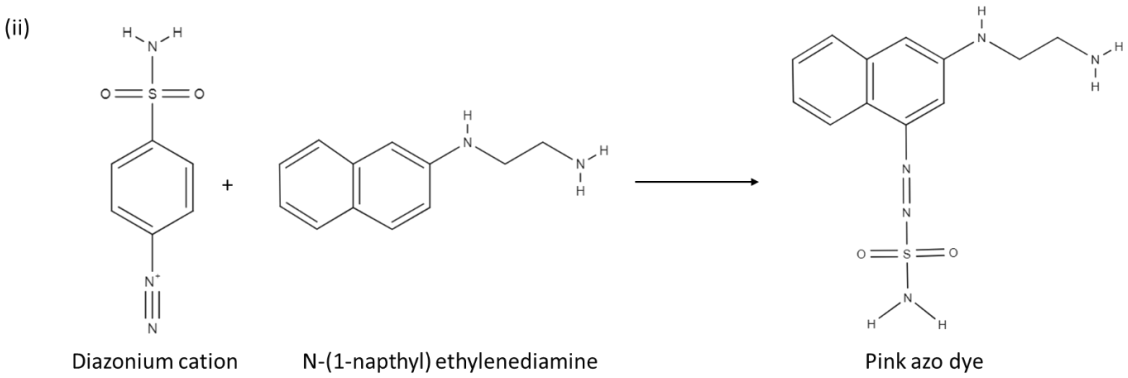


Figure 2.5 Reaction illustrating two-step conversion of colourless Griess reagent to a pink colored azo dye upon interaction with NO_2^-. Step one is the formation of diazonium cation from sulfanilamide and step two involves the coupling of the cation with N-(1-naphthyl)ethylenediamine to form a stable pink azo dye.

2.1.1 Materials and Methods

2.1.1.1 Plasma jet

The plasma jet used in this study is a single electrode system operable at atmospheric pressure [105, 106, 118, 119]. It consists of a hollow glass tube, with an outer diameter of 6 mm and an inner diameter of 4 mm. The tube is surrounded by a 15 mm long copper electrode; 40 mm away from the end of the tube. Helium gas (BOC, high purity grade) is purged into the glass tube. The gas flow is controlled using a digital mass flow controller (Apex, 0–2 slpm flow range) at a flow rate of 0.5 standard litres per minute (slpm). A PVM500 power supply (Information Unlimited) was utilised to apply a voltage of 10 kV_{p-p} (peak-to-peak) at 30 kHz. Figure 2.6 illustrates a schematic and a photograph of the He plasma jet assembly. To shield the high voltage electrode, a 10 mm thick PTFE housing was used.

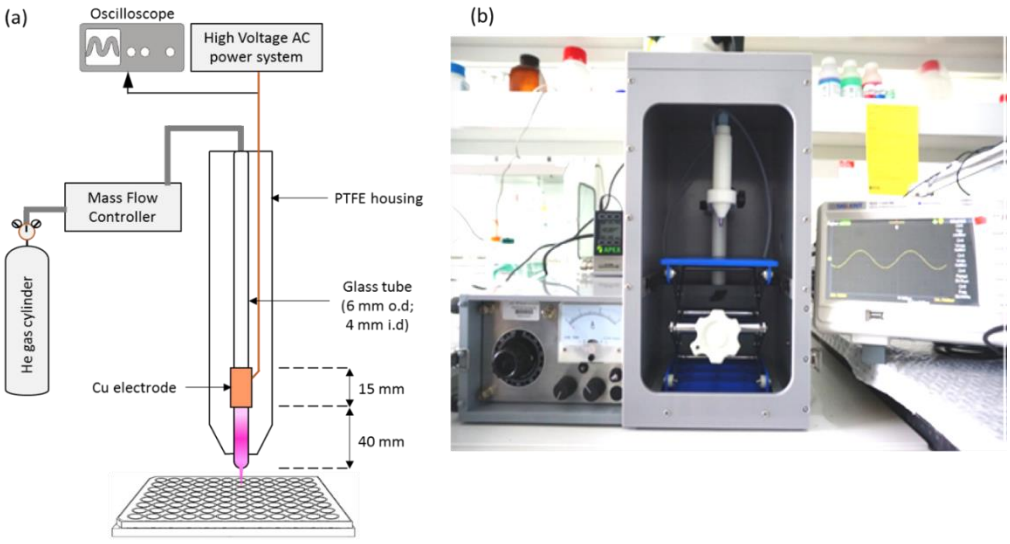


Figure 2.6 A schematic (a) and photograph (b) of the He plasma jet assembly utilised in this study.

2.1.1.2 Preparation of molecular probes

The molecular probes were prepared in each tissue fluid model using the following recipes and regents:

a) DCFH reporter system: A 2mM stock of 2′,7′-dichloro-dihydro-fluorescin diacetate (DCFH-DA, Sigma-Aldrich, catalogue number D6883) was prepared in ethanol and stored - 20°C until use. Deacetylation of DCFH-DA to DCFH was achieved by incubation of DCFH-DA in 10 mM solution of sodium hydroxide (NaOH, Sigma-Aldrich, catalogue number 367176) as shown in Figure 2.7. A 500 μL of DCFH-DA stock was added to 2 mL of NaOH solution and kept in the dark for 30 min at room temperature. The DCFH solution was neutralized by adding 10 mL of tissue fluid model solution (water, PBS or DMEM) and stored in dark at 4°C until use.

b) OPD-HRP reporter system: A solution of 2 mg/mL OPD powder (Sigma-Aldrich, catalogue number P9029) and 4 μg/ml HRP (Sigma-Aldrich, catalogue number P6782) was prepared in each of the tissue fluid model solutions and stored at 4°C until use.

c) Griess reagent reporter system: A 50 mg/mL solution of Griess reagent (Sigma-Aldrich catalogue number G4410) was prepared in each of the tissue fluid model solutions and stored at room temperature in the dark.

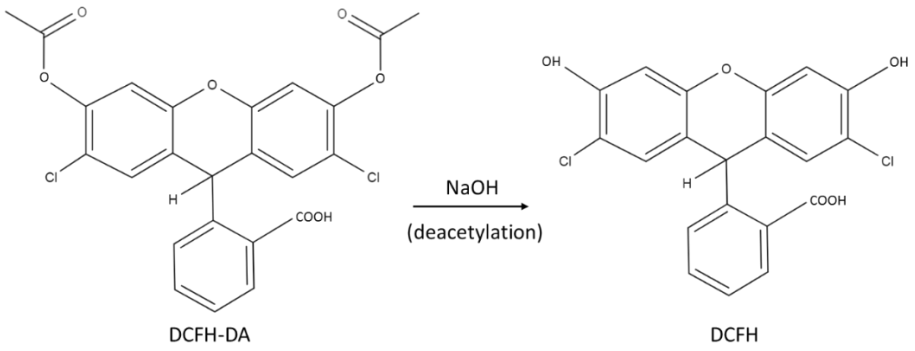


Figure 2.7 Reaction illustrating removal of the acetyl group in DCFH-DA by NaOH to form DCFH.

2.1.1.3 Measurements using a microplate reader

Fluorescence intensity and absorbance measurements were obtained using a BMG Labtech Fluostar Optima microplate reader. Fluorescence of DCF was measured using an excitation and emission filter with wavelength 498 nm and 522 nm, respectively.

Absorbance filters with wavelengths of 450 nm and 548 nm were used for the OPD-HRP and Griess reagent assays, respectively.

2.1.1.4 Plasma treatment parameters

All treatments of solution were conducted in a 96-well tissue culture plate for 15, 30 and 60 s. The distance between end of plasma jet glass tube and top of plate was fixed at 1 mm. Two types of methodologies were employed:

a) Direct detection: 200 µL of molecular probe prepared in the tissue fluid model solution was exposed *directly* to plasma in a 96-well plate. The intensities were measured immediately after the plasma treatment.

b) Indirect detection: 200 µL of tissue fluid model solution (without molecular probe) was exposed to plasma. 100 µL of this plasma treated solution was added to 100 µL of molecular probe containing 'double' the concentration as (a) to achieve the same molecular probe concentration corresponding to the direct detection method (indirect plasma exposure).

2.1.2 Results and discussion

2.1.2.1 RONS detection using DCFH

DCFH molecular probe was used to monitor the plasma jet generation of RONS in the tissue fluid models. Broadly (within the limitations noted later) the fluorescent intensities measured with DCFH can be directly correlated with RONS production. Fluorescent intensity (FI) units were normalised against untreated controls as per the following formula:

$$Normalised\ FI\ = FI\ of\ plasma\ treated\ solution / FI\ of\ untreated\ solution$$

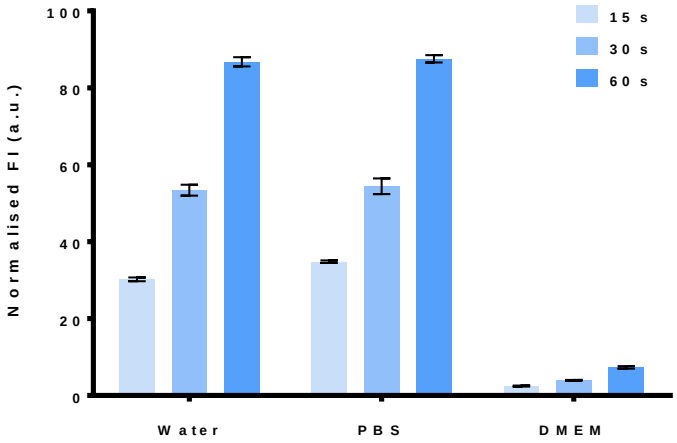


Figure 2.8 Detection of RONS using DCFH. DCFH was prepared in water, PBS, and DMEM and directly exposed to the plasma jet. Plasma jet was operated at 0.5 slpm for 15, 30 and 60 s. Each column represents the mean value and ± standard error of the mean (SEM) between 3 experiments. The experiments were performed with triplicate samples per experiment (n = 9).

Figure 2.8 shows the total RONS measured using DCFH in three tissue fluid models (water, PBS and DMEM) for the direct exposure to the plasma as a function of exposure time. The results indicate that all the tissue fluid models show an increase in FI values with increasing plasma jet exposure time of t = 15s, 30s, and 60s. This indicates that an increase in total RONS production increased as a function of plasma treatment time. Both water and PBS show similar FI, whereas the FI obtained in DMEM is much lower. The difference in intensities may indicate a low production of RONS in the DMEM, which is influenced by the composition of the fluid model. This has been further commented below.

The RONS measured are determined by three reactions occurring in 2 different phases and at their interface: namely, the gas-phase, the gas-liquid interface and the bulk liquid-phase [120, 121] (Figure 2.9). The long-lived and short-lived RONS including positive and negative ions, as well as electrons and UV photons, are generated in the gas-phase region (plasma plume). These gas-phase RONS cross the gas-liquid interface to reach the bulk liquid. This transfer is achieved by convection from the plasma jet gas flow and/or occurs via mass-transfer of RONS in the gas phase across the gas-liquid interface. The mass transfer is determined by Henry's law coefficients (or diffusion coefficients) of various species [122]. Species with higher diffusion coefficients easily reach the liquid-phase and subsequently initiate various chemical reactions to produce other secondary RONS. The generation of the •OH and H_2O_2 can also be created *in situ* in the aqueous liquid by UV photolysis. UV photons in the plasma discharge produce

the •OH in water via reaction R1 [120]. Subsequently, the •OH acts as a precursor for the formation of stable H_2O_2, as per reaction R2 [120].

$$H_2O + h\nu \rightarrow \bullet OH + H\bullet \qquad \text{- R1}$$

$$2\bullet OH \rightarrow H_2O_2 \qquad \text{- R2}$$

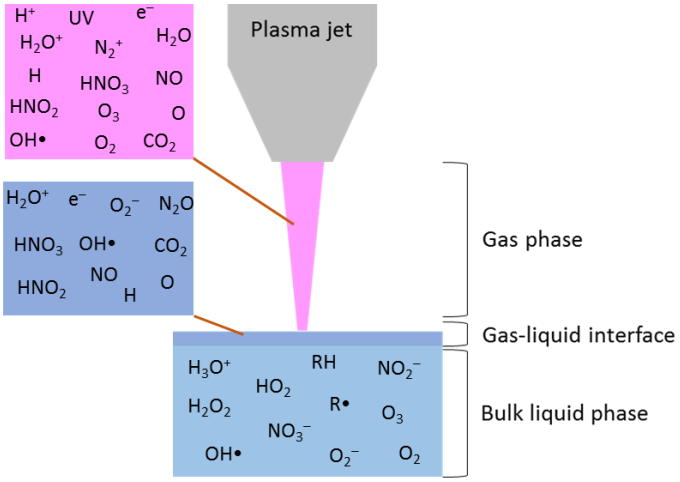


Figure 2.9 Illustration of the key phases involved in plasma-liquid interactions (for plasma operated into ambient air): gas phase, gas-liquid interface and liquid phase, and likely species to be generated in each phase.

Therefore, total RONS measured in solution is a combination of (i) RONS generated in the plasma effluent and subsequent mass transfer, and (ii) RONS produced in the liquid (after solvation) arising from the liquid chemistry. At such short plasma treatment times (15s, 30s and 60s), it is unlikely that any substantial evaporation or sputtering occurred. Therefore, it can be assumed that the type of tissue solution did not have any appreciable effects on the nature of effluent. This means that more likely explanation for the low FI with DMEM is due to the components of the DMEM inhibiting the oxidation of DCFH.

To test the hypothesis that that a constituent of DMEM is inhibiting DCFH oxidation, different types of DMEM with varied compositions were assessed. As per the manufacturer's website, DMEM with and without glutamine and phenol red were the only available variations in DMEM formulations. Therefore, DMEM with phenol red and without phenol red (Figure 2.10), and with and without L-glutamine (Figure 2.11) were compared to assess if phenol red and glutamine interfered with the DCFH assay, respectively.

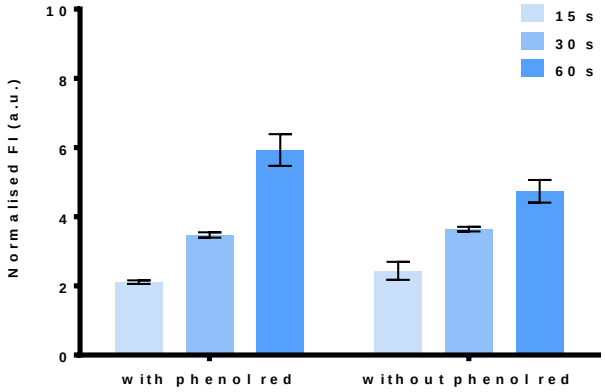


Figure 2.10 Detection of plasma delivered RONS in DMEM with and without phenol red using DCFH. Each column represents the mean value and ± standard error of the mean (SEM) between 3 experiments. The experiments were performed with triplicate samples per experiment (n = 9).

As shown in Figure 2.10, the presence of phenol red in DMEM does not impact oxidation of DCFH. This result is congruent with the study conducted by Grzelak *et al.* which shows phenol red (a pH indicator) in DMEM does not interfere with the rate of oxidation of DCFH to DCF [123].

Another difference between water/PBS and DMEM is the presence of amino acids in DMEM. As shown previously in Table 2.1, amongst the other amino acids, L-glutamine was the most abundant in the DMEM formulation. Glutamine is also the most abundant amino acid in the human body [124], and plays an important role in the synthesis of proteins, synthesis of lipids, providing energy to many cells, and maintenance of the acid-base balance in kidneys[125-127]. It is also a precursor for the production of glutathione [128], which is known to diminish the rate of oxidation of DCFH as the ROS react with glutathione instead of DCFH [129]. Therefore, DCFH prepared in DMEM with and without L-glutamine was assessed as shown in Figure 2.11.

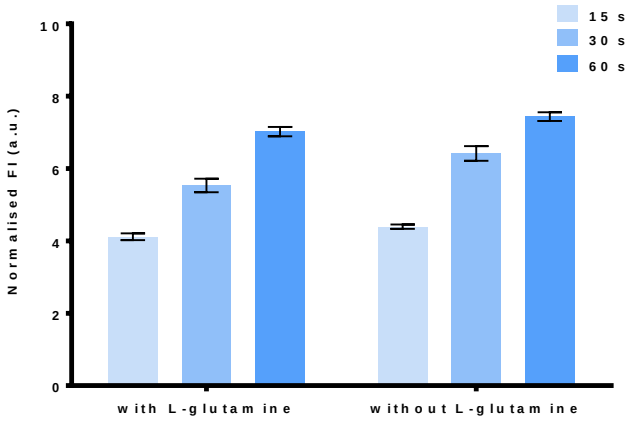


Figure 2.11 Detection of RONS generated with the plasma jet in DMEM with and without L-glutamine using DCFH. Each column represents the mean value and ± standard error of the mean

(SEM) between 3 experiments. The experiments were performed with triplicate samples per experiment (n = 9).

The results in Figure 2.11 show that presence of L-glutamine in DMEM did not influence the oxidation rate of DCFH. Although, a few studies have commented on the anti-oxidative potential of L-glutamine (and glutathione) [130-132], in this study L-glutamine did inhibit the oxidation of DCFH at a concentration of 4 mM, which was present in the commercial DMEM formulation. Many reports have demonstrated the RONS scavenging ability of other amino acids such as cysteine, tyrosine, tryptophan, methionine; and vitamins such as riboflavin in cell culture media [123, 133, 134]. Further experiments are recommended to investigate the role of the DMEM components in DCFH oxidation and RONS production, following on from this PhD.

The FI values of DCFH in each tissue fluid model can be correlated to the total RONS concentration produced by the plasma jet into the tissue fluid model using appropriate calibration curves. The calibrations would involve adding known concentrations of RONS solution to DCFH and measuring the corresponding FI. But DCFH is a broad-range RONS probe and can be oxidized by different RONS [100, 102]. It is challenging to take into account all the types of RONS generated by plasma jets in the development of these calibrations. Due to lack of appropriate calibrations curves, it cannot be confirmed that a low signal intensity of DCFH in DMEM is conclusively correlated with low RONS concentrations.

Taking into account these results, it can be elucidated that DCFH can be employed for "qualitative" assessment of RONS produced by the plasma jet into single types of tissue fluid models (e.g. monitoring RONS production as function of plasma exposure time), but cannot be used to directly compare between RONS production between different tissue fluid models (unless appropriate calibrations can be developed for these assays). Other molecular probes such as dihydroethidium, cytochrome *c* and dihydrorhodamine have also been popular for the detection of RONS [135-137]. For quantitative measurements of specific RONS, other probes such as OPD-HRP and Griess reagent can be utilised, as discussed below.

2.1.2.2 H_2O_2 detection using OPD-HRP

OPD-HRP was used to quantify H_2O_2 delivered by the plasma jet into three tissue fluid models (water, PBS and DMEM). The normalised absorbance values were calculated by

subtracting absorbance of untreated (control) OPD-HRP solution from the absorbance of plasma treated OPD-HRP. It was confirmed for this study that a neutral He gas treatment did not affect the absorbance of OPD-HRP solution; therefore untreated OPD-HRP solution was taken as a suitable control. Normalised absorbance was correlated with the concentration of H_2O_2 using calibration curves (details in Appendix A).

Figure 2.12a shows H_2O_2 concentrations measured in water, PBS and DMEM using the 'direct' method, which involves measuring H_2O_2 after direct plasma treatment of the OPD-HRP solution. Figure 2.12b shows the concentrations of H_2O_2 for the 'indirect' method, wherein the tissue fluid models (without OPD-HRP) are first treated with the plasma jet, followed by addition of the OPD-HRP solution. The detailed protocol of both methods is described previously in Section 2.1.1.4. The 'direct' and 'indirect' experimental setup proposed in this study was useful to assess the concentrations of RONS delivered by the jet in the applications where the tissue fluid is exposed 'directly' or 'indirectly' to plasma, respectively. For instance, in wound healing the wound can be either 'directly' treated with plasma jet, or treated with plasma activated liquid such that it 'indirectly' interacts with plasma jet.

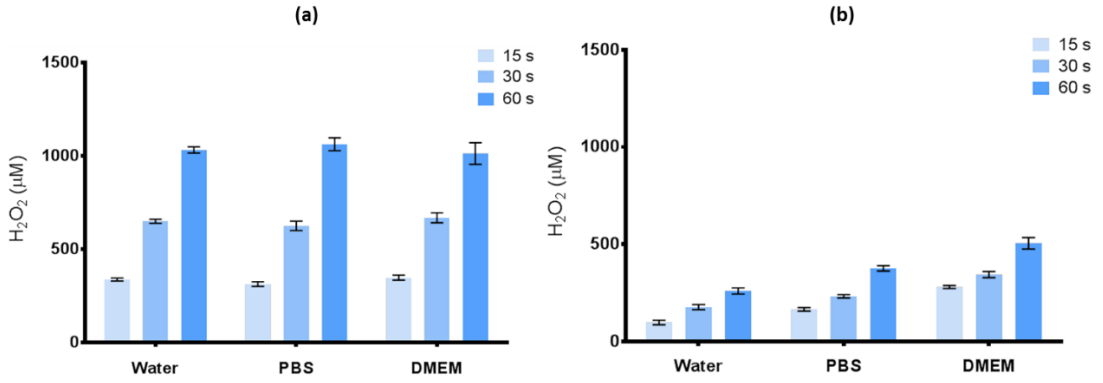


Figure 2.12 Detection of H_2O_2 in water, PBS and DMEM using the (a) direct method and (b) indirect method. The plasma jet was operated at 0.5 slpm for 15, 30 and 60 s. Each column represents the mean value and ± standard error of the mean (SEM) between 3 experiments. The experiments were performed with triplicate samples per experiment (n = 9).

The results indicate that in all three solutions, H_2O_2 was delivered in a dose dependent fashion. The concentration of H_2O_2 increased according to plasma exposure time (for t = 60s, 30s, 15s). A marked difference between the concentrations of H_2O_2 in 200 µl of solution was observed between the two methods. For the experimental range investigated in this study, H_2O_2 concentration in the range of approximately 300 µM – 1 mM was detected with the direct method, while the indirect measurements showed H_2O_2 lower concentrations in the range of 100 - 500 µM. This difference in the

concentrations can be broadly ascribed to the experimental setup for direct and indirect method, as explained below.

In the direct method, the OPD-HRP solution is in direct contact with all types of plasma components ($O_2^{-\bullet}$, •OH, and UV), along with H_2O_2. In case of the indirect method, the plasma jet is not in direct contact with the OPD-HRP solution: plasma treated solution is transferred to the OPD-HRP solution. It is suspected that the shorter-lived (and highly reactive) RONS such as $O_2^{-\bullet}$, •OH and $ONOO^-$ are extinguished before the transfer-step and it is only the longer-lived ROS (H_2O_2) which ultimately react with OPD-HRP solution. Moreover, in the indirect step, there is no possibility of UV-induced photo-oxidation of the OPD. Conversely, in case of the direct method the oxidation of OPD can be induced by both shorter-lived and longer-lived RONS. This is presumably the reason for the lower measured H_2O_2 concentrations for the indirect method than the direct method.

Figure 2.12 also shows further important differences in the concentrations of H_2O_2 detected in all of the three tissue fluid models, *vis a vis* direct *vs.* indirect: in the direct method, at any fixed treatment time (e.g. at t= 15, 30 or 60 s), the H_2O_2 concentration is within the same experimental error across the three tissue fluid models. But, in case of the indirect treatment, at any fixed treatment time the level of H_2O_2 was in the order water < PBS < DMEM. For instance, after 60 s of indirect plasma treatment, a H_2O_2 concentration of 260, 376 and 505 µM was detected in water, PBS and DMEM, respectively. Similarly, after 15 s of direct plasma treatment, 338, 314 and 348 µM of H_2O_2 was detected in water, PBS and DMEM, respectively. A possible explanation is that when directly exposed to plasma, that the reactions of the plasma-delivered, shorter-lived and species (and UV), with OPD-HRP solution "mask" (overwhelm the reactions pathways other of plasma species) and that more subtle differences present in the solution are not observed. (A useful visual observation was made in case of the direct method that the OPD-HRP solution formed a very dark-coloured product rapidly.).

In contrast, in the indirect method, the higher concentrations of H_2O_2 measured in DMEM than water and PBS (Figure 2.12b) indicates that the constituents of the tissue fluid model and/or the specificity of the molecular probe are the contributing factors to higher readings, as discussed in detail below.

Studies have shown that many reactive oxygen species (ROS) probes (both spectrometric and amperometric) fail to distinguish between ROS and reactive sulfide species (RSS) [138-140]. This cross-talk between ROS and RSS is attributed to the chemical similarities and identical mechanism of action. As shown in reactions below, while ROS formation is a multi-step one electron reduction of O_2, RSS are formed from a multiple one electron oxidation of thiols such as hydrogen sulfide (H_2S).

$$O_2 \xrightarrow{e^-} O_2^{\bullet-} \xrightarrow{e^-} H_2O_2 \xrightarrow{e^-} OH\bullet \xrightarrow{e^-} H_2O$$

$$H_2S \xrightarrow{(-)e^-} SH\bullet \xrightarrow{(-)e^-} H_2S_2 \xrightarrow{(-)e^-} S_2^{\bullet-} \xrightarrow{(-)e^-} S_2$$

DMEM is a source of thiols (RS). One electron oxidation of these thiols can generate RSS such as sulfhydryl ($HS^{\bullet-}$), thiyls ($RS^{\bullet-}$) and other persulfides. Similar to ROS, these sulfur radicals are highly reactive and react with other ROS or with each other to form more ROS and RSS, as shown below [103, 138]:

$$RS^{\bullet-} + HS^{\bullet-} \rightarrow RS_2^{\bullet-}$$

$$2HS^{\bullet-} \rightarrow H_2S_2$$

$$HS^{\bullet-} + O_2 \rightarrow O_2^{\bullet-} + HS\bullet$$

$$HS\bullet + H^+ \rightarrow H_2S$$

$$H_2S + O_2 \rightarrow H_2O_2 + S_0$$

The polysulfides (H_2S_n; n= 1-4), thus produced, can reduce disulfide bonds present in amino acids or get transferred to other thiols to form additional RSS. This illustrates that most RSS are highly reactive, can generate more ROS and could be present in abundance in thiol-rich media such as DMEM. A study by DeLeon *et al.* confirmed the 'mistaken identity' of RSS as ROS by many probes [138]. Therefore, a concrete argument can be made that the change in absorbance values of OPD-HRP in DMEM can be due to both H_2O_2 and RSS. These results become more important in cellular systems, as RSS are said to be more abundant than ROS in cells. It is likely that RSS will also react with molecular probes in cell-culture studies that could lead to an overestimation of the ROS concentrations in these studies.

Although not investigated in this thesis, two possible reasons are put forward to explain why more H_2O_2 is detected in PBS compared to water. The first possible explanation is that other oxidising molecules might be generated by the plasma treatment of PBS such

as hypochlorites that might cross-react with the molecular probe [141]. The second is since the plasma jet is contact with the solution, the higher conductivity of PBS [142] might increase the intensity of the plasma discharge and hence increase ROS production in the solution.

2.1.2.3 NO_2^- detection using Griess reagent

The concentration of NO_2^- delivered by the plasma jet in water, PBS and DMEM was measured using Griess reagent with both the direct method (Figure 2.13a) and indirect method (Figure 2.13b). The absorbance of Griess reagent after plasma treatment was normalised against the absorbance of the untreated Griess reagent. It was confirmed that the neutral He gas jet treatment did not change the absorbance of the Griess reagent. Therefore, the untreated Griess reagent was used as a suitable control for this experiment. Using calibration curves the absorbance values were converted to concentrations of NO_2^- (details in Appendix B).

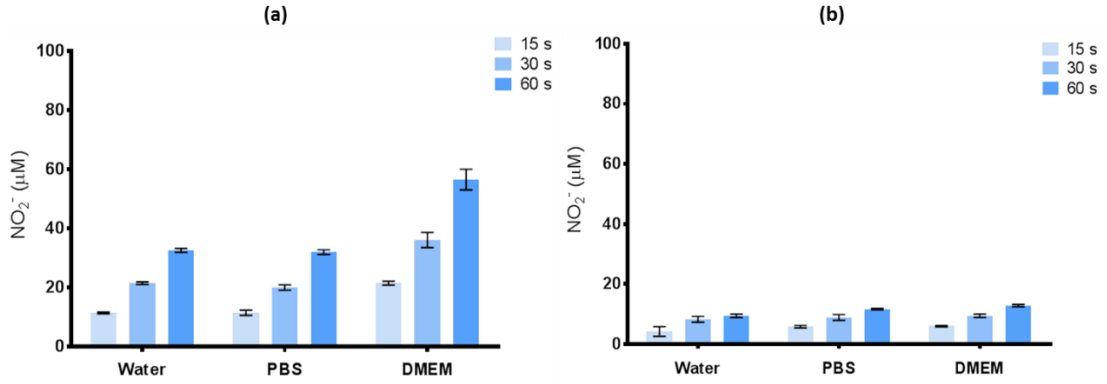


Figure 2.13 Detection of NO_2^- in water, PBS and DMEM using the (a) direct method and (b) indirect method. The plasma jet was operated at 0.5 slpm for 15, 30 and 60 s. Each column represents the mean value and ± standard error of the mean (SEM) between 3 experiments. The experiments were performed with triplicate samples per experiment (n = 9).

Results from both the direct and indirect methods show that the concentration of NO_2^- increased as function of plasma exposure time in all of the tissue fluid models. Approximately 10–60 µM of NO_2^- was detected in water, PBS and DMEM with the direct method (Figure 2.13a) and 4–12 µM with the indirect method (Figure 2.13b). Similar results were obtained with OPD-HRP in Figure 2.12, wherein the higher level treatment in the direct method was attributed to the role of other plasma components, such as shorter-lived ROS and UV in OPD oxidation. The results with Griess reagent could also imply that the absorbance of Griess reagent is affected by shorter-lived RNS species such as $ONOO^-$ (and UV) in case of the direct method, but not in case of

indirect. Therefore, higher concentrations of NO_2^- were detected in the direct method than the indirect method.

With both the direct and indirect method of detection using Griess assay, the concentration of NO_2^- in DMEM was slightly higher than water and PBS. With the direct method, after 15 s of treatment, approximately 11.5 µM of NO_2^- was detected in water/PBS but 21.5 µM in DMEM. Similarly, after 30 s of treatment approximately 21 µM of NO_2^- was detected in water/PBS but 36 µM in DMEM at 30 s; and after 60 s of treatment approximately 32 µM of NO_2^- in water/PBS but 56.5 µM in DMEM. In case of the indirect method, after 15 s of plasma treatment, the NO_2^- concentration in water, PBS and DMEM was 4.1, 5.7 and 5.9 µM, respectively. After 30 s of plasma treatment, the concentrations were 8.2, 8.8 and 9.3 µM; and with 60 s of plasma treatment they were 9.3, 11.6 and 12.8 µM in water, PBS and DMEM, respectively. Overall, using a two-way ANOVA multiple comparison in the GraphPad Prism, it was confirmed that the concentration NO_2^- in DMEM was significantly higher than water or PBS.

This enhanced production of NO_2^- in DMEM (as H_2O_2, above) could arise from the protein (sulfur) content of DMEM. In this case, a likely explanation is the sulfoxidation or nitration of the thiol groups [143, 144]. As described in section 2.1.2.3, RSS are highly reactive species and can interact with neighboring RONS to form more reactive species such as in the reactions R1 and R3 of $HS^{\bullet-}$ and $RS^{\bullet-}$ with $ONOO^-$ to form NO (which is a source of NO_2^-) and NO_2^-, respectively [145-148].

$$HS^{\bullet-} + ONOO^- \rightarrow HSNO_2 + \bullet OH \quad -(R1)$$
$$HSNO_2 \rightarrow HSO\bullet + NO \quad -(R2)$$
$$RS^{\bullet-} + ONOO^- \rightarrow RSOH + NO_2^- \quad -(R3)$$

The presence of ferric nitrate [$Fe(NO_3)_3$] in DMEM acts as a source of NO_3^- ions (R4), which can undergo following reactions (R5 or R6) to form additional NO_2^- [149, 150].

$$Fe(NO_3)_3 \rightarrow Fe^{+3} + 2NO_3^- \quad -(R4)$$
$$NO_3^- + 2e^- + 2H^+ \longleftrightarrow NO_2^- + H_2O \quad -(R5)$$
$$NO_3^- + h\nu \longleftrightarrow NO_2^- + O(^3P) \quad -(R6)$$

It is evident from the results obtained using OPD-HRP and Griess reagent that the plasma jet delivers more H_2O_2 than NO_2^- in solution (as shown in Figure 2.12 and 1.13). For instance, approximately 1 mM of H_2O_2 and approximately 45 µM of NO_2^-

was detected after a 60 s plasma treatment of water (using the direct method). Since NO_2^- is an indirect measurement of NO, it can be elucidated from this study that the He plasma jet used in this study delivers more H_2O_2 in solution than NO. This is can be explained using Henry's law coefficient [122].

RONS have to cross the gas-liquid interface to penetrate into the solution. As per Henry's law, the solubility of a gas in the liquid is directly proportional to its partial pressure in the gas phase at a fixed temperature [122]. As per the formula below, a Henry's law coefficient (H) can determine the concentration of a gas in a liquid (C) at the gaseous partial pressure (p). Herein, the units of 'C' and 'p' are moles of gas per litre of solution (M) and atmospheric absolute pressure (atm).

$$C \propto p$$

$$C = H\ X\ p$$

$$H = C / p$$

This implies that higher the H value of a gaseous molecule, the quicker it will solvate into a liquid and vice versa. At 300 K and 1 atm, the H value for H_2O_2 and NO are 1.96 x 10^6 and 4.4 x 10^{-2} [93]. Therefore, H_2O_2 is able to be transported more quickly from the gas phase into the liquid than NO, and its concentration is higher than NO.

A higher concentration of H_2O_2 can also be ascribed to the process of UV photolysis in plasma-liquid interactions. The interaction between the UV photons and liquid surface leads to the production of the OH•, which is a short-lived highly reactive radical, and can be subsequently converted to stable H_2O_2 as shown in the reactions below [120]:

$$H_2O + h\nu \rightarrow {\bullet}OH + H{\bullet}$$

$$2\,{\bullet}OH \rightarrow H_2O_2$$

2.2 Amperometric probes to measure H_2O_2 in solution

The amperometric probe (or electrochemical sensor) used for H_2O_2 detection in this study is a so-called Clark type electrochemical sensor (Figure 2.14). A Clark type sensor has a Platinum (Pt) wire working electrode and a silver/silver chloride (Ag/AgCl) reference electrode. Both the electrodes are enclosed in a Faraday shielded stainless steel sleeve, which is filled with electrolyte solution to form a 'combination electrode' setup. The end of stainless sleeve (2 mm in diameter) is covered with a

polymeric membrane, which works on the principle of size exclusion, and is pervious to H_2O_2 with an average diameter of 0.25-0.28 nm [151].

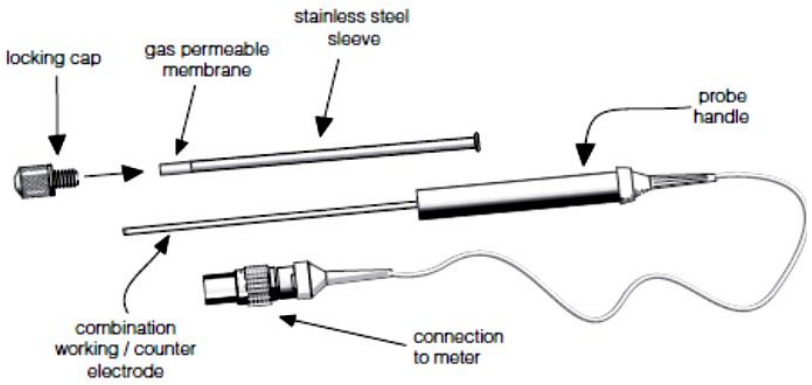


Figure 2.14 A schematic of components of the membrane-electrochemical sensor used to measure H_2O_2.

An external voltage of 0.45 V was applied and oxidation occurred at site of the electrode surface as per reaction R7 [152]. This reaction is a multi-step process as stated in reactions R8, R9 and R10. A complex is formed between the electrode surface and H_2O_2 molecule (R3), which further undergoes internal charge transfer (R9) and oxidation (R10) to reform a new binding site at the electrode surface [153, 154]. The current produced during the reaction can be directly correlated to the H_2O_2 concentrations.

$$H_2O_2 \rightarrow O_2 + 2H^+ + \mathbf{2}\boldsymbol{e}^- \quad \text{- (R7)}$$

$$H_2O_2 + Pt(OH)_2 \rightarrow Pt(OH)_2.H_2O_2 \quad \text{- (R8)}$$

$$Pt(OH)_2.H_2O_2 \rightarrow Pt + 2H_2O + O_2 \quad \text{- (R9)}$$

$$Pt + 2H_2O \rightarrow Pt(OH)_2 + 2H^+ + \mathbf{2}\boldsymbol{e}^- \quad \text{- (R10)}$$

2.2.1 Materials and Methods

2.2.1.1 Plasma jet

The plasma jet used in this study is same as described in section 2.1.1.1.

2.2.1.2 Electrochemical sensor

Prior to its use the sensor (ISO-HPO-2, World Precision instruments) was assembled and polarized as per manufacturer's instructions [155]. It was interfaced with a free radical analyzer (TBR4100-416, World Precision instruments) to record the electrochemical signals (Figure 2.15).

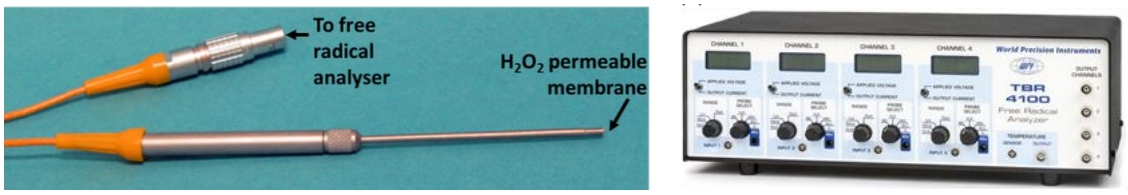


Figure 2.15 Photograph of the membrane-electrochemical sensor ISO-HPO-2 (on left) and free radical analyzer TBR4100 (on right) from World Precision Instruments used to measure H_2O_2.

2.2.1.2.1 2.2.1.3 Plasma treatment parameters

200 µL of tissue fluid was plasma treated in a 96 well plate for 15, 30 and 60 s. The distance between the end of the plasma jet glass tube and top of the plate was approximately 1 mm. Change in current measurements were measured immediately after the plasma treatment by submerging the sensor membrane tip into the test solution.

2.2.2 Results and discussion

Figure 2.16 shows the concentrations of H_2O_2 in water, PBS and DMEM measured using the ISO-HPO-2 probe. The current measured after plasma treatments were converted to H_2O_2 concentrations using calibration curves (details in Appendix C).

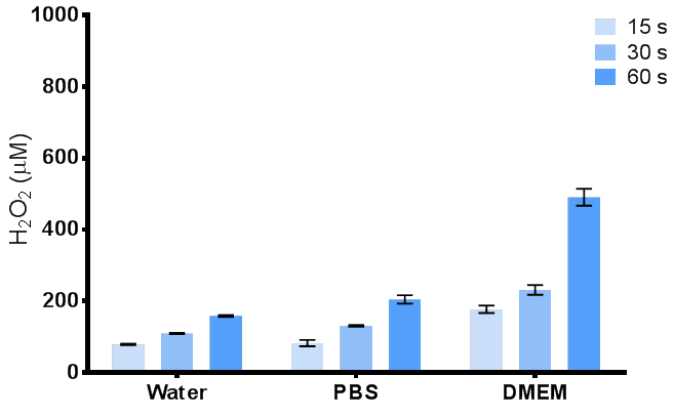


Figure 2.16 Concentrations of H_2O_2 measured using ISO-HPO-2 in water, PBS and DMEM after plasma treatment for 15 s, 30 s and 60 s. Each column represents the mean value and ± standard error of the mean (SEM) in the experiment performed with triplicate samples (n = 3).

Results show that plasma jet delivered H_2O_2 in a dose-dependent manner; longer plasma exposures delivered more H_2O_2 in all three tissue fluid models. The statistical difference between the concentrations measured in water, PBS and DMEM were measured using a two-way ANOVA with multiple comparisons (in GraphPad Prism). The results showed that the concentrations measured at each time point in PBS and water were statistically insignificant ($p>0.05$), while the concentrations measured in PBS and water when compared with DMEM were both statistically significant ($p<0.05$). The highest

concentrations of H_2O_2 were measured in DMEM when compared with water or PBS for the corresponding treatment times. This is further commented below.

It is possible that the ISO-HPO-2 sensor reacts with other types of reactive species such as RSS, like some small molecular probes. Although there is no direct experimental evidence in this study to support this assumption, a study conducted by DeLeon *et al.* focused on the false identification of RSS as ROS by amperometric (as well as spectrometric) sensors [138]. They demonstrated that the membrane of ISO-HPO-2 not only senses RSS, but also is more sensitive towards RSS than H_2O_2 – 30 times more sensitive for H_2S, 3 times more for H_2S_2 and 2 times more towards H_2S_3 and H_2S_4. Therefore, possibilities exist that ISO-HPO-2 detects both H_2O_2 and various H_2S_n species in plasma treated DMEM.

In order to obtain further insights into the reliability of the H_2O_2 detection methods, a direct comparison of the H_2O_2 concentrations was made between the measurements performed with OPD-HRP (both direct and indirect methods) and with the ISO-HPO-2 sensor. The results are presented in Figure 2.17.

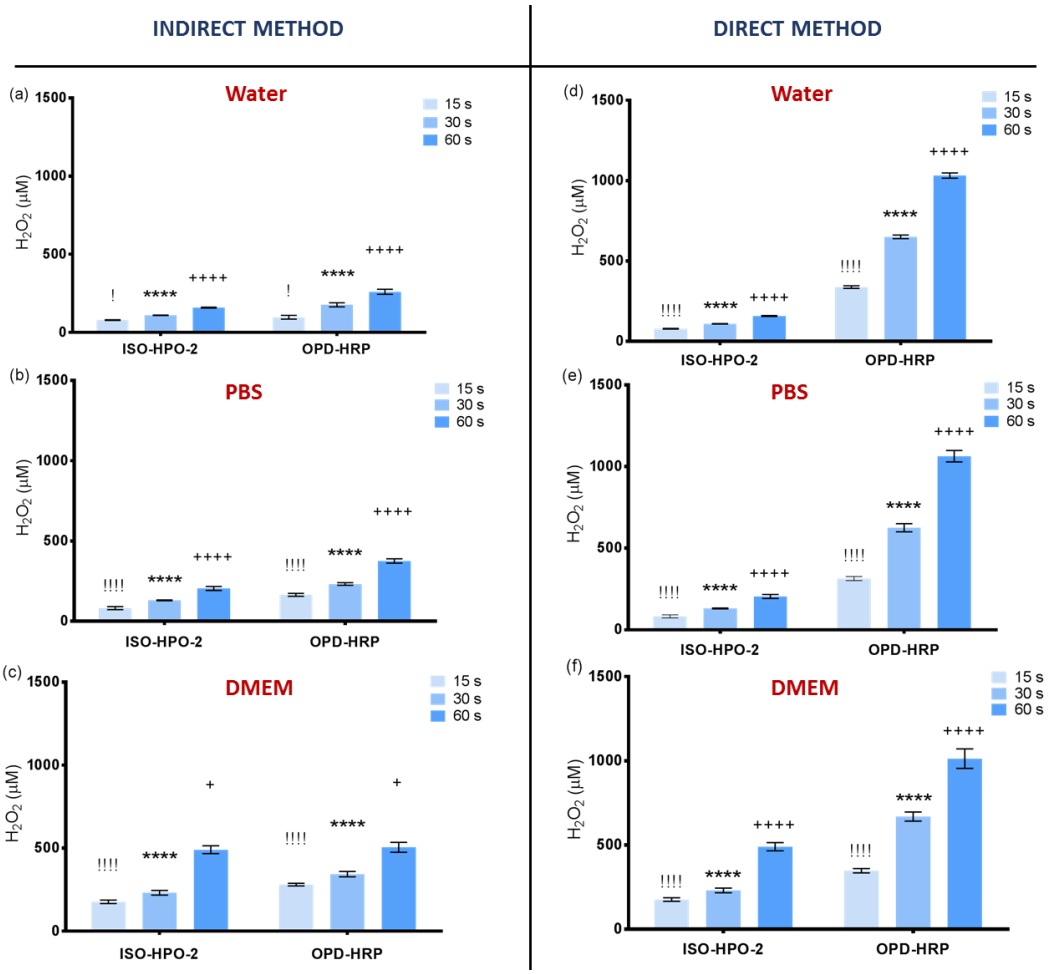


Figure 2.17 Comparison between the concentrations of H_2O_2 measured using amperometric probe ISO-HPO-2 and molecular probe OPD-HRP for H_2O_2 detection in water (a,d), PBS (b,e) and DMEM (c,f). In the panel, figures a, b and c panel represent the measurements with indirect method; and d, e and f represent the measurements with direct method Two-way ANOVA was used to determine the statistical significance of the values. The values with **,!!!! and ++++ marks represent statistically significantly different values ($p < 0.05$), whereas ! and + were statistically insignificant. The marks *, ! and + denote statistical difference in 15 s, 30 s and 60 s values.**

The data in Figure 2.17 shows that both the probes (OPD-HRP and ISO-HPO-2) could detect an increase in H_2O_2 production with plasma treatment time in all three tissue fluid models. However, a significant difference was observed in the concentrations of H_2O_2 measured by the two types of probe. Ideally under same experimental conditions and plasma treatment parameters, similar concentrations of H_2O_2 should be detected using both probes. But, the concentrations of H_2O_2 measured using the ISO-HPO-2 sensor were significantly lower than OPD-HRP, comparing both direct and indirect methods of detection. This may indicate that the molecular probe OPD-HRP is perhaps sensitive to a broader range of other components of plasma such as the shorter-lived ROS such as •OH. (And the ISO-HPO-2 is unable to detect ROS other than H_2O_2.) To investigate further, the factorial difference between ISO-HPO-2 and OPD-HRP (direct and indirect)

was also calculated to understand whether the difference is consistent (Table 2.2). Factorial difference was calculated using following formula:

$$Factorial\ difference = \frac{Concentration\ of\ H_2O_2\ with\ OPD - HRP}{Concentration\ of\ H_2O_2\ with\ ISO - HPO - 2}$$

Table 2.2 The factorial difference between the concentrations of H_2O_2 measured with the ISO-HPO-2 sensor and OPD-HRP molecular probe (indirect or direct method). The difference was calculated by dividing the concentrations measured from OPD-HRP (direct or indirect) with the measurements from ISO-HPO-2.

Tissue fluid model		**Water**	**PBS**	**DMEM**
Indirect OPD-HRP vs ISO-HPO-2	15 s	1.229697	2.011886	1.584319
	30 s	1.610597	1.775072	1.487221
	60 s	1.643785	1.837642	1.029545
Direct OPD-HRP vs ISO-HPO-2	15 s	4.296882	3.830898	1.969260
	30 s	5.947850	4.787891	2.896790
	60 s	6.531542	5.199089	2.065790

As shown in Table 2.2, in the majority of cases, the factorial difference for the OPD-HRP indirect method vs ISO-HPO-2 is similar. But, in contrast, in case of OPD-HRP direct method vs ISO-HPO-2, the average factorial difference is more variable. This indicates that for the indirect method, there is a consistent error between the molecular probe and electrochemical sensor methods. This error would require checking with a third method of H_2O_2 detection in future studies. The increased variability for the direct method is possibly attributed to other components in the plasma discharge (e.g. UV photons and electrons) interacting with the molecular probe or electrochemical sensor leading to discrepancies in measurements.

In order to (possibly) explain the discrepancies between the direct method and the ISO HPO-2 the reader is referred back to Figure 2.12, where OPD-HRP is used as a probe for both direct and indirect H_2O_2 production. In explaining the higher OPD-HRP results obtained for the direct method, it was speculated that in the direct method of detection, the absorbance of OPD may be perturbed by other components of plasma (i.e. plasma

itself, UV or short-lived reactive species), but with the indirect method only longer-lived species react with OPD. In the electrochemical probe ISO-HPO-2 method the plasma treated solution was transferred to ISO-HPO-2 electrode (after plasma treatment). This means that, like indirect method of detection with OPD-HRP, the plasma jet was not in direct contact with the ISO-HPO-2 sensor. As a result, only the longer-lived species e.g. H_2O_2 interacting with the ISO-HPO-2 sensor, the two methods (indirect OPD-HRP and ISO-HPO-2) are giving a reasonable agreement in terms of absolute H_2O_2 concentration. Furthermore, keeping aside the complications associated with direct plasma, the ISO HPO-2 sensor also shows greater H_2O_2 production and its trends in DMEM as compared to water and PBS, just like OPD-HRP does.

To summarise, the results presented in this chapter indicate that the commonly used molecular probes for RONS detection can undergo cross-reactivity with shorter-lived RONS and other components of plasma such as UV (depending on the experimental protocol used). Secondly, the ingredients of DMEM may act as source for RSS, involved in cross-reactivity of both molecular and electrochemical probes designed for the detection of H_2O_2 [138].

2.3 Conclusion

The aim of this study was to analyse the plasma-generation of RONS into the tissue fluid. Simple protocols using models of tissue fluid (water, PBS and DMEM) were established for the detection of RONS. For this study two types of RONS probes were utilised: molecular probes (DCFH, OPD-HRP and Griess reagent) and an amperometric probe (ISO-HPO-2). While DCFH is a broad range RONS probe to measure total RONS production, OPD-HRP and Griess reagent were more specific and were used to detect H_2O_2 and NO_2^-, respectively. The amperometric probe available was used to detect H_2O_2.

One of the major aspects of this study was to determine how the composition of tissue fluid model influence the production of RONS. DCFH results showed that the total RONS production in DMEM is much lower than in water and PBS. On the other hand, contrasting results with OPD-HRP (and ISO-HPO-2) and Griess reagent show a reasonably higher concentration of H_2O_2 and NO_2^-, respectively, produced in DMEM than in water and PBS upon plasma treatment. Furthermore, a comparison of the measured H_2O_2 concentrations was made between the ISO-HPO-2 sensor and OPD-

HRP molecular probe methods. It was concluded that the concentrations of H_2O_2 determined using ISO-HPO-2 and OPD-HRP were significantly different, although the average factorial difference between the ISO-HPO-2 and OPD-HRP (indirect method) was consistent. This significant difference can be an artefactual over-estimation of H_2O_2 in case of OPD-HRP. Due to the highly complex nature of plasma and plasma-liquid chemistry, it is difficult to determine the exact cause of the artefactual increase in H_2O_2 concentrations, if any, but should be the subject of future research. Nonetheless, the comparisons made between the probes in this chapter, draws attention to potential errors in measurement of RONS, and the need to cross-validate measurements of RONS with different detection methods.

The major challenge in case of the RONS probes is the cross-reactivity or sensitivity towards other type of reactive species such as RSS which are known to be produced in DMEM. Studies elsewhere have suggested that certain RONS probes exhibit higher sensitivity towards the RSS than the ROS. This case of mistaken-identity of RSS is rarely taken into account in plasma-based studies. Another challenge is associated with the DCFH probe [100, 102]. Since DCFH reacts with a broad range of RONS (and RSS) produced by plasma, it is difficult to take into account the concentrations of each type of RONS in calibrations curves. Although this may not be a concern for the studies aimed at assessing the total RONS production, but in context to this study knowing the precise concentrations of the RONS from DCFH can be helpful to corroborate the data obtained from OPD-HRP and Griess reagent.

The results obtained from direct and indirect methods have implications in the biomedical applications of plasma. The experimental setup used for direct method of RONS detection can be correlated to applications where the biological target (tissue fluid or tissue) is directly exposed to plasma. An examples includes the ‘direct’ plasma treatment of wound and tissue fluid. The indirect method can be correlated to the application of plasma activated water and plasma activated media on the wound site or to the tumor, such that the target is ‘indirectly’ exposed to plasma (or RONS). Knowing the accurate concentration of RONS delivered by the plasma jet into the tissue fluid (as well as tissue) is needed to ensure the correct dosages are delivered for the treatment.

With simple experimental setup and easy-to-use RONS probes, this study raises significant questions on the fundamental knowledge of plasma-liquid chemistry. A few

questions include – (i) how accurate are the results obtained from the commonly used RONS probes? (ii) what are the exact reaction mechanisms between the probe and plasma during the treatment? (iii) how can the tissue fluid models be improved to mimic the real physiological fluid? It also outlines the absolute necessity of developing precise calibrations for each method and careful correlations between one or more methods. The protocols and conclusions established in this study serve as a guide to study the interactions of plasma with tissues, cells and other components in the upcoming chapters of this thesis.

2.4 References

1. Dröge, W., *Free Radicals in the Physiological Control of Cell Function.* Physiological Reviews, 2002. **82**(1): p. 47-95.
2. D'Autreaux, B. and M.B. Toledano, *ROS as signalling molecules: mechanisms that generate specificity in ROS homeostasis.* Nature reviews. Molecular cell biology, 2007. **8**(10): p. 813-24.
3. Miller, E.W., B.C. Dickinson, and C.J. Chang, *Aquaporin-3 mediates hydrogen peroxide uptake to regulate downstream intracellular signaling.* Proceedings of the National Academy of Sciences of the United States of America, 2010. **107**(36): p. 15681-6.
4. Frank, S., et al., *Nitric oxide triggers enhanced induction of vascular endothelial growth factor expression in cultured keratinocytes (HaCaT) and during cutaneous wound repair.* FASEB J., 1999. **13**(14): p. 2002-14.
5. Radomski, M.W., R.M. Palmer, and S. Moncada, *The anti-aggregating properties of vascular endothelium: interactions between prostacyclin and nitric oxide.* British journal of pharmacology, 1987. **92**(3): p. 639-46.
6. Bryan, N., et al., *Reactive oxygen species (ROS)–a family of fate deciding molecules pivotal in constructive inflammation and wound healing.* European Cells & Materials, 2012. **24**(1): p. 249-265.
7. Alberts, B., et al., *Cell junctions, cell adhesion, and the extracellular matrix,* in *Molecular Biology of the Cell. 4th edition.* 2002, Garland Science: New York.
8. Rizk, M., M.B. Witte, and A. Barbul, *Nitric Oxide and Wound Healing.* World Journal of Surgery, 2004. **28**(3): p. 301-306.
9. Doughan, A.K. and S.I. Dikalov, *Mitochondrial redox cycling of mitoquinone leads to superoxide production and cellular apoptosis.* Antioxidants & redox signaling, 2007. **9**(11): p. 1825-36.
10. Zhu, G., et al., *Hydrogen Peroxide: A Potential Wound Therapeutic Target?* Medical principles and practice : international journal of the Kuwait University, Health Science Centre, 2017. **26**(4): p. 301-308.
11. Yip, W.L., *Influence of oxygen on wound healing.* International Wound Journal, 2015. **12**(6): p. 620-624.
12. Tandara, A.A. and T.A. Mustoe, *Oxygen in wound healing—more than a nutrient.* World journal of surgery, 2004. **28**(3): p. 294-300.
13. Bekeschus, S., et al., *Hydrogen peroxide: A central player in physical plasma-induced oxidative stress in human blood cells.* Free Radical Research Communications, 2014. **48**(5): p. 542-9.

14. Schulz, G. and J. Stechmiller, *Wound healing and nitric oxide production: too little or too much may impair healing and cause chronic wounds.* The international journal of lower extremity wounds, 2006. **5**(1): p. 6-8.
15. Isenberg, J.S., et al., *Nitric oxide in wound-healing.* Microsurgery, 2005. **25**(5): p. 442-451.
16. Tipa, R.S. and G.M. Kroesen, *Plasma-stimulated wound healing.* Plasma Science, IEEE Transactions on, 2011. **39**(11): p. 2978-2979.
17. Sen, C.K., et al., *Oxidant-induced vascular endothelial growth factor expression in human keratinocytes and cutaneous wound healing.* Journal of Biological Chemistry, 2002. **277**(36): p. 33284-33290.
18. Loo, A.E. and B. Halliwell, *Effects of hydrogen peroxide in a keratinocyte-fibroblast co-culture model of wound healing.* Biochemical and biophysical research communications, 2012. **423**(2): p. 253-8.
19. Sen, C.K. and S. Roy, *Redox signals in wound healing.* Biochimica et Biophysica Acta (BBA) - General Subjects, 2008. **1780**(11): p. 1348-1361.
20. Pignatelli, P., et al., *Hydrogen peroxide is involved in collagen-induced platelet activation.* Blood, 1998. **91**(2): p. 484-90.
21. Loo, A.E., et al., *Effects of hydrogen peroxide on wound healing in mice in relation to oxidative damage.* PLoS One, 2012. **7**(11): p. e49215.
22. Sies, H., *Hydrogen peroxide as a central redox signaling molecule in physiological oxidative stress: Oxidative eustress.* Redox biology, 2017. **11**: p. 613-619.
23. Sen, C.K., *The general case for redox control of wound repair.* Wound Repair and Regeneration, 2003. **11**(6): p. 431-438.
24. Babior, B.M., *Phagocytes and oxidative stress.* The American Journal of Medicine, 2000. **109**(1): p. 33-44.
25. Lee, K.S., et al., *Hydrogen peroxide induces vascular permeability via regulation of vascular endothelial growth factor.* American journal of respiratory cell and molecular biology, 2006. **35**(2): p. 190-7.
26. Bao, P., et al., *The Role of Vascular Endothelial Growth Factor in Wound Healing.* Journal of Surgical Research, 2009. **153**(2): p. 347-358.
27. Nishio, E. and Y. Watanabe, *The involvement of reactive oxygen species and arachidonic acid in alpha 1-adrenoceptor-induced smooth muscle cell proliferation and migration.* British journal of pharmacology, 1997. **121**(4): p. 665-70.
28. Roy, S., et al., *Dermal Wound Healing Is Subject to Redox Control.* Molecular Therapy, 2006. **13**(1): p. 211-220.
29. Stallmeyer, B., et al., *The function of nitric oxide in wound repair: inhibition of inducible nitric oxide-synthase severely impairs wound reepithelialization.* The Journal of investigative dermatology
1999. **113**(6): p. 1090-8.
30. Soneja, A., M. Drews, and T. Malinski, *Role of nitric oxide, nitroxidative and oxidative stress in wound healing.* Pharmacological reports, 2005. **57 Suppl**: p. 108-19.
31. Witte, M.B. and A. Barbul, *Role of nitric oxide in wound repair.* The American Journal of Surgery, 2002. **183**(4): p. 406-412.
32. Luo, J.-d. and A.F. Chen, *Nitric oxide: a newly discovered function on wound healing.* Acta Pharmacologica Sinica, 2005. **26**: p. 259.
33. Lee, R.H., et al., *Nitric oxide in the healing wound: a time-course study.* The Journal of surgical research, 2001. **101**(1): p. 104-8.

34. Nathan, C.F. and J.B. Hibbs, *Role of nitric oxide synthesis in macrophage antimicrobial activity.* Current Opinion in Immunology, 1991. **3**(1): p. 65-70.
35. Witte, M.B., et al., *Enhancement of fibroblast collagen synthesis by nitric oxide.* Nitric Oxide, 2000. **4**(6): p. 572-82.
36. Spear, M., *Wound cleansing: solutions and techniques.* Plastic Surgical Nursing, 2011. **31**(1): p. 29-31.
37. Tóth, T., et al., *Evaluation of LHP® (1% hydrogen peroxide) cream versus petrolatum and untreated controls in open wounds in healthy horses: a randomized, blinded control study.* Acta Veterinaria Scandinavica, 2011. **53**(1): p. 45.
38. Yamada, Y., et al., *Topical treatment of oral cavity and wounded skin with a new disinfection system utilizing photolysis of hydrogen peroxide in rats.* The Journal of Toxicological Sciences, 2012. **37**(2): p. 329-335.
39. Mohammadi, A.A., et al., *Efficacy of debridement and wound cleansing with 2% hydrogen peroxide on graft take in the chronic-colonized burn wounds; a randomized controlled clinical trial.* Burns, 2013. **39**(6): p. 1131-1136.
40. Finnen, M.J., et al., *Topical application of acidified nitrite to the nail renders it antifungal and causes nitrosation of cysteine groups in the nail plate.* British Journal of Dermatology, 2007. **157**(3): p. 494-500.
41. Weller, R. and M.J. Finnen, *The effects of topical treatment with acidified nitrite on wound healing in normal and diabetic mice.* Nitric Oxide, 2006. **15**(4): p. 395-399.
42. Hardwick, J., et al., *A novel method for the delivery of nitric oxide therapy to the skin of human subjects using a semi-permeable membrane.* Clinical Science, 2001. **100**(4): p. 395-400.
43. Masters, K.S.B., et al., *Effects of nitric oxide releasing poly (vinyl alcohol) hydrogel dressings on dermal wound healing in diabetic mice.* Wound Repair and regeneration, 2002. **10**(5): p. 286-294.
44. Muscará, M.N., et al., *Wound collagen deposition in rats: effects of an NO-NSAID and a selective COX-2 inhibitor.* British journal of pharmacology, 2000. **129**(4): p. 681-686.
45. Shabani, M., et al., *Enhancement of wound repair with a topically applied nitric oxide-releasing polymer.* Wound Repair Regen, 1996. **4**(3): p. 353-62.
46. Shekhter, *Beneficial effect of gaseous nitric oxide on the healing of skin wounds.* 2005.
47. Miller, C., *Nitric oxide gas (gO) as a cosmetic and wound healing agent*. 2007, Google Patents.
48. Heinlin, J., et al., *Plasma applications in medicine with a special focus on dermatology.* Journal of the European Academy of Dermatology and Venereology, 2011. **25**(1): p. 1-11.
49. von Woedtke, T., et al., *Introduction to Plasma Medicine*, in *Comprehensive Clinical Plasma Medicine: Cold Physical Plasma for Medical Application*, H.-R. Metelmann, T. von Woedtke, and K.-D. Weltmann, Editors. 2018, Springer International Publishing: Cham. p. 3-21.
50. Izadjoo, M., et al., *Medical applications of cold atmospheric plasma: state of the science.* Journal of Wound Care, 2018. **27**(Sup9): p. S4-S10.
51. Schmidt, A., et al., *A cold plasma jet accelerates wound healing in a murine model of full-thickness skin wounds.* Experimental Dermatology, 2017. **26**(2): p. 156-162.

52. Graves, D.B., *Mechanisms of Plasma Medicine: Coupling Plasma Physics, Biochemistry, and Biology.* IEEE Transactions on Radiation and Plasma Medical Sciences, 2017. **1**(4): p. 281-292.
53. Andrei Vasile Nastuta, I.T., Constantin Grigoras, Valentin Pohoata, Gheorghe Popa, *Stimulation of wound healing by helium atmospheric pressure plasma treatment.* J. Phys. D: Appl. Phys., 2011. **44**: p. 105204.
54. Isbary, G., et al., *Successful and safe use of 2 min cold atmospheric argon plasma in chronic wounds: results of a randomized controlled trial.* Br J Dermatol, 2012. **167**(2): p. 404-10.
55. Kos, S., et al., *Safety aspects of atmospheric pressure helium plasma jet operation on skin: In vivo study on mouse skin.* PLOS ONE, 2017. **12**(4): p. e0174966.
56. Fluhr, J.W., et al., *In vivo skin treatment with tissue-tolerable plasma influences skin physiology and antioxidant profile in human stratum corneum.* Experimental Dermatology, 2012. **21**(2): p. 130-134.
57. Graves, D.B., *The emerging role of reactive oxygen and nitrogen species in redox biology and some implications for plasma applications to medicine and biology.* Journal of Physics D: Applied Physics 2012. **45**: p. 263001.
58. Bekeschus, S., et al., *The plasma jet kINPen – A powerful tool for wound healing.* Clinical Plasma Medicine.
59. Arndt, S., et al., *Comparing two different plasma devices kINPen and Adtec SteriPlas regarding their molecular and cellular effects on wound healing.* Clinical Plasma Medicine, 2018. **9**: p. 24-33.
60. Cheng, K.-Y., et al., *Wound Healing in Streptozotocin-Induced Diabetic Rats Using Atmospheric-Pressure Argon Plasma Jet.* Scientific Reports, 2018. **8**(1): p. 12214.
61. Brehmer, F., et al., *Alleviation of chronic venous leg ulcers with a hand-held dielectric barrier discharge plasma generator (PlasmaDerm((R)) VU-2010): results of a monocentric, two-armed, open, prospective, randomized and controlled trial (NCT01415622).* Journal of the European Academy of Dermatology and Venereology, 2015. **29**(1): p. 148-55.
62. Schmidt, A., et al., *Non-thermal plasma treatment is associated with changes in transcriptome of human epithelial skin cells.* Free radical research, 2013. **47**(8): p. 577-592.
63. Liebmann, J., et al., *Biological effects of nitric oxide generated by an atmospheric pressure gas-plasma on human skin cells.* Nitric Oxide, 2011. **24**(1): p. 8-16.
64. Thomas, D.D., et al., *The chemical biology of nitric oxide: Implications in cellular signaling.* Free Radical Biology and Medicine, 2008. **45**(1): p. 18-31.
65. Bashan, N., et al., *Positive and Negative Regulation of Insulin Signaling by Reactive Oxygen and Nitrogen Species.* Physiological Reviews, 2009. **89**(1): p. 27-71.
66. Klyubin, I.V., K.M. Kirpichnikova, and I.A. Gamaley, *Hydrogen peroxide-induced chemotaxis of mouse peritoneal neutrophils.* European journal of cell biology, 1996. **70**(4): p. 347-351.
67. Murrell, G.A., M.J. Francis, and L. Bromley, *Modulation of fibroblast proliferation by oxygen free radicals.* Biochemical Journal, 1990. **265**(3): p. 659-665.
68. Stone, J.R. and T. Collins, *The role of hydrogen peroxide in endothelial proliferative responses.* Endothelium, 2002. **9**(4): p. 231-238.

69. Fridovich, I., *Superoxide Dismutases.* Annual Review of Biochemistry, 1975. **44**(1): p. 147-159.
70. Wende, K., et al., *Identification of the biologically active liquid chemistry induced by a nonthermal atmospheric pressure plasma jet.* Biointerphases, 2015. **10**(2): p. 1-16.
71. Halliwell, B., *Biochemistry of oxidative stress.* Biochemical Society Transactions, 2007. **35**(5): p. 1147-1150.
72. Kong, M.G., B.N. Ganguly, and R.F. Hicks, *Plasma jets and plasma bullets.* Plasma Sources Science and Technology, 2012. **21**(3): p. 030201.
73. Ojha, N., et al., *Assessment of wound-site redox environment and the significance of Rac2 in cutaneous healing.* Free Radical Biology and Medicine, 2008. **44**(4): p. 682-691.
74. Hibbs, J., R. Taintor, and Z. Vavrin, *Macrophage cytotoxicity: role for L-arginine deiminase and imino nitrogen oxidation to nitrite.* Science, 1987. **235**(4787): p. 473-476.
75. Lundberg, J.O., E. Weitzberg, and M.T. Gladwin, *The nitrate–nitrite–nitric oxide pathway in physiology and therapeutics.* Nature Reviews Drug Discovery, 2008. **7**: p. 156.
76. Butler, A.R. and M. Feelisch, *Therapeutic Uses of Inorganic Nitrite and Nitrate.* Circulation, 2008. **117**(16): p. 2151-2159.
77. Ulrich, C., et al., *Clinical use of cold atmospheric pressure argon plasma in chronic leg ulcers: A pilot study.* J Wound Care, 2015. **24**(5): p. 196, 198-200, 202-3.
78. Matthes, R., et al., *Antimicrobial Efficacy of Two Surface Barrier Discharges with Air Plasma against In Vitro Biofilms.* PLOS ONE, 2013. **8**(7): p. e70462.
79. Kim, P.Y., et al., *Bacterial inactivation of wound infection in a human skin model by liquid-phase discharge plasma.* PLoS One, 2011. **6**(8): p. e24104.
80. Kamgang-Youbi, G., et al., *Evidence of temporal postdischarge decontamination of bacteria by gliding electric discharges: application to Hafnia alvei.* Appl Environ Microbiol, 2007. **73**(15): p. 4791-6.
81. Julak, J., et al., *The persistent microbicidal effect in water exposed to the corona discharge.* Phys Med, 2012. **28**(3): p. 230-9.
82. Klebes, M., et al., *Combined antibacterial effects of tissue-tolerable plasma and a modern conventional liquid antiseptic on chronic wound treatment.* Journal of Biophotonics, 2015. **8**(5): p. 382-391.
83. Oehmigen, K., et al., *The Role of Acidification for Antimicrobial Activity of Atmospheric Pressure Plasma in Liquids.* Plasma Processes and Polymers, 2010. **7**(3-4): p. 250-257.
84. Lukes, P., et al., *Aqueous-phase chemistry and bactericidal effects from an air discharge plasma in contact with water: evidence for the formation of peroxynitrite through a pseudo-second-order post- discharge reaction of H_2O_2 and HNO_2.* Plasma Sources Science and Technology, 2014. **23**: p. 015019.
85. Graves, D.B., *Oxy-nitroso shielding burst model of cold atmospheric plasma therapeutics.* Clinical Plasma Medicine, 2014. **2**: p. 38-49.
86. Babaeva, N.Y. and M.J. Kushner, *Intracellular electric fields produced by dielectric barrier discharge treatment of skin.* Journal of Physics D: Applied Physics, 2010. **43**(18): p. 185206.
87. Tongtong, H., et al., *A 'tissue model' to study the barrier effects of living tissues on the reactive species generated by surface air discharge.* Journal of Physics D: Applied Physics, 2016. **49**(20): p. 205204.

88. Lu, X., et al., *Reactive species in non-equilibrium atmospheric-pressure plasmas: Generation, transport, and biological effects.* Physics Reports, 2016. **630**: p. 1-84.
89. Begum, A., M. Laroussi, and M.R. Pervez, *Atmospheric pressure He-air plasma jet: Breakdown process and propagation phenomenon.* AIP Advances, 2013. **3**(6): p. 062117.
90. Szili, E.J., J.W. Bradley, and R.D. Short, *A 'tissue model' to study the plasma delivery of reactive oxygen species.* Journal of Physics D: Applied Physics, 2014. **47**: p. 152002.
91. Yusupov, M., et al., *Synergistic effect of electric field and lipid oxidation on the permeability of cell membranes.* Biochimica et Biophysica Acta (BBA) - General Subjects, 2017. **1861**(4): p. 839-847.
92. Wikipedia. *Body water*. 2017 [cited 2018 27 January 2018]; Available from: https://en.wikipedia.org/w/index.php?title=Body_water&oldid=791849932.
93. Wei, T. and J.K. Mark, *Atmospheric pressure dielectric barrier discharges interacting with liquid covered tissue.* Journal of Physics D: Applied Physics, 2014. **47**(16): p. 165201.
94. Bartosz, G., *Use of spectroscopic probes for detection of reactive oxygen species.* Clinica Chimica Acta, 2006. **368**(1–2): p. 53-76.
95. Miranda, K.M., M.G. Espey, and D.A. Wink, *A rapid, simple spectrophotometric method for simultaneous detection of nitrate and nitrite.* Nitric Oxide, 2001. **5**(1): p. 62-71.
96. Hempel, S.L., et al., *Dihydrofluorescein diacetate is superior for detecting intracellular oxidants: comparison with 2',7'-dichlorodihydrofluorescein diacetate, 5(and 6)-carboxy-2',7'-dichlorodihydrofluorescein diacetate, and dihydrorhodamine 123.* Free Radical Biology and Medicine, 1999. **27**(1): p. 146-159.
97. Wardman, P., *Fluorescent and luminescent probes for measurement of oxidative and nitrosative species in cells and tissues: Progress, pitfalls, and prospects.* Free Radical Biology & Medicine, 2007. **43**: p. 995-1022.
98. Karlsson, M., et al., *What does the commonly used DCF test for oxidative stress really show?* Biochemical Journal, 2010. **428**(2): p. 183-190.
99. Burkitt, M.J. and P. Wardman, *Cytochrome c Is a Potent Catalyst of Dichlorofluorescin Oxidation: Implications for the Role of Reactive Oxygen Species in Apoptosis.* Biochemical and Biophysical Research Communications, 2001. **282**(1): p. 329-333.
100. Bonini, M.G., et al., *The oxidation of 2',7'-dichlorofluorescin to reactive oxygen species: a self-fulfilling prophesy?* Free Radic Biol Med, 2006. **40**(6): p. 968-75.
101. Chen, X., et al., *2',7'-Dichlorodihydrofluorescein as a fluorescent probe for reactive oxygen species measurement: Forty years of application and controversy.* Free Radical Research, 2010. **44**(6): p. 587-604.
102. Chen, X., et al., *2',7'-Dichlorodihydrofluorescein as a fluorescent probe for reactive oxygen species measurement: Forty years of application and controversy.* Free Radical Research Communications, 2010. **44**(6): p. 587-604.
103. Luther, G.W., 3rd, et al., *Thermodynamics and kinetics of sulfide oxidation by oxygen: a look at inorganically controlled reactions and biologically mediated processes in the environment.* Frontiers in microbiology, 2011. **2**: p. 62-62.
104. Gaur, N., et al., *Combined effect of protein and oxygen on reactive oxygen and nitrogen species in the plasma treatment of tissue.* Applied Physics Letters, 2015. **107**(10): p. 103703.

105. Jun-Seok, O., et al., *How to assess the plasma delivery of RONS into tissue fluid and tissue.* Journal of Physics D: Applied Physics, 2016. **49**(30): p. 304005.
106. Endre, J.S., et al., *The assessment of cold atmospheric plasma treatment of DNA in synthetic models of tissue fluid, tissue and cells.* Journal of Physics D: Applied Physics, 2017. **50**(27): p. 274001.
107. Fornera, S. and P. Walde, *Spectrophotometric quantification of horseradish peroxidase with o-phenylenediamine.* Analytical Biochemistry, 2010. **407**(2): p. 293-295.
108. Bystryak, S.M. and V.M. Mekler, *Photochemical amplification for horseradish peroxidase-mediated immunosorbent assay.* Analytical Biochemistry, 1992. **202**(2): p. 390-393.
109. Tarcha, P.J., V.P. Chu, and D. Whittern, *2,3-Diaminophenazine is the product from the horseradish peroxidase-catalyzed oxidation of o-phenylenediamine.* Analytical biochemistryAnal Biochem, 1987. **165**(1): p. 230-3.
110. Hempen, C., et al., *Liquid chromatographic/mass spectrometric investigation on the reaction products in the peroxidase-catalyzed oxidation of o-phenylenediamine by hydrogen peroxide.* Analytical and Bioanalytical Chemistry, 2005. **382**(1): p. 234-238.
111. Bratton, A.C., et al., *A new coupling component for sulfanilamide determination.* Journal of Biological Chemistry, 1939. **128**(2): p. 537-550.
112. Awad, H.H. and D.M. Stanbury, *Autoxidation of NO in aqueous solution.* International Journal of Chemical Kinetics, 1993. **25**(5): p. 375-381.
113. Verdon, C.P., B.A. Burton, and R.L. Prior, *Sample Pretreatment with Nitrate Reductase and Glucose-6-Phosphate Dehydrogenase Quantitatively Reduces Nitrate While Avoiding Interference by NADP+ When the Griess Reaction Is Used to Assay for Nitrite.* Analytical Biochemistry, 1995. **224**(2): p. 502-508.
114. Motomizu, S. and M. Sanada, *Photo-induced reduction of nitrate to nitrite and its application to the sensitive determination of nitrate in natural waters.* Analytica Chimica Acta, 1995. **308**(1): p. 406-412.
115. Wang, J., et al., *Effects of pH and H2O2 on ammonia, nitrite, and nitrate transformations during UV254nm irradiation: Implications to nitrogen removal and analysis.* Chemosphere, 2017. **184**: p. 1003-1011.
116. Machado, A., et al., *A greener alternative for inline nitrate reduction in the sequential injection determination of NOx in natural waters: replacement of cadmium reduction by UV radiation.* Analytical Methods, 2017. **9**(12): p. 1876-1884.
117. Zhang, Y. and L. Wu, *Photochemical reduction of nitrate to nitrite in aqueous solution and its application to the determination of total nitrogen in water.* Analyst, 1986. **111**(7): p. 767-769.
118. Endre, J.S., et al., *Modelling the helium plasma jet delivery of reactive species into a 3D cancer tumour.* Plasma Sources Science and Technology, 2018. **27**(1): p. 014001.
119. Oh, J.-S., et al., *How plasma induced oxidation, oxygenation, and de-oxygenation influences viability of skin cells.* Applied Physics Letters, 2016. **109**(20): p. 203701.
120. Bruggeman, P., et al., *Plasma–liquid interactions: a review and roadmap.* Plasma sources science and technology, 2016. **25**(5): p. 053002.
121. Du, J., et al., *Concentration distributions and reaction pathways of species in the mass transfer process from atmospheric pressure plasma jet to water.* The European Physical Journal D, 2018. **72**(10): p. 179.

122. Sander, R., *Compilation of Henry's law constants (version 4.0) for water as solvent.* Atmospheric Chemistry & Physics, 2015. **15**(8): p. 4399-4981.
123. Grzelak A, *e.a.*, *Light-dependent generation of reactive oxygen species in cell culture media.* Free Radical Biology & Medicine, 2001. **30**(12): p. 1418-1425.
124. Stehle, P. and K.S. Kuhn, *Glutamine: An Obligatory Parenteral Nutrition Substrate in Critical Care Therapy.* BioMed Research International, 2015. **2015**: p. 7.
125. de Vasconcelos, M.I. and J. Tirapegui, *[Nutritional importance of glutamine]*. Arq Gastroenterol, 1998. **35**(3): p. 207-15.
126. Aledo, J.C., *Glutamine breakdown in rapidly dividing cells: waste or investment?* BioEssays, 2004. **26**(7): p. 778-785.
127. Corbet, C. and O. Feron, *Metabolic and mind shifts: from glucose to glutamine and acetate addictions in cancer.* Current Opinion in Clinical Nutrition & Metabolic Care, 2015. **18**(4): p. 346-353.
128. Yu, J.-C., Z.-M. Jiang, and D.-M. Li, *Glutamine: a precursor of glutathione and its effect on liver.* World journal of gastroenterology, 1999. **5**(2): p. 143-146.
129. Jakubowski, W. and G. Bartosz, *2,7-dichlorofluorescin oxidation and reactive oxygen species: what does it measure?* Cell biology international, 2000. **24**(10): p. 757-60.
130. Marques, C., et al., *Antioxidant properties of glutamine and its role in VEGF-Akt pathways in portal hypertension gastropathy.* World journal of gastroenterology, 2013. **19**(28): p. 4464-74.
131. Kerksick, C. and D. Willoughby, *The antioxidant role of glutathione and N-acetyl-cysteine supplements and exercise-induced oxidative stress.* Journal of the International Society of Sports Nutrition, 2005. **2**(2): p. 38-44.
132. Lobo, V., et al., *Free radicals, antioxidants and functional foods: Impact on human health.* Pharmacognosy reviews, 2010. **4**(8): p. 118.
133. Lewinska, A., et al., *Total anti-oxidant capacity of cell culture media.* Clinical and Experimental Pharmacology and Physiology, 2007. **34**(8): p. 781-786.
134. Stadtman, E.R. and R.L. Levine, *Free radical-mediated oxidation of free amino acids and amino acid residues in proteins.* Amino Acids, 2003. **25**(3): p. 207-218.
135. Kalyanaraman, B., et al., *Recent developments in detection of superoxide radical anion and hydrogen peroxide: Opportunities, challenges, and implications in redox signaling.* Archives of biochemistry and biophysics, 2017. **617**: p. 38-47.
136. Dikalov, S.I. and D.G. Harrison, *Methods for detection of mitochondrial and cellular reactive oxygen species.* Antioxidants & redox signaling, 2014. **20**(2): p. 372-382.
137. Kalyanaraman, B. and J. Zielonka, *Green fluorescent proteins induce oxidative stress in cells: A worrisome new wrinkle in the application of the GFP reporter system to biological systems?* Redox biology, 2017. **12**: p. 755-757.
138. DeLeon, E.R., et al., *A case of mistaken identity: are reactive oxygen species actually reactive sulfide species?* American Journal of Physiology-Regulatory, Integrative and Comparative Physiology, 2016. **310**(7): p. R549-R560.
139. Eghbal, M.A., P.S. Pennefather, and P.J. O'Brien, *H2S cytotoxicity mechanism involves reactive oxygen species formation and mitochondrial depolarisation.* Toxicology, 2004. **203**(1-3): p. 69-76.
140. Joyner-Matos, J., et al., *Hydrogen sulfide induces oxidative damage to RNA and DNA in a sulfide-tolerant marine invertebrate.* Physiological and biochemical zoology : PBZ, 2010. **83**(2): p. 356-365.

141. Jirásek, V. and P. Lukeš, *Formation of reactive chlorine species in saline solution treated by non-equilibrium atmospheric pressure He/O2 plasma jet.* Plasma Sources Science and Technology, 2019. **28**(3): p. 035015.
142. Chaparro, C.V., et al., *Considerations on electrical impedance measurements of electrolyte solutions in a four-electrode cell.* Journal of Physics: Conference Series, 2016. **687**: p. 012101.
143. Eisuke, T., et al., *Chemical modification of amino acids by atmospheric-pressure cold plasma in aqueous solution.* Journal of Physics D: Applied Physics, 2014. **47**(28): p. 285403.
144. Zhou, R., et al., *Interaction of Atmospheric-Pressure Air Microplasmas with Amino Acids as Fundamental Processes in Aqueous Solution.* PloS one, 2016. **11**(5): p. e0155584-e0155584.
145. Li, Q. and J.R. Lancaster, *Chemical foundations of hydrogen sulfide biology.* Nitric Oxide, 2013. **35**: p. 21-34.
146. Filipovic, Milos R., et al., *Biochemical insight into physiological effects of H2S: reaction with peroxynitrite and formation of a new nitric oxide donor, sulfinyl nitrite.* Biochemical Journal, 2012. **441**(2): p. 609-621.
147. Vermeiren, J., et al., *Sulfide- and nitrite-dependent nitric oxide production in the intestinal tract.* Microbial biotechnology, 2012. **5**(3): p. 379-387.
148. Bryan, N.S. and M.B. Grisham, *Methods to detect nitric oxide and its metabolites in biological samples.* Free Radic Biol Med, 2007. **43**(5): p. 645-57.
149. Tresp, H., et al., *Effects of Atmosphere Composition and Liquid Type on Plasma-Generated Reactive Species in Biologically Relevant Solutions.* 2013. **3**(1-2): p. 45-55.
150. Jankowski, J.J., D.J. Kieber, and K. Mopper, *Nitrate and nitrite ultraviolet actinometers.* Photochemistry and Photobiology, 1999. **70**(3): p. 319-328.
151. Bienert, G.P., J.K. Schjoerring, and T.P. Jahn, *Membrane transport of hydrogen peroxide.* Biochimica et Biophysica Acta (BBA) - Biomembranes, 2006. **1758**(8): p. 994-1003.
152. Hall, S.B., E.A. Khudaish, and A.L. Hart, *Electrochemical oxidation of hydrogen peroxide at platinum electrodes. Part 1. An adsorption-controlled mechanism.* Electrochimica Acta, 1998. **43**(5): p. 579-588.
153. Khudaish, E.A., *The electrochemical oxidation of hydrogen peroxide on platinum electrodes at phosphate buffer solutions : a thesis presented in partial fulfilment of the requirements for the degree of Doctor of Philosophy in Chemistry at Massey University, Palmerston North, New Zealand*. 1999, Massey University.
154. Hall, S.B., E.A. Khudaish, and A.L. Hart, *Electrochemical oxidation of hydrogen peroxide at platinum electrodes. Part IV: phosphate buffer dependence.* Electrochimica Acta, 1999. **44**(25): p. 4573-4582.
155. Instruments, W.P. *Hydrogen Peroxide Macro Sensor*. [cited 2018 06-Dec-2018]; Available from: https://www.wpiinc.com/pub/media/wysiwyg/pdf/ISO-HPO-2_IMs.pdf.

Chapter 3 Assessing plasma delivery of reactive species through tissue

The potential value of plasma jets for medical applications is assigned to the fact they can be used to deliver RONS to tissues [1]. It is well established in the literature that RONS can upregulate and/or downregulate certain cellular processes [1]. Plasma-generated RONS are generated in the plasma gas-phase, in tissue fluid, and within the tissue itself. To date, most studies of the effects of plasma have been conducted *in-vitro* and have utilised cell culture – investigating the effects of plasma at "whole" cell level (for example on viability, proliferation and migration) [2-9]. However, more recently, there is a growing literature that focuses on the interactions of plasma at a molecular and cellular level such as on the modifications to proteins [10-12], DNA [13-17] and amino acids [18-20] and on the up-regulation/down-regulation of key proteins [11, 21-24]. In contrast, there has been little attention (with few reported studies) on the interactions of plasma at the tissue level.

Plasma-tissue interactions are important as to explain how plasma-generated RONS are delivered "deep'' into the tissue – where their effects manifest. The "direct" delivery of RONS by plasma jet is (generally thought to be) restricted to a few nanometers below the tissue target [25-27]. Therefore, most likely, the deep penetration of RONS to several micrometers (μm) [28-30] or millimeters (mm) [31] is an "indirect" phenomenon.

Broadly, the plasma treatment of tissue begins with the generation of shorter-lived species such as •OH near the gas-liquid interface. The •OH radicals can be generated through a complex set of reactions, and a few have been listed below (R1-R3). After the evaporation of the thin liquid layer covering the tissue surface by plasma, water vapours undergo a dissociative reaction to form •OH (R1) [32]. Additionally, •OH radicals can also be produced via dissociation of water ions (R2) and ion neutralization between $O_2^{-\bullet}$ and water ions (R3) [32].

$$e^- + H_2O \rightarrow H + {\bullet}OH + e^- \qquad -(R1)$$

$$e^- + H_2O^+ \rightarrow H + {\bullet}OH \qquad -(R2)$$

$$O_2^{-\bullet} + H_2O^+ \rightarrow H + O_2 + {\bullet}OH \qquad -(R3)$$

The •OH has a lifetime of 10^{-9} s, and can cross the gas-liquid interface and are reported to diffuse into 0.009 µm within mammalian cells [33]. $O_2^{\bullet-}$, NO and $ONOO^-$, with half lives of few milliseconds, are also formed near the gas-liquid interface [34, 35], which potentially can solvate into the tissue.

Being highly reactive in nature, these short lived species undergoes rapid reactions with other species to form longer-lived (and also highly) reactive RONS such as H_2O_2, NO_2^- and NO_3^- [32, 36]. These secondary RONS, thus formed, diffuse from the sub-surface deep into the tissue wherein a cascade of reactions between neighbouring RONS occur, leading to an *in situ* RONS production even post discharge [34, 36]. Studies by Szili *et al.* and Oh *et al.* have successfully shown the real-time transport of H_2O_2, NO_2^- and NO_3^- to mm depths [37-40].

An alternative mechanism of plasma-generation/delivery of RONS in tissue is associated with the UV photons produced by plasma. During plasma treatment, the UV photons are absorbed by the tissue target (covered with tissue fluid) and result in photolysis of water molecules to form hydrated electrons, ground state and excited oxygen atoms; and shorter- lived reactive species such as •OH. [35, 41, 42]. These highly reactive and shorter-lived species produced via photochemical reactions, are formed in top-layer (few µm) of tissue and undergo subsequent reactions to form more stable RONS such as H_2O_2. This is discussed in detail in Section 3.1.2.

A few studies have also commented on the role of electric fields from plasma in facilitating the delivery of RONS into the tissue. For instance, the study by Szili *et al.* showed that RONS are delivered in a star-shape patterns in a tissue model by the plasma jet [31]. These patterns formed by plasma jets are similar to the star-shaped Lichtenberg figures formed by plasma surface streamers across the insulator [43]. In another study, He *et al.* have successfully demonstrated the increase in plasma delivery of RONS in real tissues by the application of an extra electric field of 20 V/cm [44]. Further investigations are required to understand the mechanisms involved in deep-transport of RONS mediated by electric fields in the plasma.

The deep molecular effects induced by plasma in the real tissues has been explained using the "oxy-nitroso shield burst model" proposed by Graves [45] (Figure 3.1). According to this model, the process begins with a short term "burst" of plasma generated shorter-lived RONS in gas-phase, which react with sub-surface cells or fluids,

as explained above. The longer-lived species (such as H_2O_2, NO_2^- and NO_3^-), produced after cascade of secondary redox reactions, diffuse to interact with deeper lying cells and cause oxidative stress. Depending on the type of stress – distress or eustress – various signaling processes are actuated. The stressed cells interact with neighboring cells (adjacent and distant) via "cell-to-cell bystander communication" [46, 47]. During this communications, nearby cells may undergo cascade of redox signaling producing more RONS. This localised production of RONS in a tissue leads to further cell-to-cell communication and eventually stimulate the immune system. Activation of immune system is beneficial for the cell to undergo tissue repair, bacterial resistance and combat tumors. This model is attractive as it explains how plasma can induce biological effects associated with shorter-lived species such as •OH [1, 48].

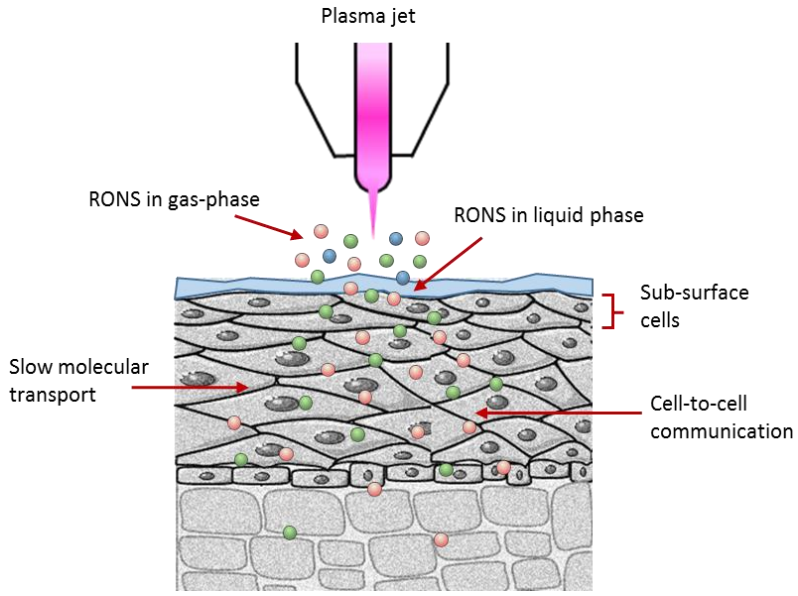


Figure 3.1 'Oxy-nitroso shield burst model' illustrating transport of plasma generated RONS deep into the tissue via cell-to-cell communication.

Hitherto, there has been a lack of substantiate experimental methods to probe the delivery of RONS within tissue. In this Chapter, hydrogels are employed as synthetic tissue models (or "tissue surrogates") to mimic real tissues (removing any influence from the cell components). Previously, a wide range of different types of hydrogels (or polymeric hydrogels) have been utilised as tissue surrogates in the studies involving imaging techniques such as MRI, X-rays and ultrasound. Materials that have been used include polyvinyl alcohol (PVA) [49-52], gelatin [53-55], agarose [56-59], polyacrylamide [60], alginate [61], polyurethane [62], collagen [63], chitosan [64], carboxymethylcellulose [65] and 2-hydroxylethylacrylate [66]. The hydrogels used in

this chapter are ideal as tissue surrogates to study the plasma-tissue interactions due to following properties:

i. Hydrogels are a network of 'hydrated' proteins and/or polysaccharides. The high water content in hydrogels is similar to the extracellular matrix of the real tissues [67].

ii. Hydrogels can be easily modified to closely mimic the physical and mechanical properties of real tissues. For example, a 10% weight by volume (w/v) gelatin film has elastic modulus of 38–54 MPa similar to that of human skin (20–80 MPa) [68]. Similarly, the elastic modulus of a 10% w/v PVA matrix (10.4 ± 0.3–13.4 ± 1.0 kPa) falls within the range for brain cerebellum (7.09 ± 0.65–31.5 ± 4.1 kPa) [69].

iii. Hydrogels are highly versatile, allowing for variation in experimental methodologies. For example, different biomolecules such as molecular reporters [31], proteins [70], oligonucleotides [71], cells [72], etc. can be dispersed within a hydrogel matrix. This is advantageous to mimic different types of real-tissues.

iv. They are robust, non-hazardous and easy to handle [73].

Tissue models made of agarose, gelatin and PVA have been utilised in this chapter. Agarose is the most widely used and well characterised tissue mimic [74]. It had been used in studies involved with radiotherapy [75], neuroscience [76] and ultrasound imaging [74] to mimic different tissues such as skin [77], liver [78], prostate [59] and brain [79]. Gelatin is a hydrolysed form of collagen and a major protein in skin, bone, and connective tissues [80, 81]. Gelatin matrix have been used as skin mimic in various studies such as elastography [82], testing cosmetics and topical creams [83, 84], and adhesives for skin [85]. PVA is a non-proteinaceous tissue model, which has been widely used in optical tomography [86], X-ray imaging [87] and magnetic resonance techniques [69].

Besides RONS, O_2 also plays vital role in wound healing [88-91]. Insufficient levels of O_2 (also termed as hypoxemia or hypoxia) caused by failed vasculature hinders wound healing processes such as reduced granulation tissue production and delayed epithelialization [92-94]. By improving tissue O_2 content (oxygen tension), regeneration

of tissues can be enhanced by promoting collagen deposition and the tensile strength of collagen can be improved [95]. O_2 also serves as an antimicrobial as it undergoes redox reactions to form RONS such as H_2O_2 and NO, which promote wound disinfection [96-101]. RONS produced from O_2 redox chemistry also act as secondary messengers and promote wound healing (as discussed previously in Chapter 1) [39, 91, 102-105]. It has been reported that plasma can elevate levels of oxygen within tissue targets [i.e. O_2 (aq)] [7, 32, 70, 106-108]. For instance, in a live mouse model the partial pressure of O_2 increased rapidly upon plasma treatment (for 5 min) from 20 mm Hg to 65 mm Hg [106]. Therefore, the potential of plasma to elevate O_2 (aq) in tissue models is also evaluated in this chapter.

The delivery of RONS and O_2 (aq) by plasma treatment into tissue targets is assessed using a variety of techniques – molecular probes, UVAS, OES and mass spectrometry. The reported data have been produced as a result of ongoing collaborations between the University of South Australia and two Japanese Universities. Thereby, studies with molecular probes were conducted in University of South Australia, whilst experiments with UVAS and mass spectrometry were conducted in Meijo University and Kochi University of Technology. The framework of this chapter is as follows:

i. Section 3.1 : Molecular probes to track RONS delivered by plasma through tissue models

ii. Section 3.2 : Real-time monitoring of plasma delivered RONS through tissue model using UVAS

iii. Section 3.3 : Tracking penetration of RONS delivered by plasma in tissue model using mass spectrometry

The pros and cons associated with each technique (molecular probes, UVAS and mass spectrometry) are discussed in detail in each relevant section. Readers are encouraged to consider each section as a distinct study in its own right: although all studies utilised plasma jets and tissue models, there exists differences in type of power supply used in plasma jet unit, experimental setup and plasma treatment parameters. However, a number of general conclusions are drawn from all these studies, which are significant for interactions between any plasma jet and tissue (Section 3.4).

3.1 Molecular probes to track RONS delivered by plasma through tissue models

In this chapter, RONS delivery in gelatin and PVA tissue models is monitored using molecular probes. The working principle of molecular probes has been explained in Chapter 2. Upon interaction with RONS, an increase in absorbance and fluorescence intensity of colorimetric and fluorescence probes, respectively, is observed. DCFH is used as a broad range RONS probe to measure total redox species generated by plasma. As stated earlier, both longer- and shorter- lived species generated by plasma play key role in redox signaling and generation of RONS deep below sub-surface cells. Therefore, it is essential to meter delivery of both longer-lived species such as H_2O_2 and NO_2^- and shorter-lived species such as •OH through tissues. H_2O_2 was measured using OPD-HRP, NO_2^- using Griess reagent and •OH using terepthalic acid (TA).

It has been shown that presence of proteins influence RONS production. For instance, in case of both light-dependent [109] and plasma generation of RONS in aqueous solution [32], the presence of protein (or serum) diminishes production of ROS. Quite contrary results have been obtained by Szili *et al.* wherein serum enhanced RONS generation in solution upon plasma treatment [110]. Therefore, role of proteins in plasma delivery of RONS still remains obscure.

In this chapter, the combined effect of both protein and O_2 (aq) in plasma delivery of RONS has been evaluated. To stimulate real tissues, both fluid proteins and protein in tissue were mimicked by dissolving bovine serum albumin (BSA) in solution and dispersing BSA in tissue hydrogel matrix (Figure 3.3).

3.1.1 Materials and Methods

3.1.1.1 Plasma jet

A two-electrode He plasma jet unit was used in this study (Figure 3.2). A glass pipette tube, with an inner diameter of 1 mm, was surrounded by two external hollow electrodes separated at a distance of 10 mm. From the bottom electrode, 1 mm of the end of glass tube protrudes out. He gas (BOC, high purity grade) at 100 ml min^{-1} was purged into the glass tube. A voltage potential of 5.5 $kV_{peak-peak}$ and a frequency of 10 kHz was applied yielding a plasma plume of 5 mm in length.

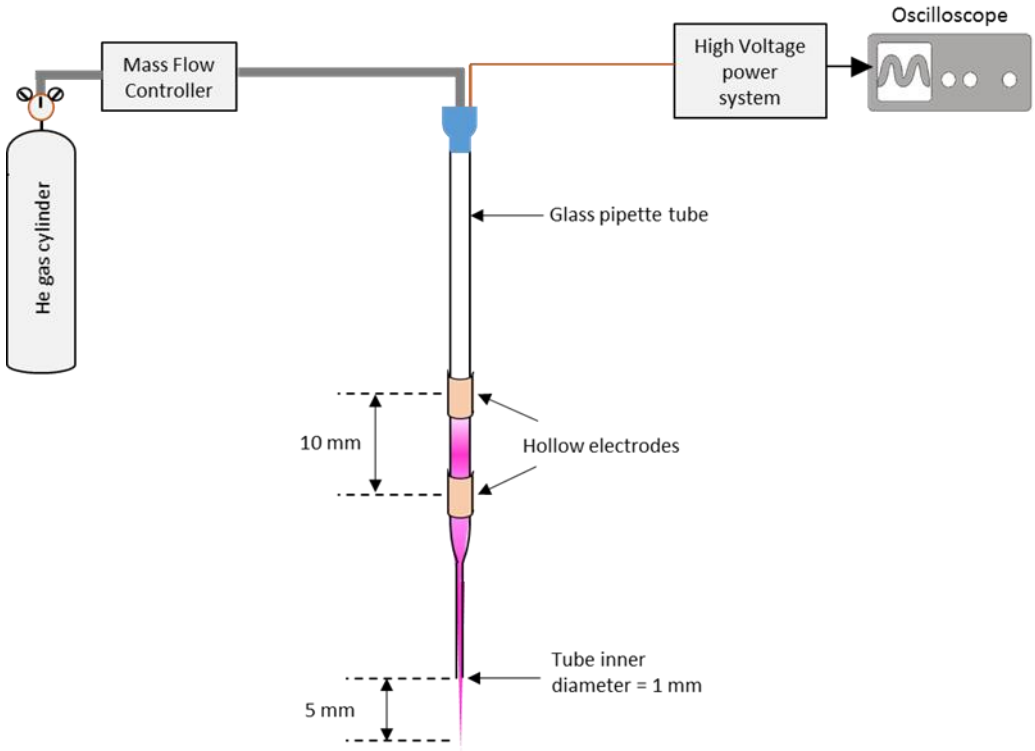


Figure 3.2 Schematic of the He plasma jet used for this study.

3.1.1.2 Preparation of the tissue model

(a) 5% (w/v) gelatin film: 50 mg ml^{-1} gelatin powder (Sigma-Aldrich, catalogue number G1890) was dissolved in 1 x PBS (Sigma-Aldrich, catalogue number P4417) by placing in a hot water bath at 40°C with continuous stirring for 15-20 minutes. 9 ml of this solution is poured into an 85 mm diameter (plastic) petri dish lined with parafilm® (Beemis, catalogue number PM-996) and evenly spread to get a 1 mm thick film. The gelatin was allowed to set at 4˚C for 12 h before use. Square sections of approximately 10 x 10 mm were cut.

(b) 10% (w/v) PVA film: 100 mg ml-1 PVA powder (Sigma-Aldrich, catalogue number 363065) was dissolved in 1 x PBS solution by placing in a hot water bath at 40°C with continuous stirring for 45-50 minutes. The solution was allowed to cool to 90°C for 30 min. Protocol similar to gelatin was used to prepare 1 mm thick films.

3.1.1.3 Preparation of the molecular probes solution

(a) DCFH: The DCFH-DA powder (Sigma-Aldrich, catalogue number D6883) was dissolved in ethanol to get an end concentration of 2 mM; the solution was stored at -20°C until use. 500 µl of stock DCFH-DA was added to 2 ml of 10 mM NaOH and incubated for 30 min at 25°C in the dark to induce ester hydrolysis

and deacetylation of DCFH-DA. The DCFH (deacetylated) solution was then neutralised by adding 10 ml of PBS. The solution was stored in the dark until use. Fluorescence was measured at an excitation wavelength of 485 nm and emission wavelength of 520 nm.

(b) *OPD-HRP*: A mixture of 18.5 mM OPD powder (Sigma-Aldrich, catalogue number P9029) and 4 µg ml-1 HRP powder (Sigma-Aldrich, catalogue number P6782) was dissolved in PBS. bsorbance was measured at 450 nm.

(c) *Griess reagent*: A 50 mg ml^{-1} solution of Griess reagent (Sigma-Aldrich, catalogue number G4410) was prepared in PBS. Absorbance was measured at 492 nm.

(d) *TA*: A 500 mM solution of TA (Sigma-Aldrich, catalogue number 185361) was prepared in PBS. Fluorescence was measured at excitation wavelength of 310 nm and emission wavelength of 420 nm.

3.1.1.4 UV-absorption spectroscopy

The levels of oxygen in PBS post plasma treatment were measured using a UV absorption spectrometer (Hitachi, U-3900). All measurements were carried out in a 100 µm optical path cuvette cells (Hellma, 106-QS). After plasma treatment of PBS (in a 96-well plate) with and without the tissue target on top, a 100 µl aliquot of test solution was diluted to 1 ml deionized water before measurements. As a positive control, absorbance was also measured corresponding to 100% O_2 by purging pure oxygen in PBS.

3.1.1.5 Experimental setup

400 µl of molecular probe solution (referred as RONS reporter solution thereafter) in a 96-well plate (Costar®, catalogue number 3596) was plasma treated for 1, 5 and 10 min at a distance of 1 mm between the end of the glass capillary tube and top of the target surface (RONS reporter solution or the gelatin / PVA targets). It was ensured that the tissue targets were in contact with the RONS probe solution at all times. 100 µl of the plasma treated reporter solution was then transferred to another 96-well plate for absorbance and FI measurements. Figure 3.3 illustrates the experimental scheme utilised in this chapter to study the role of proteins and O_2 in plasma generation of RONS through a tissue target.

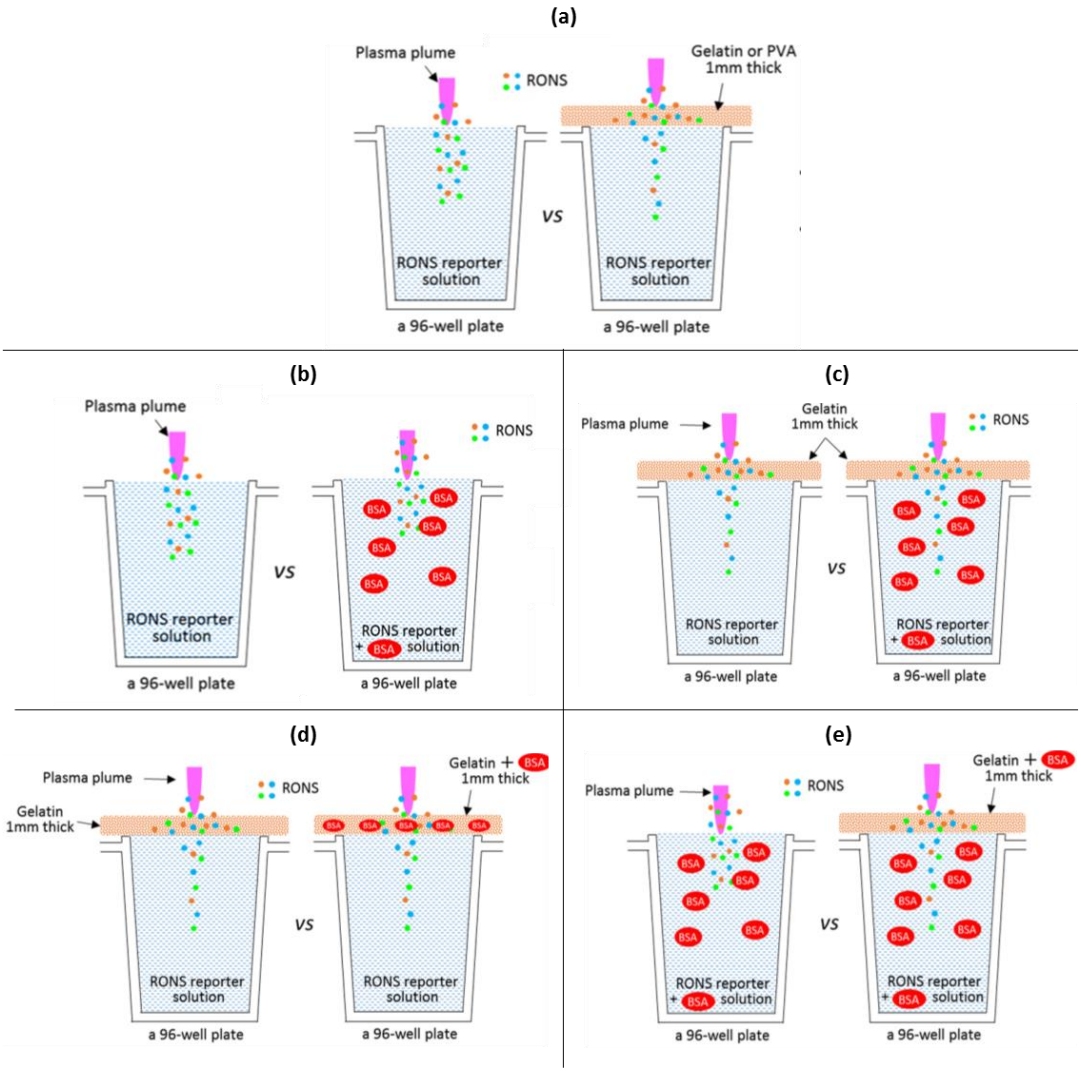


Figure 3.3 Schematic of the experimental set-up to assess (a) concentration of RONS delivered by plasma through gelatin and PVA tissue target; (b) the role of fluid proteins in plasma delivery of RONS upon direct plasma exposure; (c) the role of fluid proteins in delivery of RONS through gelatin tissue target; (d) how proteins embedded in gelatin tissue model impact RONS delivery; and (e) how fluid proteins and tissue-embedded proteins together influence plasma generation of RONS. In all cases the plasma plume is in contact with the target.

The role of proteins on the transport of RONS through targets into PBS was investigated using BSA. BSA powder (Sigma-Aldrich A7906) was dissolved in PBS at a concentration of 1, 25 and 50 mg ml^{-1} to mimic fluid proteins. BSA was also incorporated in gelatin targets at 50 mg ml^{-1} to understand how transport and/or generation of RONS is affected when protein is present in the tissue itself (Figure 3.3d and 3.3e). Appropriate controls were considered for each scenario to understand the roles of proteins and oxygen in RONS delivery. For instance:

(i) the direct plasma exposure of RONS reporter solution for 1 min[1] was the control for plasma delivery of RONS through the tissue target (Figure 3.3a);

(ii) the use of BSA-free solution was the control to study the influence of fluid proteins (Figure 3.3b and 3.3c),

(iii) the delivery of RONS through BSA-free tissue is compared with tissue incorporating BSA (Figure 3.3d), and

(iv) the direct exposure of BSA reporter solution is compared with the indirect exposure of BSA reporter solution through a BSA- tissue matrix (Figure 3.3e).

3.1.2 Results and discussion

The first step was to meter RONS including H_2O_2, NO_2^- and •OH delivered by plasma through the tissue target using specific RONS reporter solutions (OPD-HRP, Griess reagent and TA). Reporter solution was directly exposed to plasma as a control. The absorbance of plasma treated OPD-HRP and Griess reagent was correlated to H_2O_2 (Figure 3.4b) and NO_2^- (Figure 3.4c) concentrations using calibration curves (See Appendix A and B). Due to lack of a calibration curve for •OH, its generation is presented as a normalised FI (Figure 3.3d) and was calculated using the formula below:

$$Normalised\ FI = \frac{FI\ after\ plasma\ treatment}{FI\ before\ plasma\ treatment}$$

[1]1 min of direct plasma treatment was conducted to avoid significant evaporation of the solution

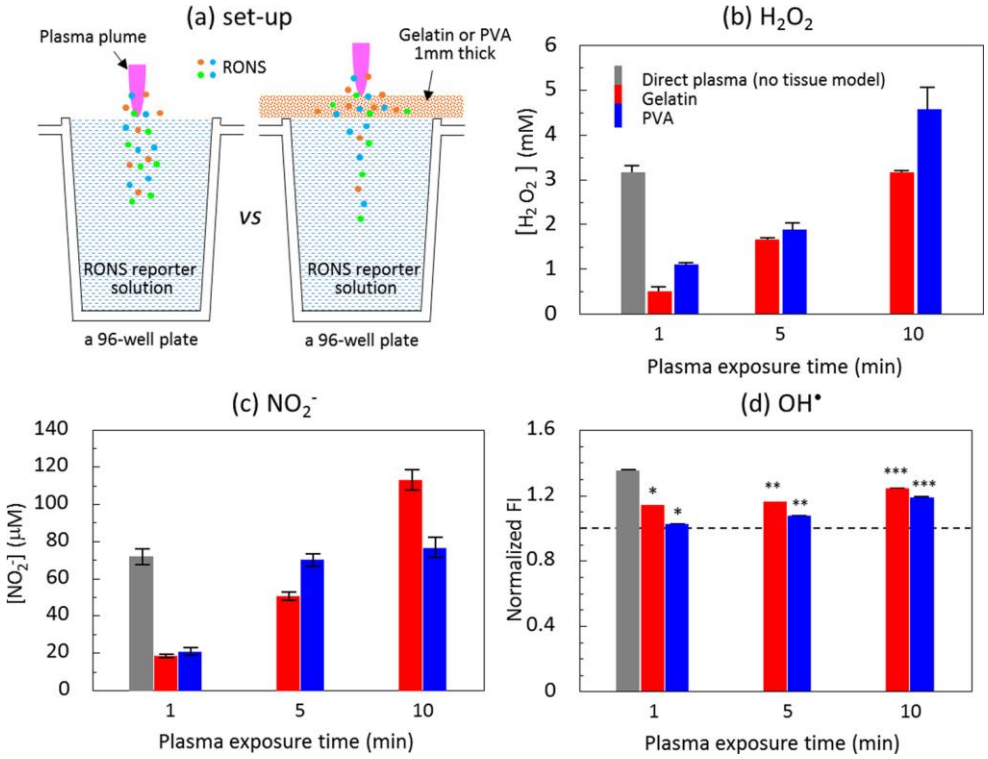


Figure 3.4 (a) Experimental scheme for the plasma-delivery of RONS in the reporter solution with and without gelatin and PVA tissue targets. The absolute concentrations of (b) H_2O_2 and (c) NO_2^- were elucidated using the calibrations curves, and (c) •OH data is presented as a normalised FI. Direct plasma exposure for 1 min was the control. The symbols *, **, * indicate a significant difference ($p<0.05$) between corresponding datasets. Below the dashed line, all numbers are effectively zero. Each column represents the mean value and ± standard error of the mean (SEM) between triplicate samples (n = 3).**

Figure 3.4b and 3.4c show the concentration of H_2O_2 and NO_2^- generated by plasma in PBS as a function of plasma exposure time, respectively. The production of •OH was denoted as normalised FI, also as a function of plasma exposure time (Figure 3.4d). From these figures, it can be concluded that the production of RONS increased with plasma exposure time (10 > 5 > 1 min).

At 1 min plasma treatment of reporter solution, the presence of gelatin and PVA targets significantly reduced the delivery of RONS as compared to direct plasma exposure. The delivery of H_2O_2 and NO_2^- was more effective through PVA than gelatin in most cases, except in case of a 10 min plasma treatment wherein more NO_2^- could be delivered through gelatin than PVA.

Within these experimental conditions, the plasma jet delivered very high concentrations of H_2O_2 (up to 5 mM and 3 mM with and without tissue model, respectively) when compared with NO_2^- (up to 120 µM and 20 µM with and without the tissue target, respectively). A high concentration of H_2O_2 can be credited to a higher Henry's diffusion coefficient value of 1.96×10^6, which is much higher than those reported for

reactive nitrogen species (approximately 10^{-2}) [41]. The high production of H_2O_2 could also be linked to UV-mediated production of •OH, as discussed below. It was recently shown that the •OH can be created *in situ* within a tissue model through UV photolysis [111].

Despite their highly reactive nature and short half-life of 10^{-9} seconds in physiological solution [45, 112], •OH radicals were detected in PBS even after plasma exposure through gelatin and PVA (Figure 3.4d). The detection of •OH in solution also brings into question whether all RONS are delivered by plasma through slow molecular transport processes. It is reported that •OH detected in solution is formed via UV-photolysis of water (R1). •OH eventually undergoes reaction R2 to form H_2O_2 in solution [35, 113].

$$H_2O + UV \rightarrow \bullet OH + H\bullet \qquad -(\mathrm{R1})$$

$$2\bullet OH \rightarrow H_2O_2 \qquad -(R2)$$

It is evident from Figures 3.4a and 3.4b that a much higher concentrations of H_2O_2 (in mM range) are generated by plasma than NO_2^- (in µM range). Therefore (acknowledging that measuring H_2O_2 captures >95% of RONS), the experimental protocols were modified to focus on the ROS production by plasma (later in section 3.2.2, it is shown by direct UVAS of the RONS in solution, that H_2O_2 is by far the major component). Consequently, DCFH was utilised as a broad range ROS reporter to study the role of proteins (DCFH also fluoresces upon reaction with RNS, as explained previously in Chapter 2). ROS production is presented as normalised FI value.

First, the role of fluid proteins upon direct plasma exposure (without tissue target) was assessed by dissolving BSA at 0 and 50 mg ml^{-1} in DCFH reporter solution, as illustrated in Figure 3.5.

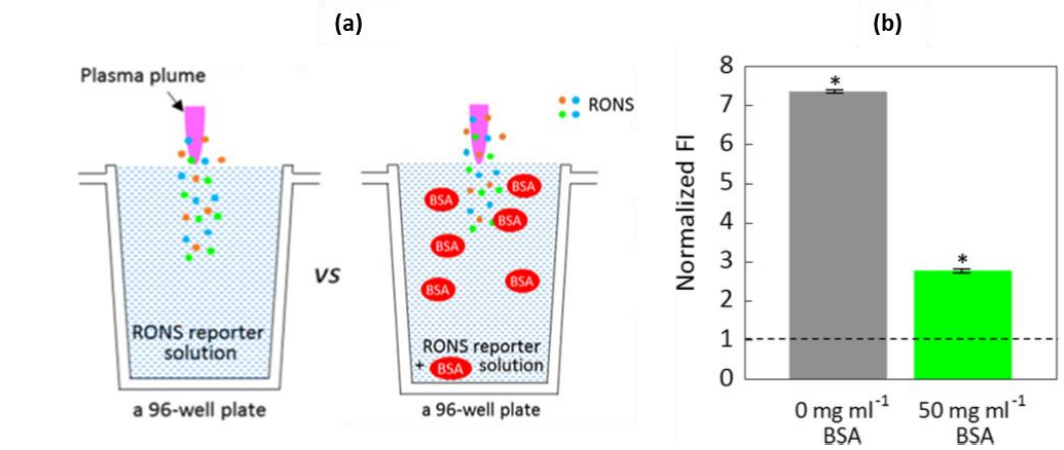


Figure 3.5 (a) The experimental setup for assessing the role of proteins in plasma generation of ROS. (b) The production of ROS is measured as normalised FI without (0 mg ml^{-1}) and with (50 mg ml^{-1}) BSA dispersed in DCFH solution. The symbol * indicates a significant difference ($p<0.05$) between corresponding datasets. Below the dashed line all numbers are effectively zero. Each column represents the mean value and ± standard error of the mean (SEM) between triplicate samples (n = 3).

The results in Figure 3.5 show that after 1 min of plasma treatment, a higher fluorescence intensity was observed for DCFH solution without BSA (0 mg ml^{-1}) than DCFH with BSA (50 mg ml^{-1}). By correlating the normalised FI with the total RONS production, it is evident that the presence of BSA suppressed the production of RONS in solution after direct exposure to plasma.

To further understand the combined effect of BSA and O_2 (aq), BSA was added to the DCFH reporter solution at concentrations of 0, 1, 25 and 50 mg ml^{-1} and these solutions were exposed to plasma through the gelatin tissue target (see Figure 3.6).

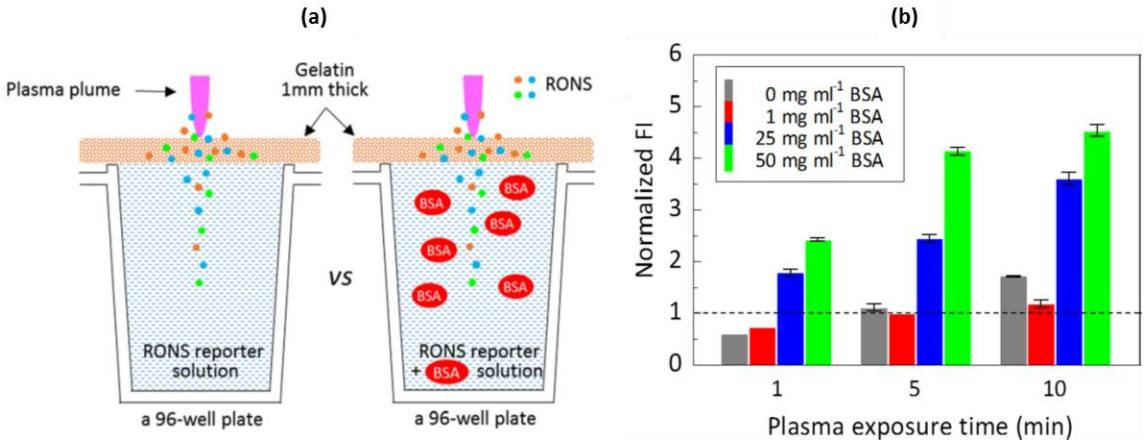


Figure 3.6 (a) The experimental setup to assess the plasma generation of ROS without BSA (0 mg ml^{-1}) and with BSA (1, 25 and 50 mg ml^{-1}) through gelatin using DCFH reporter solution. (b) Total ROS production after plasma treatment of 1, 5 and 10 min is depicted as normalised FI. Below the dashed line all numbers are effectively zero. Each column represents the mean value and ± standard error of the mean (SEM) between triplicate samples (n = 3).

The results in Figure 3.6 indicate that the production of ROS in PBS increases as a function of plasma treatment time. The presence of BSA enhanced the appearance of ROS in PBS, compared to BSA-free PBS. With a higher concentration of BSA (50 mg ml^{-1}), a greater quantity of ROS were produced at short plasma exposure times of 1 and 5 min. But, at a longer exposure time of 10 min, the generation of ROS is less dependent on BSA concentrations.

Comparing the results in Figure 3.5 with Figure 3.6, it is evident that the presence of BSA in PBS inhibits the production of ROS when the solution is directly exposed to plasma (i.e. in the absence of tissue target), but BSA stimulates the production of ROS when PBS is exposed through gelatin. This inhibitory and stimulatory effect of BSA in ROS production can be linked to O_2 (aq) content in PBS after plasma treatment. The main difference in the two experimental setups is the presence of tissue target. Previous studies have suggested that partial pressure of O_2 (aq) in sub-cutaneous tissue increases upon plasma exposure [106, 114]. To validate whether the presence of tissue model target elevates the levels of O_2 (aq) in PBS, UVAS was utilised to determine the levels of O_2 (aq) after plasma exposure. The UVAS results, which are discussed later (and in more details) in section 3.2, confirm that plasma treatment of PBS through tissue target had higher concentrations of O_2 (aq) than the PBS treated directly (without a target). These results were expected as a direct exposure to plasma causes He to replace O_2 (aq) (ie. sparging).

From all the data above (Figure 3.5 and 3.6), it can be hypothesised that levels of O_2 (aq) considerably affects the production of ROS in plasma treatment. At low levels of O_2 (aq), BSA may be acting as a sink for RONS and suppresses ROS formation. But at higher levels of O_2 (aq) after plasma exposure, production of ROS is enhanced via plasma-BSA- O_2 reactions.

This hypothesis is further tested by monitoring the delivery of ROS when BSA, at the concentrations of 0 and 50 mg ml^{-1}, is incorporated within the gelatin tissue matrix (as illustrated in Figure 3.7). In the first set of experiments, ROS production after plasma treatment of BSA-free PBS solution through a BSA-loaded gelatin target (dispersed at 50 mg ml^{-1}) is compared to ROS production after treatment through a BSA-free gelatin target (Figure 3.7b). In the second set of experiments, ROS production in PBS (with BSA at 50 mg ml^{-1}) after plasma treatment through a BSA-loaded gelatin target (Figure

3.7e) is compared to ROS production after the direct plasma treatment of the same BSA/PBS solution (Figure 3.7d).

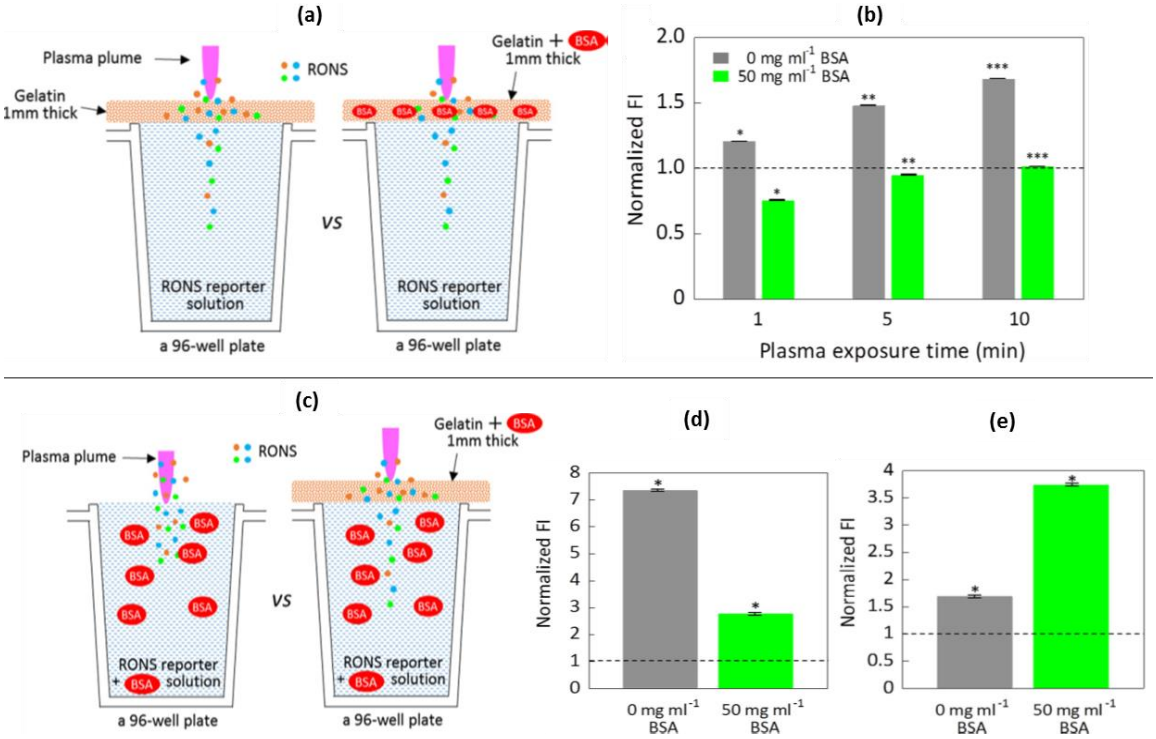


Figure 3.7 The experimental setup to assess the effect of gelatin incorporating BSA ("BSA-loaded") on plasma generation of ROS in PBS (a) without BSA and (c) with BSA. BSA is dispersed in gelatin ("BSA-loaded") at concentrations of 0 and 50 mg ml^{-1}. (b) Total ROS production in) PBS (without BSA) after the plasma treatment for 1, 5 and 10 min through agarose with BSA. Total ROS production in PBS (with BSA) after plasma treatment for 1 min (d) directly and (e) indirectly through a BSA-loaded agarose. The symbols *, **, * indicate a significant difference ($p<0.05$) between corresponding datasets. Below the dashed line all numbers are effectively zero. Each column represents the mean value and ± standard error of the mean (SEM) between triplicate samples (n = 3).**

The results from Figure 3.7b indicate that when embedded within the gelatin, BSA lowers the generation of ROS in PBS (without BSA). A similar effect is observed when PBS-BSA solution is directly treated with plasma (Figure 3.7d). But the production of RONS increased when a PBS-BSA solution is treated through a BSA-loaded gelatin, as shown in Figure 3.7e. To further understand these results and unravel the key trends in plasma-BSA-O_2 (aq) interactions, it is important to take into account the structure of BSA.

BSA is a negatively charged protein which consists 583 amino acids and 17 disulfide bonds (RSSR) and 1 sulfhydryl group (RSH) [115]. Cysteine and other polar amino acids such as aspartic acid and glutamic acid, are the major amino acids in BSA [116]. Tryptophan, methionine, glycine and isoleucine are also present in BSA, although at low concentrations [116]. Therefore, a BSA-PBS solution is abundant in amino acids

bearing alkyl and aryl groups (collectively referred as RH), and thiol groups (RSH) [32] in BSA. These groups undergo chemical modifications (oxidation, hydroxylation, sulfoxidation, amidation and nitration) upon interaction with various ROS [18].

A few potential reactions of •OH with RH and RSH are shown in the reactions R3 –R15 [117-120]. RH and RSH produce alkyl radicals (R•) and thiyl radicals (RS•), respectively, as shown in reaction R3 and R10. At low levels of O_2, the R• and RS• undergo reactions with neighboring RH and RSH molecules (R4, R11) or amongst themselves (R5, R6 and R12) to form stable alkyl, aryl and thiol products such as RH, R'H, RSSR, R-R, R'-R', etc. However, in presence of high levels of O_2, the R• and RS• undergo oxidation to form highly reactive alkylperoxyl radicals (ROO•) and thiol-peroxyl radicals (RSOO•), as shown in reactions R7 and R13. The ROO• and RSOO• convert to stable hydroperoxide products (ROOH), sulfinic acid (RSOOH) and other undefined RONS via reduction (R8 and R14) or hydrogen abstraction from other molecules (R9 and R15).

$$RH + \bullet OH \rightarrow R\bullet + H_2O \quad -(R3)$$

$$R\bullet + R'H \rightarrow RH + R'\bullet \quad -(R4)$$

$$2R\bullet \rightarrow R - R \quad -(R5)$$

$$2R'\bullet \rightarrow R' - R' \quad -(R6)$$

$$R\bullet + O_2 \rightarrow ROO\bullet \quad -(R7)$$

$$ROO\bullet + e^- \rightarrow ROOH \quad -(R8)$$

$$ROO\bullet + R'H \rightarrow ROOH + R'\bullet \quad -(R9)$$

$$RSH + \bullet OH \rightarrow RS\bullet + H_2O \quad -(R10)$$

$$RS\bullet + RSH \rightarrow RSSR + H\bullet \quad -(R11)$$

$$RS\bullet + RS\bullet \rightarrow RSSR \quad -(R12)$$

$$RS\bullet + O_2 \rightarrow RSOO\bullet \quad -(R13)$$

$$RSOO\bullet + e^- \rightarrow RSOOH \quad -(R14)$$

$$RSOO\bullet + RSH \rightarrow RSOOH + RS\bullet \quad -(R15)$$

Therefore, the amino acids present in BSA can act potential reservoirs for the ROS generated by plasma and BSA acts as a ROS scavenger (at low levels of O_2) [121]. This explains the results in Figure 3.5b and 3.7d, wherein presence of BSA in PBS, when directly treated with plasma (without the tissue target), leads to reduction in ROS production. But when PBS-BSA solution is exposed to plasma through a gelatin target (Figure 3.6b and 3.7e), an increase in ROS production is observed. This contrast in the results can be linked to the increase in levels of O_2 (aq) in PBS after the plasma treatment through gelatin and generation of various peroxyl radicals as shown in reactions above.

As confirmed by UVAS (Figure 3.16d), the presence of a tissue model enhances the levels of O_2 (aq) after plasma treatment of water. The role of O_2 (aq) in increasing the plasma-generation of RONS has been discussed in studies elsewhere [7, 38, 39, 106], and in more detail later in the section 3.2 of this chapter. In context with this study, the results indicate that even at similar levels of O_2 (aq) (after plasma treatment through gelatin), the presence of BSA in PBS resulted in a higher ROS production than in BSA-free PBS. The exact mechanisms involved in this stimulatory nature of BSA at increased partial pressure of O_2 (aq) remains unanswered.

Since, few studies have been conducted to understand the BSA-plasma interactions quantitatively, it is difficult to comment on the concentrations of ROS generated by plasma relative to the concentration quenched and which type of ROS generated by plasma are responsible for oxidation of amino acids.

The role of proteins embedded in the tissue target on plasma generation of ROS were also assessed (Figure 3.7b and 3.7e). The reduced production of ROS, on plasma treatment of a BSA-free PBS solution through gelatin target (with BSA) results of entrapment of ROS by BSA-molecules in gelatin. But an increase in ROS production was observed when the PBS-BSA solution was treated through the BSA-embedded gelatin target.

To summarise, the key findings of this chapter were:

i. The presence of tissue target during plasma treatment increases the partial pressure of O_2 in PBS. The increase in O_2 (aq) eventually enhances the plasma delivery of ROS.

ii. BSA can have a dual nature in plasma delivery of ROS. At low levels of O_2 (aq) i.e. plasma treatment of a BSA-PBS without a tissue target, BSA reduced the level of ROS. But at higher levels of O_2 (aq) i.e. when treated indirectly through the tissue target, BSA enhanced the production of ROS, even more than the indirect treatment of BSA-free PBS solution.

iii. When embedded within the gelatin target, BSA molecules acts as sinks for the ROS, and limits the plasma delivery of ROS into PBS (without BSA). But under same experimental conditions, the plasma generation of ROS is raised when BSA is added to PBS.

In tissues, plasma delivered ROS can convert proteins to ROOH. The cells deep within tissues interact with the ROOH molecules, which then decompose to act as reservoirs of other secondary messenger RONS. Decomposition of ROOH is a low flux process and takes places at an extended period of time (hours to days). This equips proteins to provide therapeutic shielding to tissue upon plasma exposure and protect cells from severe damage [45, 122]. In the presence of above physiological oxygen, data suggests the decomposition is faster and more ROS are generated immediately. Additional studies are an imperative in order to understand the exact mechanisms governing BSA-plasma interactions and understand the therapeutic effect of plasma.

In this section, molecular probes (OPD-HRP, Griess reagent, TA and DCFH) were utilised to assess RONS production. The molecular probes are easy to employ and do not require high expertise to perform. The molecular probes are also advantageous in measuring ROS in various types of solutions including buffered solvents and cell culture media with proteins and other biomolecules. But the accuracy of the molecular probes such as DCFH remains questionable due to the cross-reactivity with different type of ROS/RONS and auto-oxidation due to light. Due to unavailability of appropriate calibration curves, it is difficult to quantify the concentration of specific ROS delivered by the plasma jet. The molecular probes are a good tool to detect RONS generation after the plasma treatment, but the dynamic changes in concentrations of RONS during the plasma treatment is not possible.

Therefore, other RONS detection techniques including UVAS and mass spectrometry were utilised to assess the real-time changes in O_2 (aq) and RONS levels during plasma-tissue interactions (Section 3.2 and 3.3)

3.2 Real-time monitoring of plasma delivered RONS through tissue model using UVAS

In Section 3.1, the role of O_2 (aq) in plasma generation of RONS was examined. The increase in RONS concentrations in solution is a consequence of increased levels of O_2 (aq) after plasma exposure of solution (through tissue). But, detecting RONS delivery using molecular probes does not allow monitoring RONS production in real-time. In this context, UVAS has emerged to be promising tool to detect dynamic changes in RONS production and O_2 levels during plasma exposure. An absorption spectra profile can be generated using a UV-absorption spectrometer which can then be used to determine concentration of some of the key RONS species such as O_2, H_2O_2, NO_2^- and NO_3^-.

In this section, electrical and optical diagnosis of the plasma jet were also conducted. A current and voltage probe was used for the electrical measurements, and optical emission spectroscopy (OES) was utilised for the optical diagnosis of the plasma effluent. OES coupled with UVAS can be employed to provide both qualitative and quantitative analysis of RONS generation during plasma-tissue interactions. In Section 3.2.1, the working principle of all the techniques used in this chapter will be discussed in detail.

The experiments with UVAS was undertaken in Department of Electrical and Electronic Engineering at Meijo University, Japan. At this time, the plasma diagnostic tools including both electrical and optical diagnosis of the plasma jet were also available in Japan (which was not the case in Australia). Therefore, this opportunity was taken to carry out a combined study of the jet diagnosis and RONS delivery through tissue into tissue fluid.

3.2.1 Instrumentation techniques

3.2.1.1 UVAS

Figure 3.8 illustrated the working principle of UVAS. A light source (halogen or deuterium lamp for UV region or tungsten-halogen lamp for the visible region) impinges light on the sample, which absorbs some part of the light and transmits rest [123]. The diffraction grating separates the different wavelengths of the light [123]. The intensity of the light transmitted through the sample is measured as a function of wavelength using the detector to yield an absorbance profile [123]. Absorbance is

measured by comparing the transmittance of light exiting the sample (I) with the transmittance of light impinged on the sample (I_0) at a fixed wavelength (λ) as per the formula below [124]:

$$A(\lambda) = -\log \frac{I(\lambda)}{I_0(\lambda)}$$

According to Beer-Lambert's Law, the absorbance of a solution is directly proportional to the concentration of the absorbing species in the solution [125].

$$A = \varepsilon \, l \, C$$

ε is the absorption coefficient ($M^{-1}cm^{-1}$), l is the path length (cm) of light through the sample cell/cuvette and C is concentration (mol/L) of the analyte.

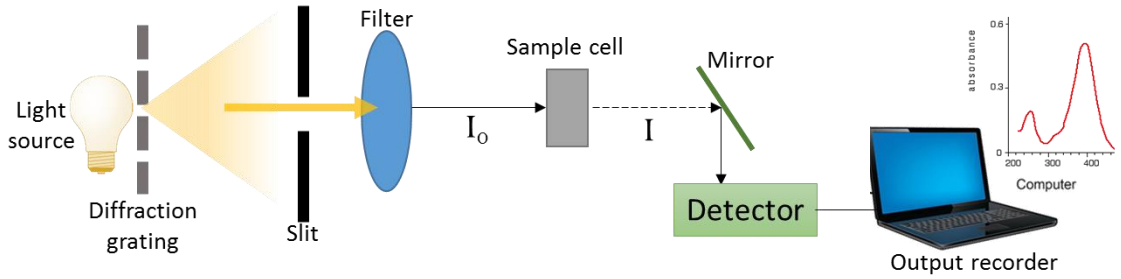


Figure 3.8 Schematic of the working principle of UVAS. The light from the source passes through a diffraction grating and slit to reach the filter. Through the filter the light then reaches the sample cell (cuvette), at fixed wavelength. The transmittance of light incident on the sample cell (I) and exiting out of the cell (I_0) is detected by a detector. The output is collected by the computer as an absorbance spectra at specific wavelengths.

3.2.1.2 Electrical diagnosis: voltage and current probe

For electrical diagnosis, the driving voltage (V) and discharge current (I_d) of the plasma jet were measured using a voltage probe and a current monitor. The current monitor used in this study is in form of a closed loop made of ferromagnetic core and a secondary coil which are grounded to an oscilloscope through a co-axial BNC cable (Figure 3.9). Values of I_d also provides information about net charge (Q_d) between the electrode and ground (tissue) using the formula [126]:

$$Q_d = \int_0^t I_d(t) \cdot dt$$

High voltage measurements are measured using a voltage probe. The voltage probe is made of voltage dividers that converts high voltage to a lower voltage in a range that

can be easily measured by an oscilloscope [127]. Values of V and I_d can be used to calculate averaged input power (P_{in}) at a fixed frequency (f) using the formula:

$$P_{in} = f \int_0^t V(t)\, X\, I_d(t) \cdot dt$$

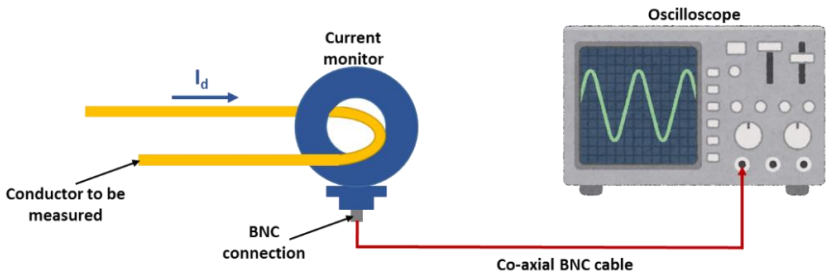


Figure 3.9 Schematic of a current monitor. The current carrying conductor to be measured passes through the current monitor. The output voltage is measured using an oscilloscope.

3.2.1.3 Optical diagnosis: OES

For optical diagnosis of the plasma jet, OES was employed with an aim to diagnose the gaseous plasma species (in the effluent). OES is used to measure the emission from the high energy components of the plasma jet, typically plotted as spectral line intensities as a function of wavelength. The OES spectra usually include the electron, vibrational and rotational transitions [128] (Figure 3.10). The electronic transitions occur rapidly from the ground state energy levels to the excited state energy levels, the vibrational transitions take place between the different vibrational levels of the same electronic energy level, and the rotational transitions occur between different rotational levels of the same vibrational state [129].

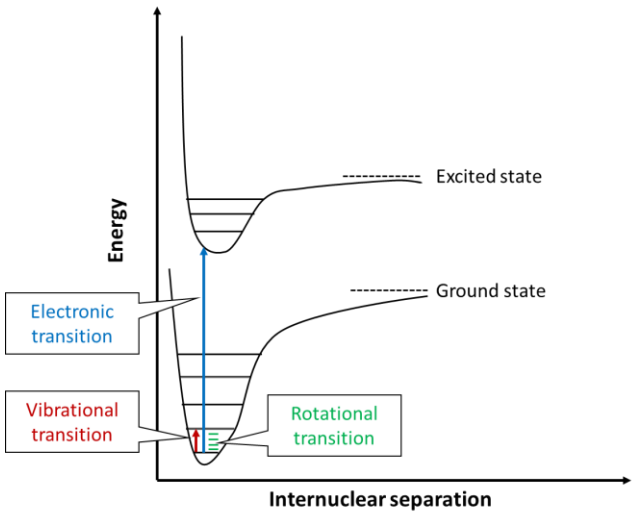


Figure 3.10 An illustration of the electronic, vibrational and rotational energy levels in a molecular spectra. The horizontal lines represent the energy levels and the vertical lines represent the transitions (electronic, vibrational and rotational) between different energy levels.

OES requires a fiber optic spectrometer to measure the emitted light from the source (here the plasma jet). The emitted light is collected by a collimating lens and directed to the spectrometer through an optic fiber (Figure 3.12). The spectrometer comprises a slit, diffraction grating filters, focusing mirrors and detector. The grating disperses the light by wavelength (and this can be used to identify transitions specific to plasma particle species) which is then collected by the detector. The detector converts the optical signal into a measurable electrical signal (i.e. emission spectral lines) displayed on the computer. The intensities of these emission spectral lines depend on various factors including the density of excited species, gas temperature, electron temperature, density of electrons, rate of quenching of the species and sensitivity of the spectrometer [130]. Therefore, the intensities cannot be directly correlated to the absolute concentration of the species. However, for qualitative analysis, the levels of the emission intensities can indicate the levels of plasma species [113].

OES generated emission spectra provide a qualitative overview of the plasma composition in a non-invasive manner. It is thought that the high-energy species generated in gas-phase, before interacting with tissue/tissue fluid, determine the redox chemistry and production of RONS in solution [131, 132]. For instance, excited state species such as He*, detected in emission spectra, form •OH and excited oxygen (O*), upon energy transfer. These highly reactive and shorter-lived species play a key role in plasma-tissue interactions and generation of new RONS in solution. The emission spectra can be also be used to evaluate the vibrational temperature (T_v), rotational temperature (T_r), gas temperature (T_g) of plasma jet, as previously demonstrated by Oh *et al.* [39, 133].

3.2.2 Materials and Methods

3.2.2.1 Plasma jet unit

A 150 mm long glass tube, with 4 mm inner diameter and tapered at the end to 800 μm, is purged with high purity helium (He) gas at 1 slpm. The glass tube has a 15 mm long copper ring electrode at a distance of 40 mm from the end of the nozzle. A plasma discharge was generated by applying a peak-to-peak voltage (V_{pp}) of 7 kV to the electrode at a fixed frequency of 10 kHz. The glass tube with high voltage powered electrode is shielded using a 10 mm thick PTFE housing. Figure 3.11 illustrates a schematic of the He plasma jet assembly.

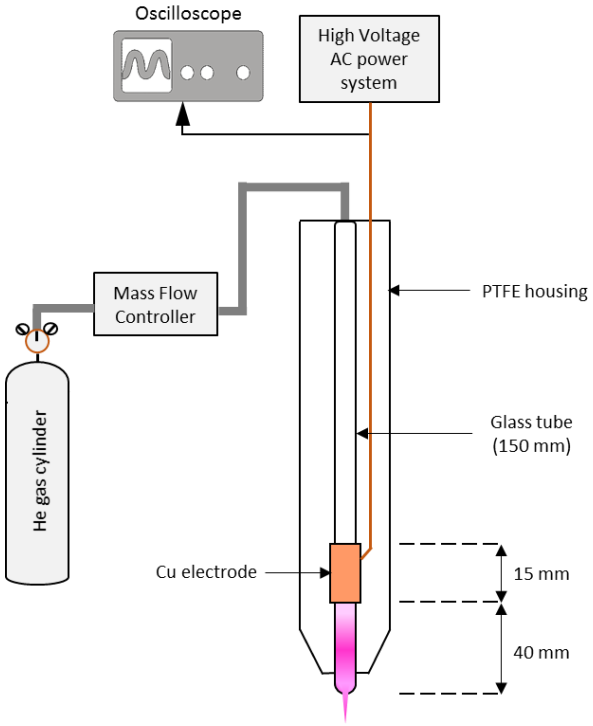


Figure 3.11 Schematic of the plasma jet used in this study. The jet consists a 150 mm glass tube which was purged with He gas at a flow rate of 1 slpm. A 15 mm long Cu electrode was wound on the glass tube such that distance between the end of glass tube and the electrode is 40 mm. An oscilloscope was used to monitor the voltage and frequency supplied to the unit by the high voltage power unit.

3.2.2.2 Agarose tissue model

2% (w/v) agarose solution was prepared by dissolving agarose powder (Sigma-Aldrich, catalogue number A9539) at a concentration of 20 mg ml^{-1} in deionized (DI) water (18.2 MΩ.cm) and heating for 1-2 min in a conventional microwave oven, until a homogeneous solution is achieved. After cooling down slightly, different thicknesses of gelatin film was achieved by pouring 15 ml for 1.3 mm thick film, 20 ml for 2.5 mm thick film and 40 ml for 5.8 mm thick film in a plastic petri-dish (85 mm diameter). By agitating the dish slightly, an evenly spread and bubble-free agarose film is achieved. The dishes were left to set at 4˚C for 12 hours before use. Square sections of 25X25 mm^2 were cut using scalpel, removed using tweezers and stored in water at 4˚C until use.

3.2.2.3 Voltage and current measurements

The applied V_{p-p} was measured using a ground-referenced high voltage probe (Tektronix P6015A). It can be attenuated to 1000x and has a high input resistance of 1 MΩ and a compensation range of 7 pF to 49 pF.

The current monitor (Pearson 2877) was placed over the high voltage cable as shown in Figure 3.12. I_d was measured by subtracting displacement current (I_{dis}) from total current (I_t) [37] as per the equation below:

$$I_d = I_t - I_{dis}$$

I_{dis} is the current measured in absence of plasma discharge but in presence of V_{p-p} and I_t is current in presence of both plasma discharge and V_{p-p}. All the electrical measurements were recorded using an oscilloscope (Tektronix TDS2014B).

3.2.2.4 Plasma treatment parameters

Agarose targets were placed on top of a quartz cuvette (Hellma Analytics, 100-QS), which was filled with 4.1 ml of DI water and exposed to plasma for 15 minutes (Figure 3.12a). For comparison, DI water without agarose was also directly exposed to the plasma jet under same treatment parameters (Figure 3.12b). The distance between end of plasma glass tube and top of tissue target/solution (d) is 15 mm.

3.2.2.5 UVAS setup

A UV-visible spectrometer (Hitachi, U-3900) was employed to detect absorption peaks in a wavelength range from 190 to 900 nm. Since no distinct absorption peaks were observed above 350 nm (in the visible and near IR range), the wavelength range was fixed at 190 – 340 nm.

The concentration of specific RONS (H_2O_2, NO_2^- and NO_3^-) were quantified from absorbance values using curve-fitting. The absorption spectra of plasma treatments were fitted against the spectra of solutions of H_2O_2, sodium nitrite ($NaNO_2$) and sodium nitrate ($NaNO_3$).

3.2.2.6 OES measurements

A fiber optic spectrometer (Ocean Optics USB4000) was used measure the emitted light from plasma. The principles of OES spectrometer have been aforementioned in Section 3.2.1. Briefly, the light is collected by the collimating lens and directed to the spectrometer via the fiber optic cable (1 mm in diameter). The intensity of emitted plasma species at specific wavelengths were collected by the detector and recorded into a measurable electrical signal. The spectral resolution of the instrument was 0.2 nm.

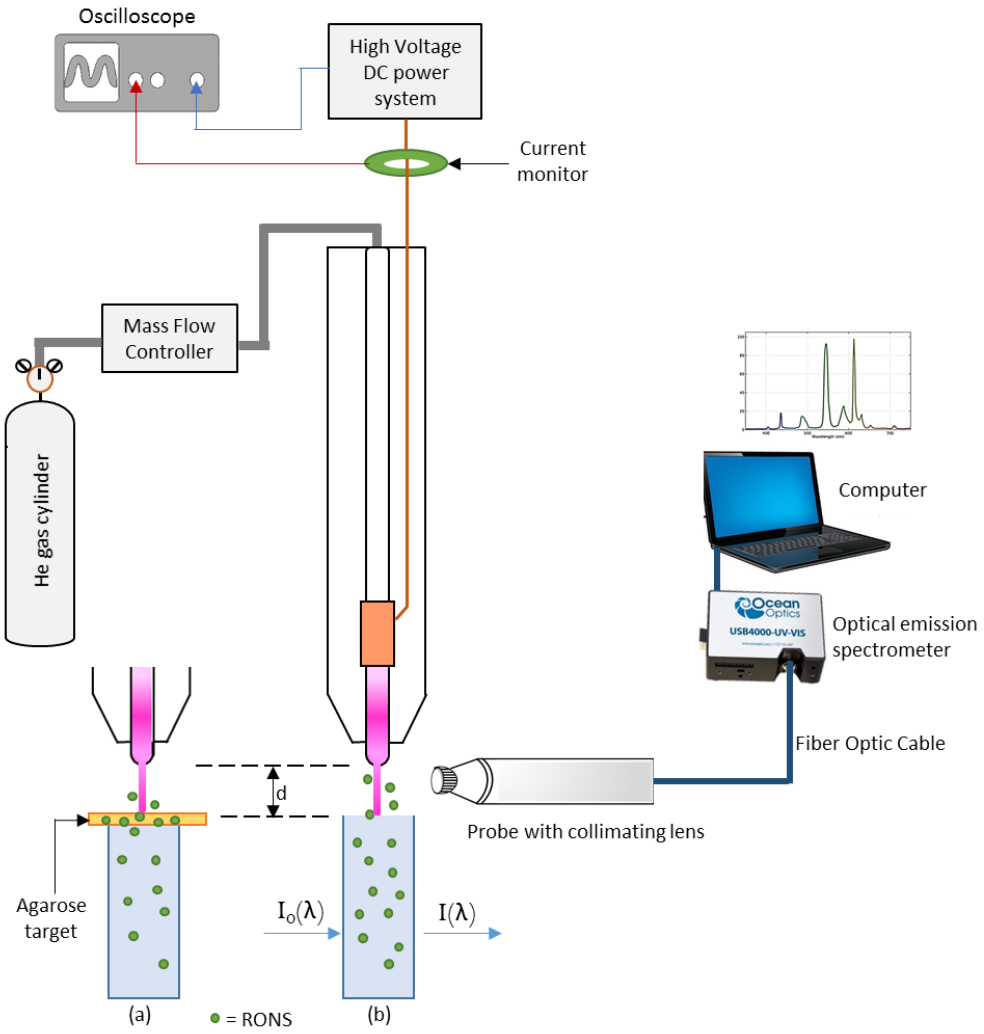


Figure 3.12 Schematic of the experimental setup utilised in this study. A volume of 4.1 ml of the DI water was exposed to the plasma jet in a cuvette (a) with and, (b) without an agarose target on top (at d = 15 mm). Electrical measurements were conducted using a current monitor and high voltage probe. UVAS was utilised to measure the transmittance in each case before (I_0) and after (I) plasma treatment at a specific wavelength (λ). OES was performed using a fiber optic probe with collimating lens and a spectrometer. The absorption and emission spectra were recorded on the computer.

3.2.3 Results and discussion

Firstly, the electrical properties of the plasma jet used in this study were measured using the current and voltage probes (Figure 3.13A, 3.13B and 3.13C).

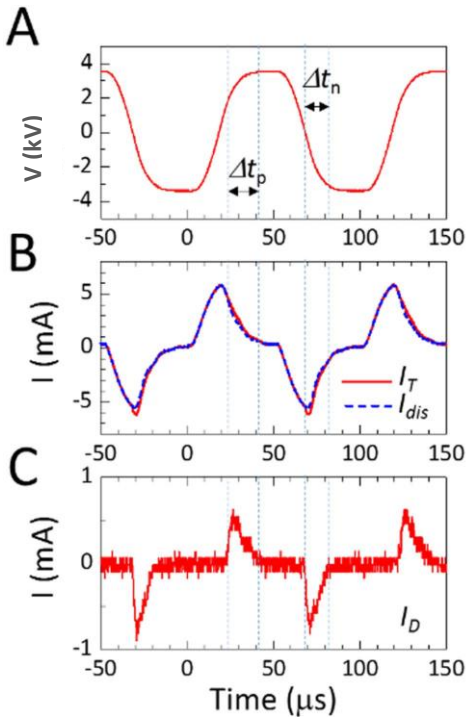


Figure 3.13 Electrical diagnosis of the He plasma jet operated at a He gas flow rate of 1 slpm. (A) The voltage waveform at an applied peak-to-peak voltage (V_{p-p}) of 7 kV were measured using the voltage probe. (B) The total current (I_t) and displacement current (I_{dis}) were measured using the current monitor. (C) The discharge current calculated (I_d) by subtracting I_{dis} from I_t. The duration of positive and negative peaks are denoted by Δt_p and Δt_n, respectively.

The results in Figure 3. 13A show the voltage waveform, at a driving V_{p-p} of 7 kV, obtained using the voltage probe. The I_{dis} and I_t were measured using the current monitor (Figure 3.13B) and then used to calculate I_d during the positive and negative cycle. The value of I_d was measured as 0.7 mA and the value of full-width-half-maximum of 10 µs. From Figure 3.13C it can be observed that the peak-to-peak amplitude and the full-width-half-maximum of both peaks (positive and negative) were similar.

The values of I_d , frequency (f) and voltage (V) over time (t) were used to calculate the average input power (P_{in}) of the plasma, using the following formula

$$P_{in} = f \int_0^t V(t)\, X\, I_d(t) \cdot dt,$$

where, f = 10 kHz and V = 7 kV, P_{in} was calculated to be 0.25 W.

After the electrical diagnosis, an optical diagnosis of the plasma jet was performed using OES. The typical emission spectra from 280-480 nm and 640-840 nm were acquired using the OES, as shown in Figure 3.14A and B, respectively. The values of T_v

and T_r were obtained from the emission spectra between 370 and 385 nm using an algorithm developed by Tokyo Institute of Technology [134].

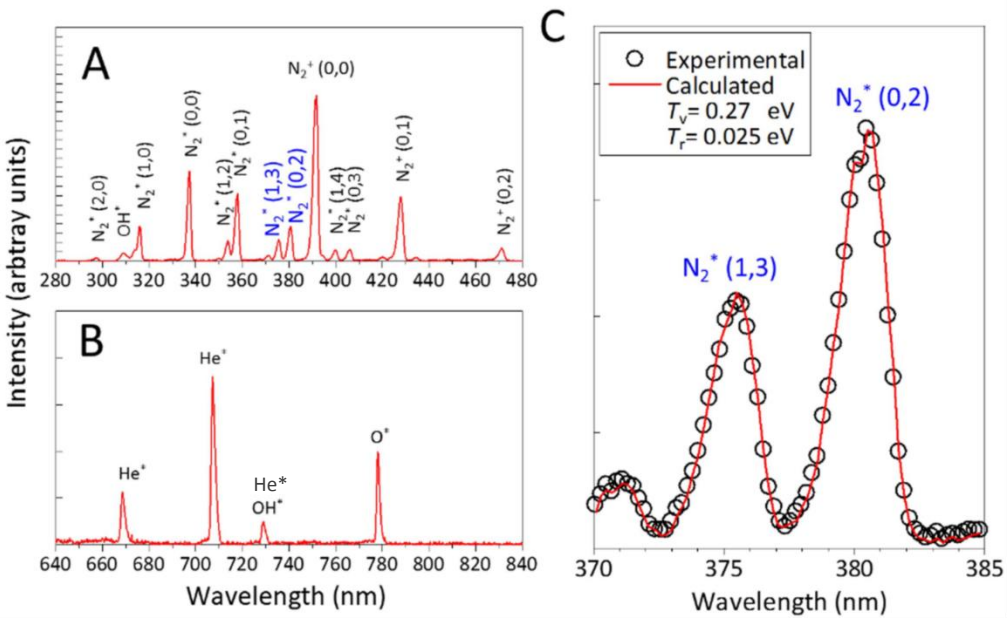


Figure 3.14 The OES generated emission spectrum of He plasma jet in the range of (A) 280-480 nm and (B) 640-840 nm. (C) The experimental spectra (circles) of N_2 second positive system from 370 nm to 385 nm was fitted against the calculated spectra (red line) provided kindly by Prof. Hiroshi Akatsuka at Tokyo Institute of Technology.

From Figure 3.14A it can be seen that the N_2 species dominated the spectra from 280-480 nm, amongst which a greater number of spectral lines were observed for the N_2 second positive systems (SPS) than the N_2^* first negative systems (FNS). To assign the signals in Fig 15A, the characteristic spectra of the N_2^+ FNS [N_2^+ ($B^2\Sigma_u^+$–$X^2\Sigma_g^+$)] and N_2^* SPS [$N_2(C^3\Pi_u$–$B^3\Pi_g)$] (ie. specific wavelengths) are listed in Table 3.1 [135].

Table 3.1 The wavelengths corresponding to the emission spectral lines in N_2^+ FNS and N_2^*SPS systems when transitioning from v' to v".

	Vibrational state transition (v', v")	**Wavelength (nm)**
N_2^+ FNS	(0,0)	391.4
	(0,1)	427.8
	(0,2)	470.9
	(2,0)	297.6
	(1,0)	319.9

N_2^* SPS	(0,0)	337.1
	(1,2)	353.6
	(0,1)	357.6
	(1,3)	375.5
	(0,2)	380.4
	(1,4)	399.8
	(0,3)	405.9

Besides signals from the N_2 system spectra, the spectral line for OH* was also observed at 308 nm (Figure 3.14A). The optical emission spectrum in the spectral region of 640-840 nm are shown in Figure 3.14B. From these data it can be observed that He* spectral lines were observed at 667.8 nm and 706.5 nm, O* at 777.5 nm and another OH* peak at 729 nm [136]. It should be noted that the peak at 729 nm can also be assigned to He*. These highly reactive species have shorter half-life and are critical in redox chemistry occurring between plasma and tissue to determine the RONS generated in DI water.

As shown in Figure 3.14C, the measured spectrum of N_2^* SPS [N_2^* (0,1) and N_2^* (2,3)] were then fitted against the calculated spectrum of N_2^* SPS between 370 and 385 nm (provided kindly by Prof. Hiroshi Akatsuka, Tokyo Institute of Technology) to calculate values of T_v and T_r [134]. The values of T_v and T_r were calculated as 0.27 eV and 0.025 eV, respectively. The calculated value of T_r for N_2 accords with the previous calculation made by Oh *et al.* for •OH [137]. Since T_r is an indicator of bulk plasma gas temperature, it confirms that the plasma jet used in this study is "cold" and appropriate for the treatment of thermally sensitive materials such as tissue. Since T_v can be affected by the inelastic collisions between the electrons and molecules, the plasma electron temperature (T_e) is considered approximately equal to T_v i.e. 0.27 eV [138, 139]. It is evident from results that value of $T_v >> T_r$, which affirms the "non-equilibrium" nature of the plasma jet. The value of T_v (0.27 eV ≈ 3000 K) indicates the presence of sufficiently high-energy components of plasma which facilitate the nitrogen-oxygen chemistry and

production of other RONS [131]. For example, the excited state species such as He* can transfer energy to ambient air and facilitate the production of O* and •OH, as shown in Figure 3.14B. These species are highly reactive and short-lived, and highly significant at gas-liquid interface [32]. For instance, it is speculated that shorter-lived highly reactive species after crossing the tissue barrier result in the generation of other types of RONS such as H_2O_2 and NO_2^- in tissue fluid (DI water is surrogate for tissue fluid) [140, 141].

The resultant RONS delivered in DI water after direct as well as indirect (through agarose target) plasma treatment were measured using UVAS (Figure 3.15). The plasma jet was operated for t=15 min and the plasma and gas flow were extinguished after 15 min. The UV absorption spectra from 190 to 340 nm were recorded after immediately after the plasma and gas flow were extinguished (t = 15 min) and at t = 30, 45 and 60 min (i.e. 15, 30 and 45 min, respectively, after the plasma and gas flow were extinguished).

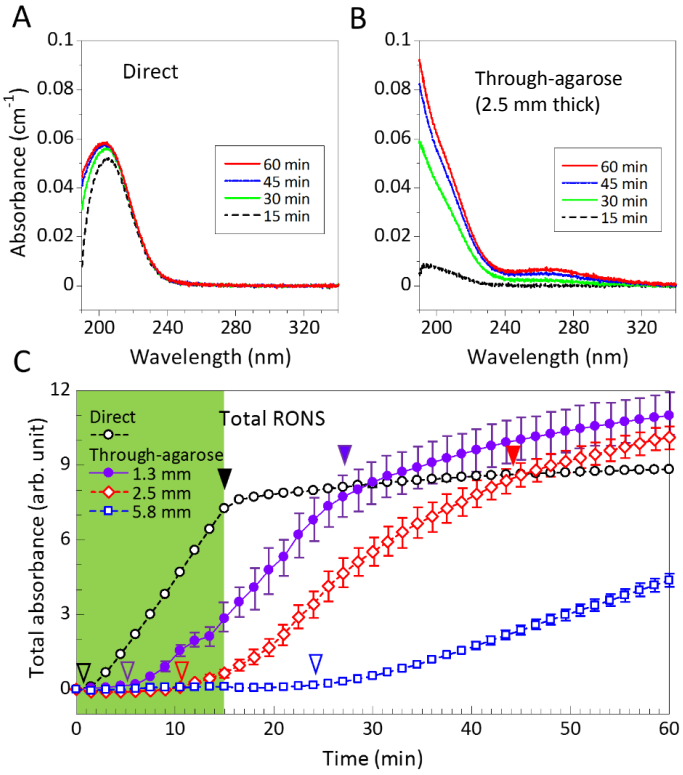


Figure 3.15 UV absorption profile showing time-dependent changes upon plasma treatment of DI water for 15 min (A) directly and (B) indirectly (through 2.5 mm thick agarose) at t=15, 30, 45 and 60 min. (C) The total absorbance between 190 and 340 nm after 15 min (green shaded region) of direct and indirect plasma treatment through the agarose target (1.3, 2.5 and 5.8 mm thick). Total absorbance was measured for up to 60 min. Open arrows indicate the point at which RONS production increased and solid arrows indicate points where rate of RONS generation slowed down. Each error bar represents ± standard error of the mean (SEM) between triplicate samples (n = 3).

Figure 3.15A shows the UVAS measurements of DI water when directly exposed to plasma at t = 15 min. A single prominent absorbance peaks at 205.8 nm was observed in this condition. From Figure 3.15A it is also evident that after the plasma and gas flow were extinguished, there was a further little change in the absorbance values over the period of t = 15 – 60 min. Interestingly, very contrasting results are obtained when plasma treatment is performed through a 2.5 mm thick agarose (Figure 3.15B). At t = 15 min, a low intensity absorbance peak at 194 nm was observed. The absorbance continued to increase at t= 30, 45, and 60 min, even after terminating the plasma and exceeded the intensity of corresponding peak for the direct plasma exposure at t = 30 min (compare 15A and 15B).

The UV absorbance values obtained from the total signal between 190 and 340 nm for both the direct and through-agarose plasma treatments were the plotted against time (t= 15, 0, 45 and 60 min), as shown in Figure 3.15C. For this experiment, the total UV absorbance values were directly correlated with total RONS and O_2 (aq) in DI water. The results in Figure 3.15C suggest that for direct plasma treatment, a rapid and monotonic increase in total RONS was observed until t=15 min (i.e. when plasma is on). However, after the plasma and gas flow are extinguished, no further increase (or a negative inflection) in RONS was observed, as marked with solid arrows. From these results it can be inferred that due to faster diffusion (or solvation) of RONS from gas phase into liquid phase, the RONS are delivered at a faster rate without any barrier (agarose) [32]

From Figure 3.15, it is also clear that unlike the direct plasma treatment, total RONS did not increase immediately with plasma treatments through agarose. The RONS appeared in DI water after some time lag of 6, 12 and 24 min (marked with open arrows) for treatment through 1.3, 2.5 and 5.8 mm thick agarose, respectively. The time lag increased with agarose thickness. Interestingly, the RONS still continued to appear even after extinguishing plasma and gas flow (after t = 15 min). The results confirm that the presence of agarose acted as a barrier and slowed the transport of RONS into DI water. The time lag in RONS appearance can be considered as a marker of RONS transport by slow molecular processes through the tissue target into DI water [38, 56]. The slow molecular transport arises when plasma jet creates a reservoir for RONS in agarose, which later solvates from agarose into DI water subsequently for at least up to 45 min after plasma (and He gas flow) are turned off.

A detailed investigation of how the appearance of total RONS (total absorbance) translates to the appearance of specific RONS is achieved by obtaining calibration curves (spectral traces) for each of the key RONS (single solution). Based on the peak-fitting (of total RONS) spectra, the UV absorption spectra of the neat solutions of neat solutions for specific RONS (H_2O_2, NO_2^-, NO_3^-) and O_2 (aq) were measured (Figure 3.16A–D). The absorbance spectra measured after plasma treatment was fitted against spectra of neat solutions, as shown in Figure 3.16E and 3.16F, using a routine established by Oh *et al.* [39]. Using this UVAS curve fitting technique, it is possible to conduct multiple, real-time and accurate RONS measurements [39]. The calibrations obtained from the curve fitting was then used to quantify the concentrations of individual RONS (mg ml^{-1}), obtained by plasma treatment of DI water from t=0 to 60 min (Figure 3.16E and 3.16F). The concentration of RONS was also plotted against time (up to t=60 min) to monitor the time-dependent changes in levels of H_2O_2, NO_2^-, NO_3^- and O_2 (aq) in DI water upon direct and indirect (through agarose) plasma treatment (Figure 3.16G-J).

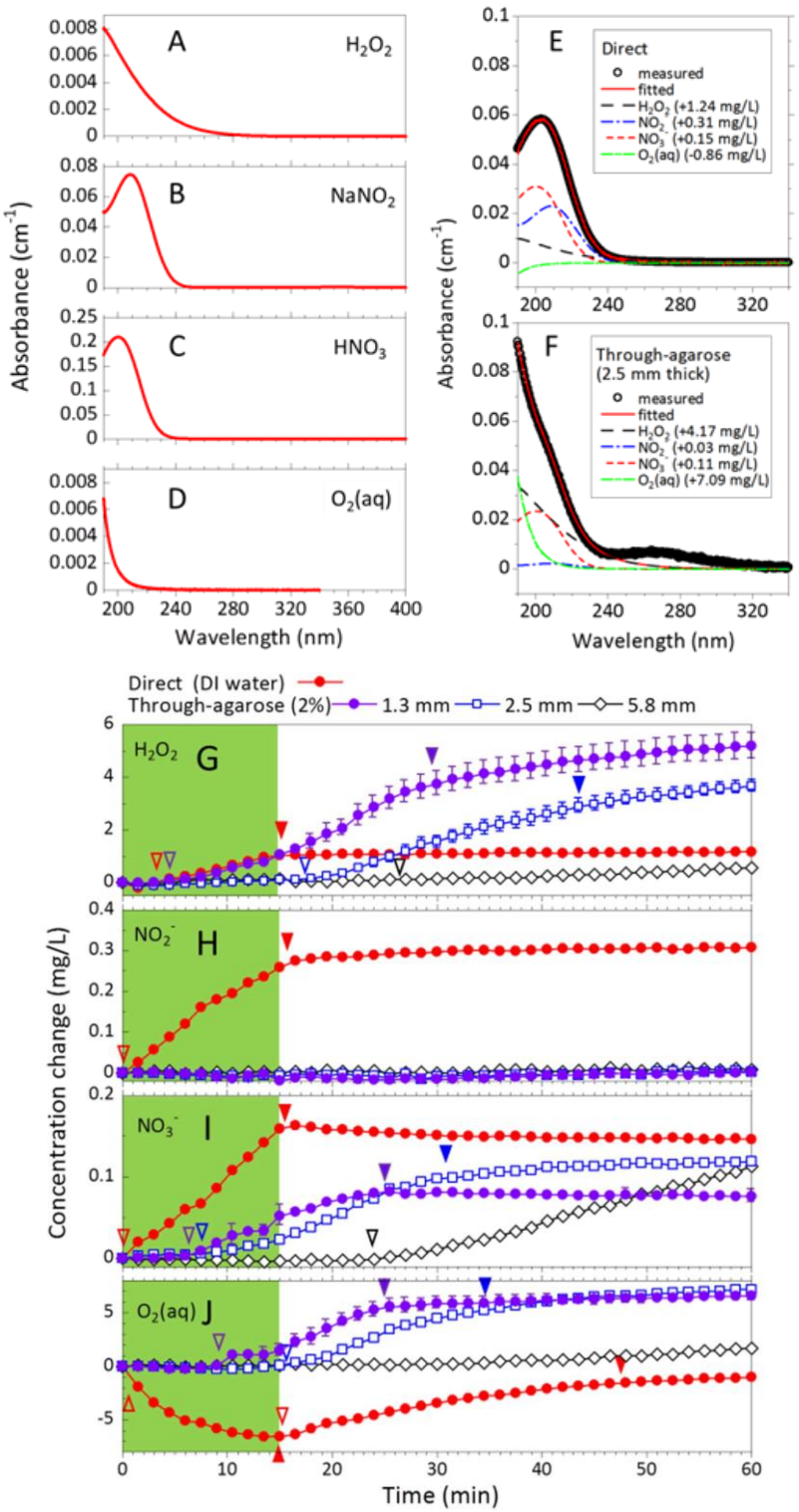


Figure 3.16 Concentrations of RONS in DI water after direct and indirect (through agarose) plasma treatment determined using an automated UVAS curve fitting technique. Reference UV absorbance peaks of neat solutions of (A) H_2O_2, (B) HNO_2, (C) HNO_3 and (D) O_2 (aq) were used to determine concentrations of RONS in DI water after plasma exposure. Plasma and helium gas flow were extinguished after 15 min (t = 15 min) as represented using green shaded region. Curve fitted spectra for (E) direct and (F) indirect plasma treatment through 2.5 mm agarose were recorded. The spectra was recorded up to t = 60 min i.e. 45 min after plasma and He gas were switched off. Dynamic changes in concentrations of (G) H_2O_2, (H) NO_2^-, (I) NO_3^- and (J) O_2 (aq) were investigated by plotting concentrations of each RONS against time. The positive and negative inflections in concentrations were shown using open and solid arrows, respectively. . Each error bar represents ± standard error of the mean (SEM) between triplicate samples (n = 3).

The measured concentrations (μM) of individual RONS (H_2O_2, NO_2^-, NO_3^-), total RONS and O_2 (aq) delivered by the plasma jet in each condition is summarised in Table 3.4.

Table 3.2 Concentrations of RONS in micromolar (μM) after direct and indirect (through agarose) plasma treatment of DI water. Plasma and gas flow were both switched off after 15 min i.e at t= 15 min. Concentrations were measured at (A) t=15 min; (B) t=30 min; and (C) t= 60 min.

	RONS type	**H_2O_2 (μM)**	**NO_2^- (μM)**	**NO_3^- (μM)**	**O_2 (μM)**	**Total RONS (μM)**
A	1.3 mm	31.2 ± 10.6	0.0 ± 0.5	0.8 ± 0.5	46.8 ± 33.6	31.6 ± 11.6
	2.5 mm	3.2 ± 2.9	0.0 ± 0.1	0.4 ± 0.1	2.8 ± 5.3	3.4 ± 3.2
	5.8 mm	4.2 ± 2.2	0.0 ± 0.0	0.0 ± 0.0	2.7 ± 2.8	4.14 ± 2.2
	Direct	30.2 ± 3.9	5.6 ± 0.2	2.6 ± 0.1	-205.3 ± 6.6	38.4 ± 5.3
B	1.3 mm	109.9 ± 29.1	0.0 ± 0.2	1.3 ± 0.2	184.4 ± 34.6	110.9 ± 29.5
	2.5 mm	45.8 ± 13.3	0.0 ± 0.3	1.6 ± 0.13	140.0 ± 22.4	47.2 ±13.7
	5.8 mm	4.3 ± 2.1	0.0 ± 0.0	0.2 ± 0.1	6.5 ± 3.5	4.5 ± 2.2
	Direct	32.0 ± 4.7	6.5 ± 0.1	2.4 ± 0.0	-107.3 ± 4.6	40.9 ± 4.9

C	1.3 mm	152.4 ± 30.5	0.1 ± 0.3	1.2 ± 0.2	206.1 ± 32.8	153.7 ±31.0
	2.5 mm	107.6 ± 13.1	0.0 ± 0.6	1.9 ± 0.1	224.6 ± 19.2	109.6 ±13.7
	5.8 mm	16.5 ± 1.1	0.2 ± 0.1	1.8 ± 0.3	52.7 ± 1.9	17.9 ± 1.4
	Direct	34.1 ± 4.0	6.7 ± 0.1	2.4 ± 0.0	-31.3 ± 4.7	43.1 ± 4.0

The first observation made from Figure 3.16 is that in case of both direct and through agarose treatments, a higher concentration of ROS (i.e. H_2O_2) are produced than RNS (NO_2^- plus NO_3^-), which was also shown previously Section 3.1 of Chapter 3, wherein gelatin was used as the tissue model (Section 3.1). These results are also consistent with concentrations of RONS measured upon direct plasma exposure of different types of tissue fluid models (water, PBS and cell culture media) using molecular probes in Chapter 2.

The RONS concentrations (mg ml^{-1}) at t=0 to 60 min, calculated using curve fitting technique, are shown in Figure 3.16E and 3.16F. The main inferences made were at t=60 min are: (i) a higher concentrations of RONS are generated in case of indirect (through agarose) plasma treatment than the direct treatment; (ii) virtually no NO_2^- was detected in DI water when treated through agarose (this is due to oxidation of NO_2^- to a stable end product– NO_3^-); and (iii) DI water was deoxygenated by direct treatment, but oxygenated by the through-agarose treatment.

The dynamic changes in concentrations of H_2O_2, NO_2^-, NO_3^- and O_2 (aq) in DI water upon direct and through-agarose plasma treatment are shown in Figure 3.16G–J. It can be observed that for the direct plasma treatment of 15 min, RONS concentrations increased in an immediate and monotonic manner (up to t=15 min). After plasma and gas flow were extinguished (after t = 15 min), no increase in RONS concentration was observed. The concentrations of RONS for direct treatment were in decreasing order of

$H_2O_2 > NO_2^- > NO_3^-$. The levels of O_2 (aq) decreased drastically after a 15 min of direct plasma treatment. Approximately 6.57 mg ml^{-1} of O_2 (aq) was lost due to replacement of O_2 molecules by He molecules. After t= 15 min O_2 solvates back into DI water and amount of O_2 (aq) was recovered, although still lower than untreated DI water.

The plasma treatment of DI water through agarose of different thicknesses had remarkable effects on production rate of RONS and O_2 (aq). As shown in 16G–J, presence of an agarose target had significant effect on the rate of delivery of RONS into DI water when compared with direct plasma treatment. The thicker agarose target presented a more substantial barrier to RONS delivery from the plasma-gas to liquid-phase, which eventually lead to a lower concentration of RONS after a 15 min of plasma treatment. However, the H_2O_2 delivery was a bit unusual (Figure 3.16G). Comparing direct vs through-agarose plasma treatment shows that the rate of delivery of H_2O_2 in DI water is not perturbed by presence of a 1.3 mm thick agarose target. The amount of H_2O_2 produced upon plasma treatment of DI water (at t = 15 min) through a 1.3 mm thick agarose target was approximately 31.2 ± 10.6 µM, which was similar to the 30.2 ± 3.9 µM produced after direct plasma treatment. However, the concentration of H_2O_2 delivered through agarose (1.3 mm thick) continued to increase even after plasma and gas flow were extinguished in contrast to direct plasma treatment. The amount of H_2O_2 in case of 1.3 mm thick agarose treatment increased from 31.2 ± 10.6 µM (at t = 15 min) to 152.4 ± 30.5 µM (at t = 60 min) as compared to just 34.1 ± 4.0 µM (at t = 60 min) for direct plasma treatments. But, as the thickness of agarose target increased, the delivery of H_2O_2 was perturbed with a time-lag in the appearance of H_2O_2. For instance, in case of 2.5 mm thick agarose, H_2O_2 appeared at 16.5 min i.e. 1.5 min after plasma and gas flow were extinguished (shown using open arrows in Figure 3.16G) and continued to increase over the 60 min time period. However, the rate of increase in H_2O_2 levels was reduced from t = 28 min and t = 43 min in case of 1.3 mm and 2.5 mm thick agarose, respectively. This negative inflection is shown by solid arrows in Figure 3.16G. The thickest agarose target of 5.8 mm was most effective barrier to H_2O_2 delivery, and levels of H_2O_2 increased gradually from 4.2 ± 2.2 µM (at t = 15 min) to 16.5 ± 1.1 µM (at t = 60 min).

The delivery of NO_2^- was only possible to detect in the direct treatment of DI water (Figure 3.16H and 3.16I). This observation is not too surprising since NO_3^- has a longer half-life and NO_2^- readily oxidised to NO_3^-, as also observed in whole blood [142]. A

time-lag of 6, 7.5 and 24 min was observed in the appearance of NO_3^- after plasma treatment through the 1.3, 2.5 and 5.8 mm thick agarose target, respectively. The concentration of NO_3^- in case of both 1.3 and 2.5 mm agarose plateaued out at t= 25.5 and 40 min, respectively. But with 5.8 mm thick agarose, the concentration of NO_3^- continued to increase up to 60 min. At t=35 min, H_2O_2 production with agarose is in the decreasing order of 1.3 > 2.5 > 5.8 mm but NO_3^- concentration at same time point were in the order 2.5 > 1.3 > 5.8 mm. The generation of NO_3^- at t=60 min increased in the order 2.5 ≈ 5.8 > 1.3 mm. It is evident from the results that post plasma treatment (after plasma and gas flow were extinguished), NO_3^- was delivered more efficiently than H_2O_2 to greater depths in a tissue model.

As discussed in Section 3.2 and shown in previous studies, unlike the direct plasma exposure of DI water, the levels of O_2 (aq) increased in plasma treatment of solution below the tissue target [39, 40]. A similar trend is observed in this study as shown in Figure 3.16J. The increase in O_2 (aq) is quite significant as untreated DI water had approximately 8 mg l^{-1} of O_2 (aq) which increased to 14.60 mg l^{-1} (at t = 60 min) after treatment through 1.3 mm thick agarose and decreased (or rather recovered) to 7 mg l^{-1} (at t = 60 min) for direct treatments (taking into account the significant reoxygenation after the plasma and gas flow are extinguished). Similar to RONS production, a time-lag was also observed before O_2 (aq) increase in DI water. After an initial delay of 9 and 15 min for 1.3 mm and 2.5 mm thick agarose target, respectively, a gradual increase in concentration of O_2 (aq) was observed after the plasma and gas flow were extinguished. The concentrations of O_2 (aq) plateaued out at t = 25.5 and 34.5 min for 1.3 and 2.5 mm thick agarose target, respectively. In case of 5.5 mm thick agarose, only a small increase of 1.7 mg l^{-1} in the concentrations of O_2 (aq) was observed at t = 60 min.

From the trends observed in Table 2, it is evident that the significant differences exist in the concentrations of RONS and O_2 (aq) treated directly and through the agarose target of different thicknesses. With the increase in thickness of agarose from 2.5 mm to 5.8 mm, the concentration of H_2O_2 and O_2 (aq) get reduced to less than one-fifth. At t = 60 min. Interestingly, the concentration of NO_3^- was not greatly influenced with the increase in agarose thickness (ranging from 1.2 ± 0.2 to 1.9 ± 0.1 µM with 1.3 mm to 5.8 mm).

The concentration of H_2O_2 gradually increased with the 1.3 mm agarose target from t = 15 min to 60 min. Although there was a time-dependent increase in transport of H_2O_2 for treatments through agarose, the initial concentrations at t = 15 min were similar to that of direct treatments. This indicates that the He plasma jet used in this chapter not only delivered H_2O_2 into the agarose target but also produced more complex secondary RONS (possibly by reaction with agarose), which were subsequently converted to H_2O_2. In Section 3.1 it was shown that RONS production increased when PBS with protein (BSA) is treated through a tissue target and suspected to be a result of secondary RONS (such as R•). These secondary RONS can react with oxygen to produce other radicals (such as ROO•), which undergo further reactions to form more stable protein ROOH. Upon their decomposition, these stable products can act reservoir for smaller messenger RONS for an extended period of time. Although, agarose target does not contain proteins, the carbohydrates and polysaccharides chains in agarose can undergo oxidation and oxidative polymerization in presence of H_2O_2 to generate potentially smaller reactive species [143, 144].

In this chapter the efficacy of UVAS to meter RONS and O_2 in solution after plasma treatment was assessed. UVAS is a promising technique to monitor the dynamic changes in plasma-production of RONS production and plasma-induced changes in levels of O_2 (aq). Unlike the molecular probes, this method can be utilised to obtain a quasi "real-time" analysis of RONS. Besides RONS, the concentrations of O_2 (aq) can also be determined using UVAS but not using the molecular probes. The use of UVAS also allows determination of multiple RONS in one experiment, without the need of multiple experiments for multiple molecular probes for a specific type of RONS. But the use of real-time UVAS still has certain limitations, which include that:

- only reactive species that have strong absorbance in UV range 190-380nm are detectable.
- only reactive species with longer life time can be detected in DI water below the target/fluid interface.
- only simple solutions can be used as tissue fluid models for UVAS; complex solutions such as BSA-PBS solution or cell culture media which scatter light are not suitable.

It should be noted that in Section 3.1, it was shown that the He plasma jet delivered 120 µM of NO_2^- after a 10 min plasma treatment of solution through the tissue model. On the other hand, in this set of experiments (Section 3.2), the He plasma jet delivered negligible amount of NO_2^- in solution even after 15 min of plasma treatment (through the tissue model). However, this results is not so surprising in the context of the major differences in the experimental setup between the studies. For instance, in Section 3.1, a two-electrode plasma jet, gelatin (polysaccharide in nature) as tissue model, PBS as tissue fluid model and 200 µL test volume in a 96-well plate were utilised. However, in Section 3.2, a single electrode plasma jet, agarose (sugar in nature) as a tissue model, water as tissue fluid model and test volume of 4 ml in a cuvette was utilised. These experimental factors can contribute to the difference in the concentration of RONS monitored in each section. Furthermore, the Griess reagent probe (used in Section 3.1) only detects NO_2^- in solution. To be able to detect NO_3^- using the Griess reagent, NO_3^- ions need to be reduced to NO_3^- via enzymatic or chemical reductants.

However, conclusively, the studies conducted with molecular probes and UVAS are in agreement in the key trends. For example, that higher concentration of ROS (H_2O_2) than RNS is delivered by the He plasma jet into tissue fluid model. Furthermore, the plasma jet has ability to enhance the oxygenation of tissue fluid in through-tissue target treatments. The increase in levels of O_2 in solution beneath tissue target can be a potential contributing factor of the slow-molecular transport of RONS deep into the tissue targets of several mm.

To develop a better understanding of the plasma-delivery of RONS through tissue target, it is also essential to understand the ionic species delivered by the plasma jet into the tissue model. In next section, the ionic species produced in the plasma effluent and penetrating the tissue model after solvation are detected in real-time using the technique of mass-spectrometry.

3.3 Tracking penetration of RONS delivered by plasma in tissue model using mass spectrometry

In sections 3.1 and 3.2, the ability of plasma to deliver RONS across tissue barriers of several mm thickness was demonstrated. As discussed in the introduction, the “deeper” effects of plasma-delivered RONS in tissues can be explained by slow molecular transport processes and/or cell-to-cell communication processes [38, 45]. Before the

slow penetration of RONS deep into the tissue, the highly reactive species present in the plasma effluent (gas-phase) interact with the tissue surface. These species in gas-phase are delivered to the tissue via “rapid transport process” in first few nms [39]. Later, these species penetrate into the tissue and get solvated. The new species thus formed emerge out on the other side of the tissue.

Molecular probes and UVAS have the potential to detect the plasma species (RONS) delivered by the plasma jet through the tisue model in tissue fluid. But, these techniques do not allow the detection of other wide range of plasma species including stable gas-phase particles, reactive radicals, ionic plasma species i.e. positive and negative ions, water cluster molecules, and even excited species such as metastables [145, 146]. This information can be acquired from the mass spectrometry, as discussed later in details, and can also be a useful tool to corroborate the results obtained from moleculr probes, UVAS and OES.

The 1980s marked the beginning of the use of mass spectrometric techniques for characterising plasma discharges [147]. Although, the use of mass spectrometry at low-pressure is well established [148-151], its application in ambient air for the plasma characterization is still newer. A few studies have utilised ambient and time-resolved mass spectrometry for identifying ionic species, neutral species and radicals produced by different types of plasma configurations including plasma needle, He parallel plate discarges, and plasma jets [137, 146, 152-157]. However, the use of mass spectrometry in the plasma treatment of tissues is still unexplored. The study presented in this thesis is the first to explore this aspect.

3.3.1 Principle and Instrumentation

Mass spectrometry can be used to identify the unknown species in a mixture (of species) by differentiating charged species on the basis of their mass-to-charge (*m/z*) ratio [147]. The working principle of mass spectrometry is illustrated in Figure 3.17. Mass spectrometry can be used to detect ions directly, or neutral species within the plasma. In the latter case, ionisation is achieved using an electron beam. Ionised species include positively charged species, such as O_2^+, N_2^+, H^+N_2, NO^+, etc. and negatively charged species, such as O_2^-, NO_2^-, CO_3^-, $O_2^-(H_2O)_2$. These are separated first according to charge and then separated by a mass analyser (an electromagnet) based on their *m/z* ratio. The m/z-resolved species reach the detector and are converted to a measurable

signal. The steps of ionization (for neutrals), sorting, and detection takes place in a high vacuum condition.

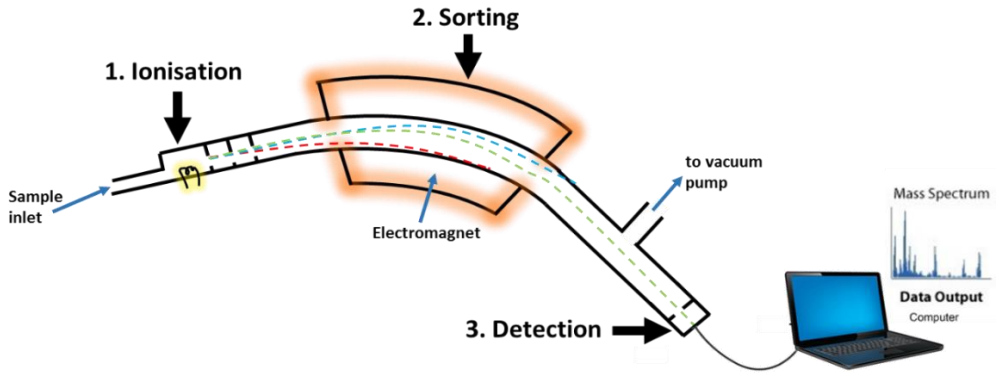


Figure 3.17 Schematic of a mass spectrometer. The species are differentiating based on the m/z ratio in three major steps – ionization by electron beam bombardment, sorting by a mass analyser and detection to get a mass spectrum.

3.3.2 Materials and Methods

3.3.2.1 Plasma jet

The physical dimensions of the body of plasma jet (glass tube in PTFE housing and electrode) was same as the unit used in section 3.2.2 (see material and methods). A high purity He gas (BOC) was purged into the glass tube at a gas flow rate of 0.5 slpm. A sinusoidal $V_{p\text{-}p}$ of 10 kV was applied with a fixed frequency of 50 kHz.

3.3.2.2 Agarose tissue model

A 2% (w/v) agarose solution was prepared using the protocol described in section 3.2.1. A 20 ml of cooled agarose solution poured in a plastic petridish and gently agitated to spread the solution evenly without forming any air bubbles. Agarose was left to set at 4^{o}C for 12 hours before use. A scalpel and plastic forceps were used to cut and gently remove 2 X 2 cm^2 pieces of 3.2 mm thick agarose film.

3.3.2.3 Mass spectrometry system

A commercially available ambient mass spectrometry system HPR60-EQP300 (Hiden Analytical Ltd.) was used to measure neutral plasma species and positively and negatively-charged plasma species [158]. The HPR60 is a three-stage differential pumping system which maintains a high vacuum environment (less than 10^{-7} Torr) during the operation. The inlet system of HPR60 is separated by three close-coupled skimmer cones – each cone has a specific orifice diameter. The orifice inlets are in fine alignment with the molecular beam axis for accurate and high intensity signals. The

HPR60 is equipped with a triple filter quadrupole mass spectrophotometer– EQP300. The molecular beam is directed into the spectrophotometer and measured by a detector. The detector sampling time was set at 1 second for all measurements. The spectrometer was operated at the residual gas (RGA) mode and secondary ion mass spectrometry (SIMS) mode to detect neutral species and ionic species (positively charged species and negatively charged species) in the region of 1-100 amu, respectively. In the RGA mode, the neutral molecular beam is internally ionised before reaching the quadrupole spectrophotometer. The SIMS mode works without an internal ioniser, which implies that the mass spectra are collected from the externally-charged species produced by applying a high voltage to the skimmer cones.

3.3.2.4 Experimental setup

The experimental setup of the plasma jet and mass spectrometry system to measure the species directly generated by plasma and generated through an agarose target are shown in Figure 3.18a and 3.18b, respectively. To achieve a maximal signal intensity and an optimal alignment of the plasma plume to mass spectrometer orifice, the plasma jet was mounted on an x-y-z stage.

The distance between end of plasma jet glass tube and mass spectrometer was determined after conducting appropriate molecular beam alignment. Firstly, mass intensity changes was monitored at the mass numbers of He (4 amu) and N_2 (28 amu) in RGA mode. This was followed by determining an optimal position at which maximum signal of He with minimum background signal of N_2 is observed. Based on this alignment, the distance between end of plasma jet glass tube and mass spectrometer orifice was fixed at 8 mm (for both direct and through agarose treatments). A custom-made sample holder was used to place agarose target at a fixed distance of 2 mm from the orifice.

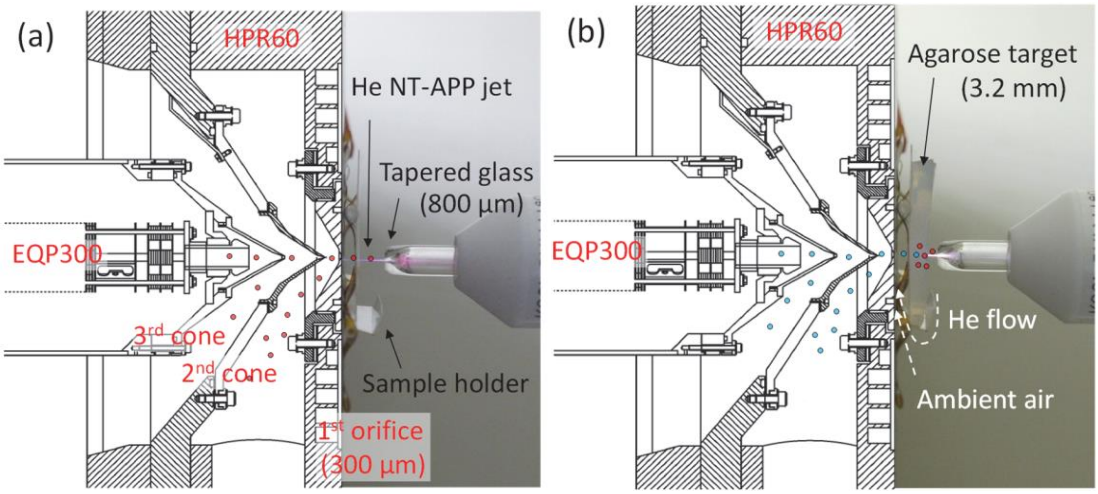


Figure 3.18 A pictorial representation of mass spectrometry of a He plasma jet. The jet was mounted onto an x-y-z stage for the molecular beam alignment. The HPR60 has a three-stage differentially pumped system which is separated by the three skimmer cones. The cones and the turbo molecular pumps help to maintain vacuum condition in the chamber. The plasma species were detected for (a) direct plasma treatment and (b) through-agarose plasma treatment.

3.3.3 Results and discussion

Using mass spectrometry, neutral and ionic species delivered by plasma jet on the other side of agarose tissue model (i.e. the side opposite surface to plasma treatment, or backside of the agarose) were detected. It was confirmed that the plasma plume is in contact with the agarose target. Due to the presence of agarose, the plasma plume is not ignited on the backside of agarose. Therefore, only the solvated species (not the plasma plume) interacted with the mass spectrometer orifice. Using the time-averaged intensities (counts/s; cps), the species were detected in the range 1–100 atomic mass units (amu); although the measurements were conducted for up to 300 amu[2]. For a 23 min of plasma treatment time, the optimum scan number was determined to be 43. Out of the 43 scans, the first and last 3 scans were without agarose target to confirm that the mass intensities had not changed.

Firstly, using the RGA mode, the mass intensities of the neutral species were detected. Figure 3.19a, 3.19b and 3.19c show the mass intensities of N_2, O_2 and H_2O produced by the plasma jet in ambient air plotted against time. The time-resolved mass spectra of He for the plasma gas and neutral He gas was also obtained (Figure 3.19d).

[2] no valuable information was available in the 100-300 amu range.

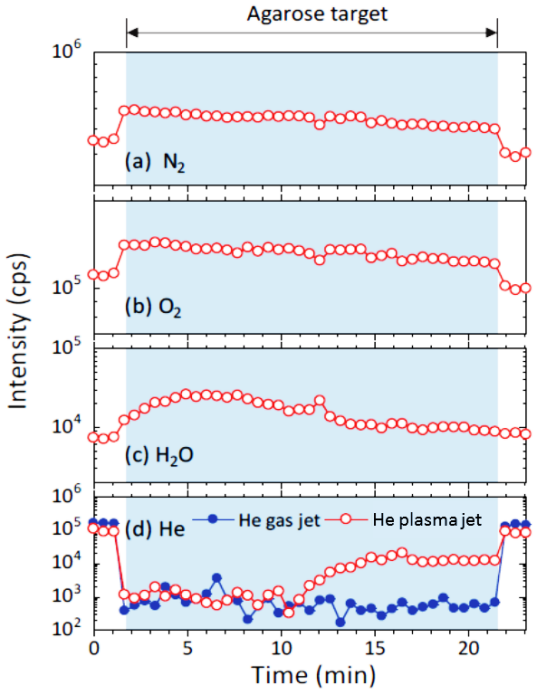


Figure 3.19 Time resolved changes in mass intensities of neutral species (a) N_2, (b) O_2, (c) H_2O (in ambient air) during plasma treatment, and (d) intensity of He during plasma jet as well as neutral He gas treatment. The species were detected in RGA mode using an internal ioniser (EQP300).

Figure 3.19 shows the spectra of N_2, O_2 and H_2O molecules in the humid ambient air, along-with the He species. In their mass spectrometric study, Stoffels *et al.* investigated the species by a He plasma needle (jet) launched into air and have reported the production of N_2, O_2 and He, similar to Figure 3.19. Figure 3.19 shows that at a fixed distance of 8 mm the intensity of N_2 is higher than other species; later the mass spectra of the positive ions (Figure 3.20) confirms that the N_2 species are also dominant over the other species. The intensity of H_2O increased immediately when an agarose target was placed between the sampling orifice and the plasma jet (Figure 3.19c). This could be due to the water vaporization from the (backside of the) hydrated agarose surface upon plasma treatment.

Comparing Figure 3.19b and 3.19d, it can be seen that the intensities of He and O_2 without an agarose target were similar (at ca. 10^5 cps). But with the presence of agarose target (blue shade), the He signal intensity decreased immediately, whilst the O_2 signal increased. The low He signal intensity is simply due to the presence of agarose target as a barrier which perturbed the flow rate of He. However, for plasma treatment the He signal intensities eventually increased between 10 to 17 min, before stabilising (Figure 3.19d). The increase in He signal intensities at 10 min was only observed with plasma treatment and not with the He gas treatment. It was speculated that this time-lag in

increase of He signal (with plasma treatment) was due to the time taken by He (as well as He metastable) species to penetrate into the agarose target. The exact mechanisms behind this phenomenon (i.e. He detection through agarose with plasma) are not completely understood, however it is possible that in the presence of plasma, the velocity of the He jet is enhanced as compared to the gas flow (without plasma). The study by Oh *et al.* supports this claim, wherein they assessed the jet structure with plasma on and with only He gas (no plasma) [159]. The results show that the jet extension (laminar region) decreases by almost 30% with the plasma ignited, which would arise from a significant increase in the gas velocity.

The increase in signal intensities of He with the plasma jet can also be ascribed to strong electric fields present in the plasma jet, absent in the gas jet. When a high voltage is applied to the He gas, high energy electrons and slower moving ions can be created and accelerated by the strong electric fields [152, 153], which can push the He species through the jet. In a study by Szili *et al.*, it was shown that a He plasma jet treatment can lead to formation of star-shaped pattern (fem mm deep) in the hydrogel tissue model, but no such patterns were observed in case of He gas jet [31]. This further indicates the role of physical forces exhibited by plasma (in form of electric field and/or plasma streamers) in the plasma-tissue interactions. Further experiments must be conducted to develop a better understanding in this context.

The next objective was to analyse the plasma delivery of ionic species (both positively- and negatively-charged plasma species). The ionic species, produced upon interactions between the plasma plume and ambient air, were detected using the SIMS mode of the spectrometer.

Firstly, the positively charged ionic species were detected at 1 min time point (t=1 min) without an agarose target (Figure 3.20a), and with an agarose target at t= 10 min (Figure 3.20b) and t = 20 min (Figure 3.20c). In Figure 3.21, the intensities of major positive species [O^+, O_2^+ and $H^+(H_2O)_4$] detected in through-agarose treatment, are plotted as function of time (over a time period of 20 min). It must be noted that the $H^+(H_2O)_4$ can also be alternatively assigned to $H_2\ O^+$ and $(H_2\ O)^+_{n-1}$.

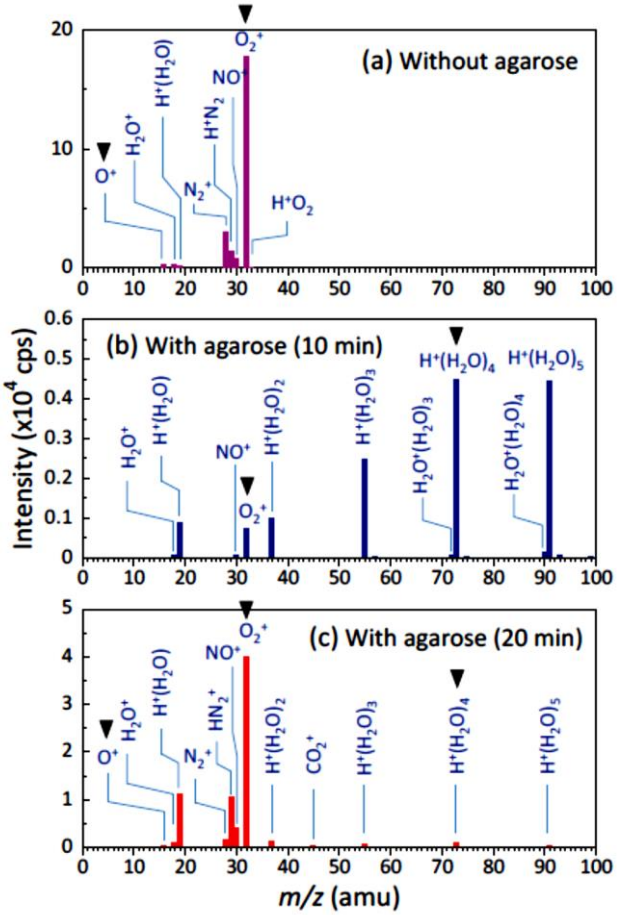


Figure 3.20 Ambient mass spectra of positive species delivered by plasma jet treatment (a) without agarose at t=1 min; (b) through agarose at t=10 min; and (c) through agarose at t=20 min. All measurements were done in positive SIMS mode.

From Figure 3.20a it can be seen that in the absence of an agarose target, the major positive ions correspond to O_2^+, N_2^+, NO^+ and H_2O^+. Other reports have also detected similar positive ions generated by plasmas launched into air [146, 152-155]. At the large distance of 8 mm between the sampling orifice and plasma jet (without agarose target), it was difficult to measure He^+. However, reducing the distance to approximately 2 mm allowed detection of He^+. For this study, all experiments were conducted at distance of 8 mm, therefore no He^+ peak is shown in Figure 3.20.

It is thought that the majority of these positive ions are generated from the Penning ionization of the molecules present in ambient air upon interactions with the highly energetic metastables of He, as shown in reactions below [153, 160, 161]:

$$He^* + N_2 \rightarrow N_2^+ + He + e^-$$

$$He_2^* + N_2 \rightarrow N_2^+ + 2He + e^-$$

$$He_2^* + N_2 \rightarrow N_2^+ + 2He + e^-$$

$$He^* + O_2 \rightarrow O_2^+ + He + e^-$$

$$He^+ + O_2^* \rightarrow O_2^+ + He$$

$$He + O_2 \rightarrow O_2^+ + He$$

Figure 3.20b and 3.20c show that the through-agarose plasma treatment still produced the same ionic species (O_2^+, H_2O^+, N_2^+, NO^+), as seen in the case of without agarose, however the signal intensities were much lower. This indicates that the presence of agarose target acts as a physical barrier to the transport of these ionic species. However, as the plasma treatment time increased to 20 min, the signal intensities of these species recover.

The mass spectra of the plasma plume (without agarose) shows peaks for the small water cluster ion– $H^+(H_2O)$ (Figure 3.20a). Such water clusters are formed due to the hydration reactions between species within the plasma plume and the water vapours in ambient air [152, 158]. Similarly, as shown in Figure 3.20b, the through-agarose plasma treatments also contains several (new) signals corresponding to water cluster ions such as H_2O^+, $H_2O^+(H_2O)_n$ [n=3-5] and $H^+(H_2O)_n$ [n=1-5]. These water clusters ions emerging to the other side of the agarose target arise from the subsequent solvation of the protonated water clusters (initially formed when plasma first interacts with the target) into the agarose target and their transport (or diffusion) to the opposite side of the target.

A major change in mass spectra of through-agarose treatment at t = 10 and 20 minutes was observed. Upon comparing Figure 3.20b with 3.20c, it is evident that the signal intensities of $H_2O^+(H_2O)_n$ [n=3-5] and $H^+(H_2O)_n$ [n=2-5] reduced at t = 20 min. However at t = 20 min, the intensities of other positive ions including O_2^+, NO^+, H_2O^+ and $H^+(H_2O)$ increased as compared to t = 10 min. With the increase in time from t = 10 min to 20 min, new spectral lines corresponding to O^+, HN_2^+ and CO_2^+ were also observed. It should be noted that the signals for CO_2^+ may coincide with the N_2O^+ (*m/z* = 44 amu). The equipment and techniques used for this study cannot differentiate between the mass spectra of two molecules/ions with the same *m/z* number, thus making the analysis difficult. But the presence of carbon-related ionic species such as CO_2^+ (Figure 3.20c) and CO_3^- and HCO_3^- (shown later in Figure 3.22) is not unusual, since the CO_2 makes 0.039% of the standard ambient conditions [162].

The time dependent changes in the mass spectra of some specific positive ions (significant in direct and through-agarose treatment) were assessed. Figure 3.21 shows the intensities of O^+, O_2^+ and $H^+(H_2O)_4$ detected in through-agarose treatment, plotted as function of time.

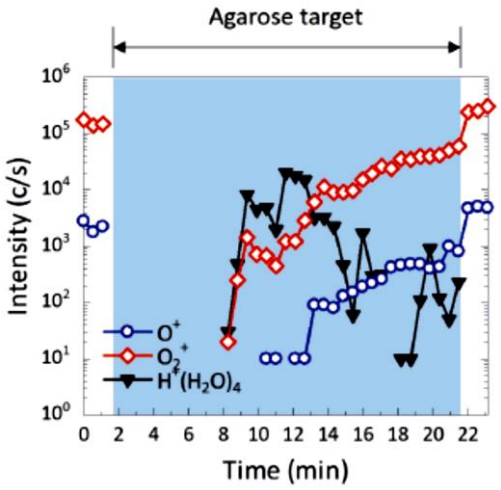


Figure 3.21 Time-dependent changes in mass intensities of positive ions O^+(16 amu), O_2^+(32 amu), and $H^+(H_2O)_4$ (73 amu).

From Figure 3.21, it can be seen that the signal intensities of O^+, O_2^+, and $H^+(H_2O)_4$ in *in-situ* measurements appear after a time-lag of several minutes. After the initial time lag of roughly 8 min, the signal intensities of O^+ and O_2^+ kept increasing with the plasma treatment time. Interestingly, the intensity of $H^+(H_2O)_4$ increased only for about 5 min before decreasing again after 12 min. This decrease can be attributed to dehydration of the agarose target and loss of water molecules (H_2O). Interestingly, after 12 min, the signal intensities for O^+ and O_2^+ increased. This could imply that as the target dehydrated, the other species (O^+ and O_2^+) begin to emerge through the agarose target.

Following the positive ion analysis, the next step was to assess the generation of negative ions produced by the plasma jet. Figure 3.22a shows the mass spectra of negative ions generated in ambient air by a He plasma jet (without agarose target). The mass spectra of the negative species for plasma treatment with agarose was also obtained, at t = 10 min (Figure 3.22b) and t = 20 min (Figure 3.22c).

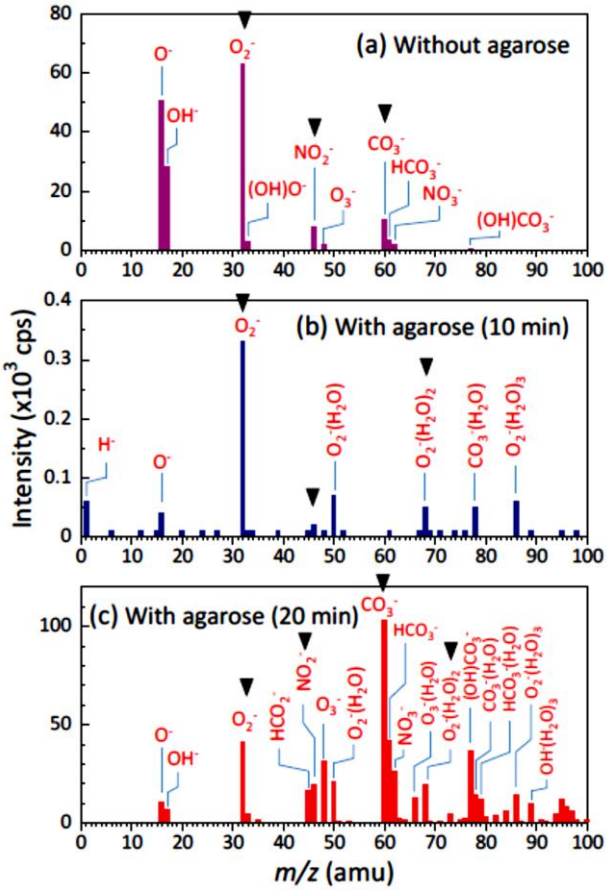


Figure 3.22 Ambient mass spectra of negative species delivered by plasma jet treatment (a) without agarose at t=1 min; (b) through agarose at t=10 min; and (c) through agarose at t=20 min. All measurements were done in negative SIMS mode.

Figure 3.22a shows that the mass spectra of the plasma without agarose corresponds to O_2, O_2^-, O_3^-, OH^-, $(OH)O^-$, NO_2^-, NO_3^-, CO_3^-, HCO_3^- and $(OH)CO_3^-$. Accepted wisdom is that negatively-charged species are produced by multi-step dissociative electron attachment, followed by further attachment with molecules present in air (M) as summarised below [153, 163]:

$$e^- + AB \rightarrow A^- + B$$

$$A^- + M \rightarrow A^-M$$

For instance, the most abundant negative species are O^-, O_2^- and O_3^- are suspected to be an outcome of the dissociative electron attachment to O_2 [164] and likely pathways as summarised below:

$$e^- + O_2 \rightarrow O^- + O$$

$$e^- + O_2 + M \rightarrow O_2^- + M$$

$$O^- + O_3 \rightarrow O_3^- \qquad (if\ sufficient\ O_3\ is\ available)$$

$$O^- + O_2 + M \rightarrow O_3^- + M \qquad (at\ low\ levels\ of\ O_3)$$

The formation of OH^- can be formed through dissociative electron attachment to water molecules [165] present in ambient air or a as shown below:

$$e^- + H_2O \rightarrow OH^- + H$$

The appearance of carbon anions such as CO_3^-, HCO_3^- and $(OH)CO_3^-$, most likely arise from reactions between the oxygen anions and carbon dioxide (CO_2) as shown below [157]:

$$O^- + CO_2 + M \rightarrow CO_3^- + M$$
$$OH^- + CO_2 + M \rightarrow HCO_3^- + M$$
$$HCO_3^- + O_2 \rightarrow (OH)CO_3^- + O$$

Figure 3.22b and 3.22c show the mass spectra of negative ions that transverse the agarose barrier and pass into the mass spectrometer. On comparing the mass spectra of plasma treatment without and with agarose, it can be seen that the several ionic water clusters including $CO_3^-(H_2O)_n$ [n=1-2], $HCO_3^-(H_2O)$, $OH^-(H_2O)_3$, $O_2^-(H_2O)_n$ [n=1-3] and $O_3^-(H_2O)$ were detected in treatment with agarose. As explained before, the water cluster ions exiting the other side of agarose are the charged water molecules (ions) which undergo solvation and diffusion in the target. Interestingly, the O_2^- species are delivered by the plasma jet even with the presence of agarose target, unlike other major species.

From comparing Figure 3.22b and 3.22c, it can be seen that there is an increase in intensities of RONS (NO_2^- and NO_3^-) from t = 10 min to t = 20 min. The NO_2^- and NO_3^- can be produced by the reactions of He metastables or other negatively charged species with the other atmospheric gases such as nitrogen oxides. These get solvated into agarose and re-emerge on the backside of the agarose. This is a time dependent process as shown in the Figures 3.22b and3.22 c. There was also a significant increase in the appearance of the anionic water clusters as the plasma treatment time increases to t = 20 min. This increase could be due to increase in water vaporisation with the treatment time.

The time dependent changes in prominent negative species – O_2^-, NO_2^-, CO_3^-, HCO_3^- and $O_2^-(H_2O)_2$ over a time period of 20 min were examined (Figure 3.23).

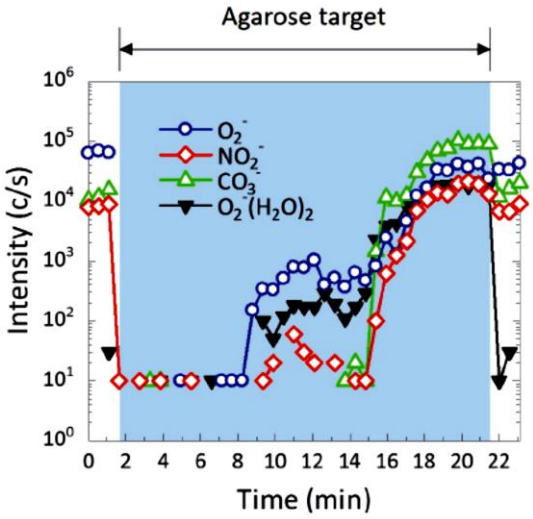


Figure 3.23 Time-dependent changes in mass intensities of negative ions O_2^-(32 amu), NO_2^-(46 amu), CO_3^-(60 amu), and $O_2^-(H_2O)_2$ (68 amu).

The results from Figure 3.23 indicate that the presence of agarose target had a significant impact on plasma delivery of negative ions. Like the positive ions, there was a time-lag before the appearance of negative species. With time, an increase in the formation of water clusters such as $O_2^-(H_2O)_2$ was also observed. The intensities of NO_2^- and CO_3^- were high in the absence of agarose, but decreased between the time points of t = 2 min (without agarose) and at t = 10 min (with agarose). Interestingly, both these species recovered again at t = 20 min (with agarose). The increase in signal intensity of NO_2^- at t=20 min is nearly double than the intensity without agarose. Similarly, the intensity of CO_3^- increased by an order of magnitude.

Overall, this initial study shows that ambient mass spectrometry can be used successfully to monitor the real-time transport of neutral gas species and plasma generated ionic (positively and negatively charged) species through agarose target. Previously, in Section 3.2, OES and UVAS was also utilised to examine the 'real-time delivery' plasma species in gas-phase and liquid-phase, respectively. But, with the OES experimental setup, the real-time transport of species through the tissue target (sub-surface) is not achievable. Another challenge associated with OES and UVAS is the inability to detect the ionic plasma species exiting on the other side of the tissue model after the plasma treatment. With mass spectrometry, short lived O_2^- could also be detected, which was challenging with UVAS as well as the molecular probes (Section 3.1).

The data from this study and previous studies (Section 3.1 and 3.2) had some common findings. For instance, the results from molecular probe and UVAS showed that the

tissue target acts as a physical barrier and perturbs the delivery of RONS, which was later confirmed by the mass spectrometry. Similarly, all the three techniques detected the OH^-, NO_2^- and NO_3^- during plasma treatment of the tissue target. Both the UVAS and mass spectrometry showed that the reactive species emerged from the other side of the tissue after some time-lag. This observation affirms that the plasma-delivery of RONS is a process of slow molecular transport. From the molecular probes and UVAS study it was speculated that the short-lived gaseous species near tissue surface, determine the formation of secondary RONS and that the tissue target may act as a reservoir for reactive species. The mass spectra obtained from this study also confirmed that the reactive (ionic) species get accumulated within the tissue target and undergo subsequent hydration or solvation before penetrating through the tissue target. The secondary ionic species and hydrated clusters, thus formed, could be detected even on the other side of the target. In other words, it can be said that mass spectrometry served a confirmatory technique to corroborate the conclusions drawn from the molecular probes and UVAS.

3.4 Conclusion

The aim of this chapter was to monitor the interactions between plasma and tissues using tissue fluid models (water and PBS) and tissue models (gelatin, agarose and PVA films). A range of detection techniques (such as molecular probes, UVAS, OES and mass spectrometry) were explored to investigate the plasma-chemistry in both the gas-phase and liquid-phase. Within this chapter, the electrical characterization of the plasma jet was also conducted using the voltage and current probes.

The plasma species generated in gas-phase were detected using OES (Section 3.2) and mass spectrometry (Section 3.3). OES results showed that the species in N_2^+ FNS [N_2^+ ($B^2\Sigma_u^+ – X^2\Sigma_g^+$)] and N_2^* SPS [$N_2(C^3\Pi_u – B^3\Pi_g)$] were dominated the plasma. Other highly reactive and shorter lived species (including metastables) such as He*, N_2*, O* and OH• were also detected. These species are known for their key role in plasma-liquid interfacial interactions and generation of RONS in liquid [34, 41, 158].

To investigate the formation of ionic species (positive and negative) when plasma interacts with ambient air and/or hydrated surface of hydrogel (tissue target) *in situ* mass spectrometry was employed. The formation of positive ions (such as O_2^+, N_2^+, H^+ N_2, and NO^+) and negative ions (such as O_2^-, NO_2^-, CO_3^- and HCO_3^-) and their

corresponding water-cluster ions were analysed in real-time. It was shown that ionic species appear in the tissue target after a time-lag. However, both positive and negative ionic species can undergo hydration and solvation inside the tissue target to form ionic water clusters such as $O_2^-(H_2O)_2$ and $H^+(H_2O)_4$, to name a few. These products are released slowly to the other side of the tissue target upon plasma jet treatment which explains the time lag experienced in appearance signal intensities of these species.

Apart from the plasma chemistry in gas-phase and within the tissue target, the chapter also focused on examining the production of RONS in solution (tissue fluid model) beneath the tissue target after plasma treatment. Molecular probes (Section 3.1) and UVAS (Section 3.2) was utilised to achieve this.

This study highlights the potential of plasma jet as a powerful tool to oxygenate tissue and increase localised partial pressure O_2 (aq) in the solution underneath the tissue (section 3.2.2). The results from UVAS are in agreement with an *in vivo* study by Collet *et al.* which showed that plasma jet can increase local oxygen tension increased in live mice [106]. From these results, the confidence in the potential use of plasma to counteract hypoxia in wounded tissues (which poses major obstacle in wound healing [93]) was re-established.

In Section 3.1, the real physiological environment of a tissue was mimicked by incorporating protein (BSA) in the tissue model (gelatin) as well as in the tissue fluid (PBS). The combined effect of protein and O_2 (aq) in plasma generation of RONS were assessed using the molecular probes. DCFH was used to detect a broad range of ROS. Specific RONS such as H_2O_2, $NO_2^-$and OH• were detected using OPD-HRP, Griess reagent and TA, respectively. From this work it was shown that in the absence of a tissue target, the tissue fluid model is deoxygenated by plasma but the levels of the O_2 (aq) are enhanced when the plasma treatments is through a tissue model such as gelatin or agarose (results confirmed using UVAS in Section 3.2). Depending on the levels of O_2 (aq), the presence of protein can either inhibit or enhance the production of ROS in the tissue fluid model. The complex protein- O_2 -plasma interactions may not be well understood but the results presented in this chapter could have direct implications in plasma treatment of real tissue as well. For instance, the proteins in tissues may act as the reservoir for secondary RONS and depending on the level of O_2 lead to a slow and gradual increase in RONS concentration is expected. This low flux of RONS mediated

by proteins can stimulate cell survival mechanisms and stimulates important cell signaling mechanisms.

Using UVAS, the tissue models of various thicknesses (1.3, 2.5 and 5.8 mm) were used to monitor the RONS delivery in tissues. It was confirmed that plasma has the potential to (i) deliver RONS deep into the tissue (up to mm); and (ii) improve levels of O_2 (aq) in solution underneath the tissue. The deep delivery of RONS occurs after a time-lag thus implicating plasma delivered RONS into tissues via slow molecular transport [38]. The analysis using different thicknesses of tissue target showed that RONS levels are more active in top levels of a tissue, also shown by Keidar *et al.* in case of tumors [166].

The studies with molecular probes and UVAS both confirmed that the He plasma jet delivered higher concentrations of H_2O_2 than the NO_2^- (and NO_3^-) in solution, as shown previously in Chapter 2 as well. These studies demonstrate conclusively that plasma delivery of RONS deep within the tissues is determined by the composition of the tissue and the tissue fluid as well as the gas-tissue interfacial interactions. Although H_2O_2 was the dominant specie quantitated in these studies, its production is also enhanced by presence of highly reactive shorter-lived species such as OH• and superoxide radicals ($O_2^{\bullet -}$) [167]. Some studies also suggest that UV component of plasma can induce photolysis of RONS and water molecules to produce highly reactive RONS [35, 41, 168, 169]. Further investigation is required to detect these shorter lived species precisely.

The simple experimental setup using hydrogels tissue fluid and tissue models, used in this chapter can serve as a platform to study plasma-tissue interactions. But, these synthetic models are not an accurate depiction of the real tissue environment. For instance, real tissues are composed of other complex biomolecules including DNA, protein, antioxidants, enzymes, etc. The physiological fluid is not static but continuously replenished with fresh fluid. Although limited parallels can be made between real tissue and experimental methodology used in this study, further developments by incorporating biomolecules (for example cells and DNA) and introducing fluid flow using microfluidic systems can strengthen our knowledge of plasma jets and potential medical applications. In the next chapter, the tissue fluid and tissue model will be improved by incorporating artificial DNA and cell models in them.

Finally, these models will be used to study the interactions of plasma with biological components present in the tissue.

3.5 References

1. Graves, D.B., *The emerging role of reactive oxygen and nitrogen species in redox biology and some implications for plasma applications to medicine and biology.* Journal of Physics D: Applied Physics 2012. **45**: p. 263001.
2. Blackert, S., et al., *Influence of non-thermal atmospheric pressure plasma on cellular structures and processes in human keratinocytes (HaCaT).* Journal of dermatological science, 2013. **70**(3): p. 173-81.
3. Moniruzzaman, R., et al., *Cold atmospheric helium plasma causes synergistic enhancement in cell death with hyperthermia and an additive enhancement with radiation.* Scientific Reports, 2017. **7**(1): p. 11659.
4. Laroussi, M. and V. Maruthamuthu, *Effects of Plasma Activated media on Epithelial Cells.* Clinical Plasma Medicine, 2018. **9**: p. 39.
5. Bekeschus, S., et al., *Basic Research in Plasma Medicine - A Throughput Approach from Liquids to Cells.* Journal of Visualized Experiments : JoVE, 2017(129): p. 56331.
6. Arndt, S., et al., *Comparing two different plasma devices kINPen and Adtec SteriPlas regarding their molecular and cellular effects on wound healing.* Clinical Plasma Medicine, 2018. **9**: p. 24-33.
7. Oh, J.-S., et al., *How plasma induced oxidation, oxygenation, and de-oxygenation influences viability of skin cells.* Applied Physics Letters, 2016. **109**(20): p. 203701.
8. Haertel, B., et al., *Surface molecules on HaCaT keratinocytes after interaction with non-thermal atmospheric pressure plasma.* Cell Biol Int, 2012. **36**(12): p. 1217-22.
9. Liedtke, K.R., et al., *Non-thermal plasma-treated solution demonstrates antitumor activity against pancreatic cancer cells in vitro and in vivo.* Scientific Reports, 2017. **7**(1): p. 8319.
10. Attri, P., et al., *Influence of reactive species on the modification of biomolecules generated from the soft plasma.* Scientific Reports, 2015. **5**: p. 8221.
11. Schmidt, A., et al., *Non-thermal plasma treatment is associated with changes in transcriptome of human epithelial skin cells.* Free radical research, 2013. **47**(8): p. 577-592.
12. Takai, E., et al., *Protein Inactivation by Low-temperature Atmospheric Pressure Plasma in Aqueous Solution.* Plasma Processes and Polymers, 2012. **9**(1): p. 77-82.
13. Antoniu, A., et al., *RETRACTED: Safety evaluation of nonthermal atmospheric pressure plasma liquid treatment: Single DNA molecule-based method.* Journal of Electrostatics, 2014. **72**(3): p. 210-217.
14. Yasuda, H., et al., *States of Biological Components in Bacteria and Bacteriophages during Inactivation by Atmospheric Dielectric Barrier Discharges.* Plasma Processes and Polymers, 2008. **5**(6): p. 615-621.
15. Tanaka, Y., et al., *Analysis of the Inactivation Mechanism of Bacteriophage X174 by Atmospheric Pressure Discharge Plasma.* IEEE Transactions on Industry Applications, 2014. **50**(2): p. 1397-1401.

16. Yasuda, H., et al., *Biological Evaluation of DNA Damage in Bacteriophages Inactivated by Atmospheric Pressure Cold Plasma.* Plasma Processes and Polymers, 2010. **7**(3-4): p. 301-308.
17. O'connell, D., et al., *Cold atmospheric pressure plasma jet interactions with plasmid DNA.* Applied Physics Letters, 2011. **98**(4): p. 043701.
18. Eisuke, T., et al., *Chemical modification of amino acids by atmospheric-pressure cold plasma in aqueous solution.* Journal of Physics D: Applied Physics, 2014. **47**(28): p. 285403.
19. Lackmann, J.W., et al., *Chemical fingerprints of cold physical plasmas - an experimental and computational study using cysteine as tracer compound.* Sci Rep, 2018. **8**(1): p. 7736.
20. Bruno, G., et al., *Mass Spectrometry Based Analysis Of The Oxidation Compounds Produced By Cold Atmospheric Plasma (CAP) Interaction With Cysteine.* Clinical Plasma Medicine, 2018. **9**: p. 33-34.
21. Grudzenski, S., et al., *Inducible response required for repair of low-dose radiation damage in human fibroblasts.* Proceedings of the National Academy of Sciences, 2010. **107**(32): p. 14205-14210.
22. Turrini, E., et al., *Cold Atmospheric Plasma Induces Apoptosis and Oxidative Stress Pathway Regulation in T-Lymphoblastoid Leukemia Cells.* Oxidative Medicine and Cellular Longevity, 2017. **2017**: p. 13.
23. Schmidt, A., et al., *A cold plasma jet accelerates wound healing in a murine model of full-thickness skin wounds.* Experimental Dermatology, 2017. **26**(2): p. 156-162.
24. Barton, A., et al., *Nonthermal plasma increases expression of wound healing related genes in a keratinocyte cell line.* Plasma Medicine, 2013. **3**(1-2).
25. Szili, E.J., et al., *Controlling the Spatial Distribution of Polymer Surface Treatment Using Atmospheric-Pressure Microplasma Jets.* Plasma Processes and Polymers, 2011. **8**(1): p. 38-50.
26. Desmet, G., et al., *On the effects of atmospheric-pressure microplasma array treatment on polymer and biological materials.* RSC Advances, 2013. **3**(32): p. 13437-13445.
27. France, R.M. and R.D. Short, *Plasma treatment of polymers Effects of energy transfer from an argon plasma on the surface chemistry of poly(styrene), low density poly(ethylene), poly(propylene) and poly(ethylene terephthalate).* Journal of the Chemical Society, Faraday Transactions, 1997. **93**(17): p. 3173-3178.
28. Matthes, R., et al., *Antimicrobial Efficacy of Two Surface Barrier Discharges with Air Plasma against In Vitro Biofilms.* PLOS ONE, 2013. **8**(7): p. e70462.
29. Lademann, J., et al., *Risk assessment of the application of tissue-tolerable plasma on human skin.* Clinical Plasma Medicine, 2013. **1**(1): p. 5-10.
30. Partecke, L.I., et al., *Tissue tolerable plasma (TTP) induces apoptosis in pancreatic cancer cells in vitro and in vivo.* BMC cancer, 2012. **12**(1): p. 473.
31. Szili, E.J., J.W. Bradley, and R.D. Short, *A 'tissue model' to study the plasma delivery of reactive oxygen species.* Journal of Physics D: Applied Physics, 2014. **47**: p. 152002.
32. Wei, T. and J.K. Mark, *Atmospheric pressure dielectric barrier discharges interacting with liquid covered tissue.* Journal of Physics D: Applied Physics, 2014. **47**(16): p. 165201.
33. Loo, A.E., et al., *Effects of hydrogen peroxide on wound healing in mice in relation to oxidative damage.* PLoS One, 2012. **7**(11): p. e49215.

34. Szili, E.J., et al., *Tracking the Penetration of Plasma Reactive Species in Tissue Models.* Trends in Biotechnology, 2017. **36**(6): p. 594-602.
35. Attri, P., et al., *Generation mechanism of hydroxyl radical species and its lifetime prediction during the plasma-initiated ultraviolet (UV) photolysis.* Scientific Reports, 2015. **5**: p. 9332.
36. Lukes, P., et al., *Aqueous-phase chemistry and bactericidal effects from an air discharge plasma in contact with water: evidence for the formation of peroxynitrite through a pseudo-second-order post- discharge reaction of H_2O_2 and HNO_2.* Plasma Sources Science and Technology, 2014. **23**: p. 015019.
37. Endre, J.S., et al., *Modelling the helium plasma jet delivery of reactive species into a 3D cancer tumour.* Plasma Sources Science and Technology, 2018. **27**(1): p. 014001.
38. Oh, J.-S., et al., *Slow Molecular Transport of Plasma-Generated Reactive Oxygen and Nitrogen Species and O2 through Agarose as a Surrogate for Tissue.* Plasma Medicine, 2015. **5**(2-4): p. 125-143.
39. Jun-Seok, O., et al., *How to assess the plasma delivery of RONS into tissue fluid and tissue.* Journal of Physics D: Applied Physics, 2016. **49**(30): p. 304005.
40. Oh, J.S., et al., *In-situ UV Absorption Spectroscopy for Monitoring Transport of Plasma Reactive Species through Agarose as Surrogate for Tissue.* Journal of Photopolymer Science and Technology, 2015. **28**(3): p. 439 – 444.
41. Bruggeman, P., et al., *Plasma–liquid interactions: a review and roadmap.* Plasma sources science and technology, 2016. **25**(5): p. 053002.
42. Jablonowski, H., et al., *Impact of plasma jet vacuum ultraviolet radiation on reactive oxygen species generation in bio-relevant liquids.* Physics of Plasmas, 2015. **22**(12): p. 122008.
43. Akiko, K., O. Shigemitsu, and H. Kunihiko, *Residual charge distribution of positive surface streamer.* Journal of Physics D: Applied Physics, 2009. **42**(9): p. 095209.
44. Tongtong, H., et al., *A 'tissue model' to study the barrier effects of living tissues on the reactive species generated by surface air discharge.* Journal of Physics D: Applied Physics, 2016. **49**(20): p. 205204.
45. Graves, D.B., *Oxy-nitroso shielding burst model of cold atmospheric plasma therapeutics.* Clinical Plasma Medicine, 2014. **2**: p. 38-49.
46. N Barekzi, M.L., *Effects of Low Temperature Plasmas on Cancer Cells.* Plasma Process. Polym. , 2013. **10**: p. 1039–1050.
47. Laroussi, M., *From Killing Bacteria to Destroying Cancer Cells: 20 Years of Plasma Medicine.* Plasma Processes and Polymers 2014. **11**(12): p. 1138-1141.
48. Graves, D.B., *Reactive Species from Cold Atmospheric Plasma: Implications for Cancer Therapy.* Plasma Processes and Polymers, 2014. **11**(12): p. 1120-1127.
49. Chmarra, M.K., et al., *Multimodal phantom of liver tissue.* 2013.
50. Jiang, S., S. Liu, and W. Feng, *PVA hydrogel properties for biomedical application.* Journal of the Mechanical Behavior of Biomedical Materials, 2011. **4**(7): p. 1228-1233.
51. Mano, I., et al., *New polyvinyl alcohol gel material for MRI phantoms.* Magnetic Resonance in Medicine, 1986. **3**(6): p. 921-926.
52. Surry, K.J., et al., *Poly(vinyl alcohol) cryogel phantoms for use in ultrasound and MR imaging.* Physics in medicine and biology, 2004. **49**(24): p. 5529-46.
53. Madsen, E.L., et al., *Tissue mimicking materials for ultrasound phantoms.* Medical physics, 1978. **5**(5): p. 391-394.

54. Madsen, E.L., et al., *Tissue-mimicking oil-in-gelatin dispersions for use in heterogeneous elastography phantoms.* Ultrason Imaging, 2003. **25**(1): p. 17-38.
55. Madsen, E.L., et al., *Anthropomorphic breast phantoms for testing elastography systems.* Ultrasound in medicine & biology, 2006. **32**(6): p. 857-74.
56. Szili, E.J., et al., *Probing the transport of plasma-generated RONS in an agarose target as surrogate for real tissue: dependency on time, distance and material composition.* J. Phys. D: Appl. Phys., 2015. **48**: p. 202001.
57. Taylor, G.D. and J.A. Cadeddu, *Training for renal ablative technique using an agarose-based renal tumour-mimic model.* BJU international, 2006. **97**(1): p. 179-181.
58. Liu, J. and C.J. Roberts, *Feasibility Studies of Model and System for Ultrasonic Characterization of Cornea Biomechanics.* Investigative Ophthalmology & Visual Science, 2004. **45**(13): p. 3825-3825.
59. D'Souza, W.D., et al., *Tissue mimicking materials for a multi-imaging modality prostate phantom.* Medical physics, 2001. **28**(4): p. 688-700.
60. Zell, K., et al., *Acoustical properties of selected tissue phantom materials for ultrasound imaging.* Physics in medicine and biology, 2007. **52**(20): p. N475-84.
61. Bush, N.L. and C.R. Hill, *Gelatine-alginate complex gel: a new acoustically tissue-equivalent material.* Ultrasound in medicine & biology, 1983. **9**(5): p. 479-84.
62. Kondo, T., M. Kitatuji, and H. Kanda. *New tissue mimicking materials for ultrasound phantoms*. in *IEEE Ultrasonics Symposium, 2005.* 2005.
63. Sakaguchi, K., et al., *In vitro engineering of vascularized tissue surrogates.* Scientific reports, 2013. **3**: p. 1316-1316.
64. Boucard, N., et al., *The use of physical hydrogels of chitosan for skin regeneration following third-degree burns.* Biomaterials, 2007. **28**(24): p. 3478-88.
65. Pasqui, D., et al., *Carboxymethyl cellulose—hydroxyapatite hybrid hydrogel as a composite material for bone tissue engineering applications.* Journal of Biomedical Materials Research Part A, 2014. **102**(5): p. 1568-1579.
66. Othman, N.S., et al., *Ultrasound speed of polymer gel mimicked human soft tissue within three weeks.* International Journal of Bioscience, Biochemistry and Bioinformatics 2011. **1**(3): p. 223.
67. Zhu, J. and R.E. Marchant, *Design properties of hydrogel tissue-engineering scaffolds.* Expert review of medical devices, 2011. **8**(5): p. 607-626.
68. Ní Annaidh, A., et al., *Characterization of the anisotropic mechanical properties of excised human skin.* Journal of the Mechanical Behavior of Biomedical Materials, 2012. **5**(1): p. 139-148.
69. Iravani, A., J. Mueller, and A.M. Yousefi, *Producing homogeneous cryogel phantoms for medical imaging: a finite-element approach.* J Biomater Sci Polym Ed, 2014. **25**(2): p. 181-202.
70. Gaur, N., et al., *Combined effect of protein and oxygen on reactive oxygen and nitrogen species in the plasma treatment of tissue.* Applied Physics Letters, 2015. **107**(10): p. 103703.
71. Endre, J.S., et al., *The assessment of cold atmospheric plasma treatment of DNA in synthetic models of tissue fluid, tissue and cells.* Journal of Physics D: Applied Physics, 2017. **50**(27): p. 274001.
72. Serena, E.M., et al., *Studying the cytolytic activity of gas plasma with self-signalling phospholipid vesicles dispersed within a gelatin matrix.* Journal of Physics D: Applied Physics, 2013. **46**(18): p. 185401.

73. Hellerbach, A., et al., *MRI phantoms - are there alternatives to agar?* PloS one, 2013. **8**(8): p. e70343-e70343.
74. Culjat, M.O., et al., *A Review of Tissue Substitutes for Ultrasound Imaging.* Ultrasound in Medicine & Biology, 2010. **36**(6): p. 861-873.
75. In, E., H.E. Naguib, and M. Haider. *Fabrication and characterization of polymer gel for MRI phantom with embedded lesion particles*. in *Health Monitoring of Structural and Biological Systems 2012*. 2012. International Society for Optics and Photonics.
76. Pomfret, R., G. Miranpuri, and K. Sillay, *The substitute brain and the potential of the gel model.* Annals of neurosciences, 2013. **20**(3): p. 118-122.
77. Widdowson, D.C., et al., *Determination of the effects of blood depth in the dermis on skin colour in a novel skin phantom using digital imaging.* Lasers in Medical Science, 2009. **25**(1): p. 55.
78. Bin, L., et al. *Elasticity and Echogenicity Analysis of Agarose Phantoms Mimicking Liver Tumors*. in *Proceedings of the IEEE 32nd Annual Northeast Bioengineering Conference*. 2006.
79. Pomfret, R., K. Sillay, and G. Miranpuri, *Investigation of the electrical properties of agarose gel: characterization of concentration using nyquist plot phase angle and the implications of a more comprehensive in vitro model of the brain.* Ann Neurosci, 2013. **20**(3): p. 99-107.
80. Liu, S.H., et al., *Collagen in tendon, ligament, and bone healing. A current review.* Clinical Orthopaedics and Related Research, 1995(318): p. 265-278.
81. Gómez-Guillén, M.C., et al., *Functional and bioactive properties of collagen and gelatin from alternative sources: A review.* Food Hydrocolloids, 2011. **25**(8): p. 1813-1827.
82. Hall, T.J., et al., *Phantom materials for elastography.* IEEE Transactions on Ultrasonics, Ferroelectrics, and Frequency Control, 1997. **44**(6): p. 1355-1365.
83. Jermann, R., M. Toumiat, and D. Imfeld, *Development of an in vitro efficacy test for self-tanning formulations.* International Journal of Cosmetic Science, 2002. **24**(1): p. 35-42.
84. Chen, S. and B. Bhushan, *Nanomechanical and nanotribological characterization of two synthetic skins with and without skin cream treatment using atomic force microscopy.* Journal of Colloid and Interface Science, 2013. **398**: p. 247-254.
85. Renvoise, J., et al., *Adherence performances of pressure sensitive adhesives on a model viscoelastic synthetic film: A tool for the understanding of adhesion on the human skin.* International Journal of Pharmaceutics, 2009. **368**(1): p. 83-88.
86. Lamouche, G., et al., *Review of tissue simulating phantoms with controllable optical, mechanical and structural properties for use in optical coherence tomography.* Biomed Opt Express, 2012. **3**(6): p. 1381-98.
87. Price, B.D., et al., *An elastically compressible phantom material with mechanical and x-ray attenuation properties equivalent to breast tissue.* Physics in Medicine & Biology, 2010. **55**(4): p. 1177.
88. Hunt, T.K., B. Zederfeldt, and T.K. Goldstick, *Oxygen and healing.* Am J Surg, 1969. **118**(4): p. 521-5.
89. Yip, W.L., *Influence of oxygen on wound healing.* International Wound Journal, 2015. **12**(6): p. 620-624.
90. T, F., *Oxygen radicals and signaling.* Curr Opin Cell Biol, 1998. **10**: p. 248-253.
91. Gordillo, G.M. and C.K. Sen, *Revisiting the essential role of oxygen in wound healing.* The American Journal of Surgery, 2003. **186**(3): p. 259-263.

92. Tandara, A.A. and T.A. Mustoe, *Oxygen in wound healing—more than a nutrient.* World journal of surgery, 2004. **28**(3): p. 294-300.
93. Sen, C.K., *Wound Healing Essentials: Let There Be Oxygen.* Wound repair and regeneration 2009. **17**(1): p. 1-18.
94. Khanna, S. and W. Wallace, *"Wound Healing: Oxygen and Emerging Therapeutics" Columbus, Ohio, September 12–15, 2002.* Antioxidants & Redox Signaling, 2002. **4**(6): p. 961-963.
95. Hunt, T., Z. Hussain, and C. Sen, *Give me ROS or give me death.* Pressure, 2001. **30**: p. 10-11.
96. Knighton, D.R., B. Halliday, and T.K. Hunt, *Oxygen as an antibiotic: The effect of inspired oxygen on infection.* Archives of Surgery, 1984. **119**(2): p. 199-204.
97. Bryan, N., et al., *Reactive oxygen species (ROS)–a family of fate deciding molecules pivotal in constructive inflammation and wound healing.* European Cells & Materials, 2012. **24**(1): p. 249-265.
98. Kanta, J., *The role of hydrogen peroxide and other reactive oxygen species in wound healing.* Acta Medica (Hradec Kralove), 2011. **54**(3): p. 97-101.
99. Schairer, D.O., et al., *The potential of nitric oxide releasing therapies as antimicrobial agents.* Virulence, 2012. **3**(3): p. 271-9.
100. Schulz, G. and J. Stechmiller, *Wound healing and nitric oxide production: too little or too much may impair healing and cause chronic wounds.* The international journal of lower extremity wounds, 2006. **5**(1): p. 6-8.
101. V. Darley-Usmar, H.W., Barry Halliwell, *Nitric oxide and oxygen radicals: a question of balance.* FEBS Lett, 1995. **369**: p. 131-135.
102. Frank, S., et al., *Nitric oxide triggers enhanced induction of vascular endothelial growth factor expression in cultured keratinocytes (HaCaT) and during cutaneous wound repair.* FASEB J., 1999. **13**: p. 2002-2014.
103. Kalghatgi, S., et al., *Endothelial cell proliferation is enhanced by low dose non-thermal plasma through fibroblast growth factor-2 release.* Annals of biomedical engineering, 2010. **38**(3): p. 748-57.
104. Finkel, T., *Oxygen radicals and signaling.* Current Opinion in Cell Biology, 1998. **10**(2): p. 248-253.
105. Sen, C.K., et al., *Oxidant-induced vascular endothelial growth factor expression in human keratinocytes and cutaneous wound healing.* Journal of Biological Chemistry, 2002. **277**(36): p. 33284-33290.
106. Collet, G., et al., *Plasma jet-induced tissue oxygenation: potentialities for new therapeutic strategies.* Plasma Sources Science and Technology, 2014. **23**(1): p. 012005.
107. Kisch, T., et al., *The repetitive use of non-thermal dielectric barrier discharge plasma boosts cutaneous microcirculatory effects.* Microvascular Research, 2016. **106**: p. 8-13.
108. Kisch, T., et al., *Improvement of cutaneous microcirculation by cold atmospheric plasma (CAP): Results of a controlled, prospective cohort study.* Microvascular Research, 2016. **104**: p. 55-62.
109. Grzelak A, *e.a., Light-dependent generation of reactive oxygen species in cell culture media.* Free Radical Biology & Medicine, 2001. **30**(12): p. 1418-1425.
110. Szili, E.J., S.-H. Hong, and R.D. Short, *On the effect of serum on the transport of reactive oxygen species across phospholipid membranes.* Biointerphases, 2015. **10**(2): p. 029511.

111. Ghimire, B., et al., *The role of UV photolysis and molecular transport in the generation of reactive species in a tissue model with a cold atmospheric pressure plasma jet.* Applied Physics Letters, 2019. **114**(9): p. 093701.
112. Vandamme, M., et al., *Antitumor Effect of Plasma Treatment on U87 Glioma Xenografts: Preliminary Results.* Plasma Processes and Polymers, 2010. **7**(3-4): p. 264-273.
113. Ghimire, B., et al., *The effect of the gap distance between an atmospheric-pressure plasma jet nozzle and liquid surface on OH and N2 species concentrations.* Physics of Plasmas, 2017. **24**: p. 073502.
114. Fluhr, J.W., et al., *In vivo skin treatment with tissue-tolerable plasma influences skin physiology and antioxidant profile in human stratum corneum.* Experimental Dermatology, 2012. **21**(2): p. 130-134.
115. Hirayama, K., et al., *Rapid confirmation and revision of the primary structure of bovine serum albumin by ESIMS and Frit-FAB LC/MS.* Biochem Biophys Res Commun, 1990. **173**(2): p. 639-46.
116. Peters, T., Jr., *Serum albumin.* Adv Protein Chem, 1985. **37**: p. 161-245.
117. Halliwell, B. and J.M. Gutteridge, *Free radicals in biology and medicine*. 2015: Oxford University Press, USA.
118. Berlett, B.S. and E.R. Stadtman, *Protein oxidation in aging, disease, and oxidative stress.* Journal of Biological Chemistry, 1997. **272**(33): p. 20313-20316.
119. Gebicki, S. and J.M. Gebicki, *Formation of peroxides in amino acids and proteins exposed to oxygen free radicals.* Biochemical Journal, 1993. **289**(3): p. 743.
120. Choe, E. and D.B. Min, *Chemistry and Reactions of Reactive Oxygen Species in Foods.* Journal of Food Science, 2005. **70**(9): p. R142-R159.
121. Roche, M., et al., *The antioxidant properties of serum albumin.* FEBS Letters, 2008. **582**(13): p. 1783-1787.
122. Yan, D., et al., *Controlling plasma stimulated media in cancer treatment application.* Applied Physics Letters, 2014. **105**(22): p. 224101.
123. Tissue, B.M., *Ultraviolet and visible absorption spectroscopy.* Characterization of Materials, 2002: p. 1-13.
124. Perkampus, H.-H., H.-C. Grinter, and T. Threlfall, *UV-VIS Spectroscopy and its Applications*. 1992: Springer.
125. Swinehart, D.F., *The Beer-Lambert Law*. Journal of Chemical Education, 1962. **39**(7): p. 333.
126. Wikipedia. *Electric current*. 2018 7 December 2018 [cited 2018 23 December 2018]; Available from: https://en.wikipedia.org/w/index.php?title=Electric_current&oldid=872501089.
127. Wolzak, G.G., *The development of high-voltage measuring techniques*, in *Department of Electrical Engineering*. 1983, Technische Hogeschool Eindhoven: Eindhoven. p. 73.
128. Wikiversity, C. *Spectroscopy/Molecular energy levels*. 12 February 2019 [cited 2019 11 May 2019]; Available from: https://en.wikiversity.org/w/index.php?title=Spectroscopy/Molecular_energy_levels&oldid=1975204.
129. Lambert, J.D. and J.D. Lambert, *Vibrational and rotational relaxation in gases*. 1977: Clarendon Press Oxford.

130. Baek, E.J., et al., *Effects of the electrical parameters and gas flow rate on the generation of reactive species in liquids exposed to atmospheric pressure plasma jets.* Physics of Plasmas, 2016. **23**(7): p. 073515.
131. Lu, X., et al., *An 11cm long atmospheric pressure cold plasma plume for applications of plasma medicine.* Applied Physics Letters, 2008. **92**(8): p. 081502.
132. XinPei, L., L. Frank, and L. Mounir, *Optical and electrical diagnostics of a non-equilibrium air plasma.* Journal of Physics D: Applied Physics, 2003. **36**(21): p. 2662.
133. Jun-Seok, O., et al., *Effect of plasma jet diameter on the efficiency of reactive oxygen and nitrogen species generation in water.* Japanese Journal of Applied Physics, 2016. **55**(6S2): p. 06HD01.
134. Shuji, K., et al., *Spectroscopic Study on Vibrational Nonequilibrium of a Microwave Discharge Nitrogen Plasma.* Japanese Journal of Applied Physics, 2004. **43**(8R): p. 5550.
135. Wallace, L., *A collection of the band-head wavelengths of N2 and N2+*. 1961, Yerkes Observatory Williams Bay WI.
136. Striganov, A.R. and N.S. Sventitskii, *Tables of spectral lines of neutral and ionized atoms*. 2013: Springer Science & Business Media.
137. Jun-Seok, O., et al., *Investigating the effect of additional gases in an atmospheric-pressure helium plasma jet using ambient mass spectrometry.* Japanese Journal of Applied Physics, 2015. **54**(1S): p. 01AA03.
138. Doering, J. *Vibrational and rotational excitation of diatomic molecules within an electronic transition (Progress Report).* in *Physics of Electronic and Atomic Collisions, Invited Papers and Progress Reports: ICPEAC VII*. 1972.
139. Kurihara, J., N. Iwagami, and K. Oyama, *N2 Temperature of Vibration instrument for sounding rocket observation in the lower thermosphere.* An Introduction to Space Instrumentation, 2003.
140. Eva Stoffels, Y.S., and David B. Graves, *Cold Atmospheric Plasma: Charged Species and Their Interactions With Cells and Tissues.* IEEE Transactions on Plasma Science, 2008. **36**(4): p. 1441-1457.
141. Lu, X., et al., *Reactive species in non-equilibrium atmospheric-pressure plasmas: Generation, transport, and biological effects.* Physics Reports, 2016. **630**: p. 1-84.
142. Moshage, H., et al., *Nitrite and nitrate determinations in plasma: a critical evaluation.* Clin Chem, 1995. **41**(6 Pt 1): p. 892-6.
143. Isbell, H.S. and P. Czubarow, *Oxidation of carbohydrates by alkaline hydrogen peroxide in the presence and in the absence of ferrous ion.* Carbohydrate Research, 1990. **203**(2): p. 287-289.
144. Duan, J. and D.L. Kasper, *Oxidative depolymerization of polysaccharides by reactive oxygen/nitrogen species.* Glycobiology, 2011. **21**(4): p. 401-409.
145. Benedikt, J., et al., *Quadrupole mass spectrometry of reactive plasmas.* Journal of Physics D: Applied Physics, 2012. **45**(40): p. 403001.
146. Stoffels, E., et al., *Mass spectrometric detection of short-living radicals produced by a plasma needle.* Plasma Sources Science and Technology, 2007. **16**(3): p. 549.
147. Thiry, D., et al., *Plasma diagnostics for the low-pressure plasma polymerization process: A critical review.* Thin Solid Films, 2016. **606**: p. 19-44.
148. Benedikt, J., *Plasma-chemical reactions: low pressure acetylene plasmas.* Journal of Physics D: Applied Physics, 2010. **43**(4): p. 043001.

149. Benedikt, J., et al., *Threshold ionization mass spectrometry of reactive species in remote Ar/C2H2 expanding thermal plasma.* Journal of Vacuum Science & Technology A, 2005. **23**(5): p. 1400-1412.
150. Liu, D., et al., *Diagnosis of dielectric barrier discharge CH4 plasmas for diamond-like carbon film deposition.* Diamond and Related Materials, 2002. **11**(8): p. 1491-1495.
151. Caldirola, S., et al., *Mass spectrometry measurements of a low pressure expanding plasma jet.* Journal of Vacuum Science & Technology A, 2015. **33**(6): p. 061306.
152. McKay, K., et al., *Mass spectrometric diagnosis of an atmospheric pressure helium microplasma jet.* Journal of Physics D: Applied Physics, 2013. **46**(46): p. 464018.
153. Oh Jun-Seok, Aranda-Gonzalvo Yolanda, and J.W. Bradley, *Time-resolved mass spectroscopic studies of an atmospheric-pressure helium microplasma jet.* J. Phys. D: Appl. Phys., 2011. **44**: p. 365202.
154. E Stoffels, *e.a., A plasma needle generates nitric oxide.* Plasma Sources Science and Technology, 2006. **15**: p. 501–506.
155. Große-Kreul, S., et al., *Mass spectrometry of atmospheric pressure plasmas.* Plasma Sources Science and Technology, 2015. **24**(4): p. 044008.
156. Ratcliffe, L.V., et al., *Surface Analysis under Ambient Conditions Using Plasma-Assisted Desorption/Ionization Mass Spectrometry.* Analytical Chemistry, 2007. **79**(16): p. 6094-6101.
157. Skalny, J.D., et al., *Mass spectrometric study of negative ions extracted from point to plane negative corona discharge in ambient air at atmospheric pressure.* International Journal of Mass Spectrometry, 2008. **272**(1): p. 12-21.
158. Oh, J.-S., et al., *Mass Spectrometry Analysis of the Real-Time Transport of Plasma-Generated Ionic Species Through an Agarose Tissue Model Target.* Journal of Photopolymer Science and Technology, 2017. **30**(3): p. 317-323.
159. Jun-Seok, O., et al., *Imaging gas and plasma interactions in the surface-chemical modification of polymers using micro-plasma jets.* Journal of Physics D: Applied Physics, 2011. **44**(15): p. 155206.
160. Pouvesle, J.M., A. Bouchoule, and J. Stevefelt, *Modeling of the charge transfer afterglow excited by intense electrical discharges in high pressure helium nitrogen mixtures.* The Journal of Chemical Physics, 1982. **77**(2): p. 817-825.
161. Martens, T., et al., *The dominant role of impurities in the composition of high pressure noble gas plasmas.* Applied Physics Letters, 2008. **92**(4): p. 041504.
162. Revelle, R. and H.E. Suess, *Carbon dioxide exchange between atmosphere and ocean and the question of an increase of atmospheric CO2 during the past decades.* Tellus, 1957. **9**(1): p. 18-27.
163. Peter, B., et al., *Mass spectrometry study of positive and negative ions in a capacitively coupled atmospheric pressure RF excited glow discharge in He-water mixtures.* Journal of Physics D: Applied Physics, 2010. **43**(1): p. 012003.
164. Itikawa, Y., *Cross Sections for Electron Collisions with Oxygen Molecules.* Journal of Physical and Chemical Reference Data, 2009. **38**(1): p. 1-20.
165. Gravendeel, B. and F.J.d. Hoog, *Clustered negative ions in atmospheric negative corona discharges in the Trichel regime.* Journal of Physics B: Atomic and Molecular Physics, 1987. **20**(23): p. 6337.
166. Keidar, M., et al., *Cold plasma selectivity and the possibility of a paradigm shift in cancer therapy.* Br J Cancer, 2011. **105**(9): p. 1295-1301.

167. Graves, D.B., *Low temperature plasma biomedicine: A tutorial review* [a)] Phys. Plasmas 2014. **21**: p. 080901.
168. Jablonowski, H. and T. von Woedtke, *Research on plasma medicine-relevant plasma–liquid interaction: What happened in the past five years?* Clinical Plasma Medicine. **3**(2): p. 42-52.
169. Goldstein, S. and J. Rabani, *Mechanism of nitrite formation by nitrate photolysis in aqueous solutions: the role of peroxynitrite, nitrogen dioxide, and hydroxyl radical.* Journal of the American Chemical Society, 2007. **129**(34): p. 10597-601.

Chapter 4 Assessing plasma interactions with cells and biological components

Using the models of tissue fluid (water, buffered solutions and cell culture media) and tissues (gelatin, agarose and PVA) in Chapters 2 and 3, it was shown that the helium (He) plasma jet can generate H_2O_2, $NO_2^-$and NO_3^-in tissue fluid and deep within a tissue mass [1-9]. These plasma-generated RONS can potentially intervene with biological pathways of the cell and induce chemical and/or physical changes in it [10, 11]. To understand the underlying mechanisms of plasma-tissue or plasma-cell interactions and to fully realise the potential of plasma in medicine, requires an understanding of how plasma interacts with cells and biological components.

While several studies have commented upon the clinical "safety" of plasma devices [12-17], the precise nature of how plasma effects cellular functions is still poorly understood. It is undoubtedly clear that the biological effects induced by the plasma depend on the intensity (or the power levels of plasma) and the plasma exposure time (or dose). Therefore, the clinically approved commercially available plasma devices are operated at strictly well-defined and clinically-tested parameters and protocols. For instance, if used as per the ISO protocols, the kINPen MED plasma jet is non-mutagenic, as shown in *in vitro* and *in vivo* studies [18, 19]. As shown by Bekeschus *et al.*, the kINPen MED does not pose any health risks in humans in terms of UV exposure, thermal damage, toxicity in tissue or mutagenicity and is therefore suitable for medical applications such as wound treatment [20]. But knowing the parameters for safe operation of the plasma jet still does not provide any insight into the mechanisms of the full range of plasma effects from benign to destructive.

In this study, the focus was to assess the effects of plasma treatment on the cell membrane and DNA. The plasma jet can generate many types of molecules in tissue fluids and tissues including the $\bullet OH$, $O_2^{\bullet -}$, $ONOO^-$ and H_2O_2 [1, 4, 21-24], which are known to induce DNA damage in the form of DNA strand breaks, modifications of DNA bases, loss of DNA bases causing production of abasic sites, DNA-protein crosslinks and chromosomal mutations [25-35].

$ONOO^-$ can induce DNA strand breaks and base modification via nitration, nitrosation, hydroxylation and deamination of DNA [27, 36]. H_2O_2 and $O_2^{\bullet-}$ can indirectly damage DNA by undergoing reactions to form the •OH, which can attack the DNA directly [34]. $O_2^{\bullet-}$ can undergo a one-electron reduction to form H_2O_2 [37]. H_2O_2 can form the •OH upon reaction with metal ions bound to the DNA (for example: copper ions present in chromosomes) [38] or present within the cells in normal conditions (such as ferric ions) [39] via Fenton chemistry. Therefore, the most important specie which can directly attack DNA is the •OH [34]. The •OH reacts with DNA by hydrogen abstraction, electron transfer and addition reactions [40].

In this study two fluorescence-based methodologies are proposed to measure DNA-strand breaks: (a) a DNA molecular beacon (MB) [28], and (b) γ-H2AX assay [41]. The structure of the MB consists of a single-stranded loop and double-stranded stem (Figure 4.1). On each side of the strand there is a fluorescence moiety (fluorophore) and a quenching moiety (quencher). When the MB-structure is intact, the fluorescence of the fluorophore is quenched. Upon DNA-strand breaks, the quencher is separated from the fluorophore resulting in fluorescence. The MB can be easily incorporated into the models of tissue fluid, tissue and cells to monitor effects of plasma on the integrity of DNA [42].

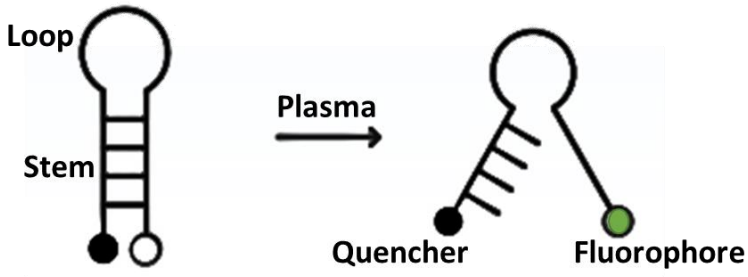


Figure 4.1 A schematic of the structure of a molecular beacon (MB). The MB used in this study consists of a single-stranded loop and double-stranded stem with a quencher (black circle) and a fluorophore (open circle) on either ends of the stem. Upon breakage of the DNA strands, the quencher separates from the fluorophore resulting in fluorescence of the fluorophore (green circle).

The damaging effects of plasma on cell membrane were also assessed using phospholipid vesicles as a cell model. The phospholipid vesicles consisted of a membrane composition of 80% dipalmitoylphosphatidylcholine (DOPC) and 20% cholesterol (further details in Chapter 1). A typical cell membrane consists phosphatidylcholines (for example DOPC) as the major lipids and approximately 20% cholesterol of the membrane lipid mass [43]. The influence of plasma jet treatments on

the integrity of the phospholipid membrane and the transport of RONS into the vesicles were assessed.

To assess how plasma influences the integrity of DNA in living cells, HaCaT keratinocyte cells that are the major skin cells important in the inflammation and reepithelization stage of wound healing, were utilised for this study. Upon induction of DNA-damage, cells initiate the DNA damage response (DDR) to ensure DNA repair and cell-survival [44]. The earliest DDR process, which occurs within seconds after DNA-damage is 'phosphorylation of the H2AX' [45]. H2AX is a histone variant which phosphorylates on serine 139 in the mega base pair chromatin region to form the γ-H2AX [46]. The three main phosphatidylinositol 3-kinase related kinases (PIKK) which phosphorylate H2AX are: ataxia telangiectasia mutated (ATM), DNA-dependent protein kinase (DNA–PK), and ataxia telangiectasia and Rad3-related (ATR) [45, 47, 48]. PIKK-mediated formation of γ-H2AX is important for recruiting the DNA-repair factors, the proteins important for cell cycle progression and the repair and remodeling of chromatin and DNA [49]. Therefore, γ-H2AX is a good marker for DNA-strand breaks. Using the technique of immunofluorescence, γ-H2AX assay can provide an insight into DNA-strand breaks in a real cell, as shown in this study.

The major aim of this chapter was to develop a method of delivering molecules that might stimulate wound healing but limit molecules that pose a potential health risk. This chapter focuses on the delivery of H_2O_2 which can have beneficial qualities for wound healing (as described in Chapter 1), but inhibit the •OH which is known to induce significant DNA damage (as aforementioned in this chapter).

To achieve this, the concept of a 'plasma screen' is introduced [50]. A plasma screen is a hydrogel dressing, placed in-between the target and the plasma jet during treatment. The dressing enables only the longer lived RONS (such as H_2O_2) to penetrate through it and reach the target, but the shorter lived and more highly reactive RONS (such as the •OH) are extinguished in the hydrogel. The ultimate eventual aim is that the plasma screen will eliminate all DNA damage in tissues, providing a means of safely stimulating regeneration of wounded tissue.

This chapter is divided into two studies. First, in Section 4.1, the DNA damaging effects of plasma using the MB in synthetic cell and tissue models are discussed. This is followed by the assessment of DNA damage in skin-like cells (HaCaT keratinocyte)

using the γ-H2AX assay, discussed in Section 4.2. The materials and methodology (Section 4.1.1 and 4.2.1) and the results and discussion (Section 4.2.1 and 4.2.2) for each section is separately presented.

4.1 Assessment of DNA damage using MB

4.1.1 Materials and methods

4.1.1.1 Plasma jet

The He plasma jet used in this study consists a 150 mm long glass tube with an inner diameter of 4 mm and tapered to 650 µm at the end of tube. A 15 mm long copper ring electrode is wound onto the glass tube, 40 mm away from the end of the glass tube. The flow of He gas (high purity grade, BOC) in the tube at 0.05 and 0.5 slpm was controlled using a mass flow controller (MFC, Apex). A peak-to-peak voltage of 10 kV was applied at 30 kHz applied to the electrode using a PVM500 power supply (Information Unlimited). For safety, the high voltage electrode and glass tube were shielded in a polytetrafluoroethylene (PTFE) housing. Figure 4.2 shows the photograph and the schematic illustration of the plasma jet device used for this study.

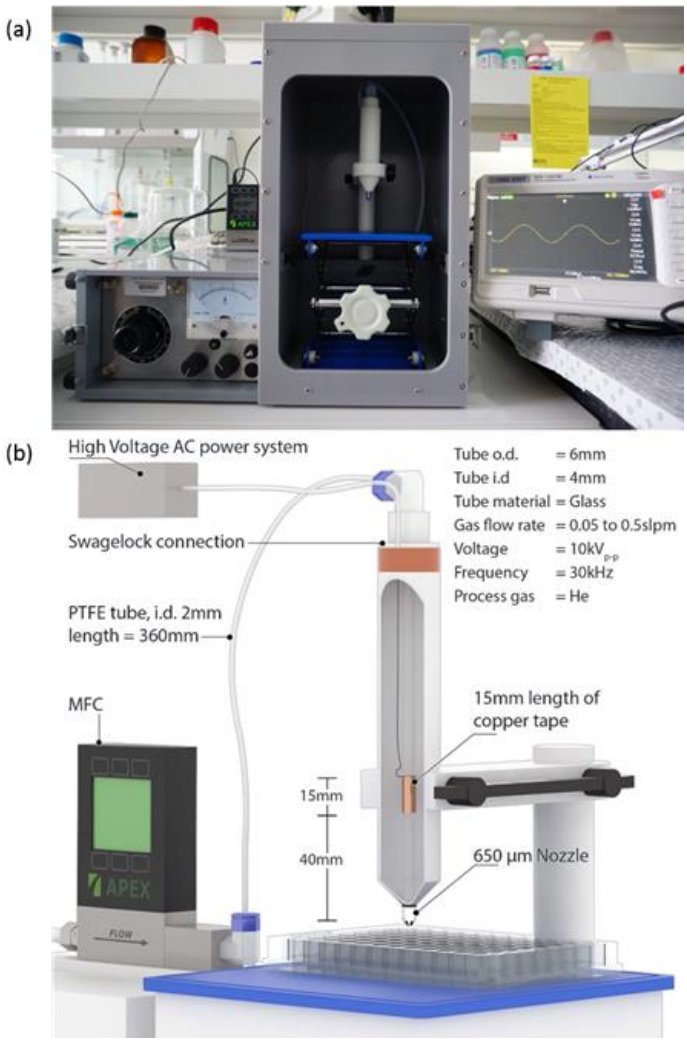


Figure 4.2 (a) A photograph of the He plasma jet. (b) A schematic of the plasma jet assembly and specifications of the plasma jet.

4.1.1.2 Tissue fluid model

4-(2-hydroxyethyl)-1-piperazineethanesulfonic acid (HEPES) buffer, composed mainly of water was used as a tissue fluid model[3]. HEPES is also commonly used in the cell culture studies as it can maintain its buffering capacity despite changes in carbon dioxide levels in the cell media. HEPES tissue fluid model was prepared by dissolving the following reagents in 100 ml of water (Sigma-Aldrich, Catalogue no. 95283):

- HEPES (Sigma-Aldrich, Catalogue no. 3375) – 238.3 mg
- Sodium chloride (NaCl; Optigen Scientific, Catalogue no. OS-22760) – 624 mg

[3] These experiments were conducted in collaboration with Dr Hirofumi Kurita at Toyohashi University of Technology (Japan), following an established protocol, which required for the MB to be dissolved in HEPES. Hence, HEPES was used as the tissue fluid model for these experiments.

- Sodium hydroxide (NaOH; Sigma-Aldrich, Catalogue no. 367176) – 22.4 mg
- Ethylenedinitrilo tetraacetic acid disodium salt (EDTA; Optigen Scientific, Catalogue no. OS-53170) – 29.22 mg

The pH of the HEPES solution was adjusted to 7.4 using 10 mM of sodium hydroxide solution. The solution was filtered using a 0.2 µm syringe filter.

4.1.1.3 Tissue model

A 10% (w/v) gelatin film was used as the tissue model. Gelatin (Sigma-Aldrich, G1890) powder was dissolved in water at 45^{o}C for 60 min. 20 mL of the gelatin solution was poured into a polystyrene petri dish (85 mm diameter) to obtain 2 mm thick gelatin films. The gelatin was allowed to set at 4^{o}C for at least 12 h before use. Gelatin pieces of 20 X 20 mm^2 dimensions were used for all experiments.

4.1.1.4 Hydrogel dressing

A commercially available hydrogel dressing, IntraSite Conformable (Smith & Nephew, Catalogue no. 66000324), was used in this study. Intrasite Conformable is a hydrogel cream on a non-woven dressing material. The dressing was cut into approximately 20 X 20 mm^2 pieces. For the plasma treatments through hydrogel dressing, 400 µl of the cell culture media or MB in a 96-well plate was treated with the plasma jet. The hydrogel dressing was slightly pressed down into the well to ensure it contacted the solution.

4.1.1.5 Phospholipid vesicle cell models

The vesicle model consisted 80% of DOPC (Avanti polar lipids, Catalogue no. 850375P) and 20% of cholesterol (Sigma-Aldrich, Catalogue no. C8667). A 100 µl of DOPC-cholesterol solution was dissolved in 200 µl of chloroform (Sigma-Aldrich, Catalogue no. 288306) and dried with nitrogen gas.

To make vesicles loaded with the MB or CF, the dried DOPC-cholesterol was mixed with 2.5 ml of 50 µM of MB or 50 mM of CF, respectively, and heated at 75^{o}C for 1 min. The MB/CF-DOPC-cholesterol solution was allowed cool to room temperature before being extruded. For extrusion, the solution was passed through two 100 nm polycarbonate membranes fixed in a hand-held syringe extruder (Avanti Polar Lipids, Catalogue no. 610000) and repeated seven times.

The vesicle solution was filtered using a Sephadex G25 column to remove non-encapsulated dye/MB. The column was supplied with an anti-bacterial solution. A volume of 5 ml of HEPES buffer was used to flush the anti-bacterial solution out of the column. This step was repeated twice and the eluate was discarded. In the next step, 2 ml of the extruded vesicle solution, followed by 1 ml of HEPES buffer was added to the column. This eluate was also discarded. Finally another 2 ml of HEPES buffer was added and this eluate was collected. The eluate (vesicles with encapsulated dye/MB) was diluted to 25% and 50% for the vesicles encapsulating the MB and CF, respectively. Preliminary experiments were conducted to determine these dilution factors to be optimal for this study.

4.1.1.6 Tris-base buffer

A stock solution of 1 M Tris-base buffer was prepared by dissolving 12.11 g of Tris(hydroxymethyl) aminomethane (Sigma-Aldrich, Catalogue no. 1545630) powder in 80 ml water. The pH of Tris-base buffer was adjusted to 7.6 by drop-wide addition of 6.2 M hydrogen chloride solution. Later, water was added to adjust the final volume to 100 ml. A concentration of 10 mM in water was made from the stock solution for preparing the MB.

4.1.1.7 MB

DNA-strand breaks were assessed using custom made MB. The MB is an oligonucleotide comprising a single-strand loop and double-strand stem structure oligomer with the sequence [6FAM]-5'-GCACTGAAGCGCCGCACGCCATGTCGACGCGCTTCAGTGC-3'-[BHQ-1].

The MB was supplied by Sigma-Aldrich at a concentration of 37 nmole in a vial. The MB was dissolved in 372 µl of 10 mM Tris-base buffer (pH 7.6) to obtain an end concentration of 100 µM (initial stock concentration). Two (working) concentrations were utilised for the experiments: 0.5 µM for treatment of the tissue fluid and tissue models, and 50 µM diluted in HEPES for vesicle encapsulation. The MB at the different working concentrations, were prepared for the experiments by denaturing the MB at 95 °C for 3 min, and allowing the MB structure to reform slowly at ambient temperature (~25 °C) for 3 h in the dark. This procedure was carried out to ensure the correct configuration of the MB.

4.1.1.8 Vesicle membrane rupture probe

Rupture of the vesicle membrane was assessed by encapsulation of 5,6-carboxyfluorescein (CF) into the vesicles. When encapsulated inside the vesicles at a high concentration, the fluorescence of CF is self-quenched. Upon membrane rupture, CF leaks out of the vesicles and dilutes resulting in a switch-on of fluorescence [6, 51]. 50 mM of CF was prepared by adding the following in 13 ml of water:

- CF (Sigma-Aldrich, Catalogue no. 21877) – 244 mg
- NaCl – 7.6 mg
- NaOH – 70.2 mg
- HEPES – 31 mg
- EDTA – 333.7 mg

4.1.1.9 Experimental setup for MB

The methodology to assess the DNA-strand breaks with the MB in models of tissue fluid, tissue and cells is shown in Figure 4.3. A volume of 200 µl or 400 µl of the MB solution in a 96-well plate was plasma treated directly or indirectly (through the tissue model or hydrogel dressing) at a distance of 1 mm from the end of jet nozzle and top of the plate. The DNA-strand breaks were assessed with the:

(a) MB dispersed in tissue fluid only;

(b) MB dispersed in tissue fluid underneath a gelatin tissue model;

(c) MB dispersed within the tissue model; and

(d) MB encapsulated within the cell model dispersed in the tissue fluid model.

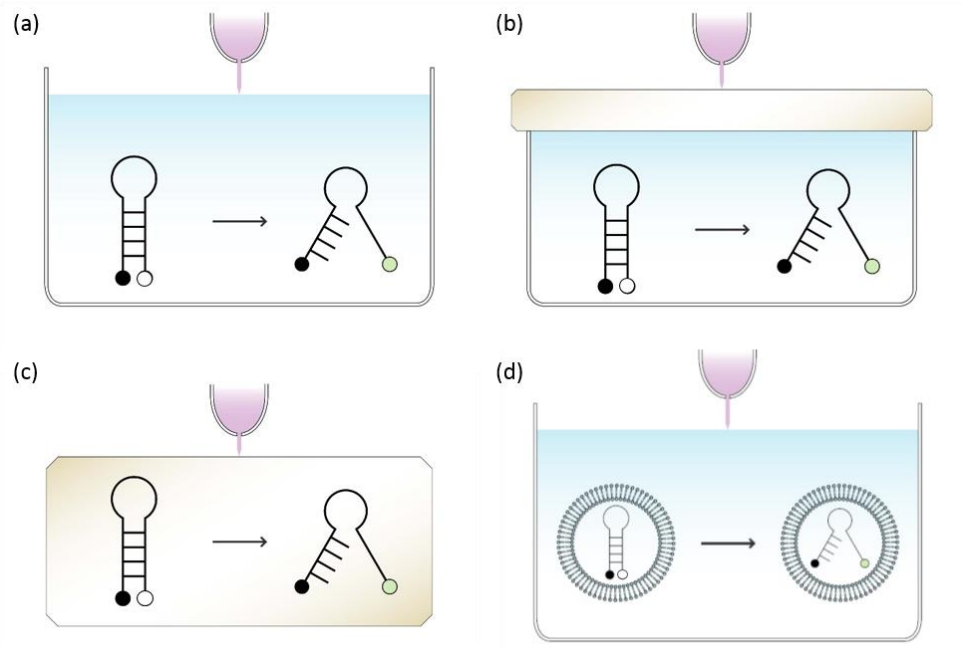


Figure 4.3 A schematic of the methodology to assess DNA-strand breaks using the MB in models of tissue fluid, tissue and cells. DNA-strand breaks were assessed with (a) the MB dispersed in the tissue fluid model, (b) dispersed within the tissue fluid model underneath the tissue model, (c) dispersed within the tissue model, and (d) encapsulated inside the cell model dispersed within the tissue fluid model.

4.1.1.10 OPD-HRP probe

The generation of H_2O_2 by the plasma jet (under same experimental conditions as described for MB above) was measured using OPD-HRP. The OPD-HRP solution was prepared by mixing 2 mg ml^{-1} of OPD (Sigma-Aldrich, Catalogue no. P9029) and 4 µg ml^{-1} of HRP (Sigma-Aldrich, Catalogue no. P6782) in water. A calibration curve was used to correlate the changes in absorbance of OPD to the concentration of H_2O_2 in the tissue fluid model (details in Appendix A).

4.1.1.11 Microplate reader measurements

The fluorescence intensity (FI) or absorbance of 100 µl of the test solutions was measured in a 96-well plate. The FI of the MB solution or CF was measured at excitation and emission wavelengths of 485 nm and 520 nm, respectively. The absorbance of oxidised OPD was measured at 450 nm.

4.1.1.12 Data processing

Preliminary experiments revealed that the neutral He gas jet (i.e. with no applied voltage) alone does not induce DNA-strand breaks of the MB in HEPES. Therefore, the raw fluorescence data were normalised to untreated MB in HEPES according to the following equation:

$$Normalised\ FI = \frac{FI\ of\ test\ MB\ suspension}{FI\ of\ untreated\ MB\ suspension} - 1$$

The same equation was also used to normalise the fluorescence data for the CF vesicles to measure membrane poration/rupture:

$$Normalised\ FI = \frac{FI\ of\ test\ CF\ vesicles}{FI\ of\ untreated\ CF\ vesicles} - 1$$

All data presented in the column charts represent the mean value from triplicate samples (n = 3) and ± standard error of the mean (SEM).

4.1.1.13 Phase-contrast and fluorescence microscopy

An inverted microscope (Nikon, TE-200) was used for the phase-contrast and fluorescence imaging with 4x magnification. The fluorescence images were captured using at 455-485 nm excitation and 500-545 nm emission. All images were recorded at the same exposure time with a Nikon DXM1200C digital camera. The image processing was done using NIS-Elements Basic Research v2.2 software.

4.1.1.14 ESR

ESR was utilised to detect the •OH in HEPES after the direct plasma treatment or through the gelatin tissue model. 5-(2,2-dimethy-1,3-propoxycyclophosphoryl)-5-methyl-1-pyrroline N-oxide (CYMPO) was the •OH radical trapping reagent used for this study. A 100 µl volume of 10 mM CYPMPO (Shidai system, Catalogue no. RR-121-A) was prepared in HEPES and treated with the plasma jet in a 96-well plate.

CYMPO reacts with the plasma-generated •OH to form the CYMPO-OH adduct at a reaction rate of 4.9×10^{9} $M^{-1}s^{-1}$. However, CYMPO can also react with $O_2^{-}\cdot$ but the rate constant of this reaction is much lower (48 $M^{-1}s^{-1}$) than that of the •OH; therefore in this study only the •OH was measured.

Following plasma exposure, the ESR reaction sample was transferred to a flat cell (JEOL resonance, Cat # DP-1055). The ESR signal was measured using an ESR spectrometer (JES-X310, JEOL Resonance, Tokyo, Japan), operating at 9.42 GHz and at 100 kHz field modulation. The settings of the spectrometer were: center magnetic field = 335.6 mT; field width = ±15.0 mT; microwave power = 4 mW; modulation

amplitude = 0.1 mT; and time constant = 0.1 s. The relative intensities of the ESR spectra were calculated by referencing against a manganese (Mn^{+2}) internal standard.

4.1.2 Results and discussion

The plasma jet operated with 0.05 or 0.5 slpm He is shown in Figure 4.4. For the experimental parameters employed in this study and as seen with the unaided eye, the visible part of the plasma jet was confined within the tube when operated at 0.05 slpm (Figure 4.4a), but extended out from the nozzle to a length of 8 mm at 0.5 slpm (Figure 4.4b). At 0.05 slpm, the plasma jet did not visibly contact HEPES for direct treatment (Figure 4.4c) but did contact at 0.5 slpm (Figure 4.4d). For treatment through gelatin, the plasma jets contacted the surface of the gelatin for both flow rates (Figure 4.4d and 4.4e); but the 0.5 slpm plasma jet exhibited a higher emission intensity and formed a larger contact area with the gelatin surface. The longer extension, higher emission intensity and larger contact area of the 0.5 slpm plasma jet indicates that the delivery rate of RONS should be higher with this plasma jet compared to the lower flow rate plasma jet.

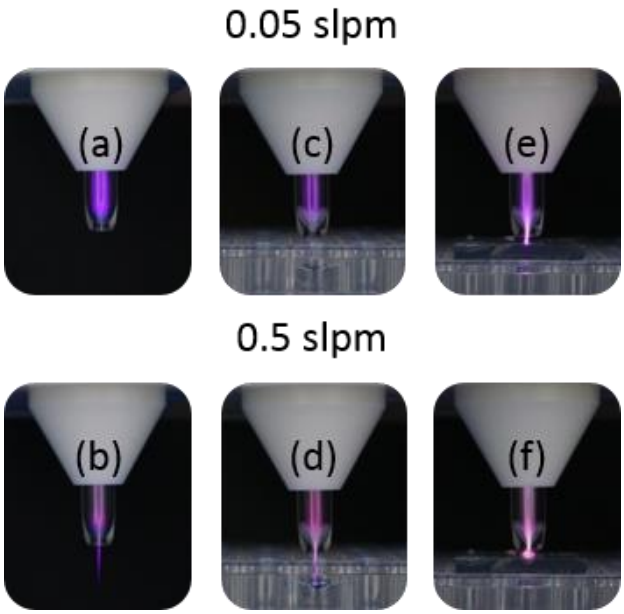


Figure 4.4 Photograph of the He plasma jet in operation under different experimental parameters. The plasma jet is shown operated at (a, c, e) 0.05 slpm or (b, d, f) 0.5 slpm into the ambient air (a, b), or during treatment of the HEPES tissue fluid model (c, d), or during treatment of the gelatin tissue model (e, f).

The frequency of DNA-strand breaks were first assessed in a tissue fluid model (HEPES) as per the experimental setup shown in Figure 4.3a. These results are shown in Figure 4.5a. Furthermore, the concentration of H_2O_2 generated by the plasma jet in

HEPES was also measured, as shown in Figure 4.5b. H_2O_2 was used to give an indication of the total RONS concentration because H_2O_2 is the major longer-lived RONS generated in aqueous solution for the plasma jet configuration utilised in this study [1, 52, 53].

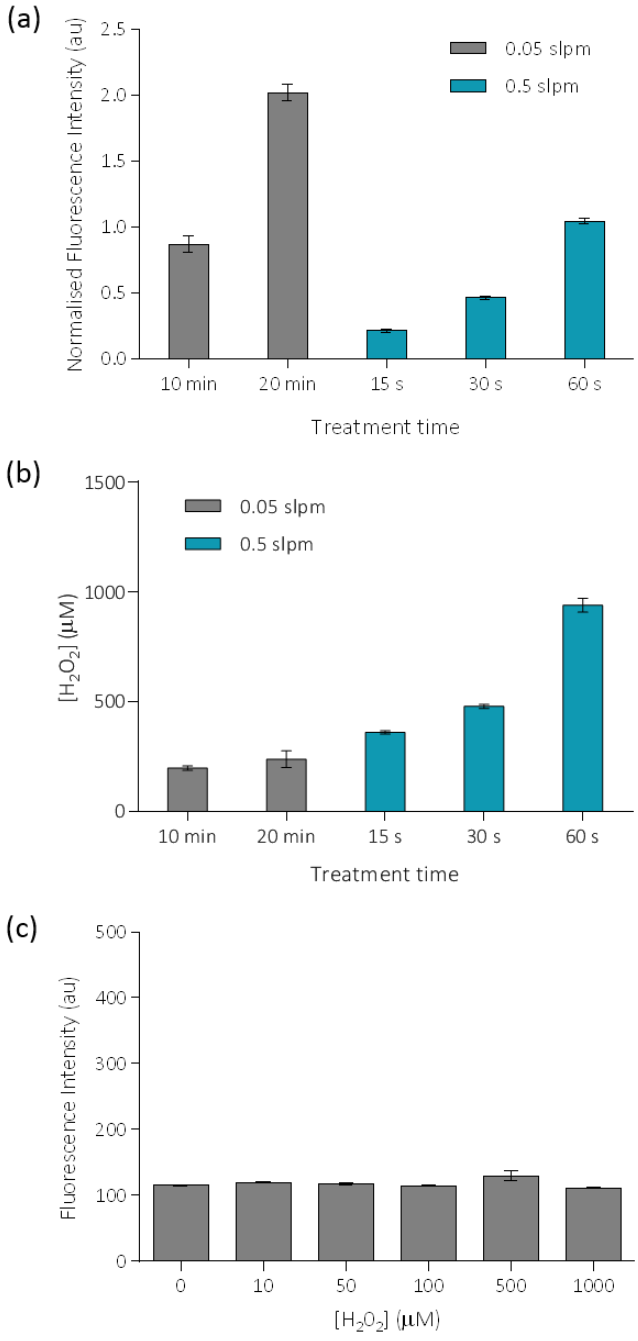


Figure 4.5 (a) DNA-strand breaks in the tissue fluid model after plasma jet treatment at 0.05 and 0.5 slpm. (b) The concentration of H_2O_2 delivered by the plasma jet under the same treatment parameters. (c) Assessment of DNA-strand breaks (shown as FI values of the MB) from different concentrations of H_2O_2 solution added to the MB suspension.

The frequency of DNA-strand breaks in HEPES was measured at 0.05 slpm plasma treatment for 10 and 20 min and at 0.5 slpm for 15, 30 and 60s, as shown in Figure 4.5a.

The results in Figure 4.5a show that DNA-strand breaks were observed under all of the plasma treatment parameters. Longer treatment times were used with the 0.05 slpm plasma jet in an attempt to obtain a similar H_2O_2 concentration compared to the higher flow rate plasma jet treatments. The frequency of DNA-strand breaks increased with plasma jet treatment time. The shortest treatment times of 15 and 30 s with the higher (0.5 slpm) flow rate plasma jet resulted in the lowest frequency of DNA-strand breaks, and the maximum amount of DNA strand breaks were observed after the longest plasma treatment time of 20 min at 0.05 slpm.

The concentrations of H_2O_2 in HEPES delivered by the plasma jet at the same treatment conditions is shown in Figure 4.5b. At a lower flow rate of 0.05 slpm, the plasma jet delivered H_2O_2 in the range of approximately 200 µM to 250 µM. Despite using much longer treatment times with the 0.05 slpm plasma jet, the concentration of H_2O_2 was still much lower in the range of 200 µM to 250 µM compared to the 0.5 slpm plasma jet that generated > 300 µM to 1 mM of H_2O_2 in HEPES. These data show a clear discrepancy in the extent of DNA-strand breaks and the delivery of RONS (using H_2O_2 as a surrogate for total RONS). To understand this discrepancy, the ability of H_2O_2 to break the DNA strands (alone) was tested over the concentration range relevant to these plasma jets (Figure 4.5c). The results clearly indicate that, H_2O_2 (added as a solution to the MB suspension) did not produce any measureable level of DNA-strand breaks in HEPES. This result is in agreement with a simulation study by Verlackt *et al*, who determined that H_2O_2 alone does not directly break the DNA strands [54].

In the next set of experiments, the DNA-strand breaks were assessed in HEPES below the gelatin tissue model. MB suspended in HEPES underneath a gelatin target was exposed to plasma (as per the experimental setup in Figure 4.3b). In Chapter 3 and in previous studies, it has been shown that the plasma jet can readily deliver H_2O_2 to several mm into the tissue models, however these targets significantly attenuate the H_2O_2 delivery, particularly in a temporal sense [1, 4, 52, 53, 55]. Therefore, for this experiment the plasma jet treatment was conducted at the higher flow rate of 0.5 slpm for 10 min to enable a higher H_2O_2 concentration to be delivered through the gelatin and into the HEPES below. The results are shown in Figure 4.6.

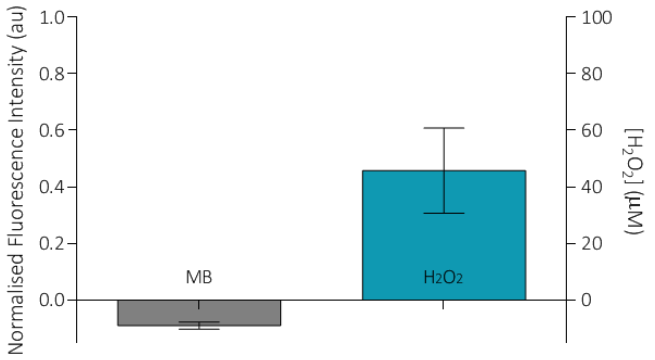


Figure 4.6 DNA-strand breaks and concentration of H_2O_2 after the plasma jet treatment of the MB through the gelatin tissue model. The plasma jet was operated at a He gas flow rate of 0.5 slpm for 10 min.

Figure 4.6 shows that the no measureable level of DNA-strand breaks were observed in HEPES, when treated through the gelatin target. This result is in contrast to the direct treatment of MB in HEPES (Figure 4.5a), where even short treatment times 15 s at 0.5 slpm induced a comparatively high amount of DNA-strand breaks. However, it should be noted that the plasma treatment of HEPES through the gelatin tissue model resulted in lower concentrations of H_2O_2 of approximately 50 µM in HEPES, when compared to the direct treatment (Compare Figure 4.5b to 4.6).

The results above indicate that there are other 'agents' involved in the plasma-induced DNA-strand breaks beyond H_2O_2. And moreover, highlight the requirement of direct proximity to the plasma jet for DNA-strand breaks to occur. Therefore to investigate this further, the plasma jet was next used to treat the MB dispersed directly and uniformly within the gelatin matrix (as shown in Figure 4.3c). DNA-strand breaks were observed by monitoring the fluorescence of the MB in the gelatin matrix using fluorescence microscopy (Figure 4.7). The image in Figure 4.7 shows an overlay of the fluorescence and phase-contrast image to illustrate the correlation between the treatment area on the gelatin surface and fluorescence as a result of DNA-strand breaks in the MB. This is a representative of typical images obtained from triplicate experiments (n = 3).

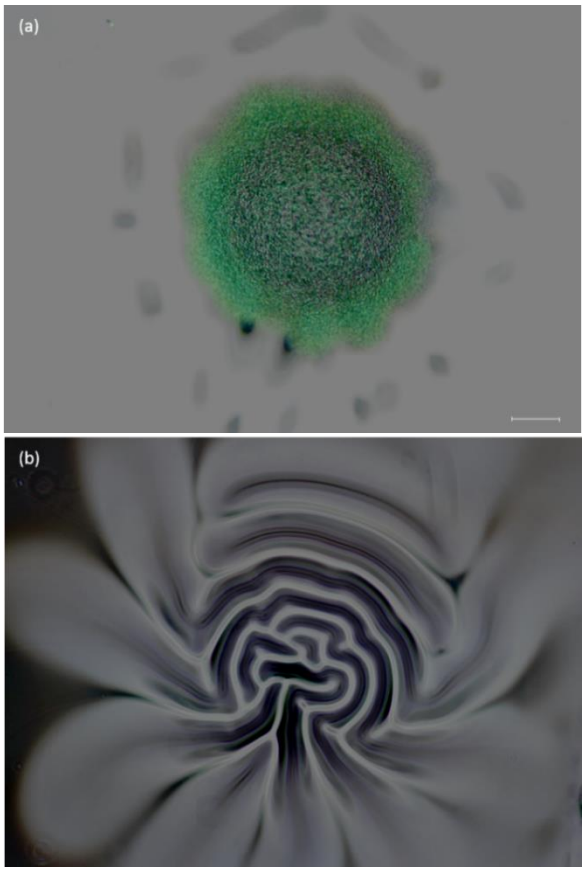


Figure 4.7 The assessment of DNA-strand breaks when MB is dispersed within the gelatin tissue matrix after the treatment with (a) He plasma jet and (b) He gas jet, both at 0.5 slpm for 10 min. The figures are the overlay of images obtained using the fluorescence and phase-contrast microscopy. The scale bar of images is 250 µm.

DNA-strand breaks were not detected in gelatin after 60 s of treatment with the 0.5 slpm plasma jet (data not shown). But, when the treatment was increased to 10 min, DNA-strand breaks were readily observed at the point of impact with the plasma jet (Figure 4.7a). In contrast, no DNA-strand breaks were observed after 10 min treatment with neutral He gas jet; although the He gas jet did partially dehydrate the gelatin surface (Figure 4.7b). Overall, these data show that the plasma jet can readily induce DNA-strand breaks in the gelatin tissue model, but this was only observed at a treatment time-scale of minutes. Possibly longer treatment times are required to observe DNA-strand breaks in the gelatin tissue model because the shorter-lived and highly-reactive RONS such as •OH (that are likely to induce significant DNA damage) are extinguished very rapidly in the gelatin matrix (compared to in HEPES). ESR was used to evaluate how the presence of gelatin target on top of HEPES affects the plasma jet delivery of the •OH in HEPES (Figure 4.8). The ESR spectrum of CYMPO-OH spin adduct was measured for the HEPES either directly exposed to plasma or indirectly through the gelatin target. An eight-line ESR spectrum with an intensity ratio of 1:2:2:1:1:2:2:1

should confirm the formation of the CYMPO-OH spin adduct, suggesting production of the OH radical in HEPES.

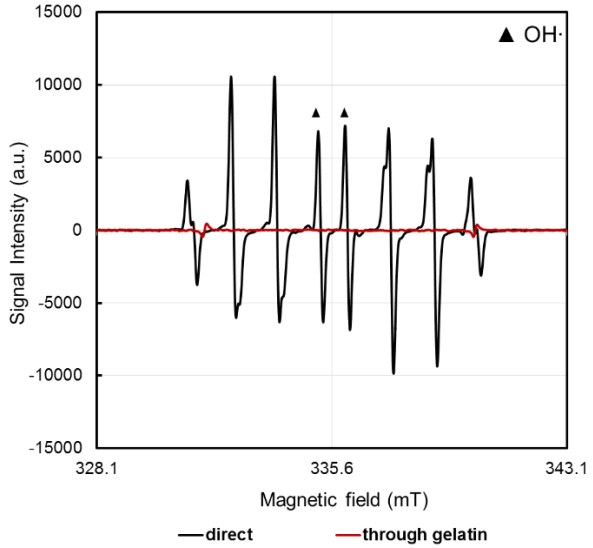


Figure 4.8 Typical ESR spectrum of HEPES containing the CYPMPO spin-trap for the •OH after plasma jet treatment. Two plasma jet treatment conditions were assessed: direct plasma treatment of HEPES and treatment of HEPES through the gelatin target. The plasma jet was operated at 0.5 slpm. The ESR spectrometer settings were: center magnetic field = 335.6 mT; and sweep width = +/- 7.5 mT.

The ESR spectrum (Figure 4.8) shows a clear signal for the •OH after the direct plasma jet treatment of HEPES, but in contrast no signal for the •OH was observed in case of the treatment of HEPES through the gelatin (covering the HEPES solution). This implies that the presence of gelatin target inhibited the plasma-delivery of the •OH in HEPES. Taking into account the results in Figures 4.5-4.7, which show DNA-strand breaks in HEPES upon the direct exposure to plasma but not when treated though the gelatin tissue model, although an appreciable amount of H_2O_2 was delivered in both conditions, the results in Figure 4.8 support the possibility that the •OH is likely to contribute to DNA-strand breaks in the plasma jet treatment of the MB.

In the treatment of biological cells it is important to consider the phospholipid cell membrane, which can protect the DNA encapsulated within the cells from exogenous RONS. Therefore, DNA-strand breaks were next assessed in the phospholipid vesicle cell models suspended in HEPES. The MB was encapsulated within the vesicles as shown in Figure 4.3d. The normalised FI of MB after the plasma jet treatment at 0.05 and 0.5 slpm was plotted as function of plasma treatment time, as shown in Figure 4.9a. Under same plasma treatment conditions, vesicle rupture was also assessed using vesicles encapsulating CF (Figure 4.9b).

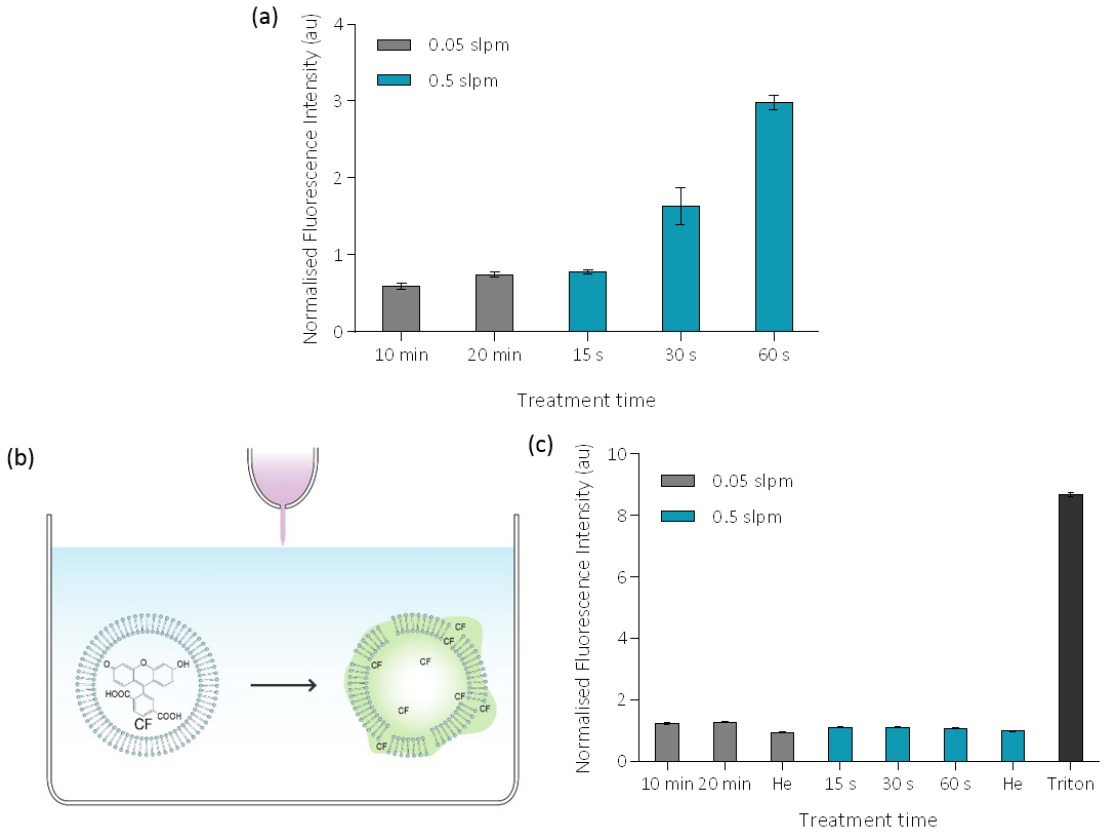


Figure 4.9 Plasma jet treatment of the MB encapsulated within the phospholipid vesicles. (a) Results showing the normalised FI of the MB treated at the two different flow rates of 0.05 slpm for 10 and 20 min, and 0.5 slpm for 15, 30 and 60 s. (b) Plasma jet treatment of the vesicles encapsulating CF and (c) corresponding results showing the normalised FI of the CF with control treatments with 0.05 slpm (for 20 min) and 0.5 slpm (for 60 s) He gas flow alone, and treatment with 0.01% (v/v) Triton X-100 solution as a positive control.

The results in Figure 4.9a shows that the normalised FI of MB (in vesicles) increased as a function of the plasma treatment time. The FI of MB (in vesicles) was higher at 0.5 slpm than the lower flow rates of 0.05 slpm. These results indicate that increasing the treatment time resulted in the increase of DNA-strand breaks in vesicles (loaded with MB). The 0.5 slpm plasma jet at the shorter treatment times induced more DNA-strand breaks within the vesicles than longer treatments with the 0.05 slpm plasma jet. The normalised fluorescence could not be directly compared between the experiments with the MB encapsulated within the vesicles (Figure 4.9a) versus the MB in suspension (Figure 4.5a). This is because (i) the concentration of MB in HEPES (0.5 µM) is different than the concentration used for vesicles (50 µM), and (ii) it was not possible to determine the final concentration of MB within the vesicle. However, for this study simply observing the relative trends, rather than absolute values, is still important as discussed in detail later.

Figure 4.9c shows the results of the CF encapsulating vesicles after plasma jet treatments. It can be seen in the graph that the measured level of CF fluorescence was similar for all plasma jet treatments. However, the intensity of CF fluorescence following plasma jet treatments was low at only 10% of the level obtained with a surfactant (Triton) known to induce complete vesicle lysis. Further, this 10% value is not significant ($p > 0.05$ from a student's *t*-test), being only marginally above the level obtained with the neutral He gas jet treatments (also shown in Figure 4.9c). These results indicate that the vesicles remained intact after the plasma jet treatments. The intact vesicle membrane further confirms that the increase in FI observed in Figure 4.9a is from the MB encapsulated within the vesicles and not in HEPES.

Another potentially interesting observation is that at the lower flow rate of 0.05 slpm (for longer treatment times) plasma jet induced more DNA-strand breaks compared to the higher flow rate of 0.5 slpm (for shorter treatment times) when the MB was suspended in HEPES (Figure 4.5a); whereas the opposite trend was observed when the MB was encapsulated within the vesicles (Figure 4.9a). These contrasting results are explained below.

Starting from the premise that H_2O_2 does not induce DNA-strand breaks, it can be suspected that it may be the short-lived and highly reactive RONS (e.g. the •OH) are responsible for the observed DNA-strand breaks. Plasma treatment of the MB in HEPES with the lower flow rate (0.05 slpm), but substantially longer treatment times, resulted in greater damage of the MB than at the higher flow rates of 0.5 slpm (at much reduced treatment times) because the total number of interactions between the short-lived, highly-reactive RONS and the MB molecules is greater in the former case. But when the MB is encapsulated, these highly-reactive RONS most probably react almost entirely with the vesicle's phospholipid membrane before reaching the DNA within. Therefore the contrast in results may arise due to the following, but not mutually exclusive reasons:

i. The higher concentrations of H_2O_2 (Figure 4.5b) generated by the plasma jet at higher flow rates is important as it facilitates the lipid-peroxidation and permeabilisation of the vesicle's membrane [56, 57], which can enhance the ingress of any remaining highly reactive RONS into the vesicles [58].

ii. At higher flow rates, the plasma jet was in contact with the liquid (Figure 4.4d), which should enhance the electric field around the vesicles. The plasma jet used in this study can generate a maximum electric field of 2.5 kV cm^{-1}. Although not investigated in this study, from a study by Oh *et al.* with a similar plasma jet it is known that the plasma jet generates small packets of charge (usually referred to as 'plasma bullets') that carry a net charge in the order of 10^{-9} C with estimated particle densities between between 10^{10} to 10^{11} cm^{-3} that can propagate to distances of several tens of millimetres from the plasma jet nozzle [59]. This phenomenon is also known as an "ionization front" [59] and has been termed as a "guided streamer" because its propagation is confined to within the He gas flow exiting the plasma jet nozzle [60-62]. Olszewski *et al.* have reported that the magnitude of electric field of the peak streamer is up to approximately 5-7 kV cm^{-1} [62]. In another study by Norberg *et al.*, it was reported that the magnitude of electric field can reach up to tens of kV cm^{-1} upon interactions with the cells in liquid [63]. A further increase in electric field from the 'plasma bullets' contacting the HEPES might have transiently increased the permeability of the phospholipid membrane during plasma jet treatment. This would enhance the ingress of the highly-reactive RONS. In a computational stimulation study, Yusupov *et al.* have shown that the synergistic action of electric field with H_2O_2 can increase the permeability of the phospholipid membrane which increases the ingress of RONS into the cells [64]. This perhaps occurs on a very fast time-scale with only small nanometre diameter pore openings in the phospholipid membrane [65]. This also explains the only minimal leakage of the encapsulated CF from the vesicles with plasma jet treatment (Figure 4.9c).

iii. The gas flow itself imparts greater mechanical forces onto the phospholipid membrane of the vesicles [66]. Consequently, greater mechanical forces exerted onto the phospholipid membrane by the higher flow rate plasma jet, enhanced the ingress of RONS.

For certain medical applications, maximising plasma induced DNA-strand breaks in the target could be advantageous, e.g. in focused cancer therapy. However, in other applications such as the treatment of an open wound, the imperative should be to limit

DNA damage. The data in Figure 4.5 showed that it is difficult to inhibit DNA-strand breaks without compromising the RONS (H_2O_2) concentration delivered by the plasma jet. Since it is possible that the the highly-reactive RONS such as the •OH can readily break DNA-strands, a challenge is to reduce or prevent the plasma jet from delivering these species to the target. Therefore, in the direct treatment of tissue fluid, one approach to inhibit DNA breaks would be to 'filter' the highly reactive RONS from the plasma jet during treatment. This could potentially be accomplished with the use of a material placed in-between the plasma jet and tissue that enables the (rapid) transport of gases or dissolved RONS from the plasma jet to the tissue. In this scenario, it is anticipated that highly reactive RONS (i.e. those that are more likely to induce DNA-strand breaks) would be extinguished in this material owing to their shorter lifetime and limited diffusion distances. This was tested in the final experiment where a commercial hydrogel dressing (Intrasite Conformable) was placed in-between the plasma jet and HEPES. A photograph during treatment and a diagrammatical representation of the experimental set-up are shown in Figures 4.10a and b for HEPES treated indirectly with the plasma jet through a hydrogel dressing. Treatment was carried out with the 0.5 slpm plasma jet for 10 min.

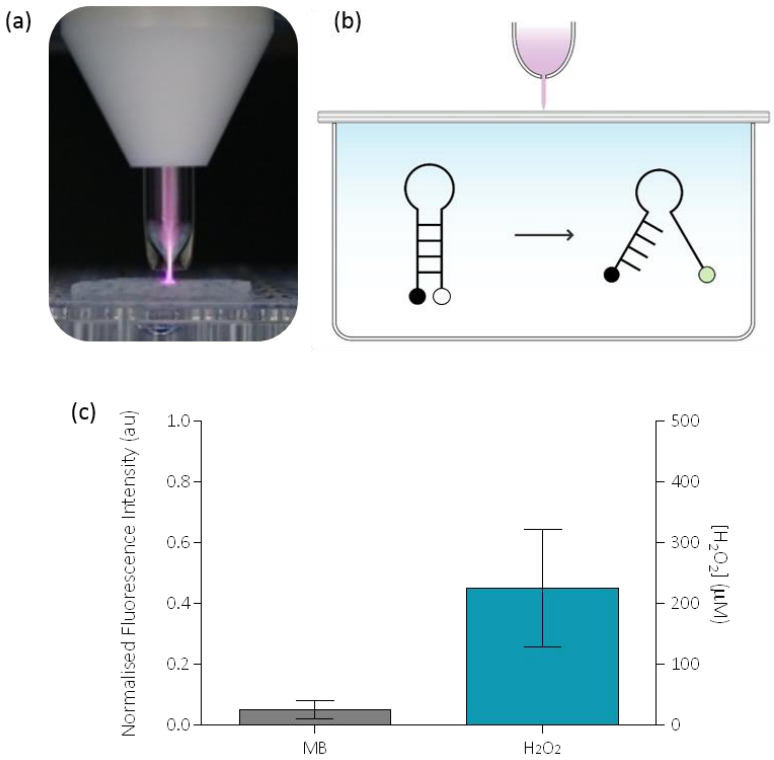


Figure 4.10 (a) Photograph and (b) schematic of the experimental methodology used to assess indirect plasma jet treatment of the MB suspended in HEPES underneath a commercial hydrogel dressing (Intrasite Conformable). (c) Corresponding results showing the normalised FI of the MB

(indicator of DNA-strand break) and concentration of H_2O_2 delivered the dressing into HEPES under the same treatment conditions. The plasma jet was operated at 0.5 slpm for 10 min.

As shown in Figure 4.10c, the hydrogel dressing significantly attenuated the level of DNA-strand breaks in HEPES but still enabled the delivery of H_2O_2 at a relatively high concentration of approximately 200 μM; a concentration comparable to HEPES directly treated with the plasma jets (compare Figure 4.10c to Figure 4.5b). This result adds to the evidence that the more stable, longer-lived RONS from plasma are not responsible for DNA-strand breaks.

To summarise, the methodology for assessing DNA-strand breaks presented in this section is reproducible, cost and time effective, does not require highly specific expertise or analytical equipment, and the data yielded is straightforward to interpret. As seen in the graphs, the SEM of the replicate data is relatively small indicating good experiment reproducibly. The good level of reproducibility and only little batch-to-batch variation in the synthetic models is because the fabrication processes are straightforward, and because experimentation with synthetic tissue models avoids biological variability. Generally, the costs of the reagents are low: the reagents to make the tissue fluid (HEPES), tissue model (gelatin) and cell models (phospholipid vesicles) are not expensive; the major cost is the MB, but the MB is used at a low concentration in 96-well formats to reduce volume requirements. The cost of the equipment is also relatively low and most of the equipment is standard to chemical and biology laboratories; such as the small handheld extruder used for making vesicles, and the microplate reader and fluorescence microscope for measuring DNA-strand breaks. In addition, the experiments can be performed quickly, especially since DNA-strand breaks in the MB give rise to an immediate and easily interpretable switch-on of fluorescence. The next issue is the versatility of the methodology. The results presented in this paper show that this methodology can be utilised to assess DNA-strand breaks from plasma jets in the tissue fluid model, within the tissue model, and within the cell models. The experiments can also be interfaced with microplates for higher through-put screening.

The major result from this study was that plasma jets have the potential to damage DNA in tissue fluid, tissue and cell models. This is not surprising because as discussed earlier, plasma jets generate highly-reactive RONS that have previously been shown to break DNA-strands [25, 28-30, 67]. In the treatment of life threatening indications such as

chronic wounds, it would be advantageous to target the destruction of bacterial cells within biofilms using plasma jets to damage DNA in these cell types. For life-threatening indications, any risk associated with respect to inadvertent DNA damage in healthy cells (in the surrounding tissue) is perhaps reasonably low considering that not all DNA aberrations cause disease and the cellular machinery of healthy cells is well equipped to repair most damaged DNA [68, 69]. On the other hand, the data in this study suggest that given there are always DNA-strand breaks (in direct application of plasma to the tissue fluid model) there remains some level of potential risk, and in such a case the risk ought to be factored in when considering non-critical clinical applications of plasma jets such as for cosmetics (e.g. wrinkle treatments and teeth whitening).

In addition to the plasma jet induced breakage of DNA-strands in HEPES (tissue fluid model), the plasma jet also induced DNA-strand breaks in gelatin (tissue model). This demonstrates that it might be possible to use plasma jets to damage DNA in a solid tissue mass such as a tumour associated with chronic wounds. Importantly, the plasma jet is unlikely to cause DNA damage far underneath a tumour because no DNA damage was observed in HEPES underneath the gelatin target. Overall, these data show that plasma jets could potentially be utilised in the future to damage DNA at specific sites within tissue for targeted decontamination of wounds and cancer therapy.

In certain circumstances, such as stimulation of wound healing or tissue regeneration, it could be advantageous to only deliver RONS that stimulate cell activity (e.g. proliferation and migration), as discussed in Chapter 1. In this study, it was shown that a hydrogel dressing placed in-between the plasma jet and HEPES or gelatin targets can significantly attenuate DNA-strand breaks but still enable the transport of H_2O_2 (and by inference other longer-lived RONS) to the targets. Delivery of controlled doses of H_2O_2 was previously shown to have beneficial effects on wound healing *in vivo* [70]. Plasma jet treatment through a hydrogel dressing is a simple method to potentially stimulate wound healing with the added advantage of not needing to remove the dressing for treatment.

Having considered the advantages, it is worth considering the limitations of the methodology, with a view to future improvements. The major limitations are that the tissue fluid, tissue and cell models are without real biological material, antioxidants and living cells, and the system is static with no physiological fluid flow. Therefore, the

level of DNA-strand breaks observed in this study could be considered as a worst case scenario. The physicochemical properties and inherent antioxidant defences of real biological tissue fluid and tissue would to some extent mitigate the transport of the RONS likely to induce DNA-strand breaks. Additional features that could be in-built to models include the incorporation of proteins, enzymes and antioxidants and cross-linking agents. These could be incorporated into either the tissue fluid or tissue models to mimic different physiological environments. In addition, it is possible to incorporate living cells into, for example, a mimic of a 3D tissue scaffold [71, 72]. This would enable us to study cellular signalling events within a tissue; intercellular signalling might also facilitate the plasma-generated signal to reach cells deeper within the tissue, which could potentially amplify DNA damage. It should also be possible to incorporate fluidic systems with small pumping systems to mimic physiological flow. These features could be incorporated into the future design of the synthetic models to help improve our understanding of plasma interactions with biological systems.

4.2 Assessment of DNA damage with the γ-H2AX assay

4.2.1 Materials and methods

4.2.1.1 Plasma jet

The plasma jet used in this study is the same as the one described in the Section 4.1.1. The plasma jet was operated at a gas flow rate of 1 slpm.

4.2.1.2 Cell culture

HaCaT keratinocyte-like cells were cultured in DMEM (Gibco®, Catalogue number 11965118) supplemented with 10% (v/v) fetal bovine serum (Gibco®, Catalogue no. 1099141), 100 IU ml^{-1} of penicillin and 100 µg ml ml^{-1} of streptomycin (Gibco®, Catalogue no. 15140122) in T75 cell culture flasks (Corning®, Catalogue no. 353110). The cells (in the flask) were cultured at 37°C in a humidified incubator with 5% CO_2.

To passage the cells, DMEM was removed and the cells were washed with 5 ml of PBS (Sigma-Aldrich, Catalogue number 79382), followed by incubating in 5 ml of 0.25% trypsin-EDTA (Sigma-Aldrich, Catalogue number 25200072) solution at 37°C, 5% CO_2 for 3-5 min (until cells were detached). The trypsin was neutralized with 10 ml of DMEM and the cell suspension was transferred to a centrifuge falcon tube. The suspension was centrifuged at 1300 rpm for 5 min before discarding the supernatant.

The cell pellet was re-suspended in 1 ml of fresh DMEM and cells were counted with a haemocytometer.

A total of 7000 cells in 200 µl of DMEM was added to wells of a 96-well tissue cell culture plate (well-depth = 6 mm) for the direct plasma treatment (without hydrogel dressing on top). The treatments were conducted at 1 slpm for 15, 30 and 60 s in two ways: (i) contact i.e. plasma plume touching the liquid and (ii) non-contact i.e. plasma plume not touching the liquid. For contact, the distance between the end of nozzle and top of the 96-well plate was 5 mm and for non-contact the distance was 10 mm.

For the plasma treatments through the hydrogel dressing, a cell culture volume of 400 µl (with 7000 cells in total) was treated for 240 s at a distance of 1 mm. The hydrogel dressing was not removed from the plate (on top of cells) until γ-H2AX assay was performed.

After the plasma jet treatment, the cells (with and without the hydrogel dressing) were incubated overnight at 37°C, 5% CO_2, prior to the γ-H2AX assay.

4.2.1.3 γ-H2AX assay

The γ-H2AX assay was performed the following day after the plasma jet treatments. First the cells were washed with PBS (Sigma-Aldrich, Catalogue no. P4417) two times, each time with an incubation of 5 min. Then, the cells were fixed with 4% (v/v) paraformaldehyde solution (ProSciTech, Catalogue no. EMS15710-S) at room temperature for 20 min. After fixation, the cells were again washed three times with PBS. After the washes, the cells were permeabalised with 0.5% (v/v) Triton X-100 (Sigma-Aldrich, Catalogue no. T8787) for 10 min at room temperature, followed by three washes with PBS. The cells were then incubated for 1 h at room temperature in 3% (w/v) BSA solution (Sigma-Aldrich, Catalogue no. A7906) made in PBS to block non-specific antibody binding. The blocked cells were washed three times with PBS, followed by a 1 h incubation at room temperature with the primary antibody Mouse monoclonal[9F3] to γ H2A.X [phospho S139] (Abcam, Catalogue no. ab26350) diluted at 1:1000. The cells were washed with PBS thrice, followed by incubation with the secondary antibody Goat Anti-Mouse IgG H&L [Alexa Fluor® 488] (Abcam, Catalogue no. ab150113), diluted at 1:1000, for 1 h in the dark at room temperature. This was followed by three washes with PBS and a rinse with deionised water.

The final step was staining of the nucleus using 4′,6-diamidino-2-phenylindole (DAPI). The DAPI solution was supplied at a concentration of 14.3 mM. A concentration of 300 µM was prepared by dissolving 2.1 µL of the 14.3 mM DAPI stock solution into 100 µL PBS. 1:1000 dilution of the 300 µM DAPI was done to achieve a final concentration of 300 nM. The cells were incubated in 300 nM DAPI solution for 5-10 min in the dark and washed three times with PBS. A 100 µl volume of PBS solution was added in each well and stored at 4^{o}C in the dark until the imaging was performed.

For imaging, the plate was transferred to the fluorescence microscope (Olympus DP80). The images were taken at an excitation/emission of 358/461 nm for DAPI and 495/519 nm for Alexa Fluor®. The exposure time for all of the images was kept the same at 137.93 ms for the DAPI channel and 500 ms for the Alexa Fluor® channel. The γ-H2AX positive and negative nuclei were counted for each condition for 3 biologically independent replicates. The images were processed using the Olympus cellSens Dimension software.

4.2.1.4 ESR

The •OH in HEPES[4] was detected using ESR for the same plasma treatment parameters as the cell culture studies. The same protocol was for ESR as described in Section 4.1.1

4.2.1.5 Electrochemical probe

The ISO-HPO-2 sensor from World Precision Instruments (USA) was used to detect the production of H_2O_2 in HEPES[5] after the plasma treatment. The calibration curves were used to correlate the measured changes in current with the concentration of H_2O_2 in solution. The details on the working of the electrochemical sensors and calibrations curves can be found in Chapter 2 and Appendix C.

4.2.2 Results and discussion

In this set of experiments the effects of plasma jet on DNA in live HaCaT cells is investigated. As shown in Figure 4.10c, the hydrogel dressing (Intrasite Conformable) can help prevent DNA-strand breaks for DNA freely suspended in solution whilst

[4] The ESR experiments were conducted at Toyohashi University of Technology Japan. DMEM was not available for use in their laboratory. Therefore, the •OH was measured in HEPES.

[5] Since ESR for the detection of the •OH was performed in HEPES, the H_2O_2 measurements were also performed in HEPES for better comparisons.

enabling the delivery of H_2O_2, which is important to stimulate cell activity important for wound healing without damage to the cells and tissue (discussed in detail in Chapter 1). In Section 4.1, the potential of the •OH to induce DNA-strand breaks was also commented upon and it was proposed that the approach should be to reduce the •OH delivery to the target. Therefore, for this cell culture study, the potential of the hydrogel dressing to reduce DNA-strand breaks in HaCaTs was also assessed, followed by measuring the production of the •OH and H_2O_2 after plasma treatment.

For this experiment, the HaCaT cells were exposed to plasma before allowing them to attach and grow on the plate surface. As mentioned earlier the two plasma treatment conditions were tested: (a) non-contact with the plasma plume not contacting the cell suspension, and (b) contact with the plasma contacting the cell suspension. The results obtained from the γ-H2AX assay are shown in Figure 4.11 and 4.12.

Figure 4.11 shows the immunofluorescence images of the DAPI-stained (blue) and γ-H2AX positive (green) nuclei captured 24 h after the plasma treatment. Additionally, the percentage of nuclei with phosphorylated H2AX was also calculated to measure the percentage of DNA-strand breaks (Figure 4.11). The percentage of DNA-strand breaks for each plasma treatment condition was calculated using the following formula:

$$Percentage\ of\ DNA\ strand\ breaks = \frac{Total\ number\ \ of gamma\ H2AX\ positive\ nuclei}{Total\ number\ of\ nuclei}\ X\ 100$$

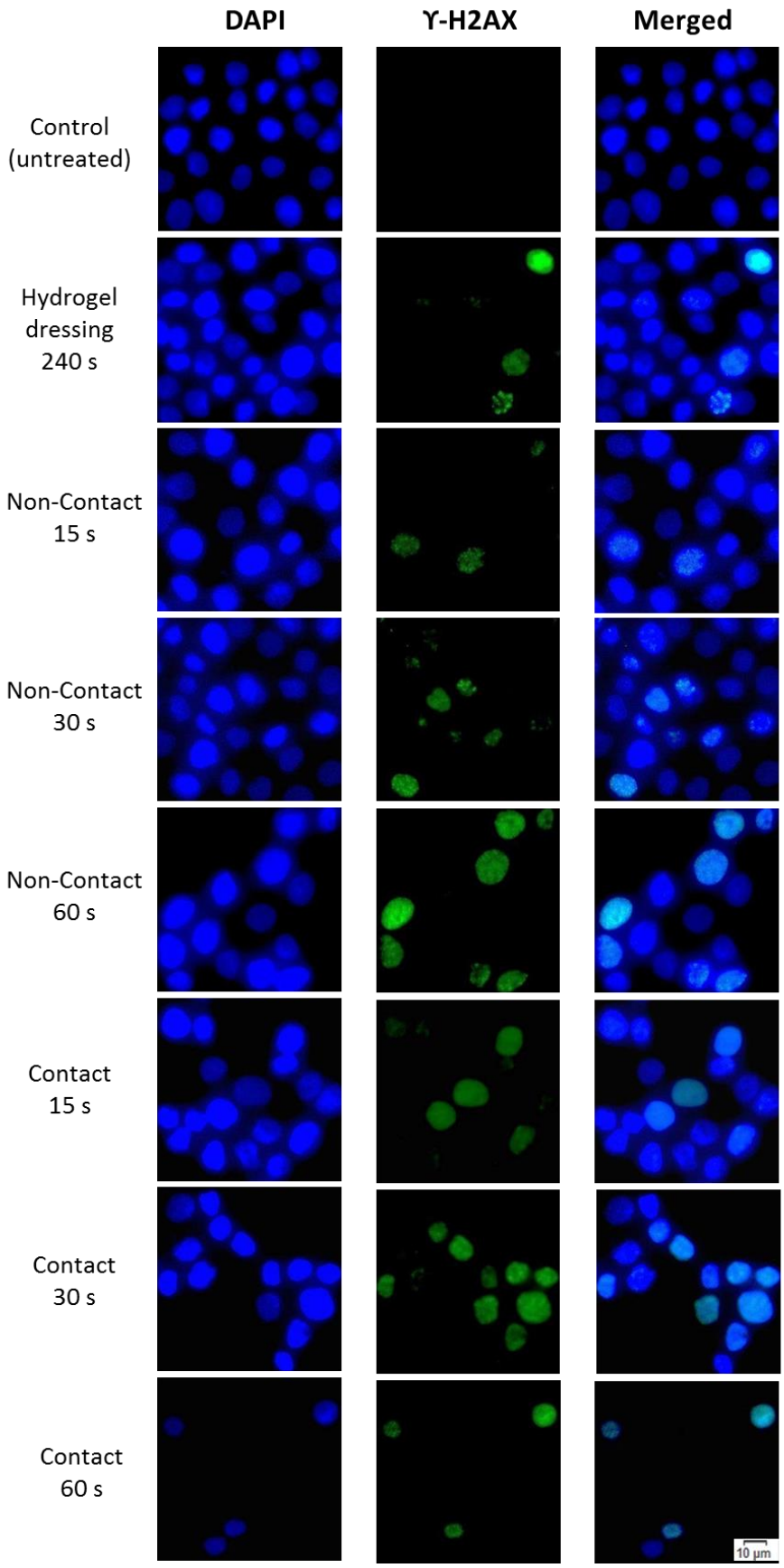


Figure 4.11 The phosphorylation of H2AX to γ-H2AX following various plasma jet treatments. The first, second and third row show the immunofluorescence images of DAPI stained nuclei, γ-H2AX positive nuclei and the merged image, respectively.

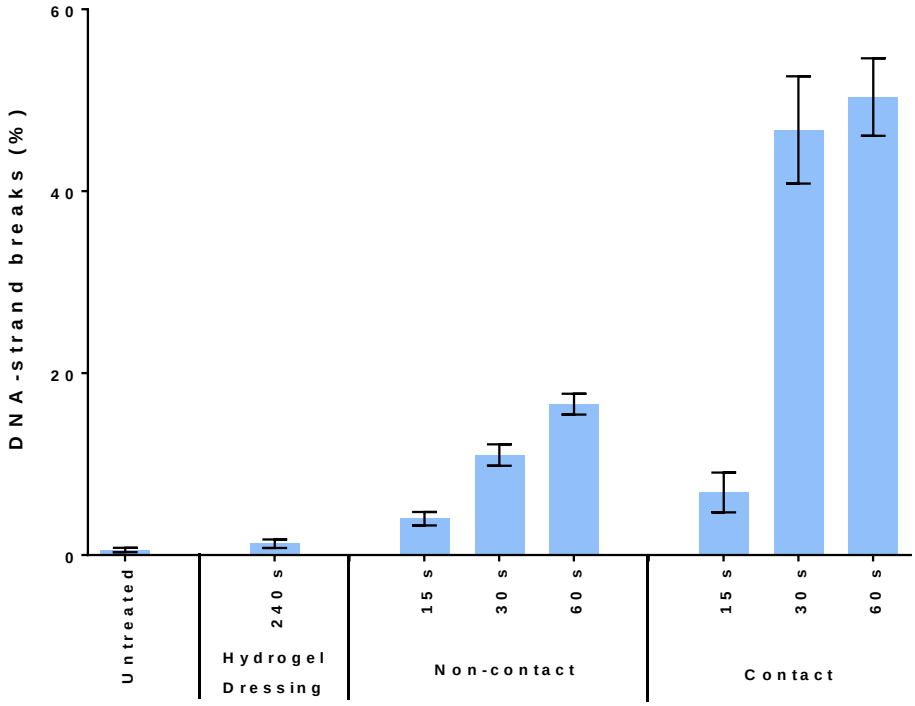


Figure 4.12 Percentage of DNA-strand breaks observed after the different plasma treatments of HaCaT cells. The cells were plasma-treated with the hydrogel dressing for 240 s and also without the hydrogel dressing (contact and non-contact) for 15, 30 and 60 s, respectively. Untreated control cells are shown for comparison.

The results in Figures 4.11 and 4.12 clearly indicate that the plasma jet treatments induced DNA-strand breaks in the cells in all cases. The DNA-strand breaks in HaCaTs were depicted by the presence of γ-H2AX positive nuclei, as shown in Figure 4.11. The number of γ-H2AX nuclei increased with the plasma treatment time and was higher when the plasma is in contact with the cells than the non-contact condition. From Figure 4.12 it can be seen that the DNA-strand breaks increased as function of the plasma treatment time in the case of the direct treatment (contact and non-contact). A higher percentage of DNA strand breaks were observed when the plasma contacted the solution (compared to non-contact treatments). All direct treatments clearly showed much higher percentages of DNA-strand breaks compared to the untreated cells (0.5 %). For instance, after 15, 30 and 60 s of non-contact plasma treatment, the percentage of strand breaks was 4%, 11% and 16%, respectively. A higher percentage of DNA-strand breaks was observed when the plasma plume contacted the cells, with 15, 30 and 60 s of treatment producing 6.8%, 46.7% and 50.3 %, respectively. When the cells were treated through a hydrogel dressing (plasma screen), the percentage of DNA-strand breaks reduced to as little as 1.2 %, close to the untreated cells (0.5 %). These results indicate

that employing the plasma screen in the plasma jet treatment can reduce the DNA strand breaks in HaCaTs.

As discussed earlier, it is speculated that the reduction in DNA-strand breaks can be achieved by inhibiting the delivery of the •OH to the target (cells). Therefore, it is possible that the decrease in DNA-strand breaks in cells after treatment through the hydrogel dressing (plasma screen) is due to the ability of the dressing to reduce the delivery of the •OH to cells. This was validated by measuring the production of •OH in HEPES (see footnote b for detail) after plasma treatment using ESR (Figure 4.13 and 4.14).

Figure 4.13 shows the typical ESR spectrum of the CYMPO/OH adduct in HEPES formed after the direct plasma treatment of the CYMPO solution and plasma treatment through the hydrogel dressing.

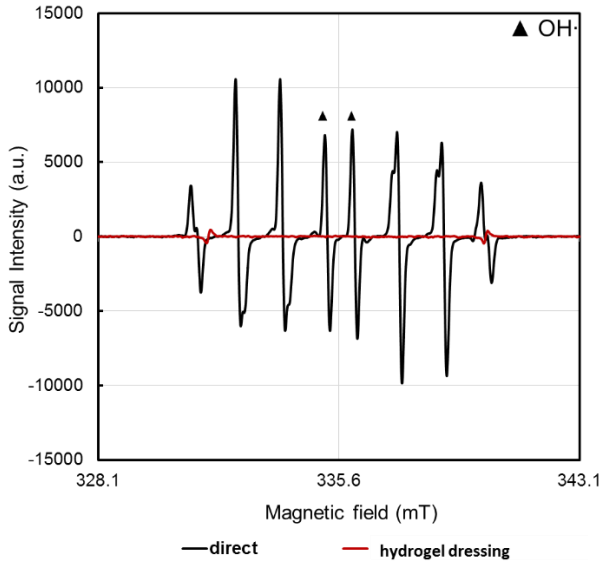


Figure 4.13 The ESR spectrum of the CYPMPO-OH adduct in HEPES adduct after it was directly treated with the plasma jet and indirectly through the hydrogel dressing. The ESR was operated with the center magnetic field at 335.6 mT and sweep width of +/- 7.5 mT.

As shown in Figure 4.13, when CYMPO solution was directly treated with plasma, the signal for the •OH were clearly observed. However, in the presence of the hydrogel dressing (plasma screen) there were no visible peaks corresponding to the •OH. This suggests that the plasma screen can readily extinguish the short-lived •OH within the hydrogel matrix. Combining these ESR results with the results in Figures 4.13, which shows a reduced percentage of DNA-strand breaks when cells were treated through hydrogel dressing, it is highly likely that the shorter-lived and highly reactive •OH plays a key role in DNA-strand breaks induced by plasma in living cells.

It was stated previously in Figure 4.12 that the frequency of DNA-strand breaks increases as a function of plasma treatment time, and that the percentage of DNA-strand breaks are increased when the plasma is in contact with the cell suspension than in the non-contact condition. To unravel how this trend is linked to the •OH, the relative signal intensities for the •OH in the ESR spectrum for each plasma treatment parameter was calculated, as shown in Figure 4.14. The relative signal intensity units were calculated using the Mn^{+2} internal standard.

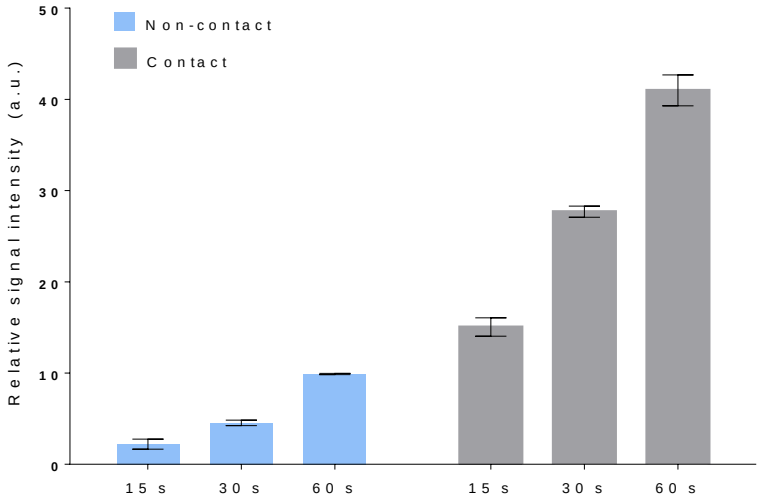


Figure 4.14 The relative signal intensities of the •OH after the direct plasma jet treatment of the CYMPO spin-trap in HEPES. The peak intensities were calculated by referencing to a Mn^{+2} internal standard. Data are expressed as the mean ± standard deviation (n=3). The plasma jet treatment of 15, 30 and 60 s was conducted in two conditions – non-contact (plasma plume not touching the liquid) and contact (plasma plume touching the liquid).

The results in Figure 4.14 indicate that the relative signal intensities of the •OH increased as function of plasma treatment time for both contact and non-contact conditions. The relative intensities of the •OH were higher when the plasma plume is in contact than when it is not in contact. In other words, the production of the •OH is higher in contact condition as compared to the non-contact. In Chapter 3, the role of UV photolysis in the generation of the •OH was discussed and can explain the differences in the •OH production in contact and non-contact condition. It could be that UV-photolysis is enhanced with a higher flux of UV photons when the plasma effluent is touching the liquid surface (contact) as compared to the non-touching condition. Overall, the production of the •OH highly correlated to the DNA-strand breaks observed in cells (Figures 4.11 and 4.12), which suggests that the plasma generation of the •OH generated in liquid is linked plasma-induced DNA-damage.

In the next set of experiments the concentration of H_2O_2 delivered by the plasma jet into the solution in contact mode, non-contact mode and in the presence of the hydrogel dressing were measured (Figure 4.15). H_2O_2 was used to give an indication of the total RONS concentration because H_2O_2 is the major longer-lived RONS generated in aqueous solution for the plasma jet configuration utilised in this study [1, 52, 53]. Moreover, H_2O_2 is desirable in wound healing therapy due to its anti-bacterial property and the ability to stimulate cell proliferation and other important signalling mechanisms (discussed in Chapter 1 in details). It must be noted that the concentrations of H_2O_2 were measured in HEPES solution and not DMEM (see Footnote 4). Nevertheless, the relative trends can be used to understand the role of H_2O_2 in this study.

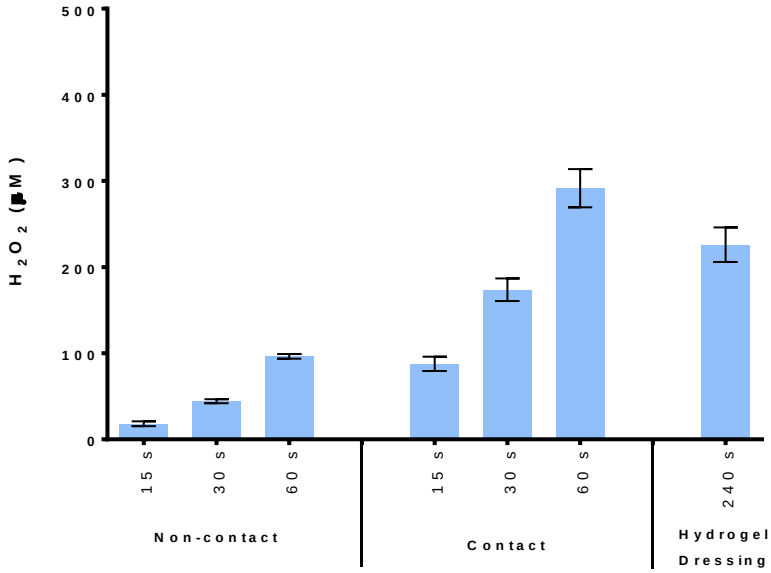


Figure 4.15 Concentrations of H_2O_2 generated by the plasma jet into HEPES after the direct plasma treatment (without hydrogel dressing) and through the hydrogel dressing. The direct treatments were performed in two conditions – (i) contact (when the plasma plume is touching HEPES), and (ii) non-contact (when the plasma plume is not touching HEPES).

Figure 4.15 shows that the concentrations of H_2O_2 increased in a dose-dependent manner. This means that as the treatment time increased, the concentrations of H_2O_2 in HEPES also increased. Higher concentrations of H_2O_2 were produced for the contact condition than non-contact. For instance, when the plasma plume is in contact with the solution, concentrations of up to 300 µM were measured, which is three times higher than the concentrations of up to 100 µM measured in the non-contact mode.

It is also evident that the plasma jet can also deliver H_2O_2 through the hydrogel dressing. The plasma treatments through the hydrogel dressing produced a high concentration of H_2O_2 (approximately 250 µM) in the solution after 4 min of treatment.

It should be noted that such high concentrations of H_2O_2 may be cytotoxic to the cells and deleterious for important cellular mechanisms, which can eventually impair the process of wound healing. Therefore, for applications in wound healing it is important to tailor (reduce) the plasma treatment time accordingly. Nonetheless, it is encouraging to see that even at such high concentrations of H_2O_2 delivered through the plasma screen, only a negligible amount of DNA damage to the MB was observed, and that this correlates very well with the small level of DNA damage observed in the live HaCaT cells. Therefore, this result not only highlights the possibility of using the plasma screen to prevent damage to cells and tissue in plasma wound treatments, but also that the high-throughput approach of the MB is a good marker for predicting DNA damage in more complex, real biological systems.

This *in vitro* study demonstrated the use of commercially available hydrogel dressing (plasma screen) as a promising tool for reducing DNA damage by acting as a "screen" to prevent the •OH from reaching cells whilst enabling the delivery of H_2O_2 which may be beneficial for wound healing. More studies are still required to investigate the prolonged/long-term potentially deleterious effects of the plasma treatments and devising plasma treatment parameters which have beneficial effects on cells.

4.3 Conclusion

The objective of this chapter was to develop a means of delivering molecules such as H_2O_2 that can potentially stimulate the beneficial signalling mechanisms in cells important for wound healing, whilst minimizing the delivery of molecules known to damage cells (e.g. the •OH radicals). In order to achieve this the concept of "plasma screen" was presented. Plasma screen is a commercially available hydrogel dressing which can be placed on top of the target during the plasma treatment. Using the technique of ESR for •OH detection and ISO-HPO-2 and OPD-HRP for H_2O_2 detection, it was shown that the plasma screen is an effective method to prevent the delivery of •OH radicals whilst still permitting the delivery of H_2O_2.

The next step was to investigate the efficiency of plasma screen to reduce or limit cell damage (in terms of DNA-strand breaks) in various biological conditions. DNA-strand breaks were assessed in tissue fluid, tissue and cells using HEPES buffer, gelatin film and phospholipid vesicles as the synthetic models, respectively as well as in HaCaTs

(keratinocytes). In this chapter two simple fluorescence-based methodologies – MB and γ-H2AX assay, are established to monitor plasma-induced DNA-strand breaks.

The results indicate that the plasma jet can induce DNA-strand breaks in the tissue fluid, tissue and cell; if the target is directly exposed to plasma. However, treating the target through the plasma screen reduced the frequency of DNA-strand breaks in cells effectively. The result obtained using the plasma screen increases confidence in its potential to be used for plasma-based wound healing therapies. For instance, placing the plasma screen on top of an open wound during the plasma-treatment can reduce the DNA-damage in skin cells (as •OH is extinguished) and can promote wound healing and decontamination (as H_2O_2 is delivered).

In Chapter 3, it was established that plasma can have significant effect on the levels of O_2 (aq), which can eventually impact the RONS production in solution. Therefore, as part of the future studies, it will be useful to measure the levels of O_2 (aq) in cell culture media during the plasma treatment. It will be also useful to detect other RONS such as $ONOO^-$ and $O_2^{\bullet-}$ generated by the plasma jet and known to induce DNA damage [34, 36, 73, 74].

With the University of Lancaster, *in vitro* and *in vivo* experiments are planned as part of future goals focusing on the activation of other markers of DNA-damage such as Chck1. This will provide further insight into the mechanisms dominating plasma-DNA and plasma-cell interactions.

It should be noted that it is necessary to also assess how the plasma jet treatment might affect the DNA and phospholipid membrane in the longer term. It can be reasonably speculated based on the present data and results presented in this chapter that any direct DNA-strand breaks induced by the plasma jet would be permanent, but further DNA strand breaks would not be expected to occur in the longer term as the highly reactive RONS would be extinguished rapidly after completion of the plasma jet treatment. In a 'real' cell, the cellular machinery can repair damaged DNA [68, 69]. However, further DNA aberrations could result in the longer term if cell function such as the cell cycle is altered by the plasma jet treatment. This is the subject of future research.

In Chapter 2-4, the plasma delivery of RONS (and O_2) in the models of tissue fluid, tissues and cells, and their effect on DNA were investigated. Briefly, an exploratory

study was undertaken with HaCaT keratinocytes skin cells to assess DNA-damage. In the next chapter, all this information will be used to develop a better understanding on the plasma-cell interactions in the two types of skin cells important for wound healing – keratinocytes and fibroblasts.

4.4 References

1. Jun-Seok, O., et al., *How to assess the plasma delivery of RONS into tissue fluid and tissue.* Journal of Physics D: Applied Physics, 2016. **49**(30): p. 304005.
2. Oh, J.-S., et al., *Slow Molecular Transport of Plasma-Generated Reactive Oxygen and Nitrogen Species and O2 through Agarose as a Surrogate for Tissue.* Plasma Medicine, 2015. **5**(2-4): p. 125-143.
3. Oh, J.S., et al., *In-situ UV Absorption Spectroscopy for Monitoring Transport of Plasma Reactive Species through Agarose as Surrogate for Tissue.* Journal of Photopolymer Science and Technology, 2015. **28**(3): p. 439 – 444.
4. Gaur, N., et al., *Combined effect of protein and oxygen on reactive oxygen and nitrogen species in the plasma treatment of tissue.* Applied Physics Letters, 2015. **107**(10): p. 103703.
5. Szili, E.J., et al., *Probing the transport of plasma-generated RONS in an agarose target as surrogate for real tissue: dependency on time, distance and material composition.* J. Phys. D: Appl. Phys., 2015. **48**: p. 202001.
6. Hong S. -H., S.E.J., *et al., Ionized gas (plasma) delivery of reactive oxygen species (ROS) into artificial cells.* Journal of Physics D: Applied Physics, 2014. **47**: p. 362001.
7. Szili, E.J., J.W. Bradley, and R.D. Short, *A 'tissue model' to study the plasma delivery of reactive oxygen species.* Journal of Physics D: Applied Physics, 2014. **47**: p. 152002.
8. Tongtong, H., et al., *A 'tissue model' to study the barrier effects of living tissues on the reactive species generated by surface air discharge.* Journal of Physics D: Applied Physics, 2016. **49**(20): p. 205204.
9. Toshiyuki, K., et al., *Two-dimensional concentration distribution of reactive oxygen species transported through a tissue phantom by atmospheric-pressure plasma-jet irradiation.* Applied Physics Express, 2016. **9**(7): p. 076202.
10. Graves, D.B., *The emerging role of reactive oxygen and nitrogen species in redox biology and some implications for plasma applications to medicine and biology.* Journal of Physics D: Applied Physics 2012. **45**: p. 263001.
11. Halliwell, B. and J.M. Gutteridge, *Free radicals in biology and medicine*. 2015: Oxford University Press, USA.
12. Heinlin, J., et al., *Plasma applications in medicine with a special focus on dermatology.* Journal of the European Academy of Dermatology and Venereology, 2011. **25**(1): p. 1-11.
13. Lehmann, A., F. Pietag, and T. Arnold, *Human health risk evaluation of a microwave-driven atmospheric plasma jet as medical device.* Clinical Plasma Medicine, 2017. **7-8**: p. 16-23.
14. Metelmann, H.-R., et al., *Clinical experience with cold plasma in the treatment of locally advanced head and neck cancer.* Clinical Plasma Medicine, 2018. **9**: p. 6-13.

15. Antoniu, A., et al., *RETRACTED: Safety evaluation of nonthermal atmospheric pressure plasma liquid treatment: Single DNA molecule-based method.* Journal of Electrostatics, 2014. **72(**3): p. 210-217.
16. Wende, K., A. Schmidt, and S. Bekeschus, *Safety Aspects of Non-Thermal Plasmas*, in *Comprehensive Clinical Plasma Medicine*. 2018, Springer. p. 83-109.
17. Isbary, G., et al., *Successful and safe use of 2 min cold atmospheric argon plasma in chronic wounds: results of a randomized controlled trial.* Br J Dermatol, 2012. **167**(2): p. 404-10.
18. Wende, K., et al., *Risk assessment of a cold argon plasma jet in respect to its mutagenicity.* Mutation Research/Genetic Toxicology and Environmental Mutagenesis, 2016. **798–799**: p. 48-54.
19. Kluge, S., et al., *Investigating the Mutagenicity of a Cold Argon-Plasma Jet in an HET-MN Model.* PLOS ONE, 2016. **11**(9): p. e0160667.
20. Bekeschus, S., et al., *The plasma jet kINPen – A powerful tool for wound healing.* Clinical Plasma Medicine.
21. Tresp, H., et al., *Quantitative detection of plasma-generated radicals in liquids by electron paramagnetic resonance spectroscopy.* Journal of Physics D: Applied Physics, 2013. **46**(43): p. 435401.
22. Arjunan K. P., C.A.M., *Hydroxyl Radical and Hydrogen Peroxide are Primarily Responsible for Dielectric Barrier Discharge Plasma-Induced Angiogenesis.* Plasma Processes & Polymers, 2011. **8**: p. 1154-1164.
23. Jablonowski, H. and T. von Woedtke, *Research on plasma medicine-relevant plasma–liquid interaction: What happened in the past five years?* Clinical Plasma Medicine. **3**(2): p. 42-52.
24. Oehmigen, K., et al., *Estimation of Possible Mechanisms of Escherichia coli Inactivation by Plasma Treated Sodium Chloride Solution.* Plasma Processes and Polymers, 2011. **8**(10): p. 904-913.
25. Hirofumi, K., et al., *Radical reaction in aqueous media injected by atmospheric pressure plasma jet and protective effect of antioxidant reagents evaluated by single-molecule DNA measurement.* Japanese Journal of Applied Physics, 2014. **53**(5S1): p. 05FR01.
26. Ames, B.N., M.K. Shigenaga, and T.M. Hagen, *Oxidants, antioxidants, and the degenerative diseases of aging.* Proceedings of the National Academy of Sciences, 1993. **90**(17): p. 7915-7922.
27. Szabó, C. and H. Ohshima, *DNA Damage Induced by Peroxynitrite: Subsequent Biological Effects.* Nitric Oxide, 1997. **1**(5): p. 373-385.
28. Kurita, H., et al., *Use of molecular beacons for the rapid analysis of DNA damage induced by exposure to an atmospheric pressure plasma jet.* Applied Physics Letters, 2015. **107**(26): p. 263702.
29. Yasuda, H., et al., *States of Biological Components in Bacteria and Bacteriophages during Inactivation by Atmospheric Dielectric Barrier Discharges.* Plasma Processes and Polymers, 2008. **5**(6): p. 615-621.
30. Yasuda, H., et al., *Biological Evaluation of DNA Damage in Bacteriophages Inactivated by Atmospheric Pressure Cold Plasma.* Plasma Processes and Polymers, 2010. **7**(3-4): p. 301-308.
31. Wiseman, H. and B. Halliwell, *Damage to DNA by reactive oxygen and nitrogen species: role in inflammatory disease and progression to cancer.* The Biochemical journal, 1996. **313 (Pt 1)**(Pt 1): p. 17-29.

32. Salgo, M.G., et al., *Peroxynitrite causes DNA damage and oxidation of thiols in rat thymocytes [corrected].* Archives of biochemistry and biophysics, 1995. **322**(2): p. 500-505.
33. Salgo, M.G., et al., *DNA Damage and Oxidation of Thiols Peroxynitrite Causes in Rat Thymocytes.* Archives of Biochemistry and Biophysics, 1995. **322**(2): p. 500-505.
34. Halliwell, B. and O.I. Aruoma, *DNA damage by oxygen-derived species Its mechanism and measurement in mammalian systems.* FEBS letters, 1991. **281**(1-2): p. 9-19.
35. Breimer, L.H., *Invited Review: Repair of DNA Damage Induced by Reactive Oxygen Species.* Free Radical Research Communications, 1991. **14**(3): p. 159-171.
36. Epe, B., et al., *DNA Damage by Peroxynitrite Characterized with DNA Repair Enzymes.* Nucleic Acids Research, 1996. **24**(21): p. 4105-4110.
37. Loschen, G., et al., *Superoxide radicals as precursors of mitochondrial hydrogen peroxide.* FEBS Letters, 1974. **42**(1): p. 68-72.
38. Prütz, W.A., *Interaction between glutathione and Cu(II) in the vicinity of nucleic acids.* The Biochemical journal, 1994. **302**(Pt 2): p. 373-382.
39. Prousek, J., *Fenton chemistry in biology and medicine.* Pure and applied chemistry, 2007. **79**(12): p. 2325-2338.
40. Valko, M., et al., *Role of oxygen radicals in DNA damage and cancer incidence.* Molecular and cellular biochemistry, 2004. **266**(1-2): p. 37-56.
41. Ivashkevich, A., et al., *Use of the gamma-H2AX assay to monitor DNA damage and repair in translational cancer research.* Cancer letters, 2012. **327**(1-2): p. 123-33.
42. Endre, J.S., et al., *The assessment of cold atmospheric plasma treatment of DNA in synthetic models of tissue fluid, tissue and cells.* Journal of Physics D: Applied Physics, 2017. **50**(27): p. 274001.
43. van Meer, G., D.R. Voelker, and G.W. Feigenson, *Membrane lipids: where they are and how they behave.* Nature reviews. Molecular cell biology, 2008. **9**(2): p. 112-24.
44. Jackson, S.P. and J. Bartek, *The DNA-damage response in human biology and disease.* Nature, 2009. **461**(7267): p. 1071-1078.
45. Burma, S., et al., *ATM phosphorylates histone H2AX in response to DNA double-strand breaks.* The Journal of biological chemistry, 2001. **276**(45): p. 42462-42467.
46. Rogakou, E.P., et al., *Megabase chromatin domains involved in DNA double-strand breaks in vivo.* The Journal of cell biology, 1999. **146**(5): p. 905-916.
47. Stiff, T., et al., *ATM and DNA-PK function redundantly to phosphorylate H2AX after exposure to ionizing radiation.* Cancer research, 2004. **64**(7): p. 2390-2396.
48. Wang, H., et al., *Complex H2AX phosphorylation patterns by multiple kinases including ATM and DNA-PK in human cells exposed to ionizing radiation and treated with kinase inhibitors.* J Cell Physiol, 2005. **202**(2): p. 492-502.
49. Mariotti, L.G., et al., *Use of the γ-H2AX assay to investigate DNA repair dynamics following multiple radiation exposures.* PloS one, 2013. **8**(11): p. e79541.
50. Short, R.D., I.M. Griffiths, and E.J. Szili, *Plasma hydrogel therapy*. 2017, Google Patents.

51. Serena, E.M., et al., *Studying the cytolytic activity of gas plasma with self-signalling phospholipid vesicles dispersed within a gelatin matrix.* Journal of Physics D: Applied Physics, 2013. **46**(18): p. 185401.
52. Oh, J.-S., et al., *Slow Molecular Transport of Plasma-Generated Reactive Oxygen and Nitrogen Species and O2 through Agarose as a Surrogate for Tissue.* Plasma Medicine, 2015. **5**: p. 125-143.
53. Oh, J.-S., et al., *In-situ UV Absorption Spectroscopy for Monitoring Transport of Plasma Reactive Species through Agarose as Surrogate for Tissue* Journal of Photopolymer Science and Technology, 2015. **28**: p. 439-444.
54. Verlackt, C.C.W., et al., *Atomic-scale insight into the interactions between hydroxyl radicals and DNA in solution using the ReaxFF reactive force field.* New Journal of Physics, 2015. **17**(10): p. 103005.
55. Szili, E.J., et al., *Probing the transport of plasma-generated RONS in an agarose target as surrogate for real tissue: dependency on time, distance and material composition.* Journal of Physics D: Applied Physics, 2015. **48**(20): p. 202001.
56. Siddique, Y.H., G. Ara, and M. Afzal, *Estimation of lipid peroxidation induced by hydrogen peroxide in cultured human lymphocytes.* Dose Response, 2012. **10**(1): p. 1-10.
57. Sakharov, D.V., et al., *Prolonged lipid oxidation after photodynamic treatment. Study with oxidation-sensitive probe C11-BODIPY581/591.* FEBS Lett, 2005. **579**(5): p. 1255-1260.
58. Van der Paal, J., et al., *Effect of lipid peroxidation on membrane permeability of cancer and normal cells subjected to oxidative stress.* Chemical Science, 2016. **7**(1): p. 489-498.
59. Jun-Seok, O., L.W. James, and W.B. James, *Plasma bullet current measurements in a free-stream helium capillary jet.* Plasma Sources Science and Technology, 2012. **21**(3): p. 034020.
60. Kong, M.G., B.N. Ganguly, and R.F. Hicks, *Plasma jets and plasma bullets.* Plasma Sources Science and Technology, 2012. **21**(3): p. 030201.
61. Boeuf, J.P., L.L. Yang, and L.C. Pitchford, *Dynamics of a guided streamer ('plasma bullet') in a helium jet in air at atmospheric pressure.* Journal of Physics D: Applied Physics, 2013. **46**(1): p. 015201.
62. Olszewski, P., et al., *Measurement and control of the streamer head electric field in an atmospheric-pressure dielectric barrier plasma jet.* Plasma Sources Science and Technology, 2014. **23**(1): p. 015010.
63. Seth, A.N., J. Eric, and J.K. Mark, *Helium atmospheric pressure plasma jets interacting with wet cells: delivery of electric fields.* Journal of Physics D: Applied Physics, 2016. **49**(18): p. 185201.
64. Yusupov, M., et al., *Synergistic effect of electric field and lipid oxidation on the permeability of cell membranes.* Biochimica et Biophysica Acta (BBA) - General Subjects, 2017. **1861**(4): p. 839-847.
65. Tero, R., et al., *Nanopore formation process in artificial cell membrane induced by plasma-generated reactive oxygen species.* Archives of biochemistry and biophysics, 2016. **605**: p. 26-33.
66. Cooper, S., et al., *Permeabilization of Adhered Cells Using an Inert Gas Jet.* Journal of visualized experiments: JoVE, 2013. **79**: p. e50612.
67. Kurita, H., et al., *Single-molecule measurement of strand breaks on large DNA induced by atmospheric pressure plasma jet.* Applied Physics Letters, 2011. **99**(19): p. 191504.

68. Taylor, E.M., et al., *The Mre11/Rad50/Nbs1 complex functions in resection-based DNA end joining in Xenopus laevis.* Nucleic Acids Research, 2010. **38**(2): p. 441-454.
69. Taylor, E.M. and H.D. Lindsay, *DNA replication stress and cancer: cause or cure?* Future Oncology, 2016. **12**(2): p. 221-237.
70. Loo, A.E., et al., *Effects of hydrogen peroxide on wound healing in mice in relation to oxidative damage.* PLoS One, 2012. **7**(11): p. e49215.
71. Divieto, C. and M.P. Sassi, *A first approach to evaluate the cell dose in highly porous scaffolds by using a nondestructive metabolic method.* Future Science OA, 2015. **1**(4): p. FSO58.
72. Loh, Q.L. and C. Choong, *Three-Dimensional Scaffolds for Tissue Engineering Applications: Role of Porosity and Pore Size.* Tissue Engineering. Part B, Reviews, 2013. **19**(6): p. 485-502.
73. Spencer, J.P., et al., *Base modification and strand breakage in isolated calf thymus DNA and in DNA from human skin epidermal keratinocytes exposed to peroxynitrite or 3-morpholinosydnonimine.* Chemical research in toxicology, 1996. **9**(7): p. 1152-8.
74. Cadet, J. and J.R. Wagner, *DNA base damage by reactive oxygen species, oxidizing agents, and UV radiation.* Cold Spring Harbor perspectives in biology, 2013. **5**(2).

Chapter 5 Assessing the effects of plasma on the skin cells

The results reported in previous chapters have provided significant optimism on the potential of plasma jets to deliver RONS as well as alter the levels of O_2 (aq)]. In Chapter 4, the influence of plasma on cells and cell membrane was studied using the artificial cell model (phospholipid vesicles). Since the effects of the plasma jet on "real" cells may be entirely different than the artificial cells, in this chapter *in vitro* cell culture study is conducted to study the effect of plasma jet on skin cells important for wound healing.

A number of studies have been conducted to explore the role of plasma-generated RONS on cells in the cell culture environment. For instance, it has been reported that plasma generated ROS can enhance endothelial cell proliferation, migration and angiogenesis by facilitating the release of cytokines such as FGF-2 or VEGF [1-6]. Some studies also emphasized on the "hormesis" effect induced by plasma, according to which low dosages of RONS delivered by plasma can stimulate proliferation while high dosages are deleterious to the cells [7-9].

To date, most studies have focused on the role of RONS in plasma-induced cellular effects, and the role of O_2 (aq) in context of cell culture studies has been seldom commented upon. A few studies have highlighted how changes in O_2 tension affect the growth of skin cells. For instance, O_2 tension above 20% impeded the growth of keratinocytes [10]. However, at a very low O_2 tension of 2%, the growth rate as well as the stratification and differentiation of keratinocytes is reduced [11]. Similarly, studies have demonstrated that the O_2 tension above 18-20% are unfavourable for the growth of fibroblasts [12, 13]. Therefore, the skin cells are sensitive to the level of O_2 in terms of their proliferation, differentiation, migration, morphology, etc. However, the role of O_2 in cells with respect to plasma jet treatment has not been studied extensively.

Since plasma jets can deliver high concentrations of oxidizing species in solution, it has been commonly misunderstood that the solution will also be oxygenated by plasma jets. However, studies by Oh *et al.* have proved that whilst inert gas plasma jets (such as argon and helium) deliver RONS into water at the same time plasma treatment can also

de-oxygenate aqueous media [14-17]. The ability of inert gases to deoxygenated liquids is well-known and has been used for a number of decades in a process referred to as "sparging"[18]. Helium (He) plasma jets are shown to be more effective at sparging (or deoxygenating liquid) than argon jets [14, 15, 19]. Therefore, in this chapter the aim is to not only understand the role of RONS in plasma treatment of cells, but also the effect of plasma-induced sparging.

The phenomenon of sparging in cells is likely to reduce their viability by inducing undesirable hypoxia (deficiency of O_2 in tissue or cell). Under hypoxic conditions, cells can undergo reduced metabolic activity thus impairing cellular health and tissue regeneration [20, 21]. Hypoxia is also a big obstacle to overcome in wound healing. Although acute hypoxia is considered to be an important of signaling inflammation and fibroblast migration in wound healing (discussed in Chapter 1 in details), a state of chronic hypoxia can impair angiogenesis and re-epithelisation [22, 23]. Therefore, in this chapter, attempts have been made to investigate the potential of plasma jet in overcoming the state of hypoxia.

Due to their significant role in the phases of wound healing, plasma-effects were studied on the keratinocytes and fibroblasts. HaCaT and HFF-1 cell lines were used as the models for keratinocytes and fibroblasts, respectively. UVAS and electrochemical probes were utilised to measure the levels of RONS and O_2 (aq) in solution during and post the jet treatments. As a starting point, first the viability of both skin cells was studied after He gas jet treatment and He plasma jet treatment, alone. Later, a combined treatment with the He gas and He plasma jet in different regime orders was explored, with an aim to understand the role of oxidative stress and sparging in cell-culture.

5.1 Materials and methods

5.1.1 Cell culture

Both the cell types – HaCaT and HFF-1, were cultured in DMEM (Gibco®, Catalogue number 11965118) supplemented with 10% (v/v) FCS (Catalogue number 1099141), 100 IU ml^{-1} of penicillin – 100 µg ml ml^{-1} streptomycin (Catalogue number 15140122) in T75 cell culture flasks (Catalogue number 430641U). The cells (in the flask) were stored at 37°C in a humidified incubator with 5% CO_2.

To passage the cells, DMEM was removed and the cells were washed with 5 ml of PBS (Catalogue number 79382), followed by incubating in 5 ml of 0.25% trypsin-EDTA (Catalogue number 25200072) solution at 37°C, 5% CO_2 for 3-5 minutes (until cells were detached). The trypsin was neutralized with 10 ml of DMEM and the cell suspension was transferred to a centrifuge falcon tube. The suspension was centrifuged at 1300 rpm for 5 minutes before discarding the supernatant. The cell pellet was re-suspended in 1 ml of fresh DMEM and cell count was performed.

A total of 5000 cells in 200 µl of DMEM was added to the 96-well tissue cell culture plate (well-depth = 6 mm) and incubated overnight at 37°C, 5% CO_2, prior to the treatments next day.

5.1.2 He plasma jet

A single electrode He plasma jet was used in this study. A 15 mm thick Cu electrode was wound at a distance of 40 mm from the end of glass tube. The glass tube has an inner diameter of 4 mm and tapered down to 650 µm at the nozzle. The electrode and glass tube are enclosed in a PTFE housing for safety. A high peak-to-peak voltage of 10 kV at 30 kHz was applied to the He gas flowing at the flow rates of 0.05 and 0.5 slpm. The treatment distance between end of glass tube nozzle and top of the 96-well was at a fixed distance of 2 mm. The He plasma jet unit and treatment setup is shown in Figure 5.1. For He gas treatment, the plasma was extinguished but He gas supply continued at the two flow rates, as mentioned previously.

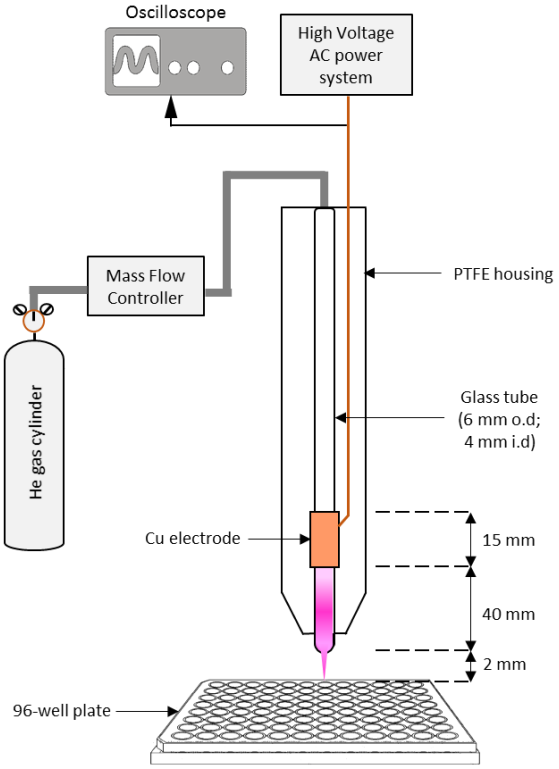


Figure 5.1 Schematic of the He plasma jet unit used in this study. 200 µl of cell suspension was exposed to plasma (or He gas) in a 96-well plate at a fixed distance of 2 mm.

5.1.3 He gas jet and plasma jet treatment

200 µl of the cell suspension (for each cell type) in 96-well plate were subjected to various combinations of plasma and/or He gas jet treatments. Following treatments were done:

a) He gas jet treatment for 60, 180 and 300 s at 0.5 slpm

b) He plasma jet treatment for 15 and 30 s at 0.05 slpm

c) He plasma jet treatment for 15 and 30 s at 0.5 slpm

d) He gas jet treatment for 300 s at 0.5 slpm, followed by He plasma jet treatment for 15 and 30 s at 0.05 slpm

e) He gas jet treatment for 300 s at 0.5 slpm, followed by He plasma jet treatment for 15 and 30 s at 0.5 slpm

f) He plasma jet treatment for 15 and 30 s at 0.05 slpm, followed by He gas jet treatment for 300 s at 0.5 slpm

g) He plasma jet treatment for 15 and 30 s at 0.5 slpm, followed by He gas jet treatment for 300 s at 0.5 slpm

5.1.4 Resazurin viability assay

A stock solution of 10 µg ml^{-1} of resazurin was prepared in PBS solution. A working solution was prepared by diluting at 1:10 in DMEM. The viability of cells was assessed 24 h after the plasma treatment. To test the viability, the media was replaced with 200 µl of the diluted resazurin solution and incubated for 2 h at 37°C, 5% CO_2. The FI of resazurin was recorded at $\lambda_{excitation}$ of 560 nm and $\lambda_{emission}$ of 590 nm in a microplate reader.

The percentage viability of cells (cell viability %) was calculated by normalising the FI values of plasma treated or He gas treated cells against untreated cells according to the following formula:

$$Normalised\ FI = \frac{FI\ of\ treated\ cells - FI\ of\ untreated\ cells}{FI\ of\ untreated\ cells}\ X\ 100\ \%$$

5.1.5 UVAS measurements

The specifications and experimental setup of the UV-vis spectrometer and curve fitting technique to determine the changes in the concentration of RONS (H_2O_2, NO_2^- and NO_3^-) and O_2 (aq) have been described previously in details in Chapter 3 (Section 3.2). All the UVAS measurements were conducted in water since water is also the main constituent (more than 98%) of DMEM.

For the cell treatments, 200 µl of liquid volume was used. But for UVAS setup, a greater volume of 4 ml in the cuvette was used in the cuvette. Consequently, the plasma and He gas exposure duration had to be extended to several minutes in order to demonstrate the effect of plasma-delivered RONS. In regards to this study, this increase in plasma treatment time was not significant because the focus was in "general trends" than absolute values.

Following plasma and He gas treatments were conducted for UVAS measurements:

a) He gas jet treatment for 30 min at 0.5 slpm

b) He plasma jet treatment for 15 min at 0.5 slpm

c) He gas jet treatment for 5 min at 0.5 slpm, followed by He plasma jet treatment for 15 min at 0.5 slpm

d) He plasma jet treatment for 15 min at 0.5 slpm, followed by He gas jet treatment for 15 min at 0.5 slpm

5.1.6 Electrochemical probe measurements

Electrochemical membrane probes combined with a Free Radical Analyzer from World Precision Instruments was used to measure the concentration of H_2O_2 and percentage of O_2 (aq) [24].

The concentration of H_2O_2 were measured using ISO-HPO-2. The method of calibration and other details have already been described in Chapter 2.

The percentage (tension) of O_2 (aq) in DMEM was measured using ISO-OXY-2. Like ISO-HPO-2, the current after each treatment condition was measured using ISO-OXY-2. These values of current were, later, correlated to the percentage (tension) of O_2 (aq) using appropriate calibration curves.

For ISO-OXY-2 calibration, first the current were measured at 0%, 21% and 100% of O_2 (aq) tension. To achieve 0% and 100% condition, DMEM was purged with nitrogen gas and O_2 gas, respectively. 21% O_2 (aq) tension was achieved by allowing the DMEM to equilibrate with ambient air at room temperature. A calibration equation was derived from the curve and the equation was used to convert the values of current from He gas and He plasma jet treatments to O_2 (aq) tension.

For treatment, 200 µl of DMEM in a 96-well plate was first treated for – (a) 15, 30, 60, 180 and 300 s with 0.05 slpm or 0.5 slpm He gas plasma jet, and for (b) 15 and 30 s with 0.05 slpm He plasma jet. Immediately after the treatments, DMEM was subjected to ISO-HPO-2 and ISO-OXY-2 for measurements.

5.2 Results and discussion

From the studies conducted in Chapter 2 and 3, it was established that the He plasma jet treatment has the potential to produce different type of RONS in tissue fluid models. Besides RONS, another major impact of He plasma jet treatment is changes in the levels of O_2 (aq) in tissue fluid. The availability of O_2 (aq) in the tissue fluid model also influences the concentrations of RONS produced. Therefore, to understand how plasma

induced changes in RONS and O_2 (aq) affect cell viability, it is essential to determine the concentrations of RONS and O_2 (aq) during and after plasma treatments. A real-time analysis of the production of H_2O_2, NO_2^-, NO_3^- and O_2 (aq) over a time period of 60 min was achieved with UVAS, as shown in Figure 5.2.

Although the cell culture experiments were performed before the UVAS experiments, for the ease of presentation, and subsequent explanation, the UVAS results are explained first.

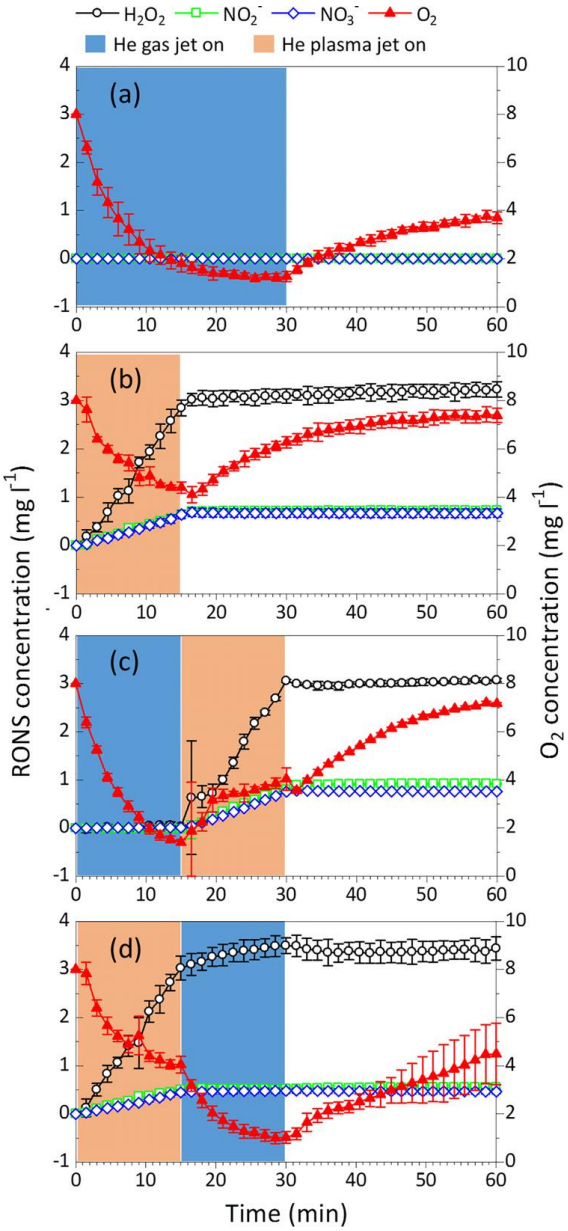


Figure 5.2 The dynamic changes in the concentration of H_2O_2, NO_2^-, NO_3^- and O_2 (aq) in water during and after the treatments with (a) 30 min of He gas jet, (b) 15 min of He plasma jet, (c) 15 min of He gas jet followed by 15 min of He plasma jet, and (d) 15 min of He plasma jet followed by 15 min of He gas jet. Both the jets were operated at a gas flow rate of 0.5 slpm.

The concentration of H_2O_2, NO_2^-, NO_3^- and O_2 (aq) in mg l^{-1} were measured using UVAS over a period of 60 min. The UVAS measurements were conducted for different jet (plasma and/or He gas) treatment conditions (significant to the cell culture data), as shown in Figure 5.2 (a-d). Each case has been discussed below.

Figure 5.2a shows the changes in H_2O_2, NO_2^-, NO_3^- and O_2 (aq) during 30 min of He gas jet treatment. It can be seen that a 30 min He gas jet treatment at 0.5 slpm does not produce any RONS species. But, there is a decrease in O_2 (aq) as He gas jet treatment increased. After only 5 min of He gas jet treatment, O_2 (aq) content decreased by more than 4 mg l^{-1}. After the gas was extinguished, i.e. between 30 min to 60 min, a gradual increase in concentration of O_2 (aq) was observed. The decrease in O_2 (aq) during the treatment is due to He gas molecules replacing the O_2 present in DI water, also referred as "sparging" [19]. When the He gas supply is terminated, the content of O_2 molecules begins to replenish in next 30 mins, although still less than the initial (pre-treatment) levels of O_2 (aq).

Figure 5.2b shows the changes in H_2O_2, NO_2^-, NO_3^- and O_2 (aq) when water was exposed to a 0.5 slpm He plasma jet treatment for 15 min. Both the He plasma jet and He gas flow were extinguished after 15 min and measurements were conducted for a further 45 min. The results indicate that He plasma jet treatment delivered H_2O_2, NO_2^- and NO_3^- into water, unlike He gas jet treatment (compare Figure 5.2a and 2b). A higher concentration of H_2O_2 was delivered by the He plasma jet than NO_2^- and NO_3^-; results also mirrored in Chapter 2 and 3, and can be explained by higher Henry's diffusion coefficient of H_2O_2 than NO_2^- and NO_3^- [25]. This finding is also important to the cell culture studies, since skin cells such as fibroblasts are known to be particularly sensitive to H_2O_2 [26, 27]. The concentrations of H_2O_2, NO_2^- and NO_3^- did not increase and stabilized after the He plasma jet and He gas supply were extinguished, i.e. after 15 mins until 60 mins. The results reveal that the while RONS concentrations increased immediately, the O_2 (aq) content decreased. In other words, He plasma jet treatment de-oxygenated water. The O_2 (aq) after post the jet treatment (after 15 min) recovered, similar to the He gas jet treatment in Figure 5.2a.

In the next set of data, a combined treatment of He gas jet and He plasma jet was done. Figure 5.2c shows the measurements when water was first treated with 15 min of 0.5 slpm He gas jet, immediately followed with a 15 min of 0.5 slpm He plasma jet

treatment, and Figure 5.2d shows the data for water first treated with 15 min of 0.5 slpm He plasma jet, immediately followed by 15 min of 0.5 slpm He gas jet treatment. In both cases, the UVAS measurements were conducted for further 30 min after He gas jet or He plasma jet were extinguished.

The results in Figure 5.2c show that He gas jet treatment does not produce any RONS (first 15 min) in water, as expected. After 15 min, the RONS production increased during He plasma jet treatment as a function of time (H_2O_2 > NO_2^- and NO_3^-). After the He plasma jet was extinguished, no further increase in RONS levels was observed (similar to results in Figure 5.2b). In terms of O_2 (aq) levels, water was deoxygenated by He gas jet (0-15 min), but the He plasma jet now oxygenated water (15-30 min) as a function of treatment time. The ability of plasma jet to oxygenated water can be linked to the production of oxygen species such as O^+, O_2^+, O_2^-, O_3^- and O^- upon plasma treatment (discussed previously in Chapter 3). After He plasma jet treatment was terminated (30-60 min), the O_2 (aq) content continued to improve. Comparing Figure 5.2b with 2c revealed that by end of all 60 min, the concentrations of RONS and O_2 (aq) were approximately equal or in similar range.

In Figure 5.2d, the order of jet treatments was reversed. The results show that during He plasma jet treatment (0-15 min), the concentration of RONS increased as treatment time increased. The concentration of H_2O_2 delivered by He plasma jet was higher than NO_2^- and NO_3^-. The He gas jet treatment (15 - 30 min) had no influence on the RONS concentration in water. After both the He plasma jet and He gas jet were extinguished i.e. after 30 mins, the concentrations of RONS did not change. During initial 15 mins of He plasma jet treatment, O_2 (aq) levels in water declined. The He gas jet treatment (after 15 min) lead to further deoxygenation of water, but had no further impact on RONS production. After 30 min when both the He plasma jet and He gas jet were extinguished, O_2 (aq) content recovered, although still lower than the initial (at 0 min) O_2 (aq) content.

Finally, from Figure 5.2(a-d) it can be concluded that both the He gas jet and the He plasma jet can deoxygenate water. But when He gas jet treatment was immediately followed with He plasma jet treatment, O_2 (aq) levels recovered. In this condition, the He plasma jet facilitated re-oxygenation. For any given condition, He gas jet had no impact on the concentration of RONS production. The delivery of RONS increased in a dose-dependent fashion during He plasma jet treatment and the plasma jet delivered

ROS (H_2O_2) more effectively than the RNS (NO_2^- and NO_3^-). Post all the treatments, the levels of RONS plateaued out and did not increase.

Knowledge of the concentration of RONS and O_2 (aq) tension produced by the He plasma jet in tissue fluid model is useful to understand the subsequent effect of plasma on skin cells in cell culture. The cell viability (%) of the two types of skin cells (HaCaT and HFF-1) was examined using the resazurin assay (Figure 5.3 and 5.4). Figure 5.3 shows the viability of HaCaT cells and Figure 5.4 shows the viability of HFF-1 cells after the different combinations of the jet treatment. The values obtained from the assay are either positive or negative which refers to the increase and decrease in cell viability relative to the untreated cells, respectively [7].

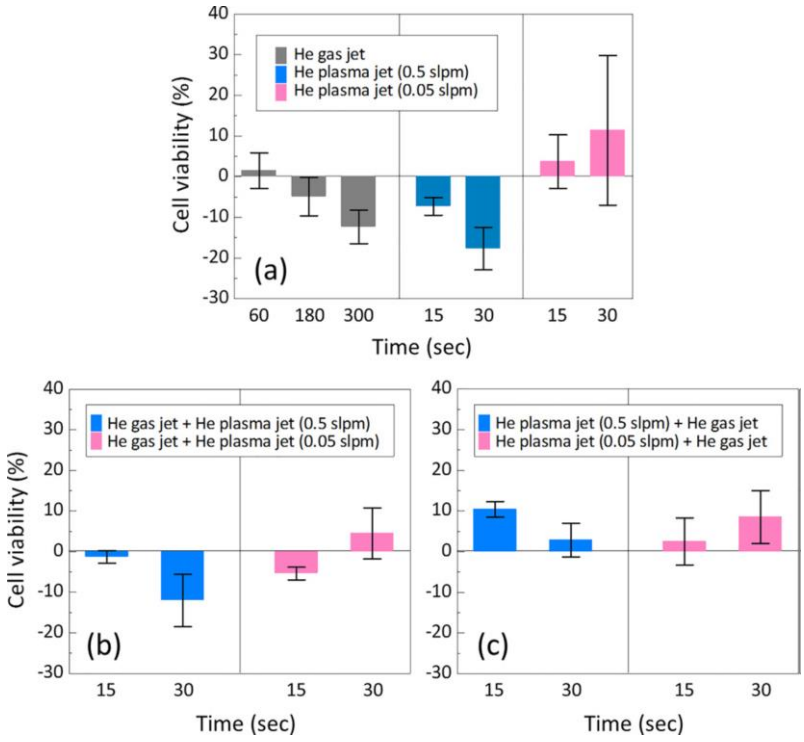


Figure 5.3 The effect on HaCaT cell viability after the treatments with (a) 60, 180 and 300 s of 0.5 slpm He gas jet and 15 and 30s of 0.5 or 0.05 slpm He plasma jet, (b) 300 s of 0.5 slpm He gas jet followed by 15 and 30s of 0.5 or 0.05 slpm He plasma jet, (c) 15 and 30s of 0.5 or 0.05 slpm He plasma jet followed by 300 s of 0.5 slpm He gas jet

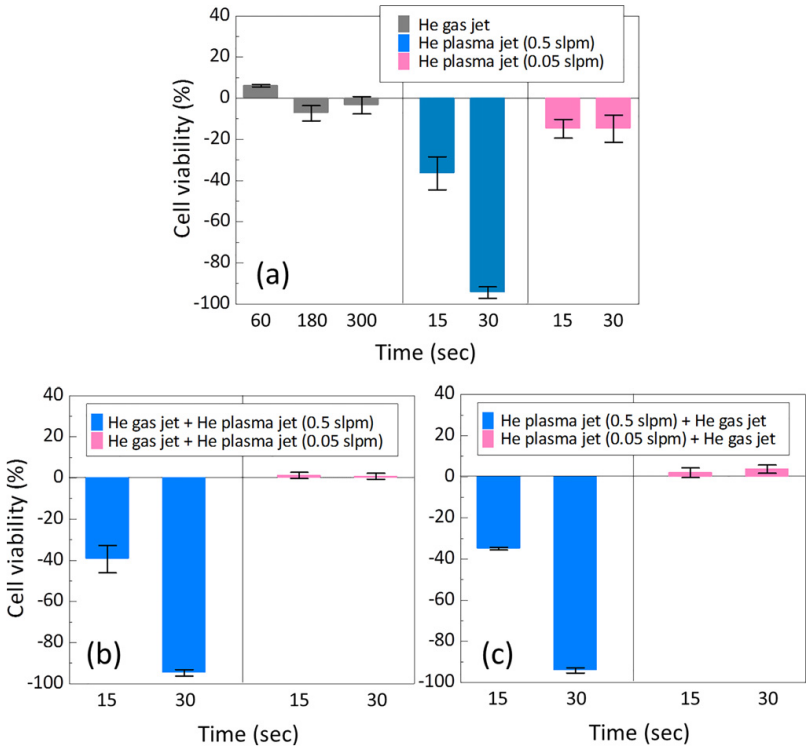


Figure 5.4 The effect on HFF-1 cell viability after the treatments with (a) 60, 180 and 300 s of 0.5 slpm He gas jet and 15 and 30s of 0.5 or 0.05 slpm He plasma jet, (b) 300 s of 0.5 slpm He gas jet followed by 15 and 30s of 0.5 or 0.05 slpm He plasma jet, (c) 15 and 30s of 0.5 or 0.05 slpm He plasma jet followed by 300 s of 0.5 slpm He gas jet

Figure 5.3a and Figure 5.4a show the viability of HaCaT and HFF-1 cells, respectively, after a He gas jet treatment (0.5 slpm) for 60, 180 and 300 s. In Figure 5.3a, it can be seen that HaCaT cell viability decreased as a function of time after He gas jet treatments of 60, 180 and 300 s. After He gas jet treatment of 300 s, HaCaT cell viability decreased by approximately 11.5%. The HFF-1 cells were less sensitive to He gas jet treatment than the HaCaT cells, as shown in Figure 5.4a. A short treatment of 60 s caused a modest increase in the viability of HFF-1 cells, but the viability decreased as treatment time increased to 180 and 300 s.

The UVAS data in Figure 5.2a show that He gas jet can significantly deoxygenate water (due to sparging) after 5 min of treatment. The decrease in the HaCaT cell viability (Figure 5.3a) and to some extent in the HFF-1 cell viability (Figure 5.4a) can be, thus, attributed to low cellular metabolism at low O_2 (aq) induced by sparging. Although not shown here, it was confirmed that the cell viability fully recovered at 72 h after the He gas jet treatment. Therefore, this implies that the effect from sparging was temporary and that the cellular metabolic activity recovered hours post treatment as the O_2 (aq) from ambient air solvated back into the DMEM (Figure 5.2a). Next, the effects of plasma jet on the cells is studied. In Figure 5.3a and 5.4a, the viability of HaCaT and

HFF-1 cells, respectively, after a He plasma jet treatment (0.5 slpm or 0.05 slpm) for 15 and 30s is shown. As seen in Figure 5.2a, at a flow rate of 0.5 slpm, He plasma jet treatment of decreased HaCaT cell viability. However, at a lower flow rate of 0.05 slpm, plasma jet treatment did not have a negative impact on cell viability, even after a longer treatment time. The HFF-1 were, however, more sensitive to He plasma jet treatment (Figure 5.4a). There was almost 100% reduction in cell viability at t=30 s after 0.5 slpm He plasma jet treatment. This reduction in viability cannot be attributed to sparging effect, as it was not observed in He gas jet treatment (Figure 5.4a). From Figure 5.2b and Table 5.1, it can be concluded that the He plasma jet treatment delivered high concentration of RONS, particularly ROS, unlike the He gas jet treatment. Collectively these results indicate that HFF-1 cells were more sensitive to RONS delivered at 0.5 slpm by the He plasma jet. At lower flow rate of 0.05 slpm, He plasma jet still decreased HFF-1 cell viability, but the effect was less marked (approximately 15% at t=30 s). The results from Figure 5.3a and 4a support the findings from previous studies where it was shown that fibroblasts are more sensitive to oxidative stress induced by reactive species, particularly H_2O_2, compared to the keratinocytes [28].

The He plasma jet used in this study delivered different type of RONS, which are also known to be able to induce oxidative stress [29-32], which can be a distress (have inhibitory effects) or eustress (induce stimulatory effects) for the cells, depending on RONS dosage [33-35]. Besides increasing RONS production, the He plasma jet also deoxygenated water (Figure 5.2b). This implies that the He plasma jet can enhance or reduce the viability of skin cells depending on the extent of oxidative stress induced by RONS versus de-oxygenation.

To understand the relative contribution from each effect (oxidative stress and deoxygenation), a combined treatment of He gas jet and plasma jet were conducted (Figure 5.3b-c and 5.4b-c).

First the He gas jet treatment, followed with He plasma jet treatment is discussed. In Figure 5.3b, the cell viability HaCaT cells after 300 s of He gas jet treatment (0.5 slpm), followed immediately with He plasma jet treatment (0.05 or 0.5 slpm) for 15 s and 30 s is shown.

As shown in Figure 5.3b, the He gas jet treatment, if followed with a 15 s He plasma jet treatment at 0.5 slpm had no effect on the HaCaT cell viability. But when the plasma jet

treatment (0.5 slpm) increased to 30 s, the HaCaT cell viability decreased. In case of He gas jet treatment followed with the He plasma jet treatment at lower flow rate of 0.05 slpm, the cell viability of HaCaTs decreased at 15 s of plasma treatment but recovered when the treatment time increased to 30 s.

Comparing Figure 5.3b with 5.3a shows that the 300 s of He gas jet treatment alone decreased the cell viability, but if followed with plasma jet treatment for 15 s at 0.5 slpm or for 30 s at 0.05 slpm, the viability of HaCaTs was broadly unaffected, or slightly higher than that of He gas jet treatment alone. This indicates that the He plasma jet can induce a "rescuing" effect on HaCaT cells viability, depending on the dosage (treatment time and flow rate).

In Figure 5.4b, the HFF-1 cell viability after He gas jet treatment of 300 s (0.5 slpm), immediately followed with 0.5 or 0.05 slpm He plasma jet treatment for 15 and 30 s is shown. These results indicate that the HFF-1 cells are highly sensitive to the He plasma jet. A 0.5 slpm He gas jet treatment followed by 0.5 slpm He plasma jet treatment had no positive impact on HFF-1 viability, as the viability reduced by almost 100% after 30 s of He plasma jet treatment. When the He plasma jet was operated at lower gas flow rates of 0.05 slpm, the viability of HFF-1 cells improved.

For the last set of experiments, the treatment order was reversed i.e. the cells were first treated with 0.5 slpm or 0.05 slpm He plasma jet for 15 and 30 s, immediately followed by 300 s of 0.5 slpm He gas jet. The viability of HaCaTs and HFF-1s under these treatment parameters are shown in Figure 5.3c and 5.4c, respectively.

From Figure 5.3c, it can be seen that reversing the order of jet treatment had a positive impact on the HaCaT cell viability. At both the gas flow rates (of He plasma jet), the viability of HaCaT cells increased (Figure 5.3c). When the cells were exposed to 0.5 slpm He plasma jet, the viability reduced as the He plasma jet treatment time increased form 15 s to 30 s; the viability after 30 s was still higher than that of the untreated cells. Interestingly, at lower flow rates, i.e. 0.05 slpm, increasing the plasma jet treatment from 15 s to 30 s improved the cell viability to some extent.

If the results in Figure 5.3c are compared with the results in Figure 5.3a, it can be seen that the HaCaTs cells, which were pre-treated with 0.5 slpm He plasma jet and later subjected to He gas jet, were more viable than the cells treated with He gas jet alone.

This implies that preconditioning the cells with plasma jet at higher flow rate before sparging (from He gas jet) can help in improving the viability of HaCaTs. At lower flow rated (0.05 slpm), the He plasma jet did not have a major impact on cell viability, when compared with 0.05 slpm He plasma jet alone.

The viability of He plasma jet treated exposed HFF-1 cells, followed by He gas jet treatment is shown in Figure 5.4c. It can be observed in Figure 5. 4c that reversing the order of treatment did not have any impact on the viability of HFF-1s. The viability of cells decreased from almost 40% to 100% as the He plasma jet treatment (0.5 slpm) time increased from 15 s to 30 s. However, at lower flow rates (0.05 slpm), the viability did not decrease significantly.

To see how this treatment regime affected cells as compared to the He gas jet alone, the results in Figure 5.4c and 5.4a are compared with each other. It can be concluded that the viability after the He gas jet treatment of pre-treated (with 0.5 slpm He plasma jet) HFF-1 cells was similar to the viability with He-gas jet treatments alone. However, the cells were less vulnerable when He plasma jet treatment was carried out at lower flow rates (0.05 slpm) when compared with He gas jet treatment alone or even He plasma jet treatment alone.

Taking into account the results obtained from UVAS, it can be seen that in case of He plasma jet treatment of water, followed with He gas jet treatment (Figure 5.2d), the He gas jet had no impact on the RONS concentration in water, but it led to reduction in the levels of O_2 (aq). This decrease in O_2 (aq) was more than that occurred with the He plasma jet treatment alone (Figure 5.2b). Since O_2 can act as reactive free radical and participate in intracellular RONS generation [36-38] (discussed in details in Chapter 2 and 3), further lowering of O_2 (aq) by He gas jet treatment helped in maintaining the RONS production at low levels. A lower RONS concentration prevents excessive oxidative stress, thus maintaining the cell viability, which can be seen in Figure 5.3c and 5.4c.

Similarly as shown in Figure 5.2c, de-oxygenated water (from He gas jet treatment) can be oxygenated again by the He plasma jet. The improvement in O_2 (aq) levels by He plasma jet can, therefore, overcome hypoxic condition and might stimulate the viability of cells, only if the flux of RONS is not very high in order to prevent oxidative stress.

This may explain why in Figure 5.3b and 5.4b, lower flow rates (0.05 slpm) result in a smaller reduction in viability than higher flow rates (0.5 slpm).

Although the UVAS technique is advantageous for real-time analysis of the plasma-delivery of H_2O_2 and O_2 (aq) in solution, the measurements were conducted in water (not DMEM) for relatively larger volumes and longer treatment times. In Chapter 2, it was demonstrated how plasma-generation of RONS (including H_2O_2) in simpler tissue fluid models such as water is different to more complex tissue fluid models such as DMEM. This chapter also highlighted the significance of correlating the quantification of RONS with other detection methods. Therefore, the UVAS data may not provide an ideal representation of the H_2O_2 and O_2 (aq) concentrations delivered by He plasma jet to the cells (in DMEM). To determine the concentration of H_2O_2 (µM) and O_2 (aq) tension (%) in 200 µl of DMEM in a 96-well plate, the ISO-HPO-2 and ISO-OXY-2 probes were used, respectively. The results obtained using these are shown in Table 5.1.

Table 5.1 The O_2 (aq) tension (%) and H_2O_2 (µM) delivered by He gas jet and He plasma jet in DMEM. The symbols … denotes values which could not be measured and * denotes the extrapolated values from calibration curves using longer treatment times of minutes.

		O_2 (%)		**H_2O_2 (µM)**	
He gas flow rate (slpm)		0.05	0.5	0.05	0.5
He gas jet treatment time (s)	15	20.0 ± 0.88	17.5 ± 1.20	…	…
	30	21.1 ± 0.11	15.3 ± 0.52	…	…
	60	…	13.3 ± 0.35	…	…
	180	…	7.52 ± 0.12	…	…
	300	…	5.29 ± 0.09	…	…

He plasma jet treatment time (s)	15	21.1 ± 0.42	19.6 ± 0.26	2.8*	17.6 ±1.33
	30	21.5 ± 0.64	18.3 ± 0.68	5.5*	73.8 ± 0.70

As discussed previously, 21% was O_2 (aq) tension in untreated DMEM at ambient air. Table 5.1 shows that at a low flow rate of 0.05 slpm, the O_2 (aq) tension remained unchanged for up to 30 s of He gas jet treatment. But at a higher flow rate of 0.5 slpm, O_2 (aq) tension decreased to 17.5% and 15.3% after 15 and 30 s of He gas jet treatment, respectively, and continued decreasing with treatment time. By the end of 300 s of He gas jet treatment, O_2 (aq) levels in DMEM reduced by 75%. Similarly, a lower flow rate (0.05 slpm) did not impact the O_2 (aq) tension after 15 and 30 s of He plasma jet treatment. But as flow rate increased to 0.5 slpm, the O_2 (aq) tension decreased; however the deoxygenation of DMEM was not of same degree as seen with 15 and 30 s of He gas jet treatment alone.

Due to the difference in test volumes used with electrochemical sensors (200 µl) and UVAS (4 ml), it is difficult to compare the absolute values of H_2O_2 obtained from each method. However, the general trends can be compared. As shown in UVAS data, He gas jet treatment did not deliver H_2O_2 in DMEM, but He plasma jet did. The He plasma jet treatment at lower flow rate of 0.05 slpm delivered lower concentrations of H_2O_2 (2.8 and 5.5 µM after 15 and 30s, respectively) than the higher flow rate of 0.5 slpm (17.6 and 73.8 µM after 15 and 30s, respectively). Due to the low signals obtained with 0.05 slpm, the concentrations of H_2O_2 in this case were determined by extrapolating the data from calibration curves using longer treatment times of several minutes (approximately 4 times longer than the original). Measuring the concentrations of H_2O_2 delivered by He plasma jet is relevant not only for this study but to assess the safety of plasma jet for tissue/cell treatment. Studies have shown that at the concentrations above 10 µM, H_2O_2 can be cytotoxic. Similar observations were made in this study wherein at higher flow rates (0.5 slpm), He plasma jet delivered 17.6 – 73.8 µM of H_2O_2 and reduced the viability of the cells.

5.3 Conclusion

The aim of this chapter was to analyse the effects of plasma jet on viability of the skin cells (HaCaT and HFF-1) important for wound healing. In Chapters 2, 3 and 4, the ability of He plasma jet to deliver RONS as well as alter the O_2 (aq) tension in biologically relevant solutions were discussed. Inspired from previous work, in this chapter the focus was to examine how He plasma jet-induced oxidation, oxygenations and de-oxygenation influence the viability of skin cells. The viability of skin cells after treatment was assessed using a resazurin assay (details in Section 5.1).

To understand the role of RONS induced oxidative stress and de-oxygenation or oxygenation, it was essential to quantify the concentrations of RONS and O_2 delivered by plasma jet into solution. The technique of UVAS and electrochemical sensing (ISO-HPO-2 and ISO-OXY-2) was used to meter H_2O_2, NO_2^-, NO_3^- and O_2 (aq) in real-time during and post the He gas jet and He plasma jet treatment of water (Figure 5.2).

The results from this study show that the He gas jet and He plasma jet can deoxygenate solution (DMEM or water) by the process referred as "sparging". Sparging had a significant effect on the viability of HaCaTs and HFF-1, as shown in Figure 5.3 and 5.4, respectively. Comparing these two figures, it was concluded that the fibroblasts (HFF-1) may be more sensitive to sparging than the keratinocytes (HaCaT). The viability of cells reduced significantly with plasma jet treatment alone. This inhibiting effect of plasma jet at high flow rates can be attribute to reduce metabolic activity of cells in state of hypoxia induced by the plasma jet.

The experiments with UVAS illustrated that besides reducing the amount of O_2 (aq), He plasma jet treatment can also deliver RONS such that higher concentrations of H_2O_2 was delivered than NO_2^- and NO_3^-. He gas jet treatment only deoxygenates the solution, with no potential to produce RONS.

To investigate the individual as well as the combined role of He gas jet and He plasma jet treatment on the cells, combined treatments of the He gas and plasma jet were conducted. In first scenario, cell were treated with 300 s of 0.5 slpm He gas jet, immediately followed by 15 and 30 s of 0.5 or 0.05 slpm He plasma jet treatment. In the next scenario, the order of treatment was reversed.

Combining the data from *in vitro* cell culture experiments with the UVAS and electrochemical probe measurements revealed that the viability of skin cells can be stimulated or inhibited depending on the "dose" of RONS and extent of de-oxygenation in the solution. While He plasma jet treatments at the higher flow rate (0.5 slpm) reduced the viability of both the skin cells significantly, reducing the gas flow rate (0.05 slpm) can improve the viability in HaCaT cells or at least have a less damaging effect in case of the HFF-1 cells.

In case of the combined He gas jet and He plasma jet treatments, it can be generalized that the skin cells were less vulnerable to He plasma jet treatment at low flow rates.. Treating the cells first with He gas jet and immediately after with low dose of He plasma jet (15 and 30 s of 0.05 slpm or 15 s of 0.5 slpm) improved the cell viability, or at least had no negative impact. Broadly, it can be said that the plasma jet had a "rescuing" effect on the cells. This effect can be linked to initial deoxygenation of the solution by He gas jet mitigated by the promoting oxygenation later by the He plasma jet, as shown using UVAS. Reversing the order of jet treatment (i.e. He plasma jet followed by He gas jet) had no major impact on the viability of skin cells, although a minor improvement in the viability was observed that can be attributed to the preconditioning by the plasma jet which mitigated the harm from sparging.

The He plasma jet used in this study can deliver high concentrations of H_2O_2 (>10 – 70 µM) to the cells (in 200 µL DMEM) at high flow rates. These concentrations are known to be deleterious to cells, as confirmed by the reduced cell viability reported in this chapter.

Taking into account the potential of O_2 to act directly as a reactive specie and in promoting RONS generation, it might be concluded that by controlling the levels of O_2 (aq) in water, excessive oxidative stress (from RONS) can be prevented. This is significant for the plasma applications, such as wound healing, where the aim is to limit or prevent the deleterious effects of plasma jet on cells.

It should be noted that, the *in vitro* cell culture experiments in this chapter were performed in a 96 well plate, while in the real physiological conditions the tissue fluid is not static and a continuous blood flow may mitigate the effect of sparging (or deoxygenation). In real cells, the RONS levels are also influenced by the presence of other biomolecules such as enzymes, proteins and antioxidants. Therefore, more follow-

up studies need to be conducted to closely mimic the "real" cellular environment, for example use of various DMEM compositions or incorporating microfluidic systems in the study.

It is also important to note that in this study the cells were directly exposed to plasma, which to some extent mimics open wounds. However in case of closed wound the effects may be very different [14, 39]. Several reports have also suggested the potential of plasma to increase sub-cutaneous blood flow and the concentration of O_2 (aq) in blood [40-42]. In Chapter 3, it was demonstrated that plasma treatment of tissue fluid model through tissue model can enhance the O_2 (aq) content within tissue or underneath the tissue. To understand the effect of plasma-induced oxygenation or de-oxygenation and RONS production in closed wounds, further studies with artificial tissue models such as gelatin or agarose can be explored. In fact at the moment, a study focusing on the viability of skin cells when plasma treated through a tissue model (agarose) is already in progress (briefly discussed in Chapter 6).

In conclusion, this chapter highlights that the levels of O_2 (aq) along-with the concentration of RONS in cell media can determine the biological outcome of plasma treatment of cells in cell culture experiments. Therefore, a prior knowledge about the plasma-induced changes in O_2 (aq) in the *in vitro* cell culture studies or *in vivo* studies can be useful to unravel the underlying mechanisms of plasma-tissue interactions. This will eventually pave way for developing strategies to control the level of oxidative stress in cells and tissue to design "safer" plasma devices.

5.4 References

1. Kalghatgi, S., et al., *Endothelial cell proliferation is enhanced by low dose non-thermal plasma through fibroblast growth factor-2 release.* Annals of biomedical engineering, 2010. **38**(3): p. 748-57.
2. Arjunan, K.P., et al., *Non-thermal dielectric barrier discharge plasma induces angiogenesis through reactive oxygen species.* Journal of the Royal Society Interface, 2012. **9**(66): p. 147-57.
3. Arjunan K. P., C.A.M., *Hydroxyl Radical and Hydrogen Peroxide are Primarily Responsible for Dielectric Barrier Discharge Plasma-Induced Angiogenesis.* Plasma Processes & Polymers, 2011. **8**: p. 1154-1164.
4. Kalghatgi, S., et al., *Effects of non-thermal plasma on mammalian cells.* PLoS One, 2011. **6**(1): p. e16270.
5. Ngo, M.-H.T., et al., *Increased Fibroblast Cell Proliferation and Migration Using Atmospheric N2/Ar Micro-Plasma for the Stimulated Release of Fibroblast Growth Factor-7.* Plasma Processes & Polymers, 2014. **11**: p. 80-88.

6. Choi, J.H., et al., *Low-temperature atmospheric plasma increases the expression of anti-aging genes of skin cells without causing cellular damages.* Archives of dermatological research, 2013. **305**(2): p. 133-40.
7. Endre, J.S., et al., *The hormesis effect of plasma-elevated intracellular ROS on HaCaT cells.* Journal of Physics D: Applied Physics, 2015. **48**(49): p. 495401.
8. Liu, J.-R., et al., *Low temperature plasma promoting fibroblast proliferation by activating the NF-κB pathway and increasing cyclinD1 expression.* Scientific Reports, 2017. **7**(1): p. 11698.
9. Bekeschus, S., et al., *Human Mononuclear Cell Survival and Proliferation is Modulated by Cold Atmospheric Plasma Jet.* Plasma Processes and Polymers, 2013. **10**(8): p. 706-713.
10. Horikoshi, T., A.K. Balin, and D.M. Carter, *Effect of Oxygen on the Growth of Human Epidermal Keratinocytes.* Journal of Investigative Dermatology, 1986. **86**(4): p. 424-427.
11. Ngo, M.A., et al., *Oxygen-Dependent Differentiation of Human Keratinocytes.* Journal of Investigative Dermatology, 2007. **127**(2): p. 354-361.
12. Balin, A.K. and L. Pratt, *Oxygen modulates the growth of skin fibroblasts.* In Vitro Cell Dev Biol Anim, 2002. **38**(5): p. 305-10.
13. Parrinello, S., et al., *Oxygen sensitivity severely limits the replicative lifespan of murine fibroblasts.* Nat Cell Biol, 2003. **5**(8): p. 741-7.
14. Jun-Seok, O., et al., *How to assess the plasma delivery of RONS into tissue fluid and tissue.* Journal of Physics D: Applied Physics, 2016. **49**(30): p. 304005.
15. Oh, J.-S., et al., *Slow Molecular Transport of Plasma-Generated Reactive Oxygen and Nitrogen Species and O2 through Agarose as a Surrogate for Tissue.* Plasma Medicine, 2015. **5**(2-4): p. 125-143.
16. Oh, J.S., et al., *In-situ UV Absorption Spectroscopy for Monitoring Transport of Plasma Reactive Species through Agarose as Surrogate for Tissue.* Journal of Photopolymer Science and Technology, 2015. **28**(3): p. 439 – 444.
17. Kotaro, O., et al., *Modulating the concentrations of reactive oxygen and nitrogen species and oxygen in water with helium and argon gas and plasma jets.* Japanese Journal of Applied Physics, 2019. **58**(SA): p. SAAB01.
18. Bakalyar, S., M.T. Bradley, and R. Honganen, *The role of dissolved gases in high-performance liquid chromatography.* Journal of Chromatography A, 1978. **158**: p. 277-293.
19. Rollie, M.E., G. Patonay, and I.M. Warner, *Deoxygenation of solutions and its analytical applications.* Industrial & Engineering Chemistry Research, 1987. **26**(1): p. 1-6.
20. Overgaard, J. and M.R. Horsman, *Modification of hypoxia-induced radioresistance in tumors by the use of oxygen and sensitizers.* Seminars in Radiation Oncology, 1996. **6**(1): p. 10-21.
21. Gray, L.H., et al., *The Concentration of Oxygen Dissolved in Tissues at the Time of Irradiation as a Factor in Radiotherapy.* The British Journal of Radiology, 1953. **26**(312): p. 638-648.
22. Yip, W.L., *Influence of oxygen on wound healing.* International Wound Journal, 2015. **12**(6): p. 620-624.
23. Sen, C.K., *Wound Healing Essentials: Let There Be Oxygen.* Wound repair and regeneration 2009. **17**(1): p. 1-18.
24. Taniguchi, N. and J. Gutteridge, *Experimental protocols for reactive oxygen and nitrogen species*. 2000: OUP Oxford.

25. Sander, R., *Compilation of Henry's law constants (version 4.0) for water as solvent.* Atmospheric Chemistry & Physics, 2015. **15**(8): p. 4399-4981.
26. Kaushik, N., et al., *Dielectric barrier discharge plasma efficiently delivers an apoptotic response in human monocytic lymphoma.* Plasma Processes and Polymers, 2014. **11**(12): p. 1175-1187.
27. Eva Stoffels, Y.S., and David B. Graves, *Cold Atmospheric Plasma: Charged Species and Their Interactions With Cells and Tissues.* IEEE Transactions on Plasma Science, 2008. **36**(4): p. 1441-1457.
28. Marionnet, C., et al., *Different Oxidative Stress Response in Keratinocytes and Fibroblasts of Reconstructed Skin Exposed to Non Extreme Daily-Ultraviolet Radiation.* PLOS ONE, 2010. **5**(8): p. e12059.
29. Halliwell, B., *Biochemistry of oxidative stress.* Biochemical Society Transactions, 2007. **35**(5): p. 1147-1150.
30. Dröge, W., *Free Radicals in the Physiological Control of Cell Function.* Physiological Reviews, 2002. **82**(1): p. 47-95.
31. Sies, H., C. Berndt, and D.P. Jones, *Oxidative Stress.* Annual Review of Biochemistry, 2017. **86**(1): p. 715-748.
32. Pruchniak, M.P., M. Araźna, and U. Demkow, *Biochemistry of Oxidative Stress*, in *Advances in Clinical Science*, M. Pokorski, Editor. 2016, Springer International Publishing: Cham. p. 9-19.
33. Burdon, R.H., Daniel Alliangana, and Vera Gill, *Endogenously generated active oxygen species and cellular glutathione levels in relation to BHK-21 cell proliferation.* Free radical research 1994. **21**(3): p. 121-133.
34. Burdon, R.H., V. Gill, and D. Alliangana, *Hydrogen Peroxide in Relation to Proliferation and Apoptosis in BHK-21 Hamster Fibroblasts.* Free Radical Research, 1996. **24**(2): p. 81-93.
35. Lundberg, J.O., et al., *Nitrate and nitrite in biology, nutrition and therapeutics.* Nature Chemical Biology, 2009. **5**: p. 865.
36. Halliwell, B. and J.M. Gutteridge, *Free radicals in biology and medicine*. 2015: Oxford University Press, USA.
37. Davies, K.J.A., *Oxidative stress: the paradox of aerobic life.* Biochemical Society Symposium, 1995. **61**: p. 1-31.
38. Giordano, F.J., *Oxygen, oxidative stress, hypoxia, and heart failure.* The Journal of Clinical Investigation, 2005. **115**(3): p. 500-508.
39. Gaur, N., et al., *Combined effect of protein and oxygen on reactive oxygen and nitrogen species in the plasma treatment of tissue.* Applied Physics Letters, 2015. **107**(10): p. 103703.
40. Collet, G., et al., *Plasma jet-induced tissue oxygenation: potentialities for new therapeutic strategies.* Plasma Sources Science and Technology, 2014. **23**(1): p. 012005.
41. Kisch, T., et al., *The repetitive use of non-thermal dielectric barrier discharge plasma boosts cutaneous microcirculatory effects.* Microvascular Research, 2016. **106**: p. 8-13.
42. Kisch, T., et al., *Improvement of cutaneous microcirculation by cold atmospheric plasma (CAP): Results of a controlled, prospective cohort study.* Microvascular Research, 2016. **104**: p. 55-62.

Chapter 6 Conclusion and future work

Chronic wounds are a major threat to the public health and economic burden in Australia, affecting almost 400,000 Australians per year and costing $3 billion per year to the Australian healthcare system [1]. Constant efforts are being made in the wound management sector to alleviate patient suffering and reduce the economic burden. It is hoped that this PhD thesis provides a contribution to tackle the issue of chronic wounds, by investigating the potential of plasma-based therapies for wound healing.

A rapid growth (over the past two decades) has been observed in the applications of cold plasma (or non-thermal plasma) for variety of biomedical applications such as bacterial disinfection [2, 3], chronic wounds [4-6], dental cavities [7] and teeth whitening [8], dermatology [9], and cancer [10-12]. For wounds treatment, clinicians have recognised that plasma devices (mainly in jet configuration) may be a promising tool to stimulate both healing and disinfect the wound site. The growing optimism in plasma is evident from the emergence of commercially-available and clinically-approved medical plasma devices, with a special focus on dermatology. Examples include Rhytec Portrait® (USA), Bovie J-Plasma® (USA), Canady Hybrid Plasma^{TM} Scalpel (USA), kINPen® (Germany) and PlasmaDerm® (Germany).

The therapeutic action of plasma is most often credited to RONS ($O_2^{\bullet-}$, •OH, H_2O_2 and NO) generated upon interactions of plasma with the ambient air. A plasma jet (as used herein) can deliver these RONS into the tissue fluid and/or deep within the tissue surface. The plasma-delivered RONS can also interact with the cell membrane and penetrate into the cell, eventually interacting with other intracellular components such as DNA. Recent *in vitro* investigations suggest that plasma-tissue and plasma-cell interactions may trigger specific cell-signalling mechanisms and this could, in part, be responsible for subsequent biological outcomes. One of the current lines of thought is that biological outcome after plasma treatment of tissues are based on the principle of 'hormesis' [13], according to which a high dosage of RONS (from plasma) has deleterious effects on the cells (such as cell cycle arrest, lipid peroxidation, reduced metabolic activity, etc.) but small doses of RONS could be beneficial and stimulate important functions such as cell migration and cell proliferation [14-16].

A Google Scholar search of the keyword “plasma medicine” shows almost 5200 studies (to date). This gives an indication of the global interest in the field of plasma medicine. However, there remains a major gap in our knowledge of the plasma jet and its interactions with real biological targets (tissue fluid, tissue and cell). The most fundamental questions which still remain unanswered are:

i. Whilst the types of species generated by the plasma jet are known, there is lack of knowledge about which specie and in what concentration reach the biological targets?

ii. How do these active species reach deep into tissue and to the cells located /embedded deep within the tissue?

iii. What are the mechanisms behind the observed biological outcomes after plasma treatment?

iv. What are the safe doses of the plasma treatment? And, how are these established?

Considering these questions (of this type) are very crucial to the development of any medical therapy and given that a number of plasma devices are already commercially available for use in the clinic (in the USA and Germany), it is rather surprising that we do not have better answers to these ‘obvious’ questions.

This PhD is an attempt to answer the above mentioned questions and can be broadly categorised into two parts – the first part covers the ‘detection and quantification of RONS’ delivered by a plasma jet into tissue fluid and the second part involves ‘assessing the biological effects of plasma’ on cells and cellular components.

In the first half of the thesis, i.e. Chapter 2 and 3, the development of methods to ‘accurately’ measure the RONS delivered by a plasma jet into tissue model targets was addressed. In Chapter 2, different types of RONS detection probes/techniques were utilised to accurately measure the concentrations of ROS such as H_2O_2 and RNS such as NO_2^- and NO_3^- delivered by a plasma jet into the tissue fluid models (water, PBS and DMEM). Amongst these techniques were small molecular probes (e.g.: DCFH, OPD and Griess reagent), electrochemical probes (ISO-HPO-2) and UVAS. While the small molecular probes are easy to use, cheaper and can be used with small volumes of test

solution, the UVAS techniques is useful to measure the dynamic changes in the levels of RONS during the plasma treatment. To measure the concentration of RONS delivered in and after the plasma treatment of tissue, hydrogel films (gelatin, agarose and PVA) of different thicknesses were utilised as tissue model targets (Chapter 3). The direct plasma treatment of tissue fluid model and through-tissue target plasma treatment can be (to some extent) linked to the plasma treatment of an 'open' wound and 'closed' wound.

From the results reported, it has been concluded that the He plasma jet(s) used in this thesis delivered higher concentrations of H_2O_2 in the tissue fluid model as compared to NO_2^- and NO_3^-. A higher concentration of RONS are generated in liquid at higher gas flow rates (1 > 0.5 > 0.05 slpm) and longer exposure times. This implies that the dosage of RONS during plasma treatment can be modulated by adjusting the plasma treatment parameters carefully.

It was elucidated that the tissue model acted as a barrier and perturbed the delivery of RONS into the tissue fluid below, however, RONS could be transported by the plasma jet deep into the tissue (mm of depths). The direct plasma treatment (without tissue) of tissue fluid and treatment through the tissue model were significantly different. The rate of RONS production (or appearance) in tissue fluid during direct plasma treatment was a faster process, as compared to treatment through the tissue model. Also, the RONS production during direct treatment ceased immediately after the plasma jet was extinguished, but in case of through-tissue model treatment, the RONS continued to appear tens of minutes after the plasma jet was extinguished. These observations indicated that the plasma-delivery of RONS deeper into the tissue is a process of 'slow molecular transport'.

Using UVAS and an electrochemical sensor (ISO-OXY-2), it was shown that while direct plasma treatment can deoxygenate a tissue fluid model, the treatment through a tissue target elevated the levels of O_2 (aq) tension in the tissue fluid and tissue model. Potentially, the ability of plasma to oxygenate tissue could be exploited to overcome the state of hypoxia (deficiency of O_2) in tissues which is a major hurdle in wound healing.

To match the tissue fluid model more closely with a real biological fluid, BSA (protein) was added to the tissue fluid model. This study was designed to investigate the combined effect of O_2 (aq) and protein in the plasma-generation of RONS. It was shown

that depending on the level of O_2 (aq) in tissue fluid, proteins can inhibit or enhance the production of RONS after plasma treatment. At low levels of O_2 (aq), such as in case of direct plasma exposure of tissue fluid model, the protein molecules quenched the RONS. But as the O_2 (aq) level increased, such as upon plasma treatment of tissue fluid though the tissue target, the presence of protein enhanced the production of RONS. The protein molecules could also acted as "reservoirs" for the plasma-generated RONS and release the RONS slowly over an extended period of time. This property could beneficial to provide a sustained and low flux of RONS which can stimulate the cellular signaling processes important for wound healing.

To complement the bulk-liquid phase RONS measurements, the reactive species generated by plasma in gas-phase were also measured, providing further insight into plasma-liquid interface reactions. The technique of OES was utilised for the optical characterization of the plasma effluent and ambient mass spectrometry was utilised to determine the neutral and ionic species transported through the tissue target during plasma treatment. The emission spectra in OES showed peaks for •OH, thus highlighting the possible role of plasma-assisted UV photolysis in RONS generation. The UV component of plasma can induce photolysis of a liquid covering tissue and produce •OH radicals at the gas-liquid interface. The highly reactive and shorter lived •OH radicals undergo subsequent reactions to form H_2O_2, the most abundant RONS detected during plasma jet treatment. The results from mass spectrometry revealed the generation of a range of charged species within the plasma and a tissue target, which could not be detected by other RONS detection techniques (i.e. small molecular probes, electrochemical sensors, UVAS or ESR). These species included O_2^+, N_2^+, H^+ N_2, NO^+, O_2^-, O_3^-, OH^-, $(OH)O^-$, NO_2^-, NO_3^-, CO_3^-, HCO_3^- and $(OH)CO_3^-$ in plasma (i.e. without tissue target), and O_2^+, N_2^+, H^+ N_2, NO^+, H_2O^+, $H_2O^+(H_2O)_n$, $H^+(H_2O)_n$, O_2^-, NO_2^-, CO_3^-,$CO_3^-(H_2O)_n$, $HCO_3^-(H_2O)$, $OH^-(H_2O)_3$, $O_2^-(H_2O)_n$ and $O_3^-(H_2O)$ during plasma treatment of the tissue target. The results from mass spectrometry also showed that the plasma-treatment of the tissue target evaporated the thin layer of water covering the target, and led to the production of water-cluster ions which solvate into the tissue model and appear on the other side of the target. A time-lag was also observed in the appearance of ionic species behind the tissue model during plasma treatment, in contrast to an abrupt increase during the direct plasma treatment. This further supports the findings from molecular probes and UVAS on the time-dependent delivery of RONS

through targets and adds to the evidence that the plasma-delivery of RONS deeper into the tissue is via a 'slow molecular transport'.

The second half of this PhD thesis i.e. Chapter 4 and 5, aims at assessing the 'harmful' effects of plasma, if any, on specific biological components and on whole cells. In chapter 4, the focus was on investigating DNA damage in the 'artificial' models of cell and biological components as well as in the skin cells (keratinocytes) using the using fluorescence-based assays. In Chapter 5, the focus is on the assessment of cell viability in two types of cells important for wound healing – keratinocytes and fibroblasts.

In chapter 4, protocols for measuring the DNA-damaging effects of plasma using the artificial DNA oligomers (or MB) and γ-H2AX assay (both fluorescence-based assays) have been developed. The MB was incorporated in the tissue fluid model, within the tissue model matrix and inside an artificial phospholipid vesicles cell model. To measure the DNA damage in 'real' cells, the phosphorylation of H2AX in keratinocytes (HaCaT cell line) was assessed. The results from both the approaches indicated that the plasma jet has the potential to induce DNA strand breaks in tissue fluid, in tissue and in cells, and the frequency of DNA strand breaks depends on the plasma dosage or treatment parameters. The intensity of DNA-strand breaks increased with plasma exposure time and gas-flow rate and decreased in with an increased distance between the plasma jet nozzle and target.

The thesis also sheds light on the probable mechanisms involved in plasma-induced DNA damage. By adding known concentrations of H_2O_2 to the MB solution, it was confirmed that the DNA-strand breaks are not induced by the longer-lived RONS such as H_2O_2. Studies have reported that H_2O_2 can also participate in DNA damage, but that is only possible through conversion of H_2O_2 to •OH (for example via Fenton reaction) [17, 18]. In other words, whilst H_2O_2 can induce DNA damage 'indirectly', the •OH radicals are the only species with the ability to 'directly' damage the DNA [19-21]. Therefore, in Chapter 4, the focus was also to assess the role of •OH produced by the plasma jet in DNA damage. Using the ESR technique, the production of •OH radicals in tissue fluid was confirmed. Combining the data from DNA-damage assays, ESR and H_2O_2 proves that the shorter-lived highly reactive species are the key "agents" facilitating DNA damage. By removing •OH for example, when the MB solution was

treated through the tissue model, no DNA-strand breaks were reported; whilst plasma continued to deliver H_2O_2 through the tissue model.

In order to safely use the plasma jet for wound healing, excessive DNA damage is undesirable. However, since microbial disinfection is another critical requirement for effective wound healing, it is desirable to deliver H_2O_2 to the wound bed/ fluid and induce a limited DNA damage (by limiting the delivery of •OH). So in an attempt to establish a "safer" plasma treatment condition, the patented 'Plasma Hydrogel Therapy' technology was tested [22]. Placing the hydrogel dressing (Smith & Nephew, Australia) between the tissue fluid model and plasma jet reduced the DNA-strand breaks significantly in both the artificial and real cells. With the help of plasma hydrogel therapy, the highly reactive •OH were filtered and only H_2O_2 reached the cells/tissue fluid. This implies that the hydrogel dressing can alleviate the deleterious effects of plasma on the cells and other biological components by "screening" the •OH radicals, and consequently the technology was referred as a "Plasma Screen" in this thesis.

In Chapter 5, the focus was to investigate the significance of plasma-induced changes in O_2 (aq) levels in RONS generation, and its impact on the viability of skin cells. The skin cells (keratinocytes and fibroblasts) were subjected to different combinations of He gas jet and He plasma jet treatments to induce oxygenation and deoxygenation in cell culture media. The viability of both cells after the jet treatments either decreased or did not change. It was also shown that the fibroblasts were more sensitive to plasma than keratinocytes. Although, under the experimental conditions used in this thesis, the plasma jet treatment (either preceded or followed by He gas jet treatment) did not have a significant positive impact on cell viability, the results provide an insight into the role of O_2 in cell-culture studies, which is often overlooked. The potential negative effects of plasma on the cellular metabolic activity, as demonstrated in this chapter, emphasises on the need of caution and care to be practised while using plasma on wounds and the importance of safety evaluation of plasma devices.

This PhD thesis is a piece of cross-disciplinary research which focused on assessing 'physics' of the plasma jet, plasma (RONS) 'chemistry' and the 'biological' effects of plasma on cells and cellular components. From establishing protocols for accurate RONS detection to proposing the concept of 'Plasma Screen', this thesis was an attempt to understand the fundamentals of RONS liquid chemistry and the more complex issues

associated with the safety of plasma and its biological effects. Although no clear and concrete experimental data showed any significant improvement in cellular functions, the knowledge obtained from this thesis paves the way for future studies aimed at developing safe and efficient plasma therapeutics.

The 'artificial' tissue and cell models used in this thesis provided new insight on the plasma-tissue/plasma-cell interactions. The results to date provide the basis for further work towards developing more 'realistic' tissue, tissue fluid and cell models, by incorporating biomolecules such as enzymes and antioxidants, or introducing fluid flow, for example in a microfluidic system. Some future projects have already been planned and are now in progress. In an ongoing collaboration with Cambridge University, UK, 3-D *in vitro* models are being utilised to create a 3-D tissue environment [23] . Skin cells are being grown in a 3-D scaffold and exposed to plasma to test for viability, migration and DNA damage. Preliminary results have shown that plasma-delivered RONS can reach cells embedded deep in the scaffolds (few mm thick) and reduced their viability. This decrease in viability could imply that the cells which are not in direct contact with the plasma (bystander cells) may be contributing to reduced viability. To evaluate the effects of plasma on bystander cells, thicker scaffolds (with cells) can be plasma treated and imaged using confocal microscopy. If cells embedded deep within the tissue exhibit DNA damage or reduced viability, then the role of 'cell-to-cell communication' in plasma-induced biological effects can be further commented upon.

In an another on-going collaboration with the York Plasma Institute, UK, the role of electric fields in plasma-generation of RONS and interactions with cells is being investigated. Two types of jet configurations- DBD and COST reference microplasma [24]. In a DBD jet there is usually plasma effluent (glow) exiting the capillary tube and in contact with the liquid. On the other hand, the plasma glow in a COST reference microplasma is contained within the glass tube and there is no visible glow in contact with the liquid. This implies that in the DBD jet, the plasma plume would induce an electric field effect on the target, while The COST microplasma does not (since the plasma plume never contacts the target). A comparison in the RONS-chemistry and subsequent biological effects induced by both the plasma devices will be useful to unravel how the orientation of electric fields influences the plasma-tissue/cell interactions.

The mechanisms governing DNA-plasma interactions also need a further investigation. Several reports have commented on the role of •OH as well as $ONOO^-$ in breaking the DNA strands [25-28]. Future studies, in collaboration with the Toyohashi University of Technology, Japan, are focused on assessing the delivery of shorter-lived and highly reactive specie $ONOO^-$ in liquid using ESR. In a complimentary study with researchers at the University of Lancaster, UK, the activation of a number of other signaling molecules, such as CHK-1, upon DNA damage are being measured.

A potential route to achieve a 'safer' plasma treatment is through fractionation of the dose. Experiments focusing on modulating the plasma (RONS) dose to stimulate cell proliferation and viability are already in progress. For instance, in an initial set of experiments, skin cells in a well (of 96-well plate) were exposed to a 60 s of plasma treatment 'once', and in other two separate wells cells were exposed to 15 s and 30 s of plasma treatment for 4 days and 2 days, respectively. The objective was to achieve a total plasma exposure duration of 60 s in each case. Interestingly, the cell proliferation decreased with one 60 s plasma treatment than the four 15 s doses of plasma, but the fractionated plasma doses had no impact on cell viability. However, in case of all plasma treatments the plasma did not improve the proliferation or viability. These experiments are still in progress. The objective is to establish the plasma treatment parameters which can positively impact the cell viability and proliferation.

Overall, this thesis provides is an initial but necessary first step towards developing an underpinning understanding of the mode of action of plasma in tissue treatment. The conclusions drawn from this PhD could have direct implications in both *in vitro* and *in vivo* research in the field of plasma medicine. The techniques used to monitor RONS delivery, the assays developed to assess harmful effects of plasma and methods proposed to limit the harmful effects for plasma will serve as a platform for the development of 'safer' plasma devices and may assist in realizing the full potential of plasma in wound healing.

6.1 References

1. Pacella, R., et al., *Solutions to the chronic wounds problem in Australia: A call To action.* 2018.
2. Lackmann, J.W. and J.E. Bandow, *Inactivation of microbes and macromolecules by atmospheric-pressure plasma jets.* Appl Microbiol Biotechnol, 2014. **98**(14): p. 6205-13.

3. Privat-Maldonado, A., et al., *Spatial Dependence of DNA Damage in Bacteria due to Low-Temperature Plasma Application as Assessed at the Single Cell Level.* Scientific Reports, 2016. **6**: p. 35646.
4. Klebes, M., et al., *Combined antibacterial effects of tissue-tolerable plasma and a modern conventional liquid antiseptic on chronic wound treatment.* Journal of Biophotonics, 2015. **8**(5): p. 382-391.
5. Brehmer, F., et al., *Alleviation of chronic venous leg ulcers with a hand-held dielectric barrier discharge plasma generator (PlasmaDerm((R)) VU-2010): results of a monocentric, two-armed, open, prospective, randomized and controlled trial (NCT01415622).* Journal of the European Academy of Dermatology and Venereology, 2015. **29**(1): p. 148-55.
6. Ulrich, C., et al., *Clinical use of cold atmospheric pressure argon plasma in chronic leg ulcers: A pilot study.* J Wound Care, 2015. **24**(5): p. 196, 198-200, 202-3.
7. Sladek, R.E.J., et al., *Plasma treatment of dental cavities: a feasibility study.* IEEE Transactions on Plasma Science, 2004. **32**(4): p. 1540-1543.
8. Lee H. W., *e.a., Atmospheric Pressure Plasma Jet Composed of Three Electrodes: Application to Tooth Bleaching.* Plasma Process. Polym., 2010. **7**: p. 274-280.
9. Heinlin, J., et al., *Plasma applications in medicine with a special focus on dermatology.* Journal of the European Academy of Dermatology and Venereology, 2011. **25**(1): p. 1-11.
10. Metelmann, H.-R., et al., *Clinical experience with cold plasma in the treatment of locally advanced head and neck cancer.* Clinical Plasma Medicine, 2018. **9**: p. 6-13.
11. Chao-Yu, C., C. Yun-Chien, and C. Yi-Jing, *Synergistic effects of plasma-activated medium and chemotherapeutic drugs in cancer treatment.* Journal of Physics D: Applied Physics, 2018. **51**(13): p. 13LT01.
12. Dubuc, A., et al., *Use of cold-atmospheric plasma in oncology: a concise systematic review.* Ther Adv Med Oncol, 2018. **10**: p. 1758835918786475.
13. Endre, J.S., et al., *The hormesis effect of plasma-elevated intracellular ROS on HaCaT cells.* Journal of Physics D: Applied Physics, 2015. **48**(49): p. 495401.
14. Halliwell, B. and J.M. Gutteridge, *Free radicals in biology and medicine*. 2015: Oxford University Press, USA.
15. Niemira, B.A., G. Boyd, and J. Sites, *Cold plasma rapid decontamination of food contact surfaces contaminated with Salmonella biofilms.* J Food Sci, 2014. **79**(5): p. M917-22.
16. Loo, A.E., et al., *Effects of hydrogen peroxide on wound healing in mice in relation to oxidative damage.* PLoS One, 2012. **7**(11): p. e49215.
17. Cadet, J. and J.R. Wagner, *DNA base damage by reactive oxygen species, oxidizing agents, and UV radiation.* Cold Spring Harbor perspectives in biology, 2013. **5**(2).
18. Park, S. and J.A. Imlay, *High levels of intracellular cysteine promote oxidative DNA damage by driving the fenton reaction.* J Bacteriol, 2003. **185**(6): p. 1942-50.
19. Balasubramanian, B., W.K. Pogozelski, and T.D. Tullius, *DNA strand breaking by the hydroxyl radical is governed by the accessible surface areas of the hydrogen atoms of the DNA backbone.* Proceedings of the National Academy of Sciences, 1998. **95**(17): p. 9738-9743.

20. Giulivi, C., Alberto Boveris, and Enrique Cadenas, *Hydroxyl radical generation during mitochondrial electron-transfer and the formation of 8-hydroxydesoxyguanosine in mitochondrial-DNA.* Archives of Biochemistry and Biophysics, 1995. **316**(2): p. 909-916.
21. Kurita, H., et al., *Use of molecular beacons for the rapid analysis of DNA damage induced by exposure to an atmospheric pressure plasma jet.* Applied Physics Letters, 2015. **107**(26): p. 263702.
22. Short, R.D., I.M. Griffiths, and E.J. Szili, *Plasma hydrogel therapy*. 2017, Google Patents.
23. Davidenko, N., et al., *Collagen–hyaluronic acid scaffolds for adipose tissue engineering.* Acta biomaterialia, 2010. **6**(10): p. 3957-3968.
24. Golda, J., et al., *Concepts and characteristics of the 'COST Reference Microplasma Jet'.* Journal of Physics D: Applied Physics, 2016. **49**(8): p. 084003.
25. Niles, J.C., J.S. Wishnok, and S.R. Tannenbaum, *Peroxynitrite-induced oxidation and nitration products of guanine and 8-oxoguanine: Structures and mechanisms of product formation.* Nitric Oxide, 2006. **14**(2): p. 109-121.
26. Salgo, M.G., et al., *DNA Damage and Oxidation of Thiols Peroxynitrite Causes in Rat Thymocytes.* Archives of Biochemistry and Biophysics, 1995. **322**(2): p. 500-505.
27. Beckman, J.S., et al., *Apparent hydroxyl radical production by peroxynitrite: implications for endothelial injury from nitric oxide and superoxide.* Proceedings of the National Academy of Sciences of the United States of America, 1990. **87**(4): p. 1620-1624.
28. Burney, S., et al., *The chemistry of DNA damage from nitric oxide and peroxynitrite.* Mutat Res, 1999. **424**(1-2): p. 37-49.

Appendix A Calibration for the detection of H_2O_2 using OPD-HRP

To quantify the concentrations of H_2O_2 delivered by the plasma jet in the tissue fluid models (water, PBS and DMEM) using OPD-HRP, following steps were followed:

1. The absorbance of plasma-treated and untreated OPD-HRP solution (prepared in the tissue fluid models) was measured using the micro-plate reader at the wavelength of 450 nm. The normalised absorbance were calculated by subtracting the absorbance of untreated solution from the absorbance of plasma-treated solution. As an example, the direct method of H_2O_2 detection in water is discussed here (Figure A.1). Similar approach was followed for all other tissue fluid models (PBS and DMEM) and for the indirect method.

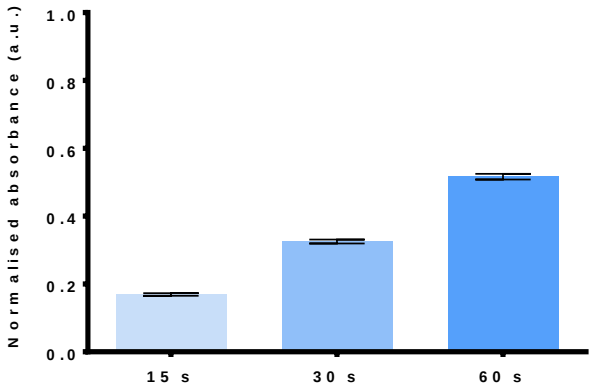


Figure A.1 Normalised absorbance of the plasma-treated OPD-HRP solution (prepared in water). Plasma treatment was conducted for 15, 30 and 60 s at 0.5 slpm.

2. In the next step, known concentrations of H_2O_2 solution were added to the OPD-HRP solution. The resultant absorbance values of H_2O_2-treated solution and untreated solution were measured. It was confirmed that that the experimental (plasma-generated) absorbance values were in the range of H_2O_2-generated absorbance values. Normalised absorbance was calculated as discussed in the step 1. The normalised calibration curve was plotted to determine the equation of chart, such that x and y variables in the equation correspond to the concentration of H_2O_2 and normalised absorbance value, respectively (Figure A.2).

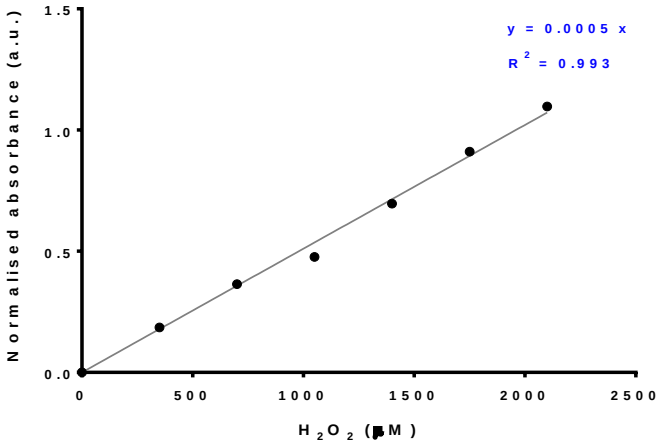


Figure A.2 Normalised absorbance of the OPD-HRP solution treated with different concentrations of H_2O_2

3. The equation in step 2 was used to translate the normalised absorbance values of plasma-treated solution into the concentration of H_2O_2. For instance, at 15 s of plasma treatment, the normalised absorbance value (or the value of 'y') was 0.169 a.u. Putting the value of 'y' in the equation y = 0.0005 x, the value 'x' (or the concentration of H_2O_2) was calculated as 338.16 µM. Similarly, other absorbance values were also converted to H_2O_2 concentrations, as shown in Figure A.3.

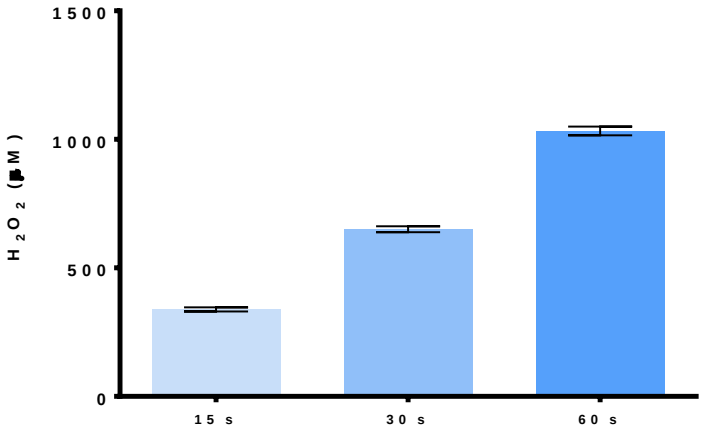


Figure A.3 The concentrations of H_2O_2 produced by the plasma jet in water. Plasma treatment was conducted for 15, 30 and 60 s at 0.5 slpm.

Appendix B Calibration for the detection of NO_2^- using Griess reagent

To quantify the concentrations of NO_2^- delivered by the plasma jet in the tissue fluid models (water, PBS and DMEM) using Griess reagent, following steps were followed:

1. The absorbance of plasma-treated and untreated Griess reagent (prepared in the tissue fluid models) was measured using the micro-plate reader at the wavelength of 548 nm. The normalised absorbance were calculated by subtracting the absorbance of untreated solution from the absorbance of plasma-treated solution. As an example, the direct method of NO_2^- detection in water is discussed here (Figure B.1). Similar approach was followed for all other tissue fluid models (PBS and DMEM) and for the indirect method.

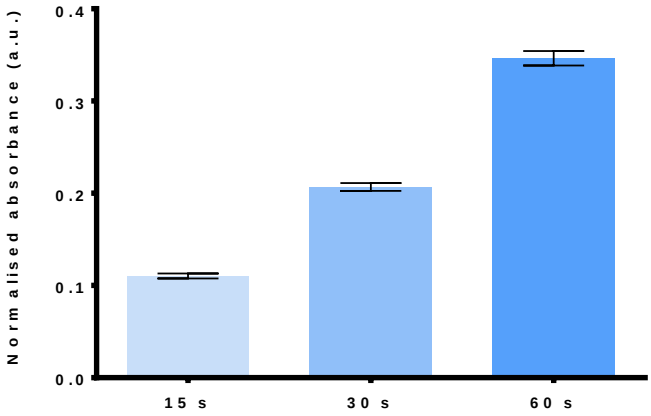


Figure B.1 Normalised absorbance of the plasma-treated Griess reagent (prepared in water). Plasma treatment was conducted for 15, 30 and 60 s at 0.5 slpm.

2. In the next step, known concentrations of HNO_2 solution (source of NO_2^-) were added to the Griess reagent. The resultant absorbance values of HNO_2-treated solution and untreated solution were measured. It was confirmed that that the experimental (plasma-generated) absorbance values were in the range of HNO_2-generated absorbance values. Normalised absorbance was calculated as discussed in the step 1. The normalised calibration curve was plotted to determine the equation of chart, such that x and y variables in the equation correspond to the concentration of NO_2^- and normalised absorbance value, respectively (Figure B.2).

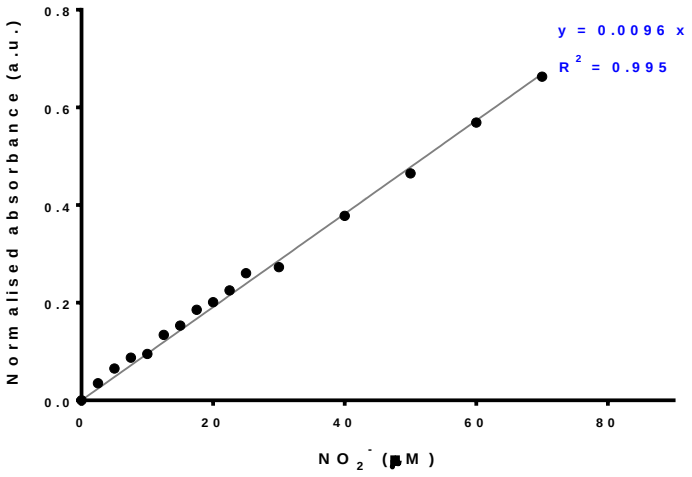


Figure B.2 Normalised absorbance of the Griess reagent treated with different concentrations of NO_2^-

3. The equation in step 2 was used to translate the normalised absorbance values of plasma-treated solution into the concentration of NO_2^-. For instance, at 15 s of plasma treatment, the normalised absorbance value (or the value of 'y') was 0.1103 a.u. Putting the value of 'y' in the equation y = 0.0096 x, the value 'x' (or the concentration of NO_2^-) was calculated as 11.49 μM. Similarly, other absorbance values were also converted to NO_2^- concentrations, as shown in Figure B.3.

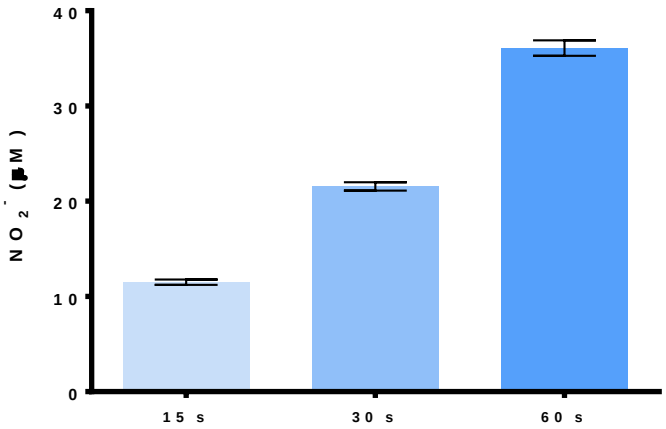


Figure B.3 The concentrations of NO_2^- produced by the plasma jet in water. Plasma treatment was conducted for 15, 30 and 60 s at 0.5 slpm.

Appendix C Calibration for the detection of H_2O_2 using ISO-HPO-2

To quantify the concentrations of H_2O_2 delivered by the plasma jet in the tissue fluid models (water, PBS and DMEM) using ISO-HPO-2, following steps were followed:

1. The current of plasma-treated and untreated tissue fluid model in a 96-well plate using ISO-HPO-2. The normalised current were calculated by subtracting the current of untreated solution from the absorbance of plasma-treated solution. As an example, H_2O_2 was detected in PBS (Figure C.1). Similar approach was followed for all other tissue fluid models (water and DMEM).

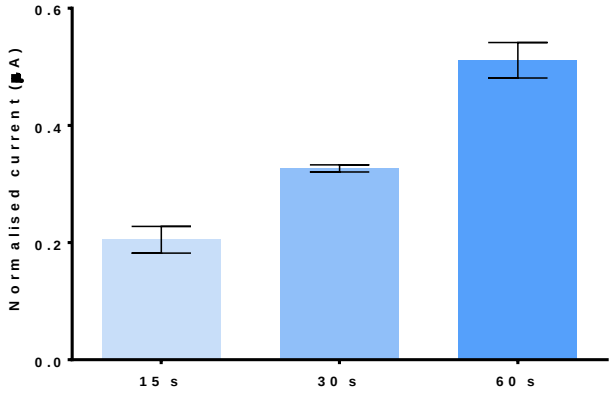


Figure C.1 Normalised current of the plasma-treated PBS. Plasma treatment was conducted for 15, 30 and 60 s at 0.5 slpm.

2. In the next step, known concentrations of H_2O_2 solution were added to PBS. The resultant absorbance values of H_2O_2-treated solution and untreated solution were measured. It was confirmed that that the experimental (plasma-generated) current values were in the range of H_2O_2-generated absorbance values. Normalised current was calculated as discussed in the step 1. The normalised calibration curve was plotted to determine the equation of chart, such that x and y variables in the equation correspond to the concentration of H_2O_2 and normalised current value, respectively (Figure C.2).

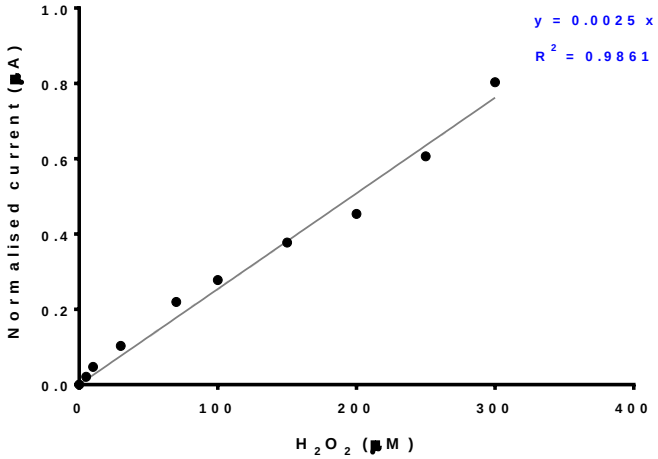


Figure C.2 Normalised absorbance of the PBS treated with different concentrations of H_2O_2

3. The equation in step 2 was used to translate the normalised absorbance values of plasma-treated solution into the concentration of H_2O_2. For instance, at 15 s of plasma treatment, the normalised current value (or the value of 'y') was 0.204 µM. Putting the value of 'y' in the equation y = 0.0025 x, the value 'x' (or the concentration of H_2O_2) was calculated as 78.49 µM. Similarly, other current values were also converted to H_2O_2 concentrations, as shown in Figure C.3.

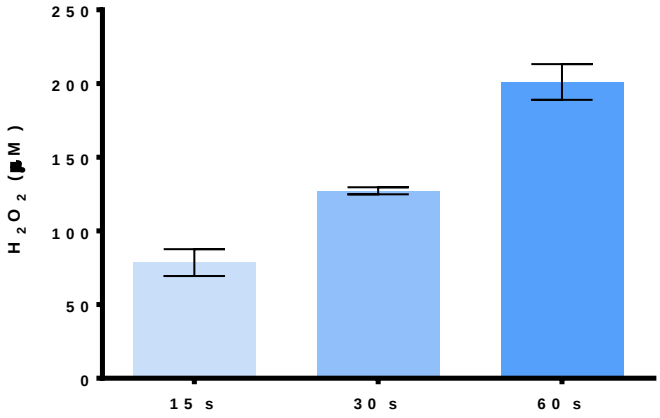


Figure C.3 The concentrations of H_2O_2 produced by the plasma jet in PBS. Plasma treatment was conducted for 15, 30 and 60 s at 0.5 slpm.

Appendix D Publishing rights for the figures in Chapter 3 (Section 3.1)

AIP PUBLISHING LICENSE
TERMS AND CONDITIONS

Jan 23, 2019

This Agreement between nishtha gaur ("You") and AIP Publishing ("AIP Publishing") consists of your license details and the terms and conditions provided by AIP Publishing and Copyright Clearance Center.

License Number	4484661062833
License date	Dec 09, 2018
Licensed Content Publisher	AIP Publishing
Licensed Content Publication	Applied Physics Letters
Licensed Content Title	Combined effect of protein and oxygen on reactive oxygen and nitrogen species in the plasma treatment of tissue
Licensed Content Author	Nishtha Gaur, Endre J. Szili, Jun-Seok Oh, et al
Licensed Content Date	Sep 7, 2015
Licensed Content Volume	107
Licensed Content Issue	10
Type of Use	Thesis/Dissertation
Requestor type	Author (original article)
Format	Electronic
Portion	Figure/Table
Number of figures/tables	5
Title of your thesis / dissertation	nvestigating plasma-tissue interactions in the context of wound healing
Expected completion date	Feb 2019
Estimated size (number of pages)	400
Requestor Location	nishtha gaur University of South Australia Mawson Lakes Boulevard MAWSON LAKES Adelaide, SA 5095 Australia Attn: nishtha gaur
Billing Type	Invoice
Billing Address	nishtha gaur University of South Australia Mawson Lakes Boulevard MAWSON LAKES Adelaide, Australia 5095 Attn: nishtha gaur
Total	0.00 AUD

Terms and Conditions

AIP Publishing -- Terms and Conditions: Permissions Uses

AIP Publishing hereby grants to you the non-exclusive right and license to use and/or distribute the Material according to the use specified in your order, on a one-time basis, for the specified term, with a maximum distribution equal to the number that you have ordered. Any links or other content accompanying the Material are not the subject of this license.

1. You agree to include the following copyright and permission notice with the reproduction of the Material:"Reprinted from [FULL CITATION], with the permission of AIP Publishing." For an article, the credit line and permission notice must be printed on the first page of the article or book chapter. For photographs, covers, or tables, the notice may appear with the Material, in a footnote, or in the reference list.
2. If you have licensed reuse of a figure, photograph, cover, or table, it is your responsibility to ensure that the material is original to AIP Publishing and does not contain the copyright of another entity, and that the copyright notice of the figure, photograph, cover, or table does not indicate that it was reprinted by AIP Publishing, with permission, from another source. Under no circumstances does AIP Publishing purport or intend to grant permission to reuse material to which it does not hold appropriate rights.
   You may not alter or modify the Material in any manner. You may translate the Material into another language only if you have licensed translation rights. You may not use the Material for promotional purposes.
3. The foregoing license shall not take effect unless and until AIP Publishing or its agent, Copyright Clearance Center, receives the Payment in accordance with Copyright Clearance Center Billing and Payment Terms and Conditions, which are incorporated herein by reference.
4. AIP Publishing or Copyright Clearance Center may, within two business days of granting this license, revoke the license for any reason whatsoever, with a full refund payable to you. Should you violate the terms of this license at any time, AIP Publishing, or Copyright Clearance Center may revoke the license with no refund to you. Notice of such revocation will be made using the contact information provided by you. Failure to receive such notice will not nullify the revocation.
5. AIP Publishing makes no representations or warranties with respect to the Material. You agree to indemnify and hold harmless AIP Publishing, and their officers, directors, employees or agents from and against any and all claims arising out of your use of the Material other than as specifically authorized herein.
6. The permission granted herein is personal to you and is not transferable or assignable without the prior written permission of AIP Publishing. This license may not be amended except in a writing signed by the party to be charged.
7. If purchase orders, acknowledgments or check endorsements are issued on any forms containing terms and conditions which are inconsistent with these provisions, such inconsistent terms and conditions shall be of no force and effect. This document, including the CCC Billing and Payment Terms and Conditions, shall be the entire agreement between the parties relating to the subject matter hereof.

This Agreement shall be governed by and construed in accordance with the laws of the State of New York. Both parties hereby submit to the jurisdiction of the courts of New York County for purposes of resolving any disputes that may arise hereunder.

V1.2

Questions? customercare@copyright.com or +1-855-239-3415 (toll free in the US) or +1-978-646-2777.

Appendix E Publishing rights for the figures in Chapter 3 (Section 3.2)

Copyright Clearance Center

Confirmation Number: 11772545
Order Date: 12/09/2018

Customer Information

Customer: NISHTHA GAUR
Account Number: 3001378544
Organization: NISHTHA GAUR
Email: nishtha.gaur@mymail.unisa.edu.au
Phone: +61 (4)14606743
Payment Method: Invoice

This is not an invoice

Order Details

Plasma Sources Science and Technology

Billing Status: **N/A**

Order detail ID:	71706432
ISSN:	0963-0252
Publication Type:	Journal
Volume:	
Issue:	
Start page:	
Publisher:	IOP Publishing
Author/Editor:	American Institute of Physics ; Institute of Physics (Great Britain)

Permission Status: **Granted**
Permission type: Republish or display content
Type of use: Thesis/Dissertation
Order License Id: 4484680047310

Requestor type	Author of requested content
Format	Print, Electronic
Portion	chart/graph/table/figure
Number of charts/graphs/tables/figures	5
The requesting person/organization	Nishtha Gaur
Title or numeric reference of the portion(s)	Figure 6, Figure 7 , Figure 8 , Table 1
Title of the article or chapter the portion is from	Modelling the helium plasma jet delivery of reactive species into a 3D cancer tumour
Editor of portion(s)	NA
Author of portion(s)	NA
Volume of serial or monograph	NA
Issue, if republishing an article from a serial	1
Page range of portion	014001
Publication date of portion	8-12-2017
Rights for	Main product
Duration of use	Current edition and up to 5 years
Creation of copies for the disabled	no
With minor editing privileges	yes
For distribution to	Worldwide
In the following language(s)	Original language of publication
With incidental promotional use	no

Lifetime unit quantity of new product	Up to 499
Title	Investigating plasma-tissue interactions in the context of wound healing
Institution name	Future Industries Institute, University of South Australia
Expected presentation date	Feb 2019

Note: This item was invoiced separately through our **RightsLink service.** More info **$ 0.00**

Total order items: 1 **Order Total: $0.00**

About Us | Privacy Policy | Terms & Conditions | Pay an Invoice

Copyright 2018 Copyright Clearance Center

Appendix F Publishing rights for the figures in Chapter 3 (Section 3.3)

Gaur, Nishtha - gauny004

From: haruyuki okamura <okamura@chem.osakafu-u.ac.jp>
Sent: Monday, 10 December 2018 2:08 PM
To: Gaur, Nishtha - gauny004
Subject: RE: Request for publishing rights
Attachments: image001.gif

Dear Nishtha Gaur,

I give you permission to use the figures appeared in https://doi.org/10.2494/photopolymer.30.317.
Thank you very much.

Sincerely yours,

Haruyuki Okamura

差出人 : Gaur, Nishtha - gauny004 <nishtha.gaur@mymail.unisa.edu.au>
送信日時: 2018年 12月10日 11:54
宛先 : 岡村 晴之
件名 : Request for publishing rights

Hello Prof. Haruyuki Okamura,

I would like to request permission to use figures of the following paper ? "Mass Spectrometry Analysis of the Real-Time Transport of Plasma-Generated Ionic Species Through an Agarose Tissue Model Target", https://doi.org/10.2494/photopolymer.30.317. I am a co-author of this paper.

I would like to use 6 figures in total for my PhD thesis to be submitted on 2-Feb-2019. I could not find "permission rights" option on the website of the Copyright Clearance Centre and Journal of Photopolymer Science and Technology. I was advised to directly contact you.

Please let me know if there is more information you need.

Many thanks,
Nishtha Gaur | PhD Research Scholar
Building V | Future Industries Institute University of South Australia, Adelaide
Work: +61-883026686 | Home: +[redacted] Alternative Email:
nishthagaur.16@gmail.com<mailto:nishthagaur.16@gmail.com>

[Please consider the environment before printing]

Appendix G Publishing rights for the figures in Chapter 4

Copyright Clearance Center

Confirmation Number: 11772720
Order Date: 12/09/2018

Customer Information

Customer: NISHTHA GAUR
Account Number: 3001378544
Organization: NISHTHA GAUR
Email: nishtha.gaur@mymail.unisa.edu.au
Phone: +61 (4)14606743
Payment Method: Invoice

This is not an invoice

Order Details

Journal of Physics D : Applied Physics

Billing Status: **N/A**

Order detail ID:	71709070
ISSN:	0022-3727
Publication Type:	Journal
Volume:	
Issue:	
Start page:	
Publisher:	IOP Publishing
Author/Editor:	Institute of Physics and the Physical Society ; Institute of Physics (Great Britain)

Permission Status: Granted
Permission type: Republish or display content
Type of use: Thesis/Dissertation
Order License Id: 4485091308343

Requestor type	Author of requested content
Format	Print, Electronic
Portion	chart/graph/table/figure
Number of charts/graphs/tables/figures	8
The requesting person/organization	Nishtha Gaur
Title or numeric reference of the portion(s)	Figure 1, Figure 2, Figure 3, Figure 4, Figure 5, Figure 6, Figure 7, Figure 8,
Title of the article or chapter the portion is from	The assessment of cold atmospheric plasma treatment of DNA in synthetic models of tissue fluid, tissue and cells
Editor of portion(s)	NA
Author of portion(s)	NA
Volume of serial or monograph	50
Issue, if republishing an article from a serial	27
Page range of portion	274001
Publication date of portion	15 June 2017
Rights for	Main product
Duration of use	Current edition and up to 5 years
Creation of copies for the disabled	no
With minor editing privileges	yes
For distribution to	Worldwide
In the following language(s)	Original language of publication

With incidental promotional use	no
Lifetime unit quantity of new product	Up to 499
Title	Investigating plasma-tissue interactions in the context of wound healing
Institution name	Future Industries Institute, University of South Australia
Expected presentation date	Feb 2019

Note: This item was invoiced separately through our **RightsLink service.** More info **$ 0.00**

Total order items: 1 **Order Total: $0.00**

About Us | Privacy Policy | Terms & Conditions | Pay an Invoice

Copyright 2018 Copyright Clearance Center

Appendix H Author declaration for the referred manuscript in Chapter 4

The assessment of cold atmospheric plasma treatment of DNA in synthetic models of tissue fluid, tissue and cells

Nishtha Gaur, Endre J. Szili, Sung-Ha Hong, Hirofumi Kurita, Jun-Seok Oh, Masafumi Ito, Akira Mizuno, Akimitsu Hatta, Allison J. Cowin, David B. Graves, Robert D. Short

(Published in Journal of Physics D: Applied Physics)

https://doi.org/10.1088/1361-6463/aa7501

Author's declaration on the statement of contribution of each author:

Author	Contribution
Nishtha Gaur*	• Synthesised MB; • Synthesised gelatin tissue models; • Synthesised HEPES tissue fluid model; • Synthesised vesicles; • Conducted plasma jet treatments; • Conducted the experiments with the commercial hydrogel dressing; • Established the OPD-HRP protocol and measured the concentrations of H_2O_2 in solution using OPD-HRP; • Assisted in manuscript writing.
Endre J. Szili*	• Developed the plasma jet; • Assisted in plasma treatments; • Performed Fluorescence and Phase-contrast microscopy; • Interpreted the results; • Wrote the manuscript.
Sung-Ha Hong	• Assisted in the synthesis of vesicles; • Assisted in MB synthesis; • Interpreting the data obtained from vesicle experiments.

* Gaur and Szili are equal co-first authors.

Hirofumi Kurita	• Provided the protocol for the synthesis of molecular beacons; • Assisted in interpreting MB-results.
Jun-Seok Oh Masafumi Ito Akira Mizuno Akimitsu Hatta Allison J. Cowin David B. Graves Robert D. Short	• Supervised all the work done; • Helped in interpreting the results; • Edited the manuscript before submission.

Principal Supervisor Confirmation:

I have sighted email or other correspondence from all Co-authors confirming their certifying authorship. The above candidate's declaration correctly reflects the contribution of each Co-author. The publication is permitted to be used as part of this thesis.

Prof. Rob D. Short

Name	Signature	Date
Rob Short	[redacted]	28.01.2019

Citation: Szili, Endre J., Nishtha Gaur, Sung-Ha Hong, Hirofumi Kurita, Jun-Seok Oh, Masafumi Ito, Akira Mizuno et al. "The assessment of cold atmospheric plasma treatment of DNA in synthetic models of tissue fluid, tissue and cells." *Journal of Physics D: Applied Physics* 50, no. 27 (2017): 274001.

Appendix I Publishing rights for the figures in Chapter 5

AIP PUBLISHING LICENSE
TERMS AND CONDITIONS

Dec 09, 2018

This Agreement between nishtha gaur ("You") and AIP Publishing ("AIP Publishing") consists of your license details and the terms and conditions provided by AIP Publishing and Copyright Clearance Center.

License Number	4485100220662
License date	Dec 09, 2018
Licensed Content Publisher	AIP Publishing
Licensed Content Publication	Applied Physics Letters
Licensed Content Title	How plasma induced oxidation, oxygenation, and de-oxygenation influences viability of skin cells
Licensed Content Author	Jun-Seok Oh, Xanthe Strudwick, Robert D. Short, et al
Licensed Content Date	Nov 14, 2016
Licensed Content Volume	109
Licensed Content Issue	20
Type of Use	Thesis/Dissertation
Requestor type	Author (original article)
Format	Print and electronic
Portion	Figure/Table
Number of figures/tables	4
Title of your thesis / dissertation	Investigating plasma-tissue interactions in the context of wound healing
Expected completion date	Feb 2019
Estimated size (number of pages)	400
Requestor Location	nishtha gaur University of South Australia Mawson Lakes Boulevard MAWSON LAKES Adelaide, SA 5095 Australia Attn: nishtha gaur
Billing Type	Invoice
Billing Address	nishtha gaur University of South Australia Mawson Lakes Boulevard MAWSON LAKES Adelaide, Australia 5095 Attn: nishtha gaur
Total	0.00 AUD

Terms and Conditions

AIP Publishing -- Terms and Conditions: Permissions Uses

AIP Publishing hereby grants to you the non-exclusive right and license to use and/or distribute the Material according to the use specified in your order, on a one-time basis, for the specified term, with a maximum distribution equal to the number that you have ordered. Any links or other content accompanying the Material are not the subject of this license.

1. You agree to include the following copyright and permission notice with the reproduction of the Material:"Reprinted from [FULL CITATION], with the permission of AIP Publishing." For an article, the credit line and permission notice must be printed on the first page of the article or book chapter. For photographs, covers, or tables, the notice may appear with the Material, in a footnote, or in the reference list.
2. If you have licensed reuse of a figure, photograph, cover, or table, it is your responsibility to ensure that the material is original to AIP Publishing and does not contain the copyright of another entity, and that the copyright notice of the figure, photograph, cover, or table does not indicate that it was reprinted by AIP Publishing, with permission, from another source. Under no circumstances does AIP Publishing purport or intend to grant permission to reuse material to which it does not hold appropriate rights.
   You may not alter or modify the Material in any manner. You may translate the Material into another language only if you have licensed translation rights. You may not use the Material for promotional purposes.
3. The foregoing license shall not take effect unless and until AIP Publishing or its agent, Copyright Clearance Center, receives the Payment in accordance with Copyright Clearance Center Billing and Payment Terms and Conditions, which are incorporated herein by reference.
4. AIP Publishing or Copyright Clearance Center may, within two business days of granting this license, revoke the license for any reason whatsoever, with a full refund payable to you. Should you violate the terms of this license at any time, AIP Publishing, or Copyright Clearance Center may revoke the license with no refund to you. Notice of such revocation will be made using the contact information provided by you. Failure to receive such notice will not nullify the revocation.
5. AIP Publishing makes no representations or warranties with respect to the Material. You agree to indemnify and hold harmless AIP Publishing, and their officers, directors, employees or agents from and against any and all claims arising out of your use of the Material other than as specifically authorized herein.
6. The permission granted herein is personal to you and is not transferable or assignable without the prior written permission of AIP Publishing. This license may not be amended except in a writing signed by the party to be charged.
7. If purchase orders, acknowledgments or check endorsements are issued on any forms containing terms and conditions which are inconsistent with these provisions, such inconsistent terms and conditions shall be of no force and effect. This document, including the CCC Billing and Payment Terms and Conditions, shall be the entire agreement between the parties relating to the subject matter hereof.

This Agreement shall be governed by and construed in accordance with the laws of the State of New York. Both parties hereby submit to the jurisdiction of the courts of New York County for purposes of resolving any disputes that may arise hereunder.

V1.2

Questions? customercare@copyright.com or +1-855-239-3415 (toll free in the US) or +1-978-646-2777.